PAST AND FUTURE HYDROLOGY NEAR THE ARCTIC TREELINE

A Thesis Submitted to the College of

Graduate and Postdoctoral Studies

In Partial Fulfillment of the Requirements

For the Degree of Doctorate of Philosophy

In the Department of Geography and Planning

(Centre for Hydrology)

University of Saskatchewan

Saskatoon

By

SEBASTIAN ALBERTO KROGH NAVARRO

Permission to Use

In presenting this thesis/dissertation in partial fulfillment of the requirements for a Postgraduate degree from the University of Saskatchewan, I agree that the Libraries of this University may make it freely available for inspection. I further agree that permission for copying of this thesis/dissertation in any manner, in whole or in part, for scholarly purposes may be granted by the professor or professors who supervised my thesis/dissertation work or, in their absence, by the Head of the Department or the Dean of the College in which my thesis work was done. It is understood that any copying or publication or use of this thesis/dissertation or parts thereof for financial gain shall not be allowed without my written permission. It is also understood that due recognition shall be given to me and to the University of Saskatchewan in any scholarly use which may be made of any material in my thesis/dissertation.

Disclaimer

Reference in this thesis/dissertation to any specific commercial products, process, or service by trade name, trademark, manufacturer, or otherwise, does not constitute or imply its endorsement, recommendation, or favouring by the University of Saskatchewan. The views and opinions of the author expressed herein do not state or reflect those of the University of Saskatchewan, and shall not be used for advertising or product endorsement purposes.

Requests for permission to copy or to make other uses of materials in this thesis/dissertation in whole or part should be addressed to:

Head of the Department of Geography and Planning
117 Science Place
University of Saskatchewan
Saskatoon, Saskatchewan S7N 1J9
Canada

OR

Dean
College of Graduate and Postdoctoral Studies
University of Saskatchewan
116 Thorvaldson Building, 110 Science Place
Saskatoon, Saskatchewan S7N 5C9
Canada

Abstract

The Arctic has warmed rapidly, increasing shrub cover and density, and thawing permafrost. Understanding, quantifying and predicting the impact of these environmental changes on the hydrological regime of Arctic headwater basins represents a great scientific challenge, particularly due to the sparse monitoring network, limited understanding of governing physical processes and their interaction, and the uncertainty in future climate projections. The purpose of this research is to better understand the impact of climate and vegetation change on the hydrology of Arctic basins near the treeline. This thesis is divided into four sections with the following objectives: (1) to test the coupling of a ground freeze/thaw algorithm with a hydrological model at two research sites in northern Yukon; (2) to diagnose the hydrology of a small Arctic basin near the treeline using a physically based hydrological model; (3) to quantify its historical long-term changes and investigate the individual and combined effect of changing climate and vegetation on its hydrology; and (4) to use high-resolution climate simulations under a high gas concentration scenario along with expected vegetation changes, to investigate changes to hydrological processes and regime.

Results revealed the importance of including vegetation dynamics such as changes in shrub extension and density in hydrological models, to capture their impact on blowing snow redistribution and sublimation, and canopy interception and sublimation of snow, something neglected by current studies. This study demonstrated that increasing shrub extension and density near the Arctic treeline slightly compensates the historical decrease in mean annual discharge produced by the decreasing precipitation, providing a small degree of hydrological resiliency. Historical change analysis revealed that hydrological processes are decelerating near the Arctic treeline, such as decreasing evapotranspiration, soil moisture, sublimation and streamflow, mostly driven by climate change. However, under sufficient climate change (38% and 6.1 °C increase in mean annual precipitation and temperature, respectively) significant hydrological changes are expected, reversing the simulated historical changes. Projections show a significant increase in mean annual streamflow discharge, shortening of the snowcover seasons, deepening of the active layer thickness, increasing peak snow accumulation and earlier and larger peak streamflow. Whilst specific to one basin, they indicate the nature of hydrological changes facing Arctic hydrology. These changes will have significant impacts on ecosystems, infrastructure, landscape evolution and atmospheric feedbacks, which are required to be properly understood and quantified to design sustainable and effective mitigation and adaptation plans. The analyses and discussions presented in this study to diagnose the past and predict future Arctic hydrology are relevant for the scientific community of hydrologists, engineers, water managers and policy makers, particularly those interested in cold regions.

Acknowledgments

I would like to thank my supervisor, Dr. John Pomeroy, for giving me the opportunity to pursue my PhD in Canada, during which I visited incredible places and met amazing people. I also want to thank for his guidance, insights and advises, which allowed me to grow as a researcher. Thank you to my committee members for their helpful insights to improve this dissertation. Thanks to my friends and colleagues from the Centre for Hydrology (Saskatoon and Canmore) for the good chats, times and valuable scientific feedback. Thanks to Joni Onclin and Phyllis Baynes for their travel and logistic support throughout this period.

I really want to thank my wife, Luci, for all her support and love during the ups and downs of this PhD, which would have been much more difficult without you by my side. Thanks to my parents for always supporting me and trying to understand why I do what I do.

Contents

List of Tables

List of Figures

List of Abbreviations

AHM: Arctic Hydrology Model

ASTER-GDEM: Advanced Spaceborne Thermal Emission and Reflection Radiometer – Global Digital Elevation Model

CCSM: Community Climate System Model

CEH: Centre for Ecology & Hydrology

CGCM4: Fourth Generation Coupled Global Climate Model

CFSR: NCEP Climate Forecast System Reanalysis

CNRM: Centre National de Recherdes Meteorologique

CRCM: Canadian Regional Climate Model

CRHM: Cold Regions Hydrological Model

DD: Dynamical Downscaling

ECMWF: European Centre for Medium-Range Weather Forecast

ECP2: Experimental Climate Prediction Center's version of the Regional Spectral Model

ECPC: Experimental Climate Prediction Center

ENSO: El Nino Southern Oscillation

FDF: Frequency Distribution Function

GCM: Global Circulation Model

GFDL: Geophysical Fluid Dynamics Laboratory GCM

HadCM3: Hadley Centre Couple Model, version 3

HRM3: Hadley Regional Model 3

HRU: Hydrological Response Unit

IPSL: Institute Pierre Simon Laplace

MM5I: PSU/NCAR Mesoscale Model

MERRA: Modern-Era Retrospective analysis for Research Applications

NARCCAP: North American Regional Climate Change Assessment Program

NARR: North American Regional Reanalysis

NCAR: National Center for Atmospheric Research

NCEP: National Center for Environmental Prediction

NWT: Northwest Territories

PDO: Pacific Decadal Oscillation

PGW: Pseudo Global Warming

RCM3: Regional Climate Model version 3

RCM: Regional Circulation Model

SD: Statistical Downscaling

SNOWTEL: Snowpack Telemetry

VWC: Volumetric Water Content

WATCH: Water and Climate Change Project

WRF: Weather Research and Forecasting Model.

Chapter 1

Introduction

Culvert filled with ice in the Glacier Creek River crossing with the Dempster Highway, June 3, 2014.

1.1 Motivation and relevance

The timing and volume of Arctic freshwater generation is critical for designing civil infrastructure (e.g. bridges and culverts), natural resources exploration and extraction, and ecological biodiversity. Despite the great importance of Arctic freshwater, the number of high-latitude research catchments have significantly decreased in the last decades (Laudon et al., 2017), diminishing the research capacity to develop a deeper understanding of Arctic freshwater systems and the potential impacts of climate and vegetation change.

Arctic regions have undergone several environmental changes in the last decades, such as rapid warming (Wanishsakpong et al., 2016; Whitfield et al., 2004), decreasing snowcover duration (Brown et al., 2010), permafrost thaw (Liljedahl et al., 2016), shrub expansion and densification (Lantz et al., 2013; Sturm et al., 2001). However, the impact of these environmental changes on runoff generation and hydrological cycling is poorly understood, mostly due to the complex interaction between mass and energy fluxes in the surface and subsurface (Kane et al., 1989; Quinton et al., 2000; Woo et al., 1982; Woo and Steer, 1982). To represent the hydrological cycling of Arctic watersheds in a realistic way, several physical processes need to be coupled, such as ground freeze and thaw, subsurface flow and storage, infiltration into partially frozen ground, snow melt and accumulation, and blowing snow redistribution; however, given the high complexity of these processes, no study has included all of them in a single modelling framework. There are only a few process-based hydrological models applied to Arctic basin headwaters: Hinzman and Kane (1991), F. Zhang et al. (2000) and Schramm et al. (2007) in Alaska, Pohl et al. (2007) and Endrizzi et al. (2011) in northwestern Canada, and Semenova et al. (2013) in northeastern Russia; although these models have a strong physical basis for some hydrological processes, they lack either a robust physical representation of key physical processes (e.g. snowmelt, sublimation, and ground freeze and thaw) or a full representation of the hydrological cycle (i.e. summer and winter processes). Therefore, there is a need for a hydrological model that includes all the key hydrological processes found in Arctic environments, allowing a reliable investigation of hydrological cycling under historical conditions and plausible scenarios of future change.

Predicting future Arctic climate and vegetation characteristics represents a great challenge for the scientific community, particularly due to the complexity of the environment and the intrinsic uncertainty of the factors that must be considered, such as CO_2 emission, anthropogenic land use changes and wild fires. Climatic projection for the Arctic show warmer and wetter conditions by the end of the century, regardless of the CO_2 emission scenario (Cai et al., 2018; Overland et al., 2013), and vegetation cover and density is expected to increase in the future (Zhang et al., 2013). Despite observed and projected changes in vegetation cover in the Arctic, hydrological models used to diagnose and/or predict future hydrology have not included transient changes in vegetation, and therefore, their impact is unknown. Regarding climate projections, studies in Arctic headwater basins have only used simple approaches to generate future climate by adding or multiplying a factor, obtained from global climate models, to observed temperature and precipitation time series

(Hinzman and Kane, 1992; Pohl et al., 2007). There are fundamental problems with using this type of approach to downscale climate projections, particularly when it is used to drive physically based hydrological models. Problems include the need for forcing data beyond temperature and precipitation (e.g. solar irradiance and relative humidity). Physical consistency between weather variables is required and future climate will most likely present different patterns, such as the frequency and intensity of precipitation (Kendon et al., 2017; Prein et al., 2015). Therefore, there is a need to incorporate more physically consistent climate projections and changes in vegetation characteristics in hydrological models to produce more reliable hydrological predictions in Arctic regions.

The following sections provide the theoretical background of this thesis, describe Arctic hydrology and the progress in hydrological processes studies in Arctic and cold regions, followed by a description of hydrological models, observed environmental changes in the Arctic and atmospheric modelling and climate projections.

1.2 Theoretical background

1.2.1 Arctic hydrology

Arctic regions are characterized by extremely cold temperatures, which condition the physical dynamics that drive its hydrology, such as snow melt and accumulation (Kane et al., 1991). This characteristic is evidenced in the development of areas with continuous and discontinuous permafrost (Beilman et al., 2001; Vitt et al., 2000). Permafrost, which is further described in Section 1.1.1.1, plays a key role in the hydrology of cold environments, affecting variables such as soil moisture storage and hydraulic conductivity (Woo, 2012, p. 15). While permafrost occurrence drives most subsurface processes, three general surface landscape categories - tundra, open subarctic forest and northern lakes (Bailey et al., 1997, p. 198-219) - determine the energy fluxes that drive key hydrological processes, such as evapotranspiration, snow melt and accumulation. The energy balance in any of these landscape classes exhibits considerable seasonality (Marsh and Pomeroy, 1996; Pomeroy et al., 2006; Woo and Guan, 2006). For instance, in tundra environments and during the winter, the energy fluxes are substantially smaller than those of the snow-free season, in which most available energy comes from the relatively warmer ground (Rouse, 1984). In contrast, during the spring and summer, a significant amount of net radiation is available, primarily as sensible and latent (evapotranspiration) heat fluxes, but also as ground heat flux, which warms and thaws the ground mainly through conduction (Woo et al., 2006). As can be expected, land cover and meteorology are not the only drivers of northern hydrology; topography also plays a key role in defining surface and subsurface drainage and energy inputs by different slopes, aspects and elevations (Carey and Woo, 2001; Quinton et al., 2004; Woo and Guan, 2006).

Numerous factors drive the hydrology of northern regions; however, to understand how these factors are reflected in the hydrological behaviour of each basin, each physical process must be properly considered. The following section describes the hydrological processes that characterize the hydrology of Arctic regions.

1.2.1.1 Hydrological processes

At a basin scale, the following physical hydrological processes can be found in cold regions: snow accumulation and melt, infiltration into frozen and unfrozen soils, permafrost thaw, canopy interception of rain/snow and its evaporation/sublimation, evapotranspiration, sublimation, blowing snow redistribution and sublimation, groundwater flow and recharge, icing formation, subsurface and surface runoff, flow through organic terrain and flow through the snowpack. At the larger river basin-scale, river discharge and stage are highly influenced by river ice processes, such as ice jamming and breakup (Beltaos, 1983). The later processes are a major concern for flood risk analysis. A detailed description and review of the main hydrological studies developed in northern Canada, specifically over the Mackenzie River Basin, are presented by Woo (2008) in the Mackenzie GEWEX Study (MAGS) project. This project provides substantial improvement in the understanding of most of the hydrological processes of this region. The most relevant advances from this project, as well as a review of more recent literature on cold regions hydrology are provided below.

Blowing snow redistribution and sublimation are key processes for cold regions hydrology; Essery et al. (1999) estimated that between 26% and 47% of total snowfall returns to the atmosphere as water vapour in an Arctic basin (Trail Valley Creek), depending on the vegetation class. In another study Pomeroy and Li (2000) calculated blowing snow losses by the end of the winter for a southern Saskatchewan prairie and an Arctic basin, in which they found that 48% and 58% of the snowfall was lost by sublimation of blowing snow, respectively. Blowing snow can be modelled as a two-mode process: saltation the dominant mode, which occurs in a narrow layer immediately above the snow surface (Pomeroy and Gray, 1990) and which particle size distribution fits a two-parameter gamma function (Schmidt, 1981); and suspension, which occurs above the saltation layer and is supported by wind turbulence (Pomeroy and Male, 1992). The mass concentration of blowing snow decreases exponentially with height and increases exponentially with friction velocity, which is a function of the atmospheric shear stress and the atmospheric density (Pomeroy and Male, 1992). Recent progress in blowing snow process understanding is presented by Aksamit and Pomeroy (2016, 2017, 2018), in which a detailed investigation of the relationship between turbulent coherent structures in atmosphere and blowing snow generation at a complex alpine terrain site is shown. Physically based models with different complexities and resolutions have been developed to simulate blowing snow transport and sublimation losses; some examples are the PIEKTUK (Déry and Yau, 1999), SnowTran-3D (Liston and Sturm, 1998) and PBSM (Pomeroy et al., 1993).

Canopy interception of snow and radiation is a critical process in the boreal forest region. Schmidt and Gluns (1991) measured snow interception from three conifer species in which, for a 10 mm snowfall, up to 50% of the snow was intercepted, and for a 20 mm snowfall that value decreased to 30%. In another experiment, Schmidt (1991) contrasted observed 15-min sublimation losses versus a 1-mm ice sphere model from an artificial conifer installed in the middle of a pine forest in Colorado, USA in which, for selected days, they had good agreement with observations. Pomeroy and Schmidt (1993) used a similar model to that used by Schmidt (1991) but included a fractal function to evaluate the dimensionless exposure coefficient (C_e) to estimate the sublimation rate of a single tree. Hedstrom and Pomeroy (1998) conducted extensive field measurements to describe the boreal forest canopy snow interception and unload processes. They developed a physically based model in which parameters such as leaf area index, canopy exposure, and species type are required to estimate canopy interception of snow, sublimation of intercepted snow and unloading rates. The complete model description and evaluations are presented by Parviainen and Pomeroy (2000), where they found that the half-hourly model provides reasonable estimates of sublimation losses and within-canopy energetics; however, they also acknowledged the need to improve canopy heat storage terms and the inclusion of a model for subcanopy energetics, which were neglected in their experiment.

Tundra shrub height and density play an important role in snow accumulation and melt patterns, primarily by: (1) changing the surface albedo, which increases when bent branches are re-exposed to the atmosphere, and (2) changing the surface roughness, which increases the snow accumulation by trapping more blowing snow (Bewley et al., 2007; Liston et al., 2002; Ménard et al., 2012; Pomeroy et al., 2006; Sturm et al., 2005, 2000).

Evapotranspiration is the combination of evaporation (from soil, canopy interception and open water surfaces), transpiration (by stomata) and sublimation (from ice and snow surfaces) processes by which water changes into the vapour phase; therefore, to evapotranspirate there must be enough available energy to produce the phase change and the atmosphere must be dry enough to capture that moisture (Davie, 2008, p. 37). Evapotranspiration has been historically addressed by four different approaches: (1) *Energy Balance*, (2) *Aerodynamic*, (3) *Combination*, and (4) *Empirical*. The Energy Balance approach is based on the conservation of energy principle which means that, for a given control volume, the difference between all the other energy terms (net radiation, ground flux sensible heat advected energy and change in internal energy storage) will result in the latent heat, which can be expressed as mm of evaporation per unit of time if it is divided by the latent heat of vaporization (Dingman, 2002, p. 274-275). The Aerodynamic approach is based on Fick's first law of diffusion, in which evapotranspiration rates are estimated using the eddy diffusivity coefficient and the specific humidity gradient (Prueger and Kustas, 2005). This approach can be used for neutral conditions (i.e. logarithmic wind profile); however, under non-neutral conditions the Monin-Obukhov Similarity Theory (MOST; Monin and Obukhov, 1954) is used. Combined methods use the Energy Balance and the Aerodynamic approach to calculate evapotranspiration. Most common approaches are the Bowen Ratio (Bowen, 1926), Penman-Monteith (Monteith,

1981) and Priestley-Taylor (Priestley and Taylor, 1972). Empirical models are the simplest approach, and they usually require very little driving data (e.g. mean temperatures); however, because of their empirical nature they are not reliable under conditions different from those in which were calibrated. Examples of this approach are the Thornthwaite model (Thornthwaite, 1948) and the Blaney-Criddle model (Blaney and Criddle, 1962). Evapotranspiration shows large seasonality in the Arctic. For example, Rouse et al. (2003) calculated the energy balance for an Arctic tundra basin in the upland and lowland area, in which during the spring the latent heat was estimated to be in between 50 and 75 (W m^{-2}), during the fall it was estimated to be 25 (W m^{-2}) for both sites, for the early winter it was about 3-5 (W m^{-2}), and for the late winter around -10 (W m^{-2}) for both sites. There have been other evapotranspiration applications over the last decades, and some examples for tundra wetlands in cold region environments are presented by Rouse (1984), Wessel and Rouse (1994) and Raddatz et al. (2009) in Churchill Manitoba.

Snow accumulation and melt is driven by several factors, some of which have been already mentioned, such as blowing snow redistribution and sublimation, and canopy interception of snow. However, not surprisingly, the exchange of energy between the snowpack and the atmosphere is also very important because it defines the available energy for snow melt and sublimation (Male and Granger, 1981). The energy balance performed at the snow surface includes solar radiation (long and short wave), diffusive energy from clouds and/or the surroundings, advection heat transfer, rainfall and snowfall advective heat, and latent and sensible heat fluxes (Gray and Landine, 1987; Marks et al., 1998). Once the energy in the snowpack allows snowmelt, the melted water flows through the snowpack. A first attempt to understand and predict this phenomenon assumed isothermal conditions, homogeneous snowpack and gravity flow (Colbeck, 1972); however, it was later updated to account for a heterogeneous and multi-layer snowpack (Colbeck, 1979, 1975). Years later, Marsh and Woo (1984a, 1984b) studied water flow through snow, including ice layer formation and preferential drainage through flow fingers. Based on detailed observations of wetting fronts through cold snowpacks, they developed a model to understand how these mechanisms (ice lens and flow fingers formation) affect the time it takes for the wetting front to reach the ground surface. Among many findings, they concluded that it is incorrect to assume that wetting fronts drain uniformly through the snowpack (faster water drainage through flow fingers), and that once the snowpack is saturated with liquid water and its temperatures reaches 0°C, all snowmelt is then available as runoff. Recently, Leroux and Pomeroy (2017) developed a 2D snowmelt model that included the effects of capillary hysteresis on preferential flow paths, which is a step forward in improving the understanding of snowmelt timing and volume. Over the last decades several models have been developed to represent snow melt and accumulation using different approaches, from simple empirical models, such as the degree-day (Hock, 2003), to more complex models such as physically based multi-layered energy and mass balance models (EBSM - Gray and Landine (1987); SNOBAL - Marks et al. (1998); SNOWPACK - Bartelt and Lehning (2002)).

Infiltration into frozen soil is characterized by two flow regimes: a transient and a quasi-steady-state regime (Zhao et al., 1997). The transient regime occurs immediately after water starts infiltrating into the frozen soil. In this regime the infiltration rate and heat transfer decrease rapidly, and the soil temperature increases by heat conduction at the surface. The quasi-steady-state is characterized by gradual changes in the infiltration rate with time; soil temperature warming is driven by latent heat released by the refreezing of melted water supplied from upper layers. Zhao et al. (1997) estimated that up to 90% of the latent heat released by the refreezing of meltwater is conducted at deeper levels and is used to increase soil temperature and melting. Gray et al. (1984) classified frozen soil infiltrability into three main groups based on studies developed in the Canadian Prairies: (i) *unlimited*, in which soils have considerable preferential flow (e.g. cracks); (ii) *limited*, in which infiltration depends on the snow water equivalent and the water/ice content of the first 30 cm of the soil layer; and (iii) *restricted*, in which infiltration is inhibited by ice lenses at the surface or shallow depth. Several studies quantifying infiltration into frozen soils have been conducted, including the development of simplified parameterization relations (Gray et al., 2001; Zhao and Gray, 1999, 1997); however, the need for further research is widely recognized. Infiltration into unfrozen soils has historically been studied more (Boughton, 1989; Philip, 1957; Romano et al., 1998) than frozen soils, yet specific processes need to be improved, such as preferential flow or macropores (Cey and Rudolph, 2009; Jarvis, 2007). Infiltration capacity depends on a series of factors: the rain rate, saturated and unsaturated hydraulic conductivity, water storage capacity, and the presence of preferential flow paths, which in turn depends on the soil structure formation and degradation, including soil biota (e.g. earthworms), soil properties (e.g. texture and porosity), topography (e.g. slope) and management (e.g. cropping and tillage) (Jarvis, 2007). Several models have been developed to simulate infiltration into unfrozen soils. They differ from each other by their complexity, parameter and data requirements, such as Richard's equations (Dingman, 2002, p. 249-251), Green-Ampt (Dingman, 2002,. 261-265), Philip's Equation (Philip, 1957), and SCS Curve Number (Boughton, 1989). The main limitations of all these methods occur when they are applied under preferential flow conditions.

Surface runoff can be classified into two groups based on its source: (1) Hortonian flow (Horton, 1933), which is produced when the water input exceeds the rate of infiltration and is common during the snowmelt period when infiltration is limited by frozen ground; and (2) saturation overland flow, which is a combination of direct rainfall and water from subsurface runoff (Woo, 2012, p. 235-236). Surface runoff routing may be estimated using Manning's equation for overland flow (Chow et al., 1994, p. 292-297) or the Muskingum method (Chow et al., 1994, p. 312). Although surface runoff can be a significant component of streamflow, for permafrost environments Quinton and Marsh (1999) found that runoff is primarily dominated by subsurface flow. Subsurface runoff is controlled, in part, by the hydraulic properties of the soil, particularly by the hydraulic conductivity and porosity (Freeze, 1972). Soil profiles in the Arctic are usually composed of: (1) an organic layer of peat at the ground surface at different stages of development and living plants such as lichens and mosses (Woo, 2008, p. 19), which have high hydraulic conductivity (with an average value of the order of m d^{-1}) that decreases with depth (up to five

orders of magnitude) (Carey et al., 2007; Quinton et al., 2000; Quinton and Gray, 2003); and (2) a deeper mineral soil layer between the permafrost and the organic layer (Mackay, 1980; Quinton et al., 2000) that can have hydraulic conductivity 3 orders of magnitude lower than that of the organic layer (Quinton et al., 2000). However, mineral soils can be also found in the ground surface, which is the result of a cryoturbation process. These features are called mineral earth hummock and are widely distributed in permafrost areas (Mackay, 1980). Between mineral earth hummocks, peat dominated (0.3 – 0.5 m depth) preferential flow paths are present, and they are referred as to inter-hummock area (Quinton et al., 2000). Given the substantial gradient of hydraulic conductivity in the soil profile, it is critical to estimate reliably the water table depth to represent successfully the subsurface runoff contribution to streamflow.

Permafrost is defined by Harris et al. (1988, p. 63) as "Ground (soil or rock) that remains at or below 0°C for at least two years". The permafrost depth defines the available soil depth capacity for water transport and storage (active layer) and, since hydraulic conductivity of organic soils can decrease several orders of magnitude with depth (Quinton and Gray, 2001); reliable tools to simulate thaw rates are essential in modelling Arctic hydrology (F. Zhang et al., 2000). Thawing primarily depends on the energy available to warm the soil and the soil's heat conductivity capacity which, in turn, depends on factors such as water/ice content, porosity, and texture (Ling and Zhang, 2004; Zhao et al., 1997; Zhao and Gray, 1997). Zhao et al. (1997) showed that highly complex and computationally intense models can be used to satisfactorily represent thaw rates for frozen soils; however, initial conditions (e.g. soil saturation and temperature) and soil properties (e.g. permeability, porosity and thermal conductivity) need to be known to run such model. Less detailed and computationally intense models such as Stefan's equation (Juminikis, 1977, p. 205) or a modified version (Hayashi et al., 2007) can also be used. Empirical equations such as the temperature-index based approach can be useful in remote areas, where sparse data are typically available, or for regional analyses (Frauenfeld et al., 2007).

Groundwater in the Arctic is highly influenced by the presence of permafrost, in which it usually acts as an aquiclude (i.e. it has poor retention and transmission of liquid water) or an aquitard (i.e. it is relatively impervious but it affects the hydraulic of the non-frozen zone) (Woo, 2012, p. 74). Active ground water can be found above, within and beneath the permafrost and is usually known as suprapermafrost, intrapermafrost and subpermafrost groundwater (Woo, 1986). Suprapermafrost is usually found in the active layer and is supplied by either snowmelt, rainfall or glacier melt in glacierized areas during the thaw season and may be stored as ice during the snow season (Woo, 2012, p. 75). Suprapermafrost may produce seepage when the water table level rises above the ground, which can be substantial input to streamflow, particularly in gravel terrains (Woo and Xia, 1995). Intrapermafrost groundwater occurs in unfrozen zones (taliks) within the permafrost, which are not subject to seasonal freezing but are subject to long-term climate changes; open taliks are produced by either an upward movement of warmer subpermafrost water (T >0°C; hydrothermal talik) or mineralized subpermafrost water (hydrochemical talik) (Sloan and van Everdingen, 1988). Because subpermafrost groundwater is beneath the permafrost, water

temperatures are greater than 0°C, and it is confined by the highly impervious permafrost; however, it is under hydrostatic pressure and has artesian conditions (Williams and Waller, 1966). In discontinuous permafrost regions, subpermafrost usually occurs in unconsolidated deposits, whereas in northern regions it is predominantly found in bedrock (Sloan and van Everdingen, 1988). Subpermafrost recharge is restricted by permafrost, particularly in continuous permafrost. However, this recharge can be enhanced by fracture systems or solution conduits such as sinkholes (Woo, 2012, p. 77).

Icings (or *aufeis* in German and *naled* in Russian) are ice formations produced by the freezing of groundwater seepage, and they can be classified into river icing, ground icing or spring icing (Carey, 1973). Ground icings are produced by saturation of the ground surface by the seepage of groundwater, whereas spring icings, as the name implies, are associated with springs or well-defined channels which form during the early winter; however, the distinction between these two categories is not entirely clear (Carey, 1973). River icings are produced on top of a river, in which the hydrostatic head of the ground water exceeds the river level, producing ice thicknesses up to three times that of normal channel flow (Kane, 1981). The detailed sequence of the physical mechanisms that produce river icing is well described by Kane (1981). Icing can produce severe problems, particularly over highway infrastructure such as culverts, in which water flow may be completely blocked by the ice layer.

1.2.1.2 Streamflow generation

The Arctic exhibits significant seasonality in radiative terms (Marsh and Pomeroy, 1996; Rouse, 1984), which are locally affected by topographic effects, such as slope and aspect (Pomeroy et al., 2006, 2003; Sicart et al., 2006) and vegetation cover (Ménard et al., 2014, 2012; Sturm et al., 2000). This considerable variation in radiative fluxes is reflected in the different mechanisms that generate streamflow. Snowmelt is the main hydrological event after the winter season, which is characterized by low streamflow during March or April followed by a peak snowmelt in May or June (Janowicz et al., 1997). However, preferential snow deposition, produced by snow redistribution and resulting in snowdrifts, contributes a significant portion of the snowmelt runoff until late summer (Marsh and Pomeroy, 1996; Pomeroy et al., 2003; Quinton and Marsh, 1999).

As temperature increases, precipitation phase changes towards liquid, producing rainfall events. Rain may then fall over the snowpack, producing rain-on-snow events, in which case a considerable amount of advected energy is added to the snowpack, leading to substantial snowmelt and runoff (Marks et al., 2001; Singh et al., 1997). This phenomenon can occur very rapidly, melting a significant percentage of the snowpack, which can also be intensified with high wind speeds (Marks et al., 2001, 1998). Devastating floods have occurred in mountainous regions due to rain-on-snow events. Some examples are the 2013 flood in Alberta, Canada (Pomeroy et al., 2016) and the 1996 flood in Oregon, U.S.A. (Marks et al., 1998).

During the snow-free period runoff from rainfall is the main source of water for streamflow, either through surface runoff or subsurface runoff through organic soils (Dingman, 1966; Kane et al., 1989, 1991). The proportion of rainfall that contributes to streamflow partly depends on the depth of the active layer, which controls subsurface storage capacity and hydraulic conductivity (Quinton et al., 2000). Rainfall events will typically occur as frontal systems or convective storms, the latter being the dominant form of precipitation during the summer season in the Mackenzie River Basin, resulting in high moisture recycling rates (Szeto, 2002). Frontal systems affect larger areas and have longer duration (several days), whereas convective storms are limited to smaller areas and shorter duration, and are usually associated with intense storms (Wallace and Hobbs, 2006, p. 349).

These mechanisms are the main generators of streamflow in Arctic regions; however, peak river stage events in large rivers (e.g. Yukon and Mayo River) can also be driven by ice jams (Janowicz, 2010), creating a damping effect in the river, raising the water level. For the period of 1885 to 2009, thirty ice jam events were reported (Whitfield, 2012) over northern latitudes. A review of these and other flood mechanisms for cold and temperate environments, and the effect of climate change on them is presented by Whitfield (2012). Janowicz (2010) presents the observed trends of the river ice regimes (freeze-up and break-up) for the mean rivers in northwest Canada over the last decades.

1.2.2 Hydrological modelling

Hydrological models are simplified representations of the physical processes that define the hydrological behaviour of any basin. They vary in complexity and computational requirements, and their selection depends on the purpose of the modelling, the characteristics of the environment in which they will be applied and the available data (Wagener et al., 2001). Hydrological models can be classified based on their spatial representation: lumped, distributed and coordinate system (Cartesian or radial), and their simulation bases: empirical/regression, stochastic time series, conceptual and physically based (Dingman, 2002, p. 29).

Lumped models represent the basin as a single point or control volume in which the spatial variability is averaged into a single representative parameter. These models cannot represent lateral flows or soil moisture redistribution and have relatively low computational requirements. In contrast, distributed models explicitly accounts for the spatial variability and, because of this, they usually require more computational resources and detailed information about the characteristics of the basin and the meteorological inputs, which might not be always available, among other problems (Beven, 2001). Some well-known distributed models are the TOPMODEL (Beven, 1997; Beven et al., 1984; Beven and Freer, 2001), WATFLOOD (Kouwen, 1988) and the SHE model (Abbott et al., 1986a, 1986b). Different coordinate system models are associated with spatial representations of 1, 2 or 3 dimensions, usually in an orthogonal system; however, a radial coordinate system, for example to model the ground water through wells, such as the MODFLOW model (Samani et al., 2004) can also be used.

Based on observed records, empirical/regression models develop relationships to simulate flow and storage processes within the watershed. Because these models are derived from observed data, their applicability is limited to that range of data. An example of an empirical/regression model is the degree-day method (Hock, 2003) which, given an air temperature and a pre-calibrated degree-day factor, estimates snow melt. Stochastic time series models use time series analysis techniques to represent system dynamics. In a similar way to empirical/regression models, stochastic time series models use records of forcing variables (e.g. precipitation) and state variables (e.g. ground water level) to characterize the system. For example, the impulse-response approach can be used to determine ground water recharge (Viswanathan, 1984). Conceptual models represent physical processes with simplified relationships, in which parameters may or may not have a physical meaning. However, most of the time these parameters cannot be observed or measured; therefore, they need to be estimated by calibration (e.g. see the VIC model; Kavetski et al., 2003). Physically based models use physical principles, such as conservation of energy and mass, to describe hydrological processes. These models are usually more complex, but they allow a much more realistic and comprehensive representation of the hydrology. Parameters in physically based models can be directly determined from observations, or be estimated by reference values in the literature. Some well-known physically based models suitable for cold regions are TOPKAPI (Ciarapica and Todini, 2002), CRHM (Pomeroy et al., 2007) and SUMMA (Clark et al., 2015).

Although a wide range of hydrological models can be found in the literature, the Arctic presents a particular and less common group of hydrological processes, in contrast with those in temperate or warmer regions. Processes such as those presented in Section 1.1.1.1 can seldom be found in classic hydrological models, and therefore the selection of a hydrological model must be made carefully.

1.2.2.1 The Cold Regions Hydrological Model (CRHM) Platform

The Cold Regions Hydrological Model Platform (CRHM, Pomeroy et al. (2007)) is physically based, modular, and user oriented platform where models with different complexity can be created, usually depending on data availability, basin knowledge and the purpose of the modelling exercise. CRHM was developed by the Centre for Hydrology at the University of Saskatchewan with the aim of improving the understanding of cold regions hydrology. The basic modelling units used in CRHM are called Hydrological Response Units (HRUs). The HRUs are spatial units that are assumed to have similar hydrological behavior and so can be simplified as one homogeneous area (control volume), which can be defined based on different basins' characteristics, such as geomorphology (e.g. elevation, aspect and slope), climatology (e.g. dry and wet) and landscape (e.g. glaciers, forest and grassland). Though HRUs are a useful and effective way to discretize a watershed, limitations arise when applied to a large watershed for which non-contiguous HRUs may produce problems in representing water exchange between them. This problem can be solved by a careful HRU delineation and a previous watershed discretization by smaller sub-basins.

CRHM allows selection from an extensive library of modules with hydrological processes for both cold and temperate environments. A list of the main physical processes and their respective representation in CRHM is presented in Table 1.1. The main advantage of the CRHM platform is that it includes a comprehensive library of cold regions hydrological processes that are not typically found in other modelling platforms.

Table 1.1: Main physical processes available in CRHM

Physical Process	**Available Modules**
Precipitation Phase	1. Psychrometric energy balance (Harder and Pomeroy, 2013) 2. Temperature threshold
Blowing Snow Transport	1. The Prairie Blowing Snow Model (PBSM; Pomeroy and Li, 2000). 2. The Walmsley simplified parameterization (Walmsley et al., 1986) of the Mason and Sykes (MS) Windflow Model (Mason and Sykes, 1979).
Evapotranspiration	1. The Granger and Gray model (Granger and Gray, 1989). 2. The Penman Monteith model (Monteith, 1981). 3. The Priestley and Taylor model (Priestley and Taylor, 1972).
Surface and Subsurface Routing	1. The Muskingum method (Chow et al., 1994, p. 312). 2. The Clark's Unit hydrograph (Clark, 1945).
Soil Moisture Storage and Flow	1. A Three-Layer Soil Model (Pomeroy et al., 2007).
Canopy Interception/Sublimation	2. The Rutter Interception Model (Valente et al., 1997) for the summer. 3. The Canopy Interception model for the winter (Hedstrom and Pomeroy, 1998; Parviainen and Pomeroy, 2000; Pomeroy et al., 1998).
Snow Melt and Accumulation	1. The Energy Balance Snow Model (EBSM; Gray and Landine, 1988). 2. The Snowcover Energy Balance model (SNOBAL; Marks et al., 1998).
Ground Freeze/Thaw	1. The XG-algorithm (Changwei and Gough, 2013) based on Stefan's equation.
Ground Surface Temperature	1. The Radiative-Conductive-Convective approach (RCC; Williams et al., 2015) 2. n-factor (Woo et al., 2007)
Infiltration	1. The Green-Ampt model (Dingman, 2002, p. 251-261) for unfrozen soils. 2. The Ayers approach (Ayers, 1959) for unfrozen soils. 3. Infiltration into frozen soils using the method described in Gray et al. (1984) and Gray et al. (1986) or the one described by Gray et al. (2001).

Physical Process	Available Modules
Radiation	1. The method presented by Annandale et al. (2002) estimates shortwave radiation based on temperature observations. 2. The snow albedo can be estimated using the method presented by (Gray and Landine, 1987). 3. Long wave radiation can be estimated using the parameterization from (Sicart et al., 2006) 4. The theoretical global radiation and the direct and diffuse solar radiation can be estimated using the parameterization from Garnier and Ohmura (1970).

1.2.3 Observed changes in Arctic regions

This section presents observed changes for some key variable in the Arctic freshwater system: air temperature, precipitation, streamflow, vegetation, permafrost and river ice. Studies are presented chronologically.

1.2.3.1 Air temperature

Temperature has been consistently increasing throughout the Arctic as documented by several studies. van Wijngaarden (2014) presents a study over the Canadian Arctic, in which 27 meteorological stations were used to estimate temperature trends during the period 1895-2014. He found that the Canadian Arctic has unequivocally increased its mean annual temperature in the last century, and that there is no significant variability between eastern and western Arctic. Particularly for the 13 stations located in Yukon and the Northwest Territories, he found an increase of 2.3, 1.6 and 1.7 ˚C per century for January, July and annual mean temperatures. Vincent et al. (2015) observed trends in climate for the period 1900-2012, and the period 1948-2012 over northern Canada (north of 60˚N), using a homogenized dataset. They found increasing air temperature throughout the country (between 1 and 3 ˚C decade^{-1}); however, the largest annual increase was found over northwestern Canada. Seasonally, the largest increase was during winter in northwestern Canada, ranging from 4 to 6 ˚C over a 65-year period. Wanishsakpong et al. (2016) investigated monthly temperature trends north of latitude 45˚N, for the period 1973 to 2013. They classified this region into 69 sub-regions, and using the dataset from the Climatic Research Unit (Brohan et al., 2006), they found significant warming in most regions, particularly those in high latitudes, such as northern Canada, Alaska, northern Pacific Ocean and eastern Siberia, where temperatures increased by at least 0.15 ˚C decade^{-1}.

1.2.3.2 Precipitation

New et al. (2001) calculated an average positive trend for high latitude regions (60 to 80 ˚N) of 3.21 mm decade^{-1} during the twentieth century; some of this is attributed to improvements in instrumentation catchment efficiency, particularly during winter, and the shift of snowfall into rainfall, which also improves catchment efficiency. Whitfield et al. (2004) investigated 5-day average changes in Arctic precipitation between two decadal periods: 1976-1985 and 1986-1995. They defined five clusters based on statistical similarity between precipitation records. Great spatial and intra-annual variability in trends were found. For example, cluster 2, which includes stations from central Russia and northern Canada, shows a significant increase during January and December winter precipitation; however, these are very small (<0.5 mm).

X. Zhang et al. (2000) showed an increase of the annual total precipitation for the period of 1950-1998, over Canada; however, there was substantial spatial variability, with greater changes in the North (>60˚N). The ratio of snowfall to total precipitation, representing the combined effect of precipitation and temperature changes, was also estimated by X. Zhang et al. (2000), showing significant positive trends for northern of Canada, produced by an increase in winter precipitation and a negative trend for the south. Zhang et al. (2001) assessed the spatial and temporal patterns of heavy precipitation over Canada. They found that there is no apparent change in the frequency and intensity of extreme events for the last century, and that a decadal variation dominates their temporal variations. Over northern Canada, they found a somewhat positive trend in the number of heavy snowfalls for autumn and winter; however, there is substantial spatial variability. Vincent and Mekis (2006) had similar results using a series of climate indices such as days with rain, cold days, diurnal temperature and consecutive dry days. Mekis and Vincent (2011) analyzed an adjusted daily precipitation dataset, which include corrections, to overcome for issues such as undercatch, evaporation and wetting losses, and trace observations for the period of 1900-2009 over Canada. Rainfall corrections for the Canadian Arctic accounted for more than 20%, compared to original values. Temporal trends over northwestern Canada presented by Mekis and Vincent (2011) appear to show an increase for both rainfall and snowfall for the period 1950-2009. Vincent et al. (2015) used an updated version of the dataset used by Mekis and Vincent (2011), for the period 1948-2012 in northern Canada, and applied an interpolation to 50-km spaced grid points. They showed an overall increasing trend with great spatial variability; however, given the limited number of monitoring stations in the north, these estimations must be used carefully.

1.2.3.3 Streamflow

Many studies have looked at observed changes in large northward flowing river basins. Over northern Canada, Déry and Wood (2005) present results in which the overall river discharge has decreased from 1964 to 2003 by -10% on average, especially for the northeast Arctic region; however, basins in the northwest area presented small changes with an average increase of 2% in

total annual discharge. McClelland et al. (2006) studied annual discharge trends of rivers to the Arctic Ocean for the period 1964-2000 and found an overall annual increase of 5.6 km^3 yr^{-1}, driven by an increase in the Eurasia water system of 6.3 km^3 yr^{-1} and moderated by a small decrease of 0.4 km^3 yr^{-1} from the North American water system. Janowicz (2008) analyzed trends in hydrologic response over permafrost basins in northwestern Canada for 45 hydrometric stations with record lengths of at least 25 years. He classified the basins based on permafrost zones: continuous, discontinuous and sporadic. Continuous and discontinuous basins showed slightly positive trends for mean annual streamflow; however, it was not statistically significant, and negative trends were also found; sporadic permafrost basins showed even more variability. Janowicz (2008) also found strong positive annual minimum streamflow trends for all three permafrost classes, which might be explained by permafrost degradation driven by warmer temperatures. Overeem and Syvitski (2010) found that major Arctic rivers such as the Mackenzie and Yukon showed an increase of 13.2 and 7.2%, respectively, in total annual streamflow for the period 1977-2007, with a shift in the snowmelt period toward an earlier melt, along with a decrease in the peak monthly discharge - around 4% for the Mackenzie and Yukon River. More recently, Rood et al. (2017) studied discharge from the Mackenzie River system in Canada and found an overall increase in the largest tributaries (Peace and Liard river basins) and also an increase in the Mackenzie River at Fort Simpson (1.5% $decade^{-1}$).

It is important to note that most of these large river basins (e.g. the Mackenzie, Lena and Yenisei River basins) have their headwaters and primary zones of runoff generation well below the Arctic Circle; therefore, they are not necessarily representative of changes in the Arctic hydrological cycle, particularly those occurring at Arctic headwaters, which have not yet been investigated in detail.

1.2.3.4 Vegetation

Changes in Arctic vegetation have been investigated by many studies using in situ photographs and measurement, and remote sensing techniques. The tundra-taiga treeline in Alaska, U.S.A., has advanced between 80 to 100 m northward in the last 200 years (Suarez et al., 1999). Payette and Filion (1985) studied white spruce (picea glauca) expansion into northern Quebec, Canada, and found that the treeline has not changed substantially over the past centuries; however, below the treeline, its density has increased. Sturm et al. (2001) investigated shrub changes in Alaska using aerial photographs and found a significant increase between 1948 and 2000. Tape et al. (2006) expanded the work showed by Sturm et al. (2001) by including many more photographs and remote sensing analysis using the Normalized Difference Vegetation Index (NDVI) from published and unpublished studies, with which they concluded that the shrub expansion is a generalized phenomenon in the Arctic. Lantz et al. (2013) studied shrub increase in the northwestern Canadian Arctic using air photographs between 1972 and 2004 and found a significant average increase in shrub cover and density of 68.1 and 35%, respectively. Myers-Smith and Hik (2017) investigated shrubline expansion in southeastern Yukon, Canada, and found consistent recruitment of alpine

willows driven by winter temperature changes. Martin et al. (2017) investigated the factors that control the expansion of shrubs into the Arctic tundra and found that there are four critical controls driving this process, hierarchically: air temperature, soil moisture, herbivory and snow dynamics.

Previous literature shows a ubiquitous expansion and densification of Arctic shrubs into the tundra; however, the studies investigating changes in the Arctic treeline show that tree density has increased in some Arctic regions (Hinzman et al., 2005) and its expansion further north is also variable and at a slower rate than shrubs, likely due to the slower reaction of trees to changes in climate forcing. Studies assessing changes in forest structure (e.g. density and height) and extent in northwestern Canada are being developed (J. Baltzer, pers. communication, 2018), which may change our understanding of northern forest; however, no studies have yet been published.

1.2.3.5 Permafrost

Lachenbruch and Marshall (1986) present one of the earliest published studies looking at changes in permafrost. They investigated top permafrost (0.2 to 2 m from ground surface) temperature in northern Alaska and found that it has increased between 2 - 4˚C during the last century. Osterkamp and Romanovsky (1999) investigated permafrost thaw along an instrumented north-south transect in the discontinuous permafrost region of Alaska during the 80s and 90s and found warmer permafrost between 0.5 and 1.5˚C. Jorgenson et al. (2006) investigated the degradation of ice wedges in Alaska at three spatial scales using field surveys, interpretation of aerial photograph time series at the surveying sites and aerial photograph for two larger domains. Aerial photograph analysis from 1945, 1982 and 2001 revealed large increases in the area covered by ice wedges. Liljedahl et al. (2016) studied ice wedge degradation but at a much larger scale using in situ observations and remote sensing techniques. They found that ice wedge degradation is a phenomenon occurring throughout the Arctic and at sub-decadal scales, impacting the water balance of lowland tundra by inducing topographic changes that drive snow redistribution and runoff.

1.2.3.6 River Ice

Magnuson et al. (2000) studied freeze-up and break-up dates between 1846 and 1995 in the northern hemisphere for which, on average, they found 5.8 days later freeze-up and 6.5 days earlier breakup per 100 years and also found that interannual variability has increased since 1950. Beltaos and Prowse (2009) reviewed the ice phenology of northern rivers, showing that significant changes have occurred in the river-ice regime during the last half of the twentieth century, such as earlier break-up and jamming, later freeze-up and ice thinning. They highlight the importance of properly characterizing these processes under changing climate and using this knowledge to inform decision making in the Arctic. Janowicz (2010) studied river ice regime trends for both freeze-up and break-up in Yukon. He found for the Yukon River in Whitehorse a delay of 30 days in the date of freeze-

up since 1902, a statistically significant earlier break-up of 5 days per century for the same river at Dawson, and that breakup severity is increasing. Janowicz attributed these changes not only to climate change but also to teleconnections with low frequency indexes, such as Pacific Decadal Oscillation (PDO) and El Nino Southern Oscillation (ENSO).

1.2.4 Atmospheric models and climate projections

Atmospheric models are simplified (yet computationally intensive) representations of the real dynamic processes that occur in the atmosphere, usually on a global or regional scale, such as cloud formation and transport, and land-ocean-cryosphere-atmosphere interactions (Manabe et al., 1975). These parameterizations have been historically used to better understand the relation between the mechanisms that drive the behaviour of the atmosphere and also to make predictions over different spatial and temporal scales (Rummukainen, 2010). Over regional and global scales, numerical weather model reanalyses, and global and regional circulation models use these physical parameterizations to reproduce historical meteorological variables and to make climate change predictions.

1.2.4.1 Global circulation models

Global circulation models (GCMs) are gridded models that couple ocean-atmosphere-land-cryosphere processes. The first GCM was developed in the late 1960s by National Oceanic and Atmospheric Administration (NOAA) Geophysical Fluid Dynamics Laboratory in Princeton, New Jersey, U.S.A. (Manabe et al., 1975). At present, GCMs are forced by different anthropogenic greenhouse gas scenarios to model future climate change. The Coupled Model Intercomparison Project Phase 5 (CMIP5) used four representative concentration pathway (RCP) scenarios: RCP2.6 (van Vuuren et al., 2011), RCP4.5 (Thomson et al., 2011), RCP6.0 (Masui et al., 2011) and RCP8.5 (Riahi et al., 2011), to project future climate change. Each RCP scenario projects a stabilized net radiative forcing of 2.6, 4.5, 6.0 and 8.5 W m^{-2} for RCP2.6, RCP4.5, RCP6.0 and RCP8.5, respectively, by 2100. RCP2.6 is the most optimistic scenario for which significant changes in energy production practices and policies must be performed. On the other hand, RCP8.5 is the scenario of "business as usual" that assumes a high population increase, slow income growth, modest changes in technology and energy consumption. Under these RCP scenarios, the global mean surface temperature for 2081-2100 – relative to 1986-2005 – as simulated by the CIMP5 models ensemble is expected to increase in 1.4°C (RCP2.6), 1.5°C (RCP4.5), 1.7°C (RCP6.0) and 2.2°C (RCP8.5); however, not surprisingly these projected changes are not expected to be regionally uniform (Collins et al., 2013).

Although GCM are state of the art in terms of global atmospheric simulations, they have several limitations, especially at regional or local scales. Problems with the topographic representation have been acknowledged. For example, Gachon and Dibike (2007) showed problems associated

with temperature projection of GCMs over northern Canada, in which the Arctic Archipelago topography was misrepresented. Local extreme precipitation events such as convective storms are also problematic in GCMs, where the capacity to capture them is very limited due to parameterized process representations of convection (Del Genio et al., 2005). On a larger scale, low frequency climate indexes such as El Nino Southern Oscillation (ENSO) and the Pacific Decadal Oscillation (PDO) are also poorly represented by GCMs (Kapur et al., 2011).

A number of GCMs have been developed over the last decades; some of the most used are the HadCM3 (UK; Gordon et al., 2000), IPSL (France; Marti et al., 2009), CNRM-CM5.1 (France; Voldoire et al., 2012), ECHAM5 (Germany; Roeckner et al., 2003), and CGCM4 (Canada; Scinocca et al., 2008). Because of the computational requirements to run world simulations, GCMs spatial resolutions is only of the order of hundreds of kilometers, which restricts its direct implementation into local studies.

1.2.4.2 Regional climate models

Regional climate models (RCMs) are numerical climate prediction models run at higher horizontal spatial resolutions than GCMs, typically in the order of tens of kilometers or higher, and are laterally forced and initialized by either CGMs or reanalyses (Section 1.2.4.3). Due to their high spatial resolution, RCMs are usually limited to regional or smaller domains. High resolution RCMs have been implemented and have shown great potential in representing observed climatic features. For example, Liu et al. (2016) present results from the Weather Research and Forecasting Model (WRF) at a high spatial resolution (4-km) RCM over North America during a 13-year period (2000-2013) and forced by the ERA-Interim reanalysis. The model was compared against the snowpack telemetry (SNOWTEL) and an ensemble of gridded observational datasets and showed an overall good performance, representing annual and sub-annual precipitation and surface temperature; however, a summer and dry bias exists. Other examples of RCMs, at relatively lower spatial resolution (>20-km), are presented by the ENSEMBLE (http://ensembles-eu.metoffice.com) and NARCCAP (http://www.narccap.ucar.edu) projects in Europe and North America, respectively, which present the implementation of several RCMs over the same temporal period and spatial domains.

1.2.4.3 Reanalyses

Historical gridded long-term meteorological series, usually from 30 to 50 years, can be obtained through atmospheric reanalyses using numerical weather prediction (NWP) models. Reanalysis use NWPs and assimilate near-surface variables as well as remote sensing products (Dee et al., 2011; Uppala et al., 2005). Reanalyses are particularly useful for estimating atmospheric forcing variables for hydrological modelling of ungauged or poorly gauged basins, where no other source of information is available (Choi et al., 2009; Krogh et al., 2015; Maurer et al., 2001). Used

extensively all over the world, reanalyses have been available for roughly two decades. Examples of some that are widely used are the NCEP North American Regional Reanalysis (NARR; Mesinger et al., 2006), NCEP/NCAR 40-yr Reanalysis (Kalnay et al., 1996), ERA-40 and ERA-Interim (Dee et al., 2011 and Uppala et al., 2005, respectively), and the NCEP Climate Forecast System Reanalysis (CFSR; Saha et al., 2010). Each reanalysis has different modelling schemes, data assimilation techniques and area coverage - from regional to global - where its ability to better represent local climatic patterns is influenced by its spatio-temporal resolution and the assimilation of local data.

Projects such as the Water and Global Change Project (WATCH; Weedon et *al.*, 2011) and the North American Regional Climate Change Assessment Program (NARCCAP; Mearns et al., 2009) provide improved reanalyses products for water and atmospheric studies. The WATCH project uses ERA-40 and ERA-Interim to generate bias-corrected data especially developed for water-related studies, which is available for the largest basins of the world, such as the Mackenzie, Mississippi, Amazon and Ganges River. The NARCCAP project provides dynamically downscaled NCEP/DOE AMIP-II reanalysis data, using several RCMs, such as the Weather Research and Forecast Model (WRF; Michalakes et al., 2004), with a 50-km spatial resolution.

In North America, several projects have used reanalysis data to better represent atmospheric variability; some of them were conducted on the Mississippi River basin (Maurer et al., 2001; Music and Caya, 2007), northern Manitoba (Choi et al., 2009) and British Columbia (Cannon and Whitfield, 2002). Lindsay et al. (2014) compared seven atmospheric reanalyses: NCEP-R1, NCEP-R2, CFSR, 20CR, MERRA, ERA-Interim and JRA-25, in terms of monthly averages for variables such as: temperature, radiative fluxes and precipitation in the Arctic region. They showed that three reanalyses were superior to the others; these are the CFSR, MERRA and ERA-Interim.

1.2.4.4 Downscaling techniques

Given the relatively coarse spatial resolution of reanalyses, GCMs and some RCMs for local studies, spatial and/or temporal downscaling must be performed. Downscaling approaches are classified into two main groups: dynamical (DD) and statistical (SD) (Fowler et al., 2007; Maraun et al., 2010; Wilby et al., 2002). Dynamical downscaling is associated with the implementation of higher resolution RCMs, using the boundary conditions from the reanalysis, GCM or lower resolution RCM. Statistical downscaling establishes a long-term statistical relationship between reanalysis, RCM or GCM and observed weather. Each approach has many advantages and disadvantages, which have been previously reviewed (Fowler et al., 2007). For example, SD approaches require significantly less computational resources and technical knowledge than DD; DD is based on physical equations that provide physically connected weather variables, whereas SD is based on relatively simple empirical relationships. The latter difference is critical when using the downscaled weather time series to force physically based hydrological models, as these models

require a consistency between weather variables that it is not guaranteed by SD approaches, resulting in significant limitation.

1.3 Research design

1.3.1 Purpose of the research

The purpose of this research is to better understand the impact of climate and vegetation change on the hydrology of Arctic basins near the treeline.

Previous research investigating Arctic hydrology lacks full representation and coupling of the physical processes driving the hydrological cycling and, therefore, estimations of changing hydrological, permafrost and snow regimes are likely biased and scientifically unsatisfactory. Developing a new methodology that couples vegetation, climate and hydrological dynamics will allow a more reliable diagnosis of the historical hydrological, permafrost and snow regimes, and a coherent prediction of potential future changes for Arctic headwaters basins, which is critical in supporting decision making in this environment.

1.3.2 Research objectives and questions

The following three objectives were defined to pursue the aforementioned overarching purpose of this research.

1) Determine the temporal and spatial variability, and interactions of the states and fluxes of the hydrological cycle within an Arctic basin.

   Previous studies in Arctic regions have shown that given the number of hydrological processes and their complex interactions, models that couple mass and energy fluxes in the surface and subsurface are required to adequately represent the hydrological cycling. Despite this, current Arctic models lack full physically based representation of the key hydrological processes, as opposed to less reliable empirical approaches. This objective aims to answer the following questions:

   a) Can a spatially distributed and physically based hydrological model, based on knowledge from previous process studies in the Arctic, properly represent the observed streamflow regime, permafrost thaw, and snow accumulation and melt characteristics of an Arctic headwater near the tundra-taiga transition?
   b) What are the controlling water fluxes of an Arctic headwater basin and how do they vary spatially and temporally?

2) Diagnose the historical hydrological responses to changing climate and vegetation in an Arctic basin.

   Understanding the role of observed changes in vegetation and climate on the historical water cycling of an Arctic basin is crucial in understanding potential hydrological changes under future scenarios of change, yet no study has addressed the individual roles of changing climate and vegetation on Arctic hydrology. This objective aims to answer the following questions:

   a) What hydrological responses are caused by the individual effect of transient climate and vegetation?
   b) What are the hydrological responses to changes in both climate and vegetation?
   c) Does transient vegetation change enhance or dampen climate change?

3) Quantify future hydrological changes due to projected changes in climate and vegetation in an Arctic basin.

   Few studies have looked at the impact of climate change on the hydrology of Arctic headwaters, and the models used have been based on empirical relationships and simple methodologies to look at future climate. These approaches do not ensure the physical consistency of projected climate variables. Furthermore, changing vegetation has been neglected in these estimations. This objective aims to answer the following questions:

   a) Can a high spatial resolution (4 km) atmospheric model represent observed weather patterns sufficiently well for hydrological cycle simulations in an Arctic basin?
   b) What are the expected hydrological changes under a global warming scenario with vegetation change?
   c) Is future climate or vegetation the main driver of projected changes in the hydrological cycle of an Arctic basin near the treeline?

1.3.3 Field Campaigns

A series of field campaigns were carried out between 2014 and 2015, with the goal of installing two comprehensive hydrometeorological stations, performing seasonal maintenance, data collection and snow surveying. Details about the hydrometeorological station sensors and location are provided in the Chapter 2. During the first field campaign in June 2014, both the Windy Pass (Figure 1.1) and Rio Roca (Figure 1.2) weather stations were installed and the instrumentation started recording. During the second field campaign in September 2014, the weather stations were revised and repaired as necessary – Windy Pass had a malfunctioning anemometer - and snow thermocouples were installed at two heights. One soil pit was dug for each station to install the soil moisture soil temperature profiles, as can be seen in Figure 1.3 and Figure 1.4 for Windy Pass and Rio Roca, respectively. The third field campaign was carried out in March 2015 and involved data collection, station maintenance and a snow survey transect. Conditions during this campaign are presented in Figure 1.5 and Figure 1.6 for Windy Pass and Rio Roca, respectively. The fourth and last field campaign was in September 2015 and involved data collection and general maintenance. After this campaign, other field campaigns have been carried out to ensure the proper functioning of the stations and data collection. This has been done in collaboration between Richard Janowicz's group at the Water Resources Branch, Yukon Environment, the Centre for Hydrology, University of Saskatchewan and Sean Carey's research group at McMaster University.

Figure 1.1: Installing the Pluvio-2 at Windy Pass, June 6, 2014.

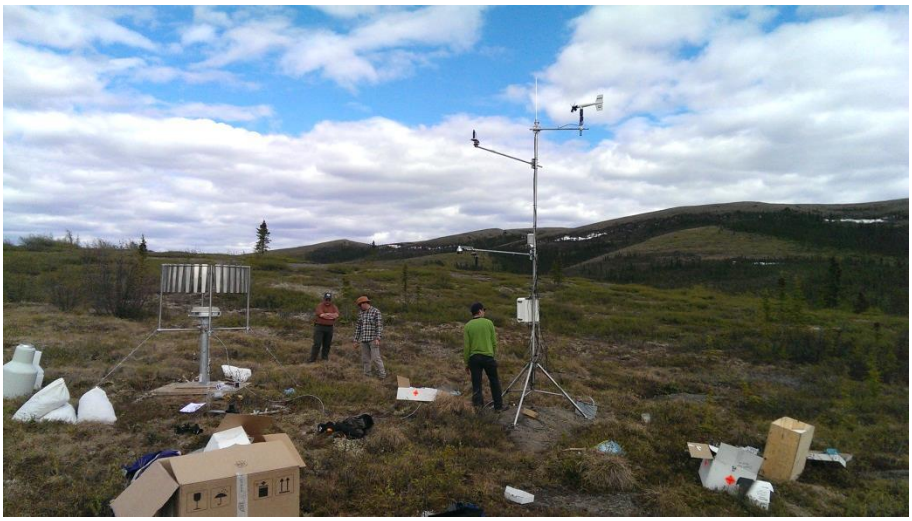

Figure 1.2: Installing the weather station at Rio Roca, June 4, 2014.

Figure 1.3: Soil profile at Windy Pass, September 6, 2014. Permafrost was not reached.

Figure 1.4: Soil profile at Rio Roca, September 7, 2014. Permafrost was likely reached.

Figure 1.5: Windy Pass conditions in March 30, 2015, during snow survey, data collection and station maintenance campaign.

Figure 1.6: Rio Roca conditions in March 31, 2015, during snow survey, data collection and station maintenance campaign.

Figure 1.7: Windy Pass conditions in September 23, 2015, during data collection and station maintenance campaign.

Figure 1.8: Windy Pass conditions in September 23, 2015, during data collection and station maintenance campaign.

1.3.4 Thesis outline

Chapter 2: This chapter presents the implementation and validation of a single-point hydrological model at two weather stations in northern Canada, for which detailed weather and subsurface measurements starting in 2014 are available. A detail validation of the new modules representing ground surface temperature and ground freeze and thaw included in the CRHM platform, as well as validation for snow accumulation and soil moisture storage are presented. Results and analysis showed in this chapter provides the basis for a further implementation of these algorithms at a larger basin-scale in the following chapters.

Chapter 3: This chapter describes in detail a spatially distributed and physically based hydrological model at Havikpak Creek, a small Arctic basin in the Northwest Territories, Canada, underlain by continuous permafrost. The model was developed using the Cold Regions Hydrological Model (CRHM) platform, and it incorporates all the key physical process found in this environment, in particular, it includes ground freeze and thaw dynamics for the first time. The model was validated against daily streamflow discharge, snow accumulation and melt, and ground thaw. The model was used to diagnose the hydrological cycling and water balance over a period of 28 years, including snowpack dynamics, permafrost thaw and runoff generation, providing the first detailed analysis of the hydrological fluxes and their variation over time and space.

Chapter 4: This chapter investigates the long-term historical effect of transient climate and vegetation (i.e. shrub expansion and density) on the simulated hydrological cycling of Havikpak Creek basin. This was approached by defining three modelling scenarios: (1) changing climate and

constant vegetation, (2) constant climate and changing vegetation, and (3) changing climate and vegetation over the period 1960-2016. A long-term time series of weather variables was reconstructed, mostly based on observations; however, atmospheric reanalyses were used to complete the records. Trend analysis using a non-parametric statistical test, change point analysis and teleconnections with climatic indexes such as El Nino Southern Oscillation, are investigated in the mass and energy fluxes.

Chapter 5: This chapter quantifies and analyses changes to the hydrological cycling in Havikpak Creek basin under scenarios of changing climate and vegetation, as projected by a high resolution (4 km), state-of-the-art atmospheric model under a pseudo-global-warming configuration, and the extrapolation of observed rates of shrub expansion and densification. A detailed validation of the weather time series produced by the atmospheric model is presented. A sensitivity analysis of the basin water balance to projected changes in vegetation characteristics is performed to investigate the uncertainty associated with vegetation projections. Changes in the hydrological regime, snowmelt and accumulation patterns, evapotranspiration, sublimation and ground thaw are detailed, quantified and discussed.

Chapter 6: This chapter concludes this thesis, synthesising all the research presented in previous chapters, providing a broader discussion on Arctic hydrological research and suggesting a potential direction for future hydrological research in Arctic regions.

Chapter 2

Simulating permafrost hydrology in northern Canada

Boreal forest and shrubs at the Windy Pass Station, Dempster Highway, Yukon, on March 3, 2015.

Abstract

Representing water cycling in permafrost-dominated regions is challenging, as it is the result of complex interactions between subsurface-surface-snowpack-atmospheric processes, yet it is critical for predicting future hydrology. Most hydrological models applied to regions with continuous and discontinuous permafrost have either neglected or used empirical representations for key hydrological processes, such as blowing snow redistribution and sublimation, snow accumulation and melt, snow interception by canopy and sublimation, and permafrost thaw. This study presents the implementation and validation of a new set of algorithms representing permafrost coupled with a single-point physically based hydrological model at two hydrometeorological stations in northern Yukon, Canada, for which detail meteorological and subsurface measurements are available. Hydrological processes included in the model are evapotranspiration, soil moisture, flow through organic terrain and mineral soil, permafrost thaw, energy balance snowmelt and snow accumulation, blowing snow redistribution and sublimation, interception and sublimation of snowfall, and infiltration in frozen and unfrozen soils. The model was able to successfully represent ground surface temperature (bias ≤ 0.2°C), ground thaw (bias $\leq$ 11cm) and soil moisture (bias $\leq$1.1 mm), but it underestimated snow accumulation (about 30 mm at both sites) likely due snow undercatch by wind. Sensitivity analysis of simulated ground thaw revealed that the soil properties of the upper organic layer dominated the model's response; however, the model showed a robust performance for a range of realistic physical parameters. This study demonstrates that a robust and yet computationally inexpensive algorithm to represent permafrost thaw can be successfully coupled with a physically based hydrological model, representing a step forward simulating permafrost hydrology.

Author contributions:

SK and JP designed the study. SK performed the simulations and analyses and prepared the manuscript with contributions from JP to the manuscript structure, readability and analysis and discussion of the results.

2.1 Introduction

The Arctic is warming producing several environmental changes such as shrub expansion and densification (Sturm et al., 2001b; Lantz et al., 2013; Myers-Smith and Hik, 2018), and permafrost thaw (Payette, 2004). Particularly, permafrost thaw has been shown to be critical for hydrological connectivity (supra- and super-permafrost groundwater exchange, hydraulic conductivity and subsurface runoff and storage; Walvoord and Kurylyk, 2016), carbon dioxide and methane release (Knoblauch et al. 2018; Herndon 2018), changes in landscape (Myers-Smith et al., 2008; Liljedahl et al., 2016) and infrastructure (building foundations and roads stability). Therefore, better understanding of the processes controlling permafrost thaw as well as robust numerical representations of various complexities and under different environmental conditions (i.e. climate, vegetation and soil) is needed.

Simulating the ground freeze and thaw regime represents a great challenge as it is the result of complex interactions between processes representing the energy and mass exchanges amongst atmosphere, land, snowpack and subsurface (Kane et al., 1991; Zhao et al., 1997; Woo, 2012). Numerical methods representing the heat transfer equation, including heat conduction, latent heat and convective heat exchange, coupled with subsurface flow have been shown to properly simulate ground freeze and thaw, using detailed ground information and forcing data (see review from Kurylyk and Watanabe, 2013). However, these approaches require detailed field information, commonly unavailable in remote regions of the Arctic, and are computationally intensive. Conversely, there are simplified, empirical representations for the active layer thickness based on empirical equations (e.g. degree-day), which have been used for hydrological modelling in cold regions (Z. Zhang et al., 2000; Schramm et al., 2007). The main disadvantage of these approaches is that they are not reliable under conditions different from which they were developed (Sivapalan, 2003), impeding their implementation in remote and ungauged regions and for climate change impact studies, for which models using physical principles should be pursued instead (Pomeroy et al., 2013b). Therefore, models of intermediate complexities are required, that can reliably represent ground freeze and thaw, and can be relatively easily implemented in hydrological model for Arctic and subarctic environments, allowing multiple model realizations to assess model uncertainty and sensitivity.

In the context of model of intermediate complexities, Stefan's Equation (Juminikis, 1977, p. 205) is a commonly used and relatively simple one-directional model that estimates ground freeze and thaw in homogeneous soils, which considers the latent heat of fusion and neglects the soil volumetric heat capacity and convective heat exchange. Modified versions of Stefan's Equation have been developed to be implemented in multilayered soils (Woo et al., 2004; Hayashi et al., 2007; Fox, 1992; Yi et al., 2006). Another modified version of Stefan's Equation developed by Changwei and Gough (2013), referred as the XG-algorithm, differs from previous approaches as it does not require averaging of soil parameters for multilayered soils and is independent of the number and thickness of soil layers. Algorithms based on Stefan's Equation require ground surface

temperature estimation as the upper boundary condition. Measuring this variable is not common and even if it is measured at a point, spatially distributed estimations are required for hydrological models. Simulation of ground surface temperature has been typically approached by implementing a ratio between ground surface temperature to air temperature, referred as the n-factor (Woo, 2012, p. 56), which is commonly assumed to be constant. Main issues associated to the use of the n-factor are its empirical basis and that it varies spatially (Klene et al., 2001) and temporally (Woo et al., 2007). Williams et al. (2015) presented a novel approach to estimate ground surface temperature based on air temperature, net radiation and ground thaw depth, referred as the radiative-conductive-convective (RCC) approach. The RCC approach showed good performance at tree experimental sites in Canada and it proved to have a much superior performance than the empirical n-factor. Both the XG-algorithm and the RCC approach were incorporated in the Cold Regions Hydrological Model (CRHM; Pomeroy et al. 2007) platform, and they are part of the Arctic Hydrology Model (AHM) developed by Krogh et al. (2017) and applied by Krogh and Pomeroy (2018) to investigate recent hydrological changes in an Arctic basin near the treeline.

The purpose of this research is to verify in detail the incorporation of the XG-algorithm and the RCC approach to the CRHM-AHM at two instrumented permafrost hydrology research sites in northern Yukon, Canada, for which detailed measurements of soil temperature and water content and ground surface temperature are available. As a secondary goal, the sensitivity of the model to changes in the soil thermal properties and porosity is also examined for model transferability and climate change studies.

2.2 Study sites and data

The sites selected for this study are permafrost hydrology study sites associated with two hydrometeorological stations located in northern Yukon, Canada (Figure 2.1), namely, Rio Roca and Windy Pass. These two locations were selected as they have good access from the nearest road (Dempster Highway), are relatively sheltered from wind and bridge the gap between existing weather stations along the Dempster Highway corridor. Windy Pass is situated within the North Ogilvie Mountain Ecoregion, which is predominantly covered by subarctic coniferous forest (50%), followed by Arctic/alpine tundra (20%), rocklands (20%), and lakes and wetland (5%), with relatively dry (mean annual precipitation 300 to 450 mm) and cold conditions (mean annual temperature -7 to -10°C) (Smith et al. 2004). The elevation at Windy Pass is 1,030 metres above sea level (m.a.s.l.) in a terrain with a mild slope estimated at 5° and is surrounded by shrubs, moss and scattered spruce (Table 2.1). The soil profile at Windy Pass is characterized by an upper partially decomposed organic layer, from the surface to 23 cm depth, followed by a denser organic matter layer (15 cm thick), underlain by mineral soil (Figure 2.2a). The second station, Rio Roca, is located within the British-Richardson Mountains Ecoregion, which is predominantly covered by alpine/subarctic tundra (65%), followed by subarctic coniferous forest (20%) and rocklands (15%), with dry (mean annual precipitation 250 to 400 mm) and cold conditions (mean annual temperature -7.5 °C) (Smith et al., 2004). The elevation at Rio Roca is 660 m.a.s.l., with a ground surface slope

estimated at 4°, surrounded by scattered shrubs and spruce, and with moss, lichen and grass on the ground. The soil profile at Rio Roca is characterized by an upper partially decomposed organic layer, from the surface to 18 cm depth, followed by a denser and organic matter layer of at least 63 cm thickness, at which point, continuous, ice-rich permafrost was reached and further sub-soil investigations were not possible (Figure 2.2b).

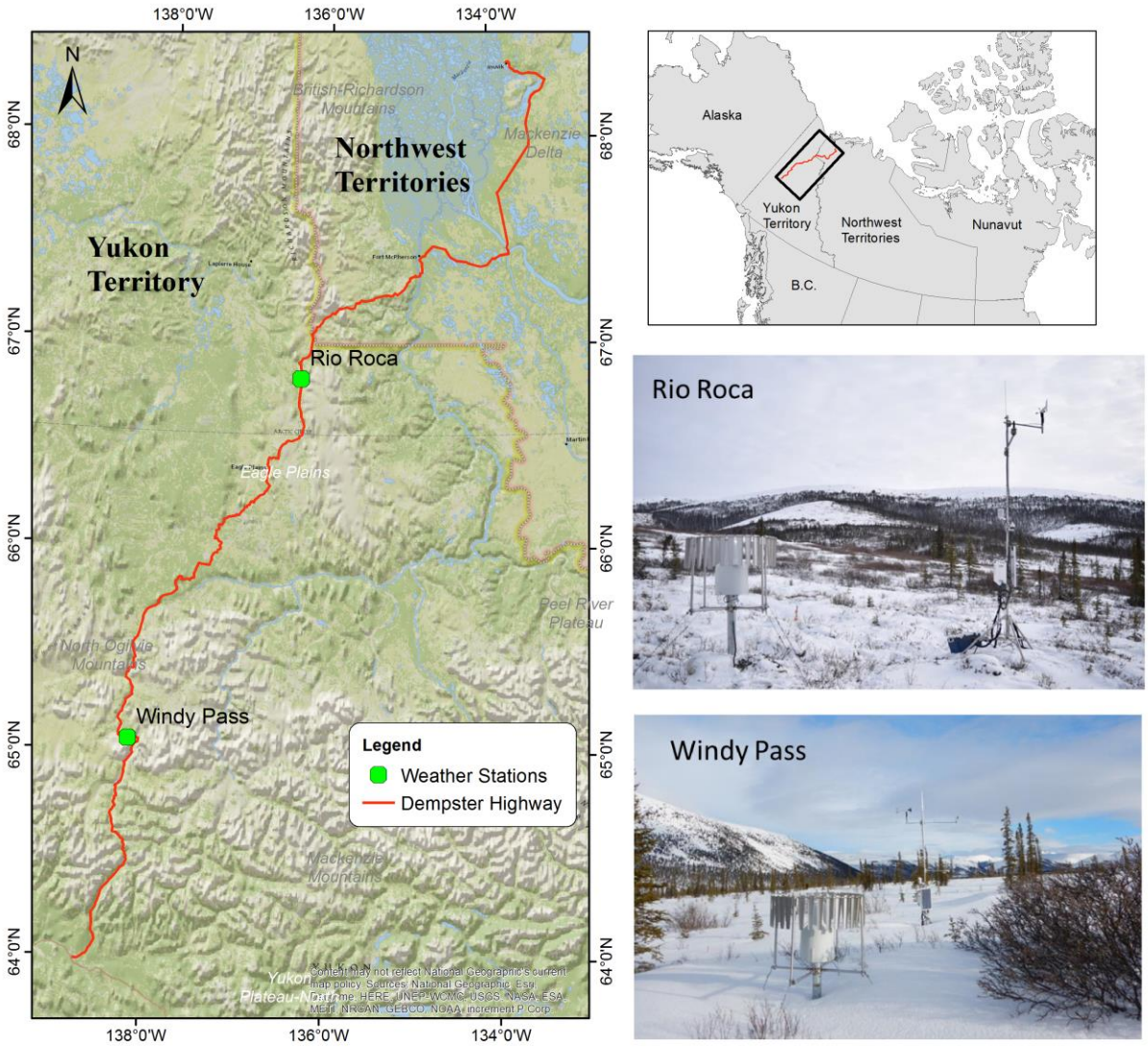

Figure 2.1: Location of permafrost hydrology study sites in northern Yukon, Canada.

Table 2.1: Study site geographical characteristics.

Station	**Geographic Coordinates**	**Elevation (m.a.s.l.)**	**Slope**	**Vegetation cover**
Windy Pass	65° 4’ 0.8’’ N 138° 14’ 46.1’’ W	1,030	5°	Shrubs, moss and scattered spruce
Rio Roca	66° 50’ 1.0’’ N 136° 20’ 0.0’’ W	660	4°	Grasses, moss, lichen and scattered spruce and shrub

Both stations were equipped with sensors to monitor the following variables: precipitation, air temperature, relative humidity, incoming and outgoing shortwave radiation, wind direction and speed, snow depth, soil heat flux, soil moisture and temperature (4 depths), ground surface temperature and snow temperature. The sensors’ models, manufacturers and height/depths are detailed in Table 2.2. The data was recorded using a CR1000 datalogger from Campbell Scientific Canada Ltd., and the frequency of measurements was every 30 minutes for all variables except for soil moisture and temperature, which were measured every 6 hours.

Table 2.2: Instrumentation at the two weather stations.

Measurement	**Manufacturer**	**Model**	**Quantity**	**Sensor height or depth (m) with respect to ground surface**	
				Windy Pass	**Rio Roca**
Precipitation	Ott	Pluvio2	1	2.0	2.0
Air Temperature and Relative Humidity	Rotronic	HC-S3-XT	1	2.1	2.9
Outgoing and Incoming Shortwave Radiation	Apogee	SP-230	1 (each)	2.0 and 2.4, respectively	4.1 and 4.3, respectively
Wind Speed and Direction	RM Young	05108-10-L	1	4.3	5.0
Snow Depth	Campbell	CSI SR50A	1	2.2	2.5
Soil Heat Flux	Hukseflux	HFP01-L	1	-0.03	-0.03
Soil Moisture and Temperature	Campbell	CS655-L	4	-0.1, -0.23, -0.51, -0.91	-0.1, -0.3, -0.5, -0.76
Ground Surface Temperature	Omega	Type E Thermocouple	1	-0.01	-0.01

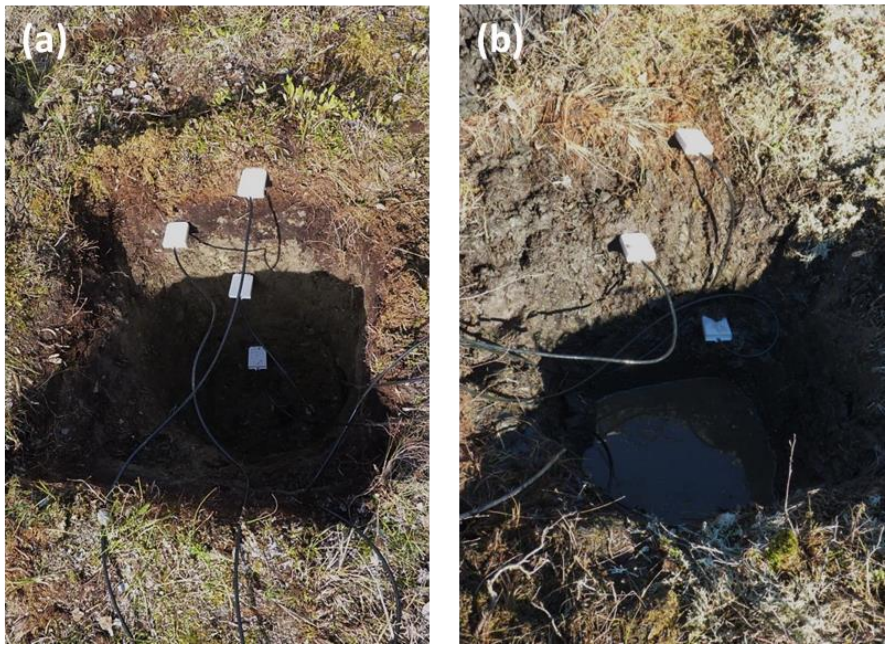

Figure 2.2: (a) Soil profile at Windy Pass, September 6, 2014. Permafrost was not reached. (b) Soil profile at Rio Roca, September 7, 2014. Ice-rich permafrost was reached.

2.2.1 Windy Pass

Continuous weather and soil data at Windy Pass is available for this study from September 2014 to June 2017, including two complete summer (2015 and 2016) and three winter (2014-2015, 2015-2016 and 2016-2017) seasons. Figure 2.3a presents mean monthly precipitation and mean daily temperature for the available period. Precipitation was corrected for the effect of wind undercatch, typically found for snowfall in cold, windy and dry environments. Smith (2008) developed the correction used, which is an empirical relationship between wind speed and undercatch. Mean annual precipitation was 407 mm after wind undercatch corrections, for which the maximum monthly precipitation occurred in August at 104 mm, followed by July and June at 88 mm and 51 mm, respectively, representing a total summer precipitation of 243 mm or 60% of the mean annual precipitation. Winter precipitation (October to April) was 107 mm or 26% of the mean annual precipitation. Mean annual temperature was -4.4 °C, and the maximum and minimum recorded temperatures were 25.0 and -42.1 °C respectively, with an average season above 0 °C of 148 days from April 28 to September 23. Figure 2.3b presents the wind rose, which shows predominant winds from the north; however, the highest wind speeds were from the south and reached up to 8 m s^{-1}. High wind speeds (> 4 m s^{-1}) were infrequent. Relative humidity ranged from 13% to 98%, with mean annual values of 70%. Daily shortwave irradiance rose to 800 W m^{-2} in mid-summer and down to 5 W m^{-2} in mid-winter. Average snow depth increased to 90, 68 and 43 cm in 2015, 2016 and 2017, respectively. End of snow ablation was May 19, 14 and 9 for the

years 2015, 2016 and 2017, respectively; whereas the beginning of the snowcover season was Oct 6, Sept 18 and Oct 8 for the years 2015, 2016 and 2017, respectively. Figure 2.3c presents mean daily soil temperature at four depths. The thawing season of 2015 was shorter than in 2016 at most recorded depths (Table 2.3 and Table 2.4), which is consistent with the warmer maximum and minimum temperatures. For example, the initiation of ground thaw at 10 cm deep started in May 19 in 2015, whereas in 2016 it started about three weeks earlier. Note that for the available measurements, the deeper in the soil the longer the thawing season is. Table 2.3 and Table 2.4 present details about ground thaw duration and initiation, ground freeze initiation, and minimum and maximum soil temperature at all depths. Liquid water content (not shown) was successfully measured at all depths but at 23 cm, for which several gaps during the summer developed.

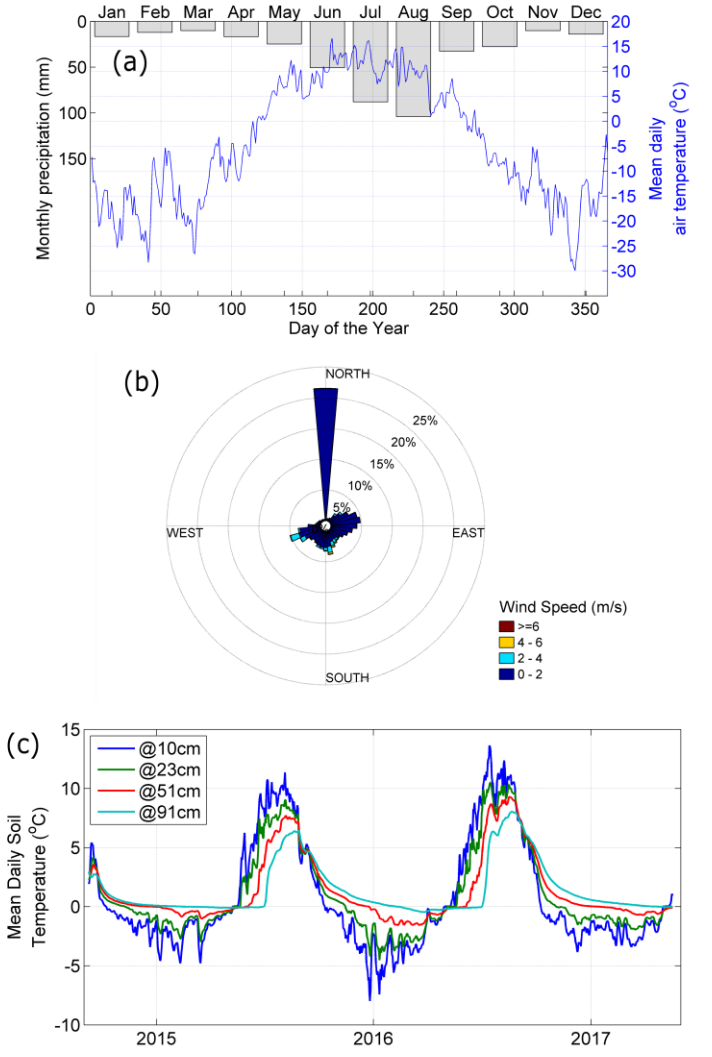

Figure 2.3: (a) Mean monthly precipitation and mean daily air temperature. (b) Wind rose. (c) Mean daily soil temperature at four depths.

Table 2.3: Soil temperature profile for the period spring 2015 – spring 2016 at Windy Pass.

Depth (cm)	Ground thaw initiation	Ground freeze initiation	Thaw season duration (days)	Maximum 6-hourly temperature (°C)	Minimum 6-hourly temperature (°C)
10	May 19	Oct 11	145	13.5	-8.1
23	May 22	Nov 15	177	9.7	-4.6
51	May 31	Dec 25	208	7.8	-1.6
91	June 30	Feb 9	255	6.5	-0.5

Table 2.4: Soil temperature profile for the period spring 2016 – spring 2017 at Windy Pass.

Depth (cm)	Ground thaw initiation	Ground freeze initiation	Thaw season duration (days)	Maximum 6-hourly temperature (°C)	Minimum 6-hourly temperature (°C)
10	April 30	Oct 9	162	16.4	-3.9
23	May 19	Nov 4	152	12.1	-1.9
51	June 5	Jan 15	224	9.3	-0.7
91	July 2	Apr 23	295	8.1	-0.1

2.2.2 Rio Roca

This station has a shorter period of record than Windy Pass, due to station damage likely produced by a bear; therefore, continuous records are only until June 2016. Only one ground thaw season (2015) and two winter seasons (2014-2015 and 2015-2016) are available. Figure 2.4a presents mean monthly precipitation and mean daily temperature. Precipitation at Rio Roca was also corrected for the effect of wind undercatch using the correction from Smith (2008). Mean annual precipitation was 439 mm, for which the maximum monthly precipitation occurred in August at 111 mm, followed by July and October at 64 mm and 55 mm, respectively. Mean summer precipitation (June to August) was 205 mm or 47% of the mean annual precipitation, whereas

winter precipitation accounted for 165 mm or 38% of the mean annual precipitation. Mean annual temperature at Rio Roca was -4.1 °C, and the maximum and minimum recorded temperatures were 25.5 and -36.3 °C, respectively, with an average season above 0 °C of 150 days, from April 25 to September 22. Figure 2.4b presents the wind rose, which shows predominant winds from the north, similar to Windy Pass station; however, the highest wind speeds were from the east and reached up to 9 m s^{-1}. Relative humidity ranged from 15% to 98%, with mean annual values of 73%. Daily shortwave irradiance increased to 750 W m^{-2} in mid-summer and down to 3 W m^{-2} in mid-winter. Snow depth from the SR50 was very noisy even after removing outlier values, and there is a substantial inconsistency when compared to the spatially averaged snow survey observations near the station. Nevertheless, the end of the snow ablation can be extracted from this and it was on May 9, 2015, and May 1, 2016.

Figure 2.4c presents mean daily soil temperature at four depths. Ground thaw at 10 cm began on May 20 and lasted until October 2, resulting in a thawing period of 135 days, whereas for the deepest measurement at 76 cm, soil thaw started on July 1 and lasted until October 15, resulting in a shorter thawing season of 102 days (Table 2.5). The opposite was found at Windy Pass, in which deeper soil layers have a longer thawing season. This is explained by the colder conditions at deep soil layers and the continuous, ice-rich permafrost at depth found at Rio Roca, resulting in faster cooling of the ground and likely shallower active layer thickness, which in turn produces a faster freezing front from the permafrost upwards.

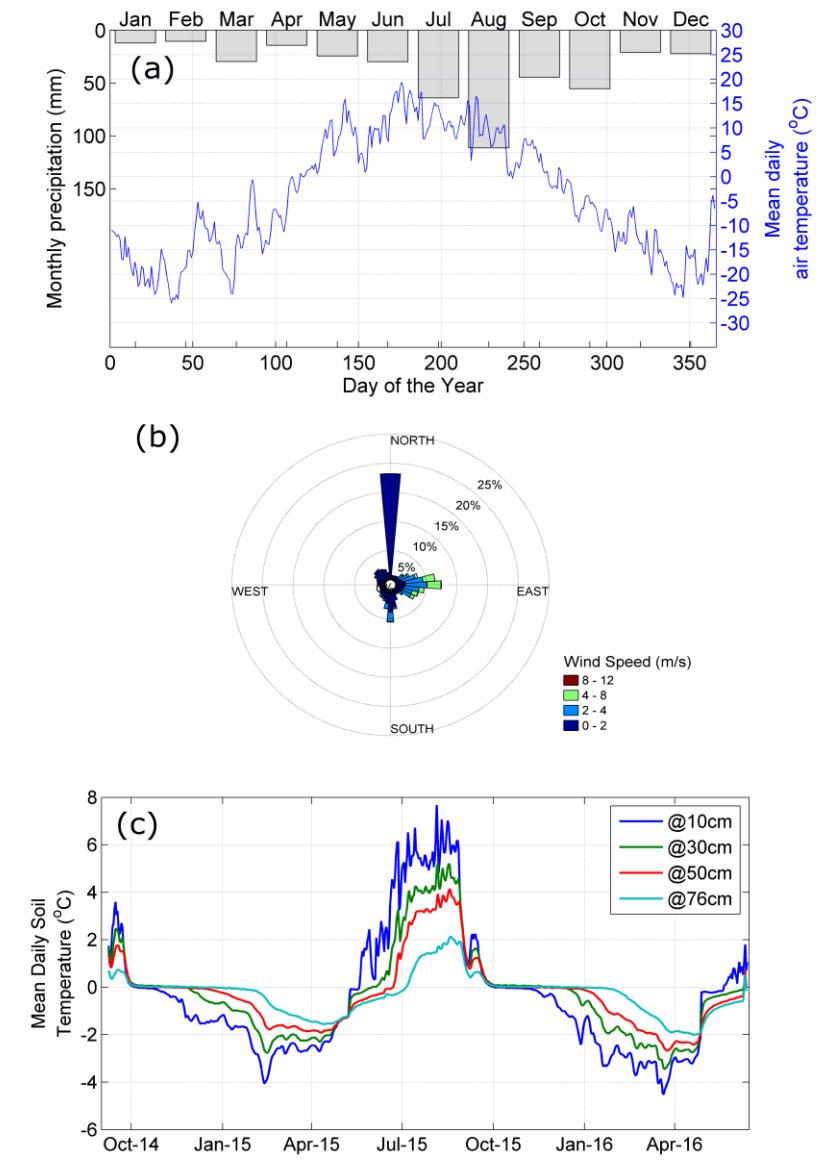

Figure 2.4: (a) Mean monthly precipitation and mean daily air temperature. (b) Wind rose. (c) Mean daily soil temperature at four depths.

Table 2.5: Soil temperature profile for the period spring 2015 – spring 2016 at Rio Roca.

Depth (cm)	Ground thaw initiation	Ground freeze initiation	Thaw season duration (days)	Maximum Temperature (°C)	Minimum Temperature (°C)
10	May 20	Oct 2	135	9.0	-4.6
30	June 1	Oct 9	130	5.5	-3.5
50	June 22	Oct 9	109	4.2	-2.7
76	July 5	Oct 15	102	2.2	-2.1

2.3 Point-scale hydrological modelling

The Arctic Hydrology Model (AHM; Krogh et al., 2017), developed using the Cold Regions Hydrological Model platform (CRHM; Pomeroy et al., 2007; 2016), was used to simulate the observations recorded at Windy Pass and Rio Roca stations. CRHM has a flexible and modular structure that allows selection from a large library of modules, the hydrological processes and the approaches (e.g. degree day or full energy balance to simulate snow accumulation and melt) to include in the model configuration. Hydrological processes included in this application include snow albedo decay, precipitation phase, sublimation/evaporation from canopy, intercepted snowfall/rainfall, snowmelt and accumulation, snow redistribution and sublimation by wind, ground freeze/thaw, evapotranspiration, surface and subsurface flow and storage, flow through organic terrain and snowpack, infiltration into frozen and unfrozen soils. The only difference between this model configuration and the one used in the CRHM-AHM is that streamflow routing was not included here as in subsequent thesis chapters. Most algorithms used to represent these hydrological processes have a strong physical base, allowing confidence model and parameter transferability between sites with similar conditions. Table 2.6 presents a brief description with the key characteristics of each module representing the hydrological processes (more details in Krogh et al., 2017 and subsequent chapters). The CRHM-AHM requires hourly input weather data consisting of precipitation, air temperature, relative humidity, wind speed and shortwave and longwave irradiance. As a single-point or 1-D implementation of the CRHM-AHM model, this application does not allow horizontal inputs of mass fluxes such as surface and subsurface flow, though water can flow out and snow can also be transferred through wind redistribution.

Table 2.6: Description of the physical processes included in the hydrological model for Rio Roca and Windy Pass.

Physical process	**Module description**
Precipitation Phase Partition	This method estimates the phase of precipitation (rain or snow) using a psychrometric energy balance approach, based on the fall velocity, air temperature and the relative humidity (Harder and Pomeroy, 2013)
Albedo Decay	Albedo decay rate is classified into three groups: premelt, melt and postmelt, each with a different decay rate for the snowcovered period. This model is suitable for cold shallow snowpacks that are not subject to frequent mid-winter melt events (Gray and Landine, 1987)
Canopy Interception, Sublimation and Evaporation	The Rutter Interception Model (Valente et al., 1997) for rain interception, linked to growing season evapotranspiration. The Canopy Interception and Sublimation Model for the snow season (Ellis et al., 2010; Hedstrom and Pomeroy, 1998; Parviainen and Pomeroy, 2000; J. W. Pomeroy et al., 1998)
Snow Melt and Accumulation	A Snowcover Energy Balance Model (SNOBAL; Marks et al., 1998) is a two-layer energy balance model that allows refreezing and uses the bulk transfer method with stability correction (Monin and Obukhov, 1954) to calculate turbulent heat fluxes.
Evapotranspiration	Penman-Monteith Algorithm (P-M; Monteith, 1981) for unsaturated surfaces and Priestley-Taylor (Priestley and Taylor, 1972) for saturated surfaces. Jarvis (1976) to estimate stomata resistance changes.
Blowing Snow Transport, Sublimation and Redistribution	Prairie Blowing Snow Model (PBSM; Fang and Pomeroy, 2009; Pomeroy and Li, 2000) is a steady-state two-phase flow model that calculates snow saltation and suspension based on friction velocity, aerodynamic roughness height, exposed vegetation and fetch distance. A coupled sublimation algorithm integrates the sublimation of a single ice particle over the saltation and suspension layers and rescales this to bulk sublimation.
Ground Thaw-Freeze	A simplified solution of Stefan's heat flow equation, the XG – algorithm (Changwei and Gough, 2013)
Snow-free ground surface temperature	Semi-empirical approach that uses air temperature, net radiation and antecedent frost table depth to estimate ground surface temperature (Williams et al., 2015).

Physical process	Module description
Water flow through snowpack and organic layer	Water flow detention produced by the celerity of flow through the snowpack or exposed organic layers above soil is calculated as per Pomeroy et al. (2016) based on Colbeck (1975, 1972) and relationships between permeability, water pressure and saturation.
Soil Infiltration	Infiltration into unfrozen soils using Ayers (1959) and into frozen soils using Gray et al. (2001). Infiltration into unfrozen soils is based on an empirical relationship between ground cover condition (e.g. bare soil or forested) and soil texture. For frozen soils, infiltration is first classified as unlimited, restricted and limited. For limited infiltration, parameterization of a finite difference heat and mass transfer model is based on initial surface saturation, average soil saturation and temperature, and infiltration opportunity time.
Soil Moisture	Subsurface vertical and lateral drainage controlled by effective hydraulic conductivity using the Brooks and Corey (1964) relationship. Three-layer model includes a recharge, lower and groundwater layer. The model allows for infiltration excess or saturation-excess overland flow, surface runoff, recharge through macropores and subsurface discharge (Fang et al., 2013). Here, no sub-permafrost groundwater recharge is allowed due to ice-rich soils and relatively shallow active layer. Lateral and vertical flows are calculated based on Darcy's law using the unsaturated hydraulic conductivity calculated with the Brooks and Corey (1964) relationship. This module is linked to XG and all water and storage capacity in the frozen layer is considered immobile and inaccessible. Liquid water below a frozen layer may drain vertically or horizontally but not be recharged from above. Liquid water above a frozen layer is restricted to the unfrozen layer and may drain horizontally and be recharged or withdrawn by evapotranspiration.
Surface and Subsurface Routing	Surface and subsurface lag and storage (Clark, 1945).

Some of the key differences with previous hydrological models using the CRHM platform are the incorporation of the XG-algorithm (Changwei and Gough, 2013) representing ground freeze and thaw, and the estimation of ground surface temperature that it is used as the upper boundary condition for the XG-algorithm. During the snow-free season, ground surface temperature is calculated using the radiative-conductive-convective approach (RCC; Williams et al., 2015), which is based on air temperature, net radiation and antecedent frost table depth. During the snowcovered season, ground surface temperature is calculated based on the lower snow layer temperature from two-layer snow energy balance model SNOBAL. The XG-algorithm is a

simplified solution for Stefan's equation (Juminikis, 1977) to represent heat transfer in multi-layered and non-uniform soils, considering the latent heat of fusion and neglecting the volumetric heat capacity of the soils (i.e. sensible heat exchange). Stefan's equation is presented in Equation 2-1, where ξ is the frost/thaw front depth, k is the thermal conductivity of the soil (W m^{-1} K^{-1}), F is the surface freeze/thaw index (°C degree-days; calculated based on the ground surface temperature), L is the latent heat of fusion (J kg^{-1}), w is the volumetric water content (m^3 m^{-3}), and ρ is the bulk density of the soil (kg m^{-3}).

$$\xi = \sqrt{\frac{2kF}{Lw\rho}} \qquad \textit{Equation 2-1}$$

Changwei and Gough (2013) defined the ratio P_{12} (Equation 2-2), where *1* and *2* are two vertically adjacent soil layers.

$$P_{12} = \frac{\xi_1}{\xi_2} = \left(\frac{k_1\rho_2 w_2}{k_2\rho_1 w_1}\right)^{0.5} \qquad \textit{Equation 2-2}$$

The P_{12} ratio is the ratio between the frost/thaw front depth of soil layer 1 and 2, which is defined only by the physical properties of each soil layer, and not by the freeze/thaw index (F). With Equations 2-1 and 2-2, and the concept of a "residual freeze/thaw index", Changwei and Gough (2013) deduced a simple relationship to estimate the freezing/thawing depth in a two layered soil system:

$$\xi = \begin{cases} \sqrt{\frac{2k_1F}{Lw_1\rho_1}} & if\ F \leq F_1 \\ Z_1 + \frac{\xi_1 - Z_1}{P_{12}} & if\ F > F_1 \end{cases} \qquad \textit{Equation 2-3}$$

where Z_1 is the thickness of the first soil layer (m) and F_1 is the freeze/thaw index required to freeze/thaw the first layer. Equation 2-3 can be generalized to calculate the freeze/thaw of an n-layered soil system. The thermal conductivity of each soil layer is estimated using the expression developed by Johansen (1975, p. 221) for unfrozen and frozen soils, based on their degree of saturation.

The majority of the parameters used in this study are presented and discussed by Krogh et al. (2017) and were taken from detailed process studies in the region or in places with similar hydrological conditions; however, parameters describing local characteristics such as elevation, aspect, slope, vegetation (Table 2.1) and soil profile are specific to each site and derived from local measurements. The soil profile configuration used in the CRHM-AHM single-point configuration consists of 20 numerical layers. The top 10 layers are 0.1 m thick and the lower 10 layers are 0.2

m thick. The top 4 layers in the Windy Pass model represent the top organic soil and the lower 16 layers represent the mineral soil (Figure 2.2a). The Rio Roca model has a much thicker organic layer represented by the top 8 layer in the model and the mineral soil represented by the remaining 12 layers (Figure 2.2b). The thermal properties and porosities used in the organic and mineral soil layers are presented in Table 2.7 and are based on reference values presented by Woo (2012).

Table 2.7: Thermal properties and porosity for the organic and mineral soil layers used in the CRHM-AHM model at Windy Pass and Rio Roca stations.

Parameter	**Organic**	**Mineral**
Porosity	0.8	0.4
Soil dry thermal conductivity (W m^{-1} K^{-1})	0.1	0.25
Soil saturated unfrozen thermal conductivity (W m^{-1} K^{-1})	0.5	2.5
Soil saturated frozen thermal conductivity (W m^{-1} K^{-1})	1.9	1.9

2.4 Results

2.4.1 Model Performance

2.4.1.1 Windy Pass

Figure 2.5 presents a comparison between observed near ground surface temperature (1 cm deep) and simulations for the snow-free period of 2015 and 2016. The model slightly underestimated ground surface temperature by -0.5°C during 2015, whereas during 2016 the model overestimated observations by 0.4°C, resulting in a mean bias of 0.02°C for the entire period. Correlation between simulations and observations during 2015 and 2016 are 0.95 and 0.94, respectively, resulting in a correlation of 0.94 for the entire period. This analysis demonstrates the capability of the radiative-conductive-convective model (Williams et al., 2015), implemented within the CRHM-AHM, to simulate daily ground surface temperature at Windy Pass. Note that the CRHM-AHM model determined the start of the snow-free period and the initiation of thaw. The top panel in Figure 2.6 presents simulated and observed ground thaw, i.e. the date and depth at which the soil temperature reaches 0°C. During the thawing season of 2015, the model underestimated ground thaw by 10, 13, 23 and 15 cm at 10, 23, 51 and 91 cm deep, respectively, resulting in a mean bias of -15 cm. During the 2016 thawing season, the model also underestimated observations by 10, 2, 7 and 3 cm

at 10, 23, 51 and 91 cm deep, respectively, resulting in a mean bias of -6 cm. The lower panel in Figure 2.6 presents a comparison of the modelled liquid water content to that observed at a depth within the top recharge layer. The recharge layer in CRHM-AHM is used as the top soil layer that receives water from infiltration and from which vegetation roots extract soil moisture for evapotranspiration. Observed water content at the recharge layer was calculated assuming a 10 cm recharge layer and a constant water content equal to the measurements at 10 cm deep. A small mean bias of 1.1 and 0.4 mm and a correlation coefficient of 0.16 and 0.61 were found for 2015 and 2016, respectively. The main differences were found at the beginning of the 2015 season, in which the water content is underestimated; however, for the remaining of the period, the model showed to adequately represent water content in the top 10 cm. A more detailed analysis including water content observations at all depths was not possible due to several gaps found in the records at 23 cm depth.

The upper panel in Figure 2.7 shows a comparison between observed and simulated snow depth. Simulated snow depth was underestimated by the model during the years 2015 and 2016, which is explained by an overestimation of the simulated snow density; however, in 2017 it was relatively well represented. There is significant spatial variability in observed snow depth, particularly during 2015, as can be seen from the snow survey standard deviation (σ = 0.18 m). Continuous "point" snow depth observations by the SR50 allow comparison of the beginning and end of the snowcover season. The observed dates for the end of snow ablation for the years 2015, 2016 and 2017 were May 19, May 14 and May 9, respectively, whereas simulations were May 19, May 11 and May 15. This demonstrates that the model simulated an earlier (3 days) and later (6 days) end of snow ablation period for the years 2016 and 2017, respectively, but captured the exact day in 2015. This is particularly important, as the end of the snow ablation triggers the initiation of ground thaw. The lower panel in Figure 2.7 presents simulated snow water equivalent (SWE), and the mean and standard deviation of SWE from the snow survey transect. The model simulations underestimated the mean observed SWE by 29 and 30 mm for 2015 and 2016, respectively. However, as previously mentioned, there is substantial spatial variability in the snow survey; standard deviations for the years 2015 and 2016 were 54 and 34 mm, respectively and so the simulations are within the standard deviations. The model simulations may be biased by uncertainty in the wind undercatch correction used (Smith, 2008), model error (e.g. calculation of turbulent fluxes or ground heat), and the small topographic features producing small scale wind redistribution. Variability in wind redistribution is expected for the snow survey transect points far from the more wind-sheltered conditions found at the meteorological station, and was not captured by the single-point model implementation. Unfortunately, there are no observations to compare simulated SWE during the year 2017.

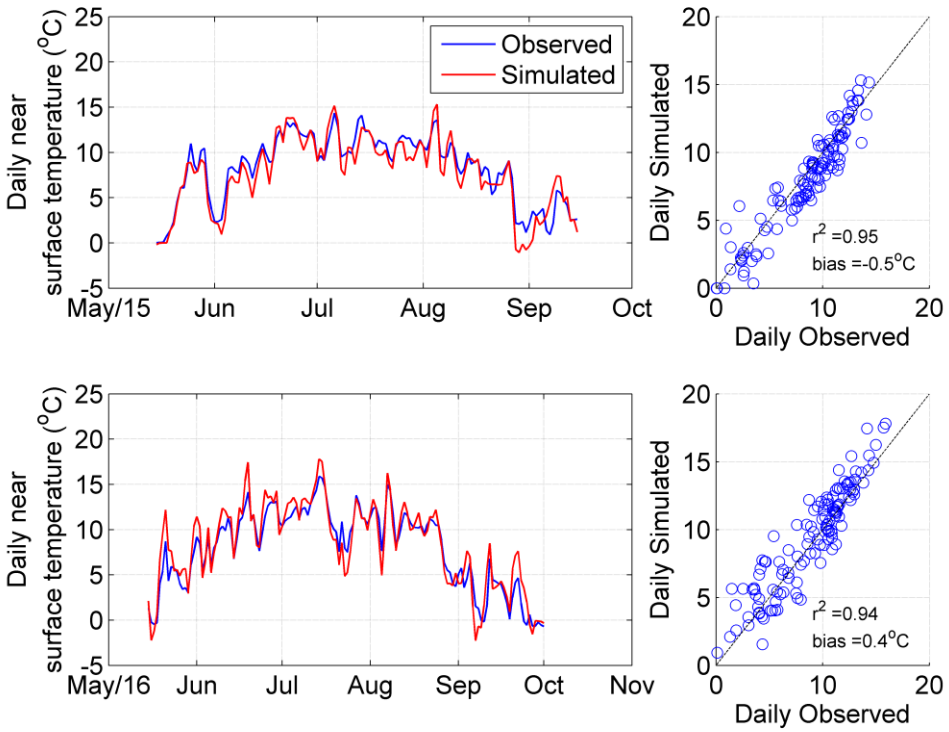

Figure 2.5 Near ground surface temperature (1 cm depth) comparison between observed and single-point model at Windy Pass.

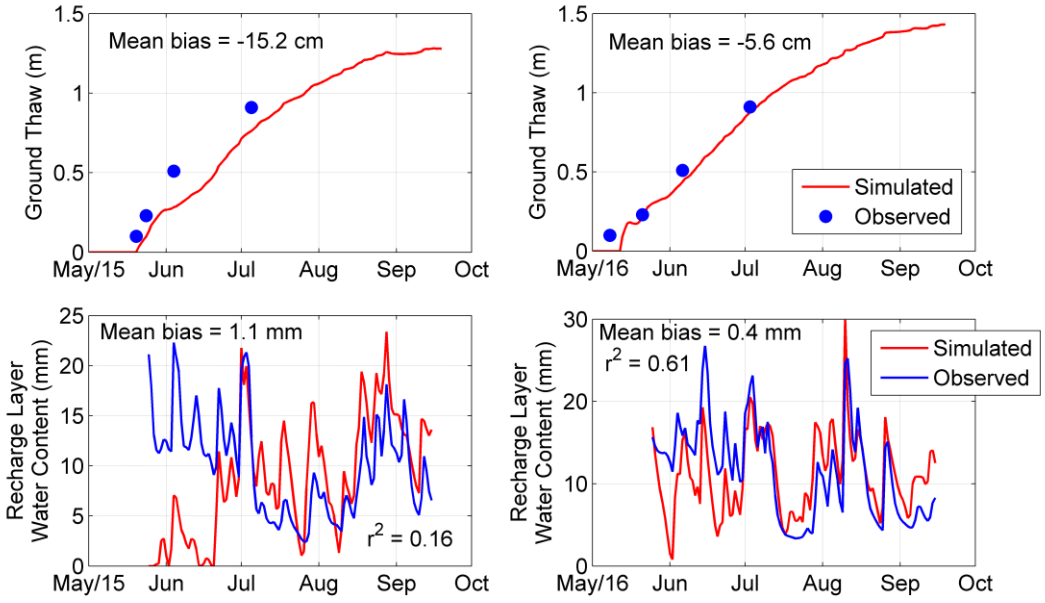

Figure 2.6: Top panels: ground thaw validation at Windy Pass. Lower panel: liquid water content at the top recharge ground layer.

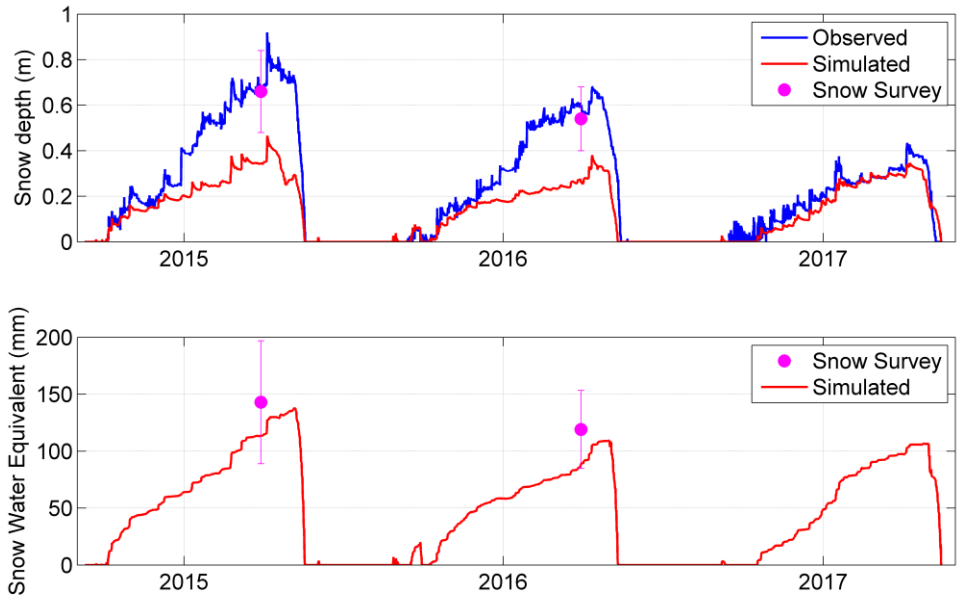

Figure 2.7: Upper panel: snow depth comparison between observed and single-point model at Windy Pass. Lower panel: snow water equivalent validation at Windy Pass. Magenta circles represent the mean value from a snow survey performed across the Windy Pass station. Error bar presents the standard deviation of the snow survey.

2.4.1.2 Rio Roca

Due to the shorter available period, there is only one ground thaw season to validate the model at Rio Roca. Figure 2.8 presents observed and simulated daily ground surface temperature, for which the model slightly overestimated observations by 0.04°C on average; however, simulations correlated well to observations, with a coefficient of correlation of 0.88. The upper panel in Figure 2.9 shows the validation of the ground thaw algorithm used in the model. A good agreement was found between observations and simulations, with differences of -10, 0.02, 0.0 and -9 cm, at 10, 30, 51 and 76 cm depths, respectively, resulting in a mean bias of -5 cm. The initiation of ground thaw was 5 days late due to late snow ablation in the model (Figure 2.8); this partially explains the bias in ground thaw.

Unfortunately, snow depth records do not allow a meaningful comparison between simulated and observed snow depth to support this ground thaw analysis. The lower panel in Figure 2.9 presents observed mean and standard deviation of SWE from two snow surveys performed in late March 2015 and 2016 against simulated SWE. Simulations for 2015 and 2016 underestimated observed mean SWE by 30 and 24 mm, respectively; however, they are both within the standard deviation (35 and 58 mm, respectively) of observations along the transect. SWE standard deviations suggest a large spatial variability along the snow transect (similarly to Windy Pass), which could be due to small topographic features producing small-scale wind redistribution, modelling errors and/or

uncertainty in the wind undercatch algorithm employed. As opposed to Windy Pass, measurements of liquid water content at the top layer are incomplete, precluding a comparison of the recharge layer water content.

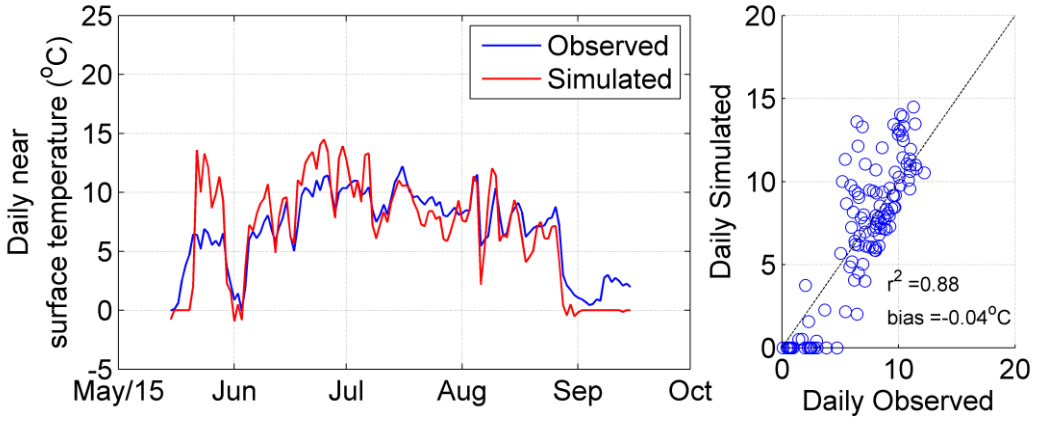

Figure 2.8: Near surface temperature validation at Rio Roca station.

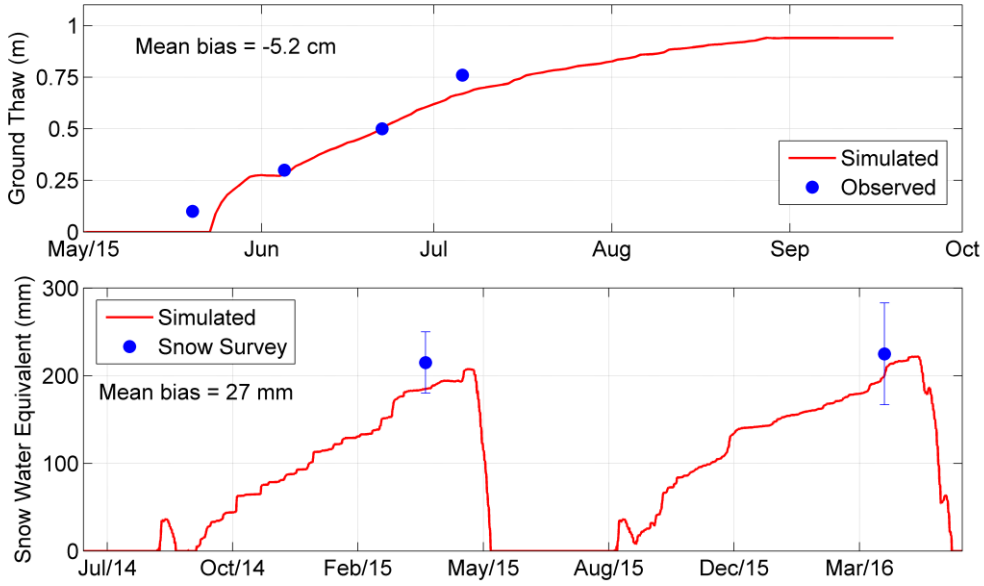

Figure 2.9: Upper panel: ground thaw validation at Rio Roca. Lower panel: snow water equivalent validation at Rio Roca. Blue circles represent the mean value from a snow survey performed across the Rio Roca station. Error bar presents the standard deviation of the snow survey.

2.4.2 Ground thaw sensitivity to thermal conductivity and porosity

Given the uncertainty associated with the parameter values chosen for the thermal conductivity and porosity, a sensitivity analysis for a range of possible and documented values was performed to understand their impact on the simulated ground thaw. The parameters and ranges used in the sensitivity analysis are presented in Table 2.8. The global sensitivity analysis presented by Razavi and Gupta (2016a and 2016b), referred as VARS (Variogram analysis of response surfaces), was used for this purpose. The mean bias between observed and simulated ground thaw was used as the metric to assess the sensitivity. Fifteen "stars" (refer to the VARS manual for details: http://homepage.usask.ca/~ser134/publications/20160219_VARS-Tool%20manual.pdf) were used to set up the sensitivity analysis, resulting in 825 simulations for the six parameters, which is considered to be sufficient for this purpose.

Figure 2.10 and Figure 2.11 present the results of the sensitivity analysis for the Windy Pass and Rio Roca models, respectively. In both cases, the parameter that had the greatest impact on the model (i.e. the largest ratio of factor sensitivity, Figure 2.10a and Figure 2.11a) was the soil dry thermal conductivity of the organic soil layer (p3), followed by the porosity of the organic layer (p1). Simulations using the different parameter-scenarios (Figure 2.10b and Figure 2.11b) suggest that for the Windy Pass model, the active layer thickness (ALT) varies between 1.17 and 1.42 m for the year 2015 and between 1.31 and 1.58 m for the year 2016, whereas for the Rio Roca model it varies between 0.93 and 1 m. This analysis revealed that the simulated ALT at Windy Pass is more sensitive to the selection of parameters, particularly those associated with the upper organic soil layer, than the simulated ALT at Rio Roca. This can be explained by the warmer and longer thawing season found at Windy Pass (Figure 2.5 and Figure 2.9), allowing a larger variability by the end of the thawing season. A histogram of mean bias in simulations (Figure 2.10c and Figure 2.11c) shows that at Windy Pass, parameters uncertainty alone does not completely explain the model underestimation of ground thaw, as for all the scenarios, the mean bias was always at least -6 cm. At Rio Roca, some simulations showed a mean bias of -3 cm, suggesting that with a different combination of realistic parameters the model bias can be further reduced to small values, though it was already relatively low.

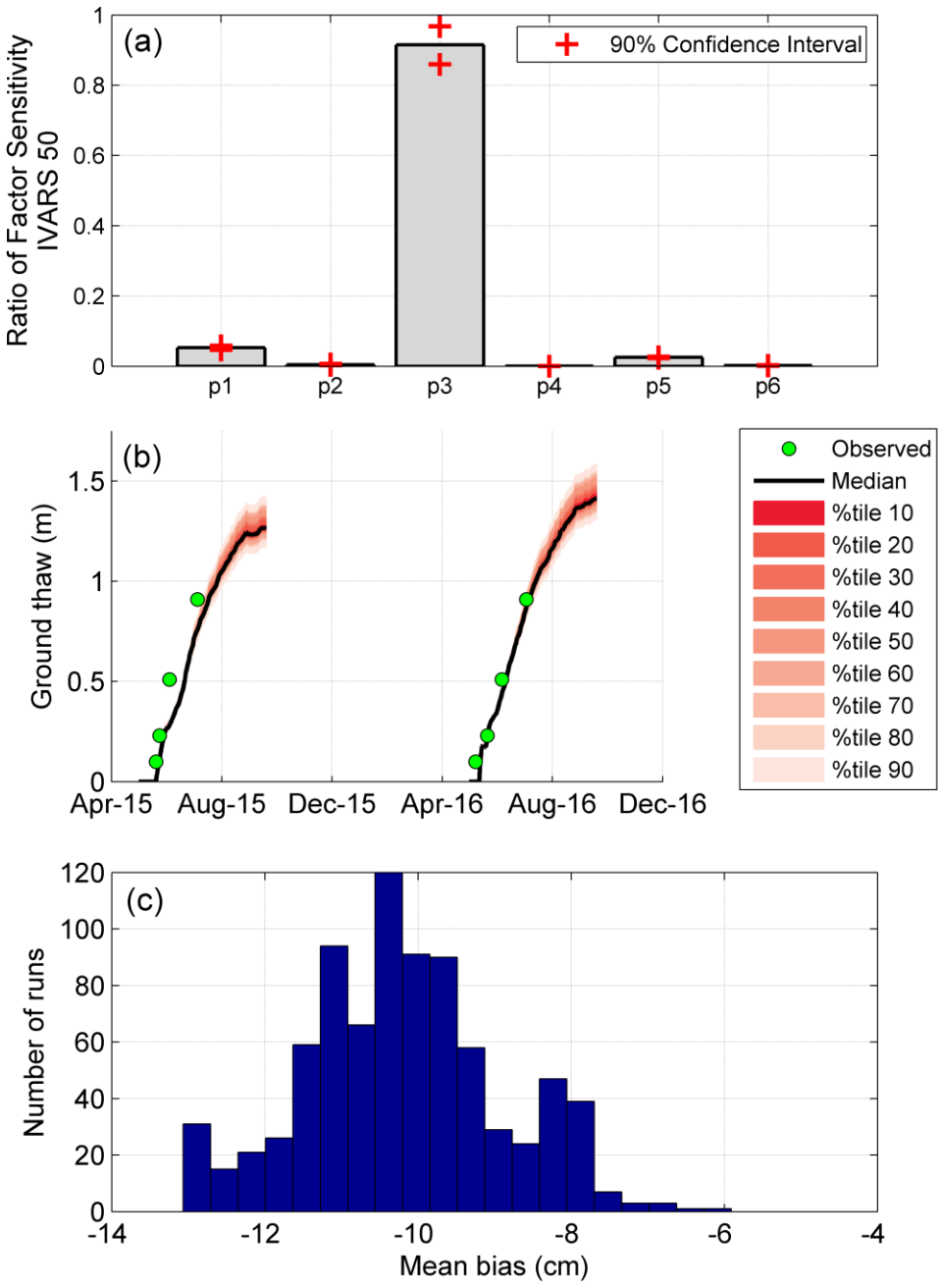

Figure 2.10: (a) Ratio of factor sensitivity of simulated ground thaw to selected parameters at Windy Pass; p1: organic layer porosity, p2: mineral soil layer porosity, p3: organic soil layer dry thermal conductivity, p4: mineral soil layer dry thermal conductivity, p5: organic soil layer saturated thermal conductivity, p6: mineral soil layer saturated thermal conductivity. (b) Sensitivity of simulated ground thaw to selected parameters against observations. (c) Histogram of simulations mean bias. 825 model simulations were performed.

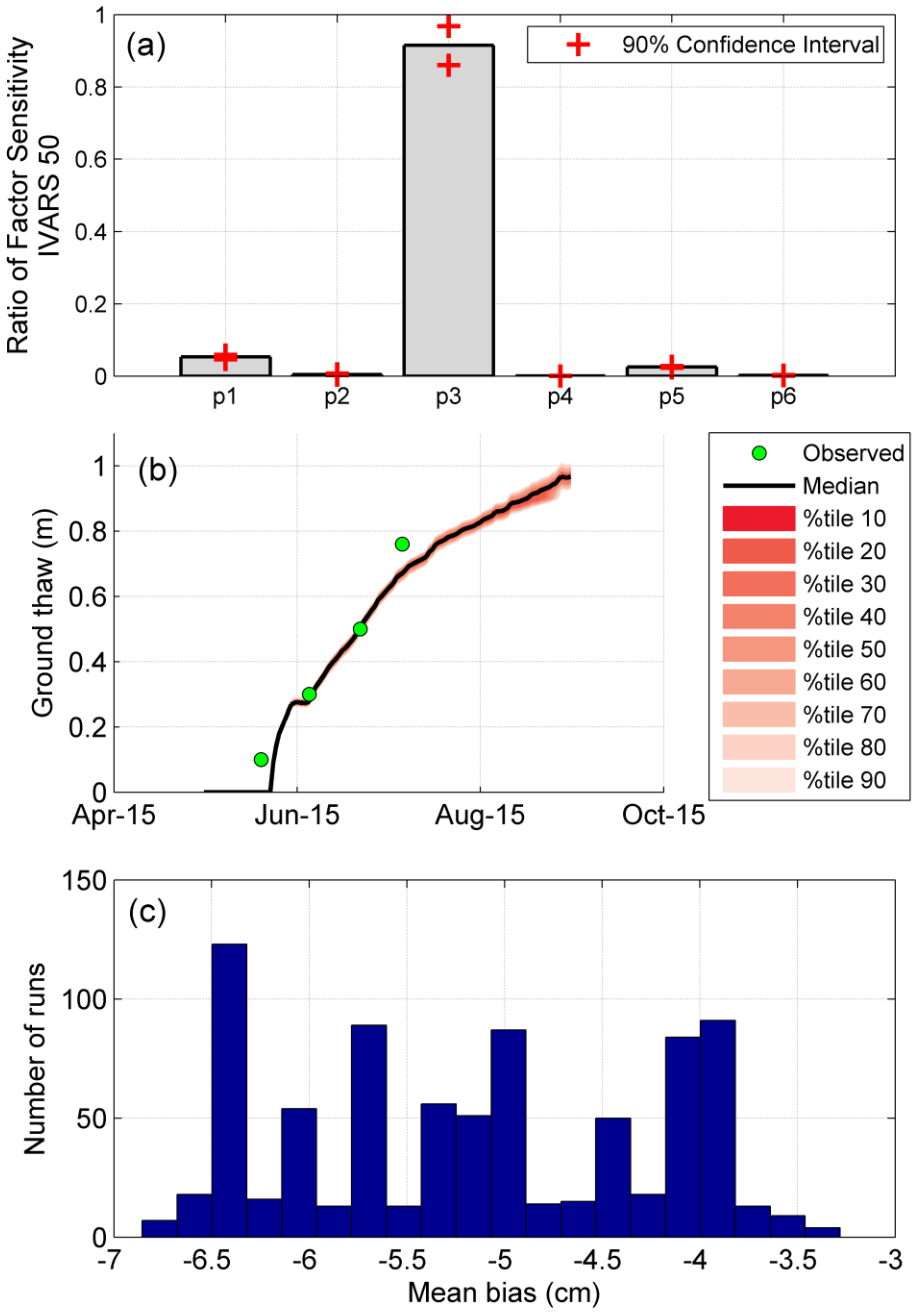

Figure 2.11: (a) Ratio of factor sensitivity of simulated ground thaw to selected parameters at Rio Roca; p1: organic layer porosity, p2: mineral soil layer porosity, p3: organic soil layer dry thermal conductivity, p4: mineral soil layer dry thermal conductivity, p5: organic soil layer saturated thermal conductivity, p6: mineral soil layer saturated thermal conductivity. (b) Sensitivity of simulated ground thaw to selected parameters against observations. (c) Histogram of simulations mean bias. 825 model simulations were performed.

Table 2.8: Parameter ranges for ground thaw sensitivity analysis at Windy Pass and Rio Roca.

Parameter	**Organic soil layer**	**Mineral soil layer**
Porosity (.)	0.7 – 0.9	0.3 – 0.5
Soil dry thermal conductivity (W m^{-1} K^{-1})	0.06 – 0.15	0.2 – 0.3
Soil saturated unfrozen thermal conductivity (W m^{-1} K^{-1})	0.25 – 0.75	2.0 – 3.0

2.5 Discussion

The CRHM-AHM model was found to successfully represent daily ground surface temperature at the two sites (Figure 2.5 and Figure 2.8); mean bias at Windy Pass and Rio Roca was 0.02 and 0.04 °C, respectively, whereas the correlation coefficient was 0.94 and 0.88, respectively, demonstrating the capacity of the RCC model to be successfully transfer and applied to different conditions. Ground surface temperature is a critical state variable in the model, as it was used as the upper boundary condition to the module simulating ground thaw, and it is typically used for that purpose by other models (Hayashi et al. 2007; Woo et al. 2007; Kurylyk et al. 2014). The model underestimated ground thaw at both sites (Figure 2.6 and Figure 2.9), with a mean bias of 11 and 5 cm at windy Pass and Rio Roca, respectively. Model underestimation of ground thaw could be due to late simulations of the initiation of ground thaw, which is controlled partially by the end of the snow ablation and meteorological inputs. Simulated end of snow ablation at Windy Pass was earlier than observed (Figure 2.7) in the season 2015 and 2016; therefore, it does not explain the underestimation of ground thaw. Unfortunately, measured snow depth at Rio Roca was too variable to extract a reasonable estimation for the end of the snow ablation. Another reason to explain the underestimation of ground thaw is an underestimation of the thermal conductivity by values taken from the literature, as well as modelling errors in representing soil moisture and its impact on thermal conductivity (Farouki 1981). In either case, the average underestimation of ground thaw is considered to be small and reasonable for hydrological applications, particularly, when parameters from the literature are being used as opposed to measured values. This is an important finding, as hydrological models of headwater basins in the Arctic have either neglected or used very simplified representations of ground thaw (i.e. degree day; Z. Zhang et al., 2000 and Schramm et al., 2007); however, the CRHM-AHM successfully represented evolution of the active layer under continuous permafrost conditions using a robust and computationally inexpensive approach.

The sensitivity analysis showed that the parameters associated with the upper organic soil layer are the most important in the model's behaviour (Figure 2.10a and Figure 2.11a). This is not

surprising, as this layer has the largest thermal conductivity. Nevertheless, this analysis also showed that mean differences between observed soil temperature and simulations (Figure 2.10c and Figure 11c) are not very sensitive to parameter selection, as observations are relatively shallow (<0.76 and <0.91 m for Windy Pass and Rio Roca, respectively) and the largest variability was found by the end of the thawing season (Figure 2.10b and Figure 2.11b). Therefore, although there is uncertainty in parameter selection, it does not significantly impact the mean ground thaw bias found in this study. This finding demonstrates the robustness of the model when using a realistic set of physical parameters.

SWE validation against a snow survey transect showed an underestimation of 30 and 27 mm at Windy Pass and Rio Roca, respectively, suggesting problems in the representation of snow accumulation. Misrepresentation of SWE is attributed to some combination of problems in measuring snowfall due to wind undercatch and differences between the point application of the model, the areal representation of the snow survey and the arbitrary point measurement of snow depth by the SR50. Although the wind regime at both sites is relatively mild and the precipitation gauges were installed in a relatively wind-sheltered locations – particularly at Windy Pass -, problems with observed snowfall, such as wind undercatch, are likely driving much of the SWE underestimation. Despite the underestimation of mean SWE, the observed standard deviation of SWE was also relatively large, about 54 and 34 mm at Windy Pass, and 38 and 58 mm at Rio Roca, for the years 2015 and 2016, respectively, and so simulated SWE is within that range of variability. The large variability in SWE measurements is due to redistribution around small topographic features and small-scale wind redistribution processes that are not captured by the single-point model. The snow survey transects extend to areas that are not sheltered from the wind, explaining the large spatial variability.

2.6 Conclusion

This study demonstrated that a robust and yet computationally inexpensive algorithm to represent active layer development in regions underlain by continuous permafrost can be successfully coupled to a physically based hydrological model for cold regions. A detail verification of the model performance in simulating continuous ground surface temperature, ground thaw and top soil liquid water content, and discontinuous snow accumulation from snow survey was performed at two northern Canadian sites. Previous hydrological models for Arctic headwater basins have either neglected or use simple representations for the development of the active layer (i.e. degree day) and, therefore, the need for a modelling framework including this and other key hydrological processes that can be easily transferred to other cold regions and under future climate conditions. The sensitivity analysis to key soil thermal properties and porosity demonstrated the robust representation of ground thaw using a realistic range for the physical parameters.

The analysis presented in this chapter showed that the XG-algorithm, driven by reference temperatures in Snobal and the radiative-conductive-convective method in CRHM, can properly capture permafrost dynamics, and therefore, it can be implemented and applied at the basin scale in CRHM. The following chapter presents the detailed description, implementation and validation of the CRHM Arctic Hydrology Model (AHM), including ground freeze and thaw calculations, at a small Artic basin near Inuvik in the Northwest Territories, Canada. The purpose of such analysis is to diagnose in detail, and for the first time, the hydrology of an Arctic basin at the tundra-taiga transition region.

CHAPTER 3

Diagnosis of the hydrology of a small Arctic treeline basin at the tundra-taiga transition using a physically based hydrological model

Forest around Havikpak Creek, Northwest Territories, April 1, 2015.

Abstract

A better understanding of cold regions hydrological processes and regimes in transitional environments is critical for predicting future Arctic freshwater fluxes under climate and vegetation change. A physically based hydrological model using the Cold Regions Hydrological Model platform was created for a small Arctic basin in the tundra-taiga transition region. The model represents snow redistribution and sublimation by wind and vegetation, snowmelt energy budget, evapotranspiration, subsurface flow through organic terrain, infiltration to frozen soils, freezing and thawing of soils, permafrost and streamflow routing. The model was used to reconstruct the basin water cycle over 28 years, to understand and quantify the mass fluxes controlling its hydrological regime. Model structure and parameters were set from the current understanding of Arctic hydrology, remote sensing, field research in the basin and region, and calibration against streamflow observations. Calibration was restricted to subsurface hydraulic and storage parameters. Multi-objective evaluation of the model using observed streamflow, snow accumulation and ground freeze/thaw state showed adequate simulation. Significant spatial variability in the winter mass fluxes was found between tundra, shrubs and forested sites, particularly due to substantial blowing snow redistribution and sublimation from the wind-swept upper basin, as well as sublimation of canopy-intercepted snow from the forest (about 17% of snowfall). At the basin scale, the model showed that evapotranspiration is the largest loss of water (47%), followed by streamflow (39%) and sublimation (14%). The model's streamflow performance sensitivity to a set of parameters was analysed, as well as the mean annual mass balance uncertainty associated with these parameters.

This manuscript has been modified for inclusion in this thesis. It was originally published as:

Krogh, S., J. Pomeroy and P. Marsh, 2017: Diagnosis of the hydrology of a small Arctic basin at the tundra-taiga transition using a physically based hydrological model, *Journal of Hydrology*, 550, 685-703, http://dx.doi.org/10.1016/j.jhydrol.2017.05.042.

Author contributions:

SK and JP designed the study. JP developed the CHRM modelling platform. SK performed the data collection, model setup and validation, and prepared the manuscript with contributions from JP to the manuscript structure, readability and analysis and discussion of the results. PM provided some of the data used in the study and contributed to the general discussion.

3.1 Introduction

The Arctic is a remote and extremely cold environment that has recently captured the attention of policy makers, engineers and scientists, particularly for the role of Arctic sea ice in global atmospheric and oceanic circulation (Budikova, 2009), observed climate change (Larsen and Anisimov, 2014) and permafrost degradation (Liljedahl et al., 2016). Precipitation and temperature changes all over Canada (including the Canadian Arctic) from 1948 to 2012 were studied by Vincent et al. (2015) and clearly showed warming (4 to 6°C) and an overall increase in precipitation with significant spatial variability.

The majority of the surface and subsurface physical processes describing the hydrology of Arctic river basins have been studied in detail, resulting in a good understanding of the main hydrological controls. The water year in the Arctic can be defined as starting after the fall-winter transition (beginning in October), during which temperatures cool rapidly, causing a substantial energy transfer from the relatively warmer ground to the atmosphere or the recently formed snowpack (Rouse, 1984). Snowfall may be intercepted by vegetation (forest or shrubs) and sublimate (Pomeroy et al., 1998). If it falls over shrubs, the snow load may bend and bury their branches, producing abrupt changes in surface albedo, especially during the quick spring transition, in which branches are re-exposed to the atmosphere (Endrizzi and Marsh, 2010; Ménard et al., 2012; Pomeroy et al., 2006). Tundra may be subject to significant blowing snow redistribution to vegetated surfaces such as shrubs and forest edges and to gullies and stream channels, and tundra snowpacks undergo sublimation during blowing snow transport (Essery and Pomeroy, 2004; Pomeroy et al., 1997; Pomeroy and Li, 2000). Spring snowmelt is the major hydrological event of the year, in which over 50% of the annual precipitation melts in a few weeks (Marsh et al., 2002; Marsh and Pomeroy, 1996). During snowmelt, partially or fully frozen ground with high ice content can restrict infiltration, producing overland flow or shallow subsurface flow (Kane, 1980; Kane and Stein, 1983; Quinton and Marsh, 1999) that may be delayed by the formation of snow-dams produced by drifts in the channels (Woo et al., 1980). Once ground has thawed, infiltration into the highly porous top organic soil layer (20 – 50 cm) is restricted by the water storage potential above the frozen layer (Gray et al., 2001; Kane and Stein, 1983; Woo and Steer, 1982), resulting in preferential subsurface flow as the dominant runoff mechanism (Kane et al., 1991; Quinton and Marsh, 1999). Subsurface runoff occurs as a shallow saturated "suprapermafrost groundwater" layer perched on top of the frost table (Quinton et al., 2000; Woo and Steer, 1982). As there is an exponential decline in hydraulic conductivity with depth in organic soils, the depth of thaw has an important control on the rate of subsurface flow (Carey et al., 2007; Quinton et al., 2000; Woo and Steer, 1983). The maximum thickness of the thawed layer defines the Active Layer Thickness (ALT) and the boundary with permafrost. The ALT controls both ground heat transfer (Halliwell and Rouse, 1987) and available soil water storage capacity for late summer (Woo, 2012, p. 216). ALT in regions such as the Boreal forest and tundra environments in northwestern Canada ranges from roughly 0.25 to 1.75 m (Woo et al., 2007).

Robust physically based hydrological models that include cold regions processes are required to diagnose the hydrological regimes of Arctic basins under climate change (Woo et al., 2008), as the complex surface and subsurface energy and mass balance hampers the successful application of conceptual models developed for more temperate regions. The relatively low density of stream gauges in the Arctic means that opportunities for calibration are limited and so model parameters must be identifiable from other observations, including those from remote sensing and research basin field studies (Pomeroy et al., 2013b). Several models have been developed for cold regions hydrology that include processes specific to the climate; however, not all have a strong physical basis. Examples of process-based hydrological models in Arctic environments are presented by Z. Zhang et al. (2000; ARHYTHM model), Kuchment et al. (2000), Schramm et al. (2007; TopoFlow model), Endrizzi et al. (2011; GEOtop Model) and Semenova et al. (2013; Hydrograph model), differentiating by the number of physical processes included and the complexity used to represent them. Although these models have strong physical bases for some hydrological processes, they lack either full representation of the hydrological cycle (i.e. summer and winter processes) or a robust physical representation of the key hydrological processes such as snowmelt, sublimation, and ground freeze-thaw or snow redistribution by wind and interception by vegetation.

The Cold Regions Hydrological Modelling platform (CRHM; Pomeroy et al., 2007) is a process-based, flexible, modular hydrological modelling platform that allows the selection of different modules from an extensive library to create a custom hydrological model. Each module represents a different approach to simulate hydrological processes. Many of the modules have a strong physical basis and describe the cold regions processes that are found in Arctic environments (Pomeroy and Marsh, 1997). CRHM has been applied in different regions, including China (Zhou et al., 2014), Patagonia (Krogh et al., 2015), Canadian Rockies (Fang et al., 2013; Pomeroy et al., 2016), German Alps (Weber et al., 2016), northern Canada (Rasouli et al., 2014) and Svaldbard (López-Moreno et al., 2016).

The purpose of this study is to investigate and reconstruct the dynamics of the water and energy budgets and resulting hydrological regime over a 28-year period for an Arctic basin underlain by permafrost in the tundra-taiga transition region. This investigation involves the implementation and validation of a comprehensive physically based cold regions hydrological model that couples atmosphere, surface and subsurface energy and mass fluxes.

3.2 Study site and available data

Havikpak Creek (HPC) was selected for diagnosis as the study basin as it is a relatively small (16.4 km^2) taiga-dominated Arctic basin in the transition treeline region, with previous hydrological process studies, good vegetation and topographic characterisation, an active, well-maintained stream gauge and high-quality driving meteorology. HPC is located 2 km north of Inuvik Airport, Northwest Territories (NWT), Canada (68.2°20'N 133°28'W) and discharges through a culvert under the Dempster Highway, which is the only road linking Inuvik with the airport and southern

Canada. This region is underlain by continuous permafrost from 350 m to over 575 m deep (Natural Resources Canada, 1995). HPC has moderate topography (mean slope of approximately 2°) and an elevation range from 60 to 240 m (Figure 3.1), with a primary SW aspect. HPC landcover classification was studied by Marsh et al. (1997) using Landsat Thematic Mapper images and a combination of supervised classification, cluster analysis, transformed thermal and vegetation indexes, and field validation. The result of this analysis was seven landcover classes: water, tundra, sparse shrub, closed shrub, sparse forest, open forest and closed forest, with forest representing over 50% of the HPC basin. The majority of the forest in HPC is comprised of black spruce taiga (*Picea mariana*) (Eaton et al., 2001), primarily restricted to the mid-low elevations (<140 masl); however, a smaller area of forest can also be found on well drained hillsides, and both shrub and some sparse tundra cover the highest elevations plateaux and gullies (Pomeroy and Marsh, 1997).

According to the Köppen-Geiger climate classification (Peel et al., 2007) the climate in Inuvik is subarctic, meaning cold temperatures, no dry seasons and cold summers. Based on the Canadian Climate Normals (1981-2010, Environment and Climate Change Canada (ECCC)), the mean annual temperature at Inuvik is -8.2 ^{o}C with a mean monthly temperature below zero from October to May, and a maximum summer temperature of 14.1 ^{o}C in July. Total mean annual precipitation is 241 mm, which is distributed throughout the year, with peak precipitation during summer between July and September. The mean annual number of days with precipitation above 0.2 mm is 130 (36% of the year), from which 93 days are associated with snowfall. Regional precipitation near HPC has a markedly decreasing south-north gradient. For example, Fort McPherson Airport weather station, located about 120 km southwest of HPC, has a mean annual precipitation of 298 mm, and Tuktoyaktuk Airport weather station, located about 160 km northeast of HPC, has a mean annual precipitation of 160 mm (Canadian Climate Normals, 1981-2010, ECCC). Precipitation variability within HPC is expected to be minimal as the basin length is only 6.5 km and localized summer convective activity is infrequent.

The location of ECCC weather stations near Inuvik, namely Inuvik Airport, Inuvik Upper Air and Inuvik Climate, are presented in Figure 3.1. General information about these stations is presented in Table 3.1.

Inuvik Airport station has been operating for the longest period and has experienced changes in its location over time. After the 1990s, there were changes in precipitation gauge type and the collection method, from manually emptied, Nipher-shielded Meteorological Service of Canada copper cylinders to automated, Alter-shielded Geonor storage gauges. Both Inuvik Climate and Upper Air have had Alter-shielded Geonor with automatic collection; these stations are adjacent to each other. Observed daily streamflow from 1995 to present for HPC basin is available from an ECCC Water Survey of Canada (WSC) hydrometric station downstream from the HPC crossing with the Dempster Highway (see Figure 3.1). Metadata associated with streamflow records acknowledge the great uncertainty associated with the measurements, particularly during the snowmelt period, as ice is found in the cross section of the hydrometric station. Snow water

equivalent on the ground has been measured regularly from 1960 to present by ECCC as a sequence of snow depth and density measurements along a sparsely shrub-covered transect surrounded by taiga forest near the Inuvik Climate station.

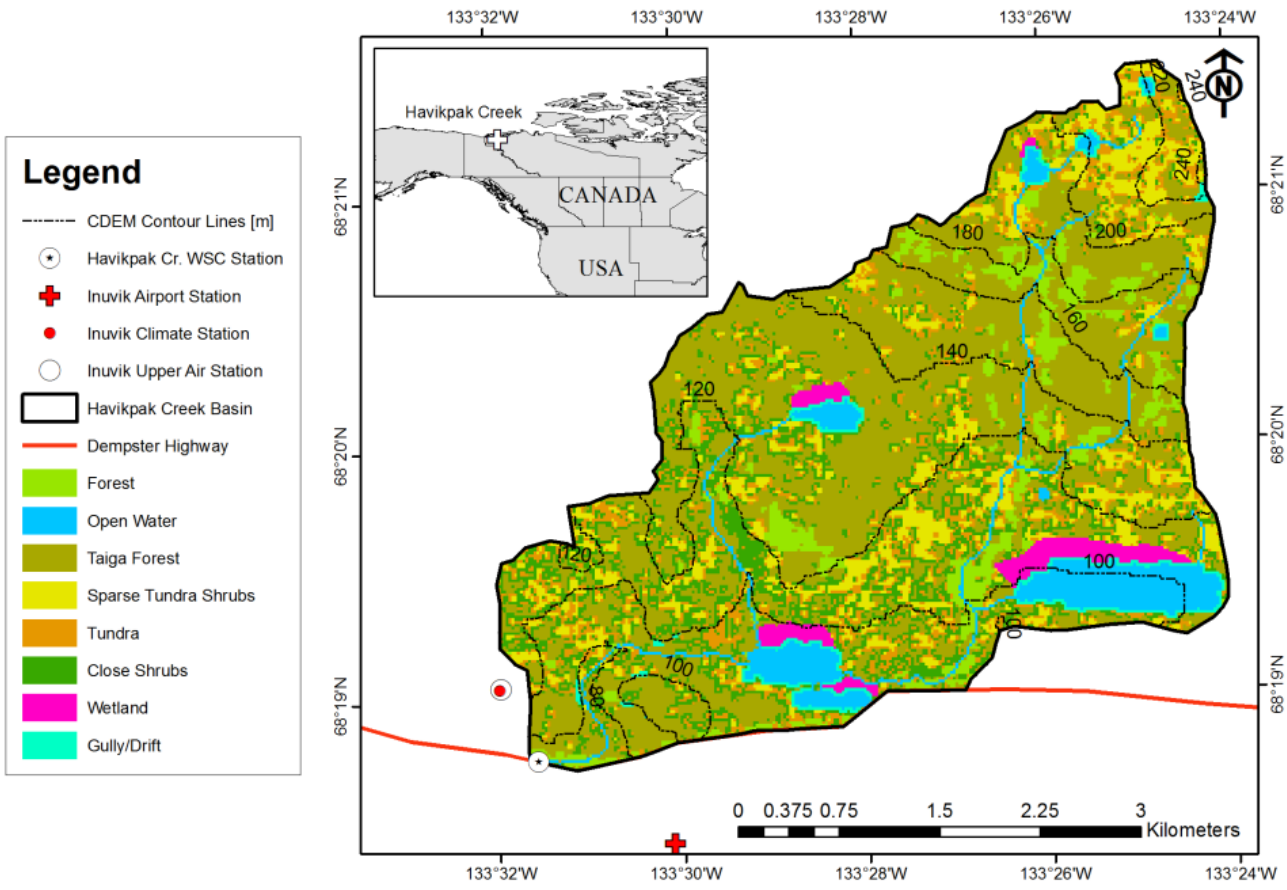

Figure 3.1. Havikpak Creek drainage area, landcover, hydrometric and weather stations.

Table 3.1. Available weather records from Environment and Climate Change Canada stations near Inuvik

EC station	Latitude	Longitude	Elevation (masl)	Start year	End year	Weather variables*	Time-step
Inuvik Airport	68º 18’ 14”	-133º 28’ 58”	67.7	1960	2005	Pp**	Daily
				1957	1979	T, RH, U	Daily
				1980	2013	T, RH, U	Hourly
Inuvik Climate	68º 18’ 59”	-133º 31’ 0”	103.0	2003	Present	Pp, T, RH, U, SD	Hourly
Inuvik Upper Air	68º 18’ 59”	-133º 31’ 0”	103.0	1995	2007	Pp, T, RH, U	Daily

* Pp: Precipitation (rain and snow), T: air temperature, RH: Relative Humidity, U: Wind Speed, SD: Snow Depth. ** There is a 1.5 years gap between June 1995 and January 1997.

3.3 Methodology

A flowchart describing input data sources and pre-processing, hydrological model setup, output data, validation and analysis is presented in Figure 3.2 to provide guidance to the methodology. In the next sections, a detailed description of each of these steps is provided

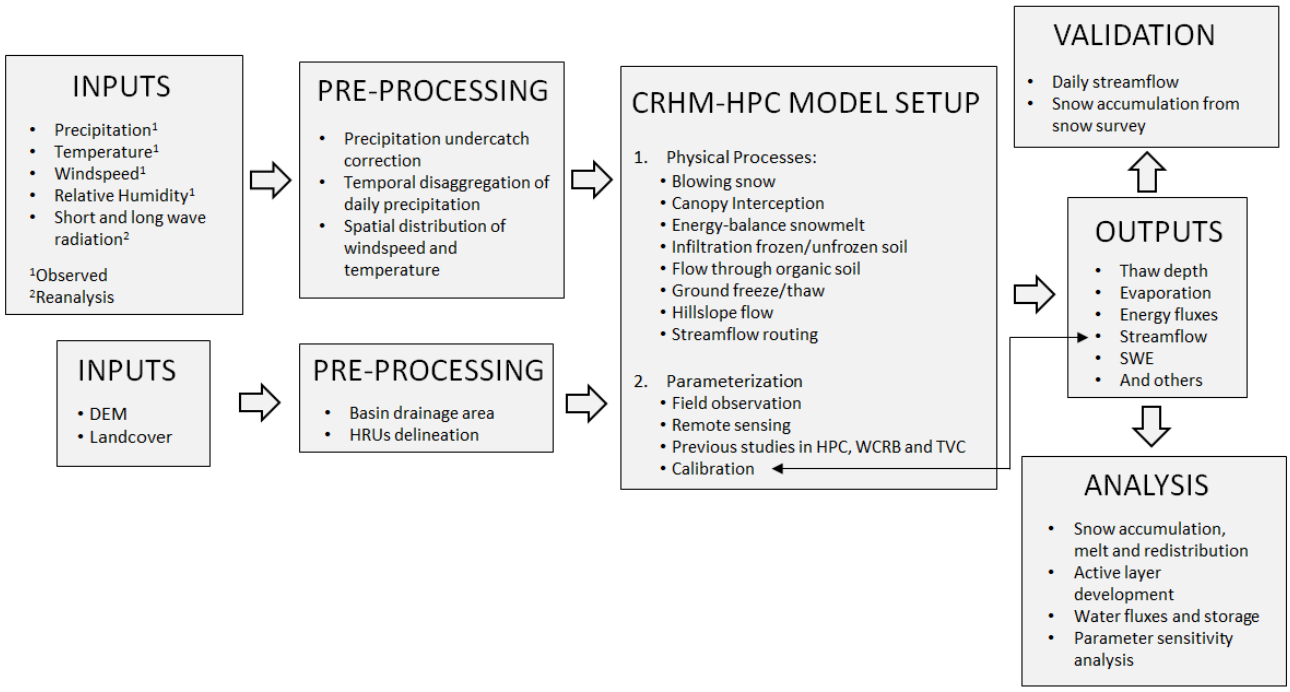

Figure 3.2 Modelling flowchart for Havikpak Creek (HPC). WCRB and TVC refer to two other research basins used in the parameterization section, namely Wolf Creek Research Basin, Yukon Territory and Trail Valley Creek, Northwest Territories

3.3.1 Weather forcing time series

To generate a single and continuous time series with weather forcing data for HPC in the period between 1980 and 2009, hourly records of temperature, wind speed and relative humidity from the Inuvik Airport station were used. Gaps in the hourly temperature records were filled using linear interpolation. Missing values for wind speed and relative humidity were filled as follows: (1) one-hour gaps were filled by linear interpolation and (2) the remaining gaps were filled with the hourly mean values calculated for each calendar month.

A continuous daily precipitation time series was reconstructed using data from (1) the Adjusted and Homogenized Canadian Climate Dataset (AHCCD; Mekis and Vincent, 2011) for the Inuvik station (station ID: 2202578) during the period between 1980 and 1995, which includes corrections for rainfall (wind speed at the orifice height, wetting of the funnel area, evaporation and wetting of the receiver or container) and snowfall (Nipher-shielded cylinder gauge wind undercatch and trace events); and (2) from a Alter-shielded weighing storage gauge wind undercatch corrected time series using daily and hourly precipitation recorded at Inuvik Upper Air (1995-2003; daily) and Inuvik Climate (2003-2009; hourly) stations.

3.3.1.1 Correction and temporal disaggregation of daily precipitation

Daily and hourly snowfall records from Inuvik Upper Air and Inuvik Climate stations were corrected for wind undercatch, using the expression developed by Smith (2008) for the Alter-shielded Geonor gauge. An hourly precipitation time series is preferred to force the hydrological model; therefore, a statistical disaggregation approach was implemented to disaggregate daily precipitation into hourly.

The temporal disaggregation of precipitation has been widely studied in the literature, particularly for hydrological applications (Gupta and Waymire, 1993; Onof et al., 2000). A common approach to disaggregate precipitation is by random cascade (Licznar et al., 2011; Molnar and Burlando, 2005). This approach is based on the assumption that, over different disaggregation levels (e.g. from 24 to 12 hr), some statistical properties are invariant (i.e. multiscaling properties; Gupta and Waymire (1990)). In this study, the multiplicative microcanonical random cascade model first created by Olsson and Berndtsson (1998) and further refined by Güntner et al. (2001) was used. The approach used in this study is referred to as the *Practical Experiment E24/0.75/1* by Güntner et al. (2001). Observed hourly precipitation from Inuvik Climate station was aggregated and used to calibrate the model and was then used to disaggregate daily precipitation from 1995 to 2009.

3.3.1.2 Spatial distribution of wind speed and temperature

Wind speed in the relatively calm lower elevations of HPC is not representative of the wind-swept upland tundra, as noted by Pomeroy and Marsh (1997). To overcome the misrepresentation of wind speed observation, Walmsley's parametric version of the Jackson-Hunt boundary layer windflow model (Walmsley et al., 1989) that simulates the effect of local topographic features was implemented. This model was developed to be used under moderate-to-high wind speeds, and it assumes a neutral thermal stratification and uniform surface roughness. The coefficients used for the upper tundra and shrubs are associated with a 3D rolling terrain, meaning moderate topographic changes in the three spatial dimensions. Temperature was spatially distributed based on elevation through a lapse rate estimated at 0.0074 $^{o}C\ m^{-1}$.

3.3.1.3 Atmospheric reanalysis data

Solar radiation records were not available for HPC; therefore, short- and long-wave radiation from atmospheric reanalysis were used to force the hydrological model. Reanalysis data has been used previously to overcome the lack of weather forcing data in remote regions for hydrological applications (e.g. Krogh et al., 2015). In this study the ERA-Interim (ERA-I; Dee et al. (2011)) reanalysis was used. Three-hour interval short- and long-wave radiation from ERA-Interim for the period between 1980 and 2009 was linearly interpolated over time to create an hourly time series.

ERA-Interim has a 0.75° spatial resolution; therefore, only one centroid (the closest) was used to extract the weather time series.

3.3.2 Basin delineation and landcover map

The HPC drainage area was estimated based on the Canadian Digital Elevation Model (CDEM – 20 x 20 m); Natural Resources Canada, 2013) using the Topographic Parameterization software (TOPAZ; Garbrecht and Martz, 1997) and the Arc Hydro Tool Version 2.0. Basin delineation was then manually corrected to account for the barrier effect of the highway, resulting in a 16.4 km^2 drainage area. The CDEM was smoothed using the *denoise* algorithm presented by Johns et al. (2003) to obtain a less disturbed aspect and slope map.

In this study the field-verified landcover classification from Marsh et al. (1997) was modified to include a Wetland class, as shown by the landcover classification from the Earth Observation for Sustainable Forest Development (EOSD; Wulder and Nelson (2003)), which is primarily covered by sparse shrubs. Also, sparse and open forest were merged in a new class called Taiga and, similar to Marsh et al. (1997), a Gully/Drift class was added where the slope is greater than 9° and around Open Water class. The vegetation in the Gully/Drift class is primarily sparse shrubs. Figure 3.1 presents the final landcover map used in this study, as well as the basin delineation.

3.3.3 Hydrological model configuration

CRHM is a spatially distributed model that uses Hydrological Response Units (HRUs; Kouwen et al., 1993)) to spatially discretize the basin. HRUs can be computed by grouping different climatological, biophysical and physiographic characteristics such as landcover, humid or arid areas, slope, aspect and elevation (Krogh et al., 2015; Pomeroy et al., 2007; Pomeroy et al., 2013a, 2013b) and need not be contiguous. HRUs for HPC basin were hierarchically defined by: (i) computing the main physiographic characteristics of the eight landcover classes (i.e. area, aspect and slope); (ii) assessing the need to split each landcover class by slope or aspect; and (iii) splitting the Tundra, Sparse Shrubs and Gully/Drift classes into two elevation bands, as the upper basin has a higher wind speed regime which is critical to properly represent blowing snow sublimation and redistribution (Pomeroy and Marsh, 1997). The result of this analysis is 11 HRUs (c.f. Table 3.2). Note that the basin was not discretized on slope or aspect, as the slopes are primarily mild (mean and maximum slope of 2.1° and 9°, respectively) and aspect is mostly southwest throughout the basin. The primary HRU physiographic characteristics are presented in Table 3.2. The model was run for the 30-year period between 1980 and 2009; however, the first two years were used to spin-up the model. These two years are relatively normal in terms of mean annual precipitation and temperature; therefore, they are considered as representative of the modelling period.

Table 3.2: HRU physiographic characteristics

HRU Name	Area (km^2)	Mean Elevation (m)	Mean Slope (°)	Mean Aspect* (°)
Upper Tundra	0.40	200	3.0	226
Lower Tundra	1.50	102	2.0	217
Upper Sparse Shrubs	0.65	207	2.8	234
Lower Sparse Shrubs	1.40	115	2.0	210
Closed Shrubs	2.60	116	2.1	226
Taiga	7.20	137	2.4	215
Forest	1.00	137	2.8	214
Upper Gully/Drift	0.05	200	4.2	235
Lower Gully/Drift	0.10	102	1.8	254
Wetland	0.40	109	2.5	187
Open Water	1.10	111	1.2	187

*0° is north and 180° is south.

A schematic representation of the key physical processes and mass fluxes governing the hydrological regime of HPC (and most Arctic basins in this region), classified into winter and summer processes, is presented in Figure 3.3. Key physical processes to simulate in this environment are precipitation phase, canopy snow/rain interception and sublimation/evaporation, snowmelt energy-balance, blowing snow sublimation and redistribution, evapotranspiration, overland runoff, infiltration into frozen and unfrozen soil, flow through organic terrain and mineral soil, ground freeze and thaw, and streamflow routing. In the CRHM platform, all of these processes

are represented by modules that can be included to generate a suitable model for this environment; hereafter this model will be referred as the CRHM Arctic Hydrology Model (AHM)

The approaches used by the CRHM-AHM to simulate each of these hydrological processes in modules are described in Table 3.3. In this table these modules are classified into atmospheric, land-atmospheric and land processes. A detailed description of the parameters used for each physical process module is provided in Section 3.4. The equations used in the ground and thaw algorithm are detailed next, as this is the first time they are used in the CRHM platform.

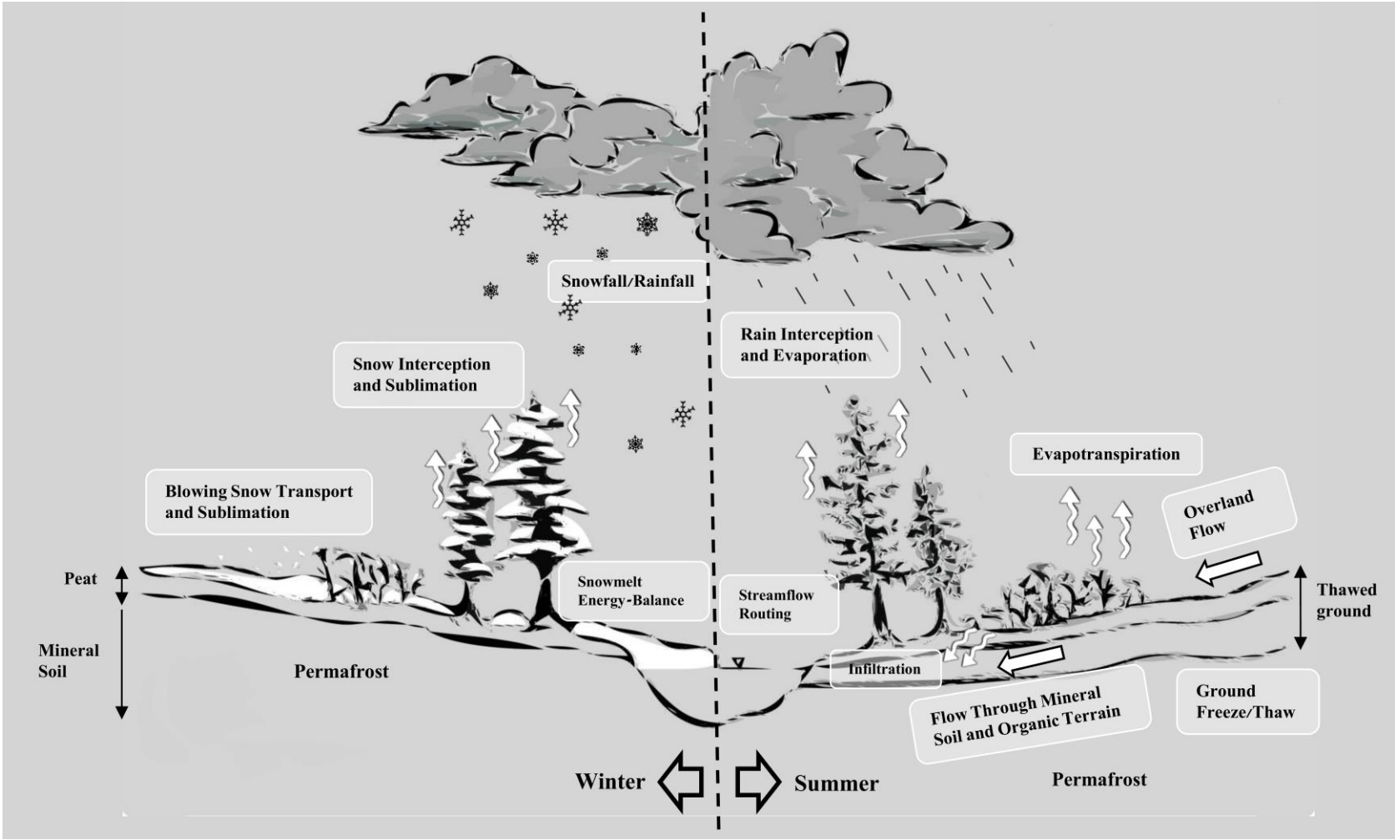

Figure 3.3 Conceptual model of Havikpak Creek Basin hydrology. Sketch by Lucia Scaff, University of Saskatchewan

.

Table 3.3 Physical processes included in the CRHM Arctic Hydrology Model (AHM)

Physical Process		**Simulation Approach**	**Main Characteristics**
Atmospheric	Precipitation Phase Partition	Harder and Pomeroy (2013)	This method estimates the phase of precipitation (rain or snow) using a psychrometric energy balance approach, based on the fall velocity, air temperature and the relative humidity.
Land-Atmospheric	Albedo Decay	Gray and Landine (1987)	Albedo decay rate is classified into three groups: premelt, melt and postmelt, each with a different decay rate for the snowcovered period. This model is suitable for cold shallow snowpacks that are not subject to frequent mid-winter melt events.
	Canopy Interception, Sublimation and Evaporation	The Rutter Interception Model (Valente et al., 1997) for rain interception, linked to growing season evapotranspiration. The Canopy Interception and Sublimation Model for the snow season (Ellis et al., 2010; Hedstrom and Pomeroy, 1998; Parviainen and Pomeroy, 2000; J. W. Pomeroy et al., 1998)	Both models estimate precipitation interception and phase change based on geometric characteristics of the forest cover (leaf area index, vegetation height and maximum canopy interception load) and atmospheric conditions (temperature, wind speed and vapour pressure).
	Snow Melt and Accumulation	A Snowcover Energy Balance Model (SNOBAL; Marks et al., 1998)	Two-layer energy balance model that allows refreezing and uses the bulk transfer method with stability correction (Monin and Obukhov, 1954) to calculate turbulent heat fluxes. Lower layer snow temperature forms an upper boundary condition for soil

Physical Process		Simulation Approach	Main Characteristics
			freeze-thaw calculations in winter using the XG module.
	Evapotranspiration	Penman-Monteith Algorithm (P-M; Monteith, 1981) for unsaturated surfaces and Priestley-Taylor (Priestley and Taylor, 1972) for saturated surfaces. Jarvis (1976) to estimate stomata resistance changes.	P-M calculates actual evapotranspiration over non-saturated surfaces based on net radiation, stomata resistance and surface roughness. Stomata resistance is calculated based on a minimum resistance and four coefficients (>1) related to atmospheric and ground conditions. Priestley-Taylor is a simplified, net radiation based method for saturated surfaces that includes horizontal advection of energy.
	Blowing Snow Transport, Sublimation and Redistribution	Prairie Blowing Snow Model (PBSM; Fang and Pomeroy, 2009; Pomeroy and Li, 2000)	Steady-state two-phase flow model that calculates snow saltation and suspension based on friction velocity, aerodynamic roughness height, exposed vegetation and fetch distance. A coupled sublimation algorithm integrates the sublimation of a single ice particle over the saltation and suspension layers and rescales this to bulk sublimation.
Land	Ground Thaw-Freeze	A simplified solution of Stefan's heat flow equation, the XG – algorithm (Changwei and Gough, 2013)	Simplified solution for Stefan's equation that can be implemented for multi-layered soils, based on layer depth and thermal conductivity. It assumes a linear temperature distribution in the thawed or frozen layers.
	Ground surface temperature	Radiative-conductive-convective approach (Williams et al., 2015)	Semi-empirical approach that uses air temperature, net radiation and antecedent frost table depth to estimate ground surface temperature as an upper

Physical Process		Simulation Approach	Main Characteristics
			boundary condition for XG in the snow-free period.
	Water flow through snowpack and organic layer	Detention flow layer (Pomeroy et al., 2016)	Water flow detention produced by the celerity of flow through the snowpack or exposed organic layers above soil is calculated as per Pomeroy et al. (2016) based on Colbeck (1975, 1972) and relationships between permeability, water pressure and saturation.
	Soil Infiltration	Infiltration into unfrozen soils using Ayers (1959) and into frozen soils using Gray et al. (2001).	Infiltration into unfrozen soils is based on an empirical relationship between ground cover condition (e.g. bare soil or forested) and soil texture. For frozen soils, infiltration is first classified as unlimited, restricted and limited. For limited infiltration, parameterization of a finite difference heat and mass transfer model is based on initial surface saturation, average soil saturation and temperature, and infiltration opportunity time.
	Soil Moisture	A three-layer soil model (Pomeroy et al., 2007). Subsurface vertical and lateral drainage controlled by effective hydraulic conductivity using the Brooks and Corey (1964) relationship.	Three-layer model includes a recharge, lower and groundwater layer. The Model allows for infiltration excess or saturation-excess overland flow, surface runoff, recharge through macropores and subsurface discharge (Fang et al., 2013). Here, no sub-permafrost groundwater recharge is allowed due to ice-rich soils and shallow active layer. Lateral and vertical flows are calculated based on Darcy's law using the unsaturated hydraulic conductivity calculated with the Brooks and Corey (1964) relationship. This module is linked to

Physical Process		Simulation Approach	Main Characteristics
			XG and all water and storage capacity in the frozen layer is considered immobile and inaccessible. Liquid water below a frozen layer may drain vertically or horizontally but not be recharged from above. Liquid water above a frozen layer is restricted to the unfrozen layer and may drain horizontally and be recharged or withdrawn by evapotranspiration.
	Surface and Subsurface Routing	Lag and Storage(Clark, 1945)	Clark's lag and storage for subsurface routing between HRUs.

In this study, the sub-permafrost groundwater layer is neglected, as the expected shallow active layer (e.g. between 0.4 and 0.8 m for Siksik Creek – 50 km from HPC; Quinton and Marsh, 1998) and ice-rich soils restrict percolation and exfiltration of groundwater in the region (Woo and Marsh, 2005); however, supra-permafrost groundwater is represented by the soil moisture module. The presence of taliks underneath the lakes and ponds in HPC is unknown and not included in the CRHM-AHM; however, if deep taliks were present, they could potentially create zones of connectivity between supra- and sub-permafrost groundwater (open taliks) as have been observed in other continuous and discontinuous permafrost regions (Johansson et al., 2015; Rowland et al., 2011). To assess properly the presence of taliks, geophysical exploration techniques or ground-based observations are required. Here, the lack of deep groundwater contribution is indicated by the absence of winter streamflow in HPC; however, this could potentially change in the future, as groundwater connectivity may increase with decreasing permafrost (Walvoord et al., 2012).

3.3.3.1 The new ground freeze/thaw algorithm included in CRHM

A new feature in the CRHM platform is explored and introduced in this study, which is the implementation of the XG-algorithm (Changwei and Gough, 2013) as a module to simulate ground freeze and thaw. The XG-algorithm provides a simplified solution for Stefan's equation (Juminikis, 1977) to represent heat transfer in multi-layered soils with non-uniform soil properties (e.g. thickness, thermal conductivity and porosity). This equation considers only the latent heat of fusion (energy released when freezing or absorbed when thawing) and ignores the volumetric heat capacity of the soil. Stefan's equation for a homogeneous soil is presented in Equation 3-1.

$$\xi = \sqrt{\frac{2kF}{Lw\rho}}$$ *Equation 3-1*

Where ξ is the frost/thaw front depth, k is the thermal conductivity of the soil (W m^{-1} K^{-1}), F is the surface freeze/thaw index (^oC degree-days), L is the latent heat of fusion (J kg^{-1}), w is the volumetric water content (m^3 m^{-3}), and ρ is the bulk density of the soil (kg m^{-3}). Changwei and Gough (2013) defined the ratio P_{12}:

$$P_{12} = \frac{\xi_1}{\xi_2} = \left(\frac{k_1\rho_2 w_2}{k_2\rho_1 w_1}\right)^{0.5}$$ *Equation 3-2*

where *1* and *2* are two vertically adjacent soil layers. The P_{12} ratio is the ratio between the frost/thaw front depth of soil layer 1 and 2, which is defined only by the physical properties of each soil layer, and not by the freeze/thaw index (F). By using a given freeze/thaw index, Equations 3-1 and 3-2, and the concept of a "residual freeze/thaw index", Changwei and Gough (2013) deduced a simple relationship to estimate the freezing/thawing depth in a two layered soil system, which can be reduced to the following equation:

$$\xi = \begin{cases} \sqrt{\frac{2k_1F}{Lw_1\rho_1}} & if\ F \le F_1 \\ Z_1 + \frac{\xi_1 - Z_1}{P_{12}} & if\ F > F_1 \end{cases}$$ *Equation 3-3*

where Z_1 is the thickness of the first soil layer (m) and F_1 is the freeze/thaw index required to freeze/thaw the first layer. Equation 3-3 can be easily generalized to calculate the freeze/thaw of an n-layered soil system, which has shown good results as demonstrated by *Changwei and Gough* (2013). The thermal conductivity of each soil layer is estimated using the expression developed by Johansen (1975, p. 221) for unfrozen and frozen soils, based on their degree of saturation, as presented in Equation 4 and 5, respectively.

$$\sqrt{k_U - k^0} = \sqrt{k^l - k^0} * S_r$$ *Equation 3-4*

$$k_F = k^0 * \left(\frac{k^l}{k^0}\right)^{S_r}$$ *Equation 3-5*

where k_U and k_F is the thermal conductivity of unfrozen and frozen soil, respectively, k^0 is the dry thermal conductivity of the soil, k^l is the saturated thermal conductivity and S_r (m^3 m^{-3}) is the degree of saturation of the soil. The units of the thermal conductivity are (W m^{-1} K^{-1}).

3.3.4 CRHM-Arctic Hydrology Model parameterization

Parameterization was performed using the deduction, induction, abduction (DIA) approach (Pomeroy et al., 2013a) as follows: (1) physiographic and vegetation parameters such as slope, aspect and vegetation type were obtained from the DEM and landcover map; (2) parameters from previous studies by Pomeroy and Marsh in HPC basin (Pomeroy et al., 1999; Pomeroy and Marsh, 1997; Marsh et al. 1997); and (3) transferring parameters from other basins with similar hydrological regimes (e.g. Trail Valley Creek, NWT (Pomeroy et al., 1997) and Wolf Creek, Yukon (Carey and Woo, 2005). The latter has shown to be a valid and successful parameter transfer approach (Dornes et al., 2008). Parameters that could not be defined using the DIA approach were calibrated (next section).

3.3.4.1 Deduction, Induction and Abduction approach (DIA)

3.3.4.1.1 Snow accumulation, melt and distribution

The albedo decay function (Gray and Landine, 1987) requires a maximum and minimum albedo, associated with fresh snow and snow free conditions, respectively. The albedo range for Open Water landcover was set to 0.9 for fresh snow (Marsh et al., 2002) and 0.1 for snow free conditions, whereas for Tundra, Tundra Shrubs, Taiga and Forest, fresh snow albedo was set to 0.8 and snow free to 0.15 (Eugster et al., 2000; Ménard et al., 2012). Snow surface roughness used by SNOBAL was set to 0.001, m similar to the one estimated by Marsh and Pomeroy (1996) and Neumann and Marsh (1998) in this region. The maximum value for the liquid water holding capacity of snow was set to 0.01 mm $mm^{-1,}$ as recommended by Marks et al. (1998). Fresh snow density was assumed to be 100 kg m^{-3}, as presented by Ménard et al. (2012) for Trail Valley Creek. SNOBAL requires observed ground temperatures to estimate ground heat flux, which are not available for HPC; here, a constant temperature of -4 °C at 10 cm from the ground surface is assumed. Leaf Area Index (LAI), used by the canopy interception module, was estimated at 0.25 and 1.2 m^2 m^{-2} (Pomeroy et al., 1999) for shrubs and forest, respectively. The maximum snow load capacity was set to 5.9 kg m^{-2}, as used by Pomeroy et al. (1998) for Black Spruce in the Canadian boreal forest and 0.5 kg m^{-2} for shrubs as used by Rasouli et al. (2014) in Wolf Creek Research Basin, Yukon. Blowing snow transport in the upper basin was simulated following the sequence from Tundra to Shrubs and Gully/Drift HRUs, with fetch of 1000 and 3000 m for Upper Tundra and Upper Shrubs HRU, respectively, according to the values observed by Pomeroy and Marsh (1997). For the lower elevations, the blowing snow redistribution sequence starts from Lower Tundra and Open Water to Lower Shrubs and then to Lower Gully/Drift HRUs, with fetch values of 40, 500, 1000 and 3000 m for the Gully/Drift, Tundra, Shrubs and Open Water HRUs, respectively, following observations made by Pomeroy and Marsh (1997).

3.3.4.1.2 Surface runoff

Surface runoff in all HRUs represents overland flow, except Open Water, where it represents streamflow. This flow occurred through the snowpack as porous media flow at the Darcy velocity, as described in the next section. When snow-free, this flow occurred only when the detention layer did not exist (Open Water) or for runoff in excess of that, which could be held in detention in the upper organic layer. For both cases, the routing of surface runoff was modelled using Clark's lag and route hydrograph technique (Clark, 1945). Two parameters were required: storage and lag constant. These parameters were calibrated and assumed constant amongst HRUs with the same land cover (Table 3.6).

3.3.4.1.3 Subsurface and hillslope flow

Many studies have acknowledged the predominance of subsurface runoff and storage in tundra-dominated Arctic environments near Inuvik (e.g. Quinton, 1997; Quinton and Marsh, 1999), especially for the high water-holding capacity of these soils (Quinton et al., 2000). Figure 3.4 shows the soil representation used in the CRHM-AHM, which is composed of three layers representing upper peat, lower peat and mineral soil layers. This three-layer system has been identified by other studies in similar environments (Carey and Woo, 2005; Quinton and Marsh, 1999). Carey and Woo (2001), Quinton and Marsh (1999) and Quinton et al. (2000) present value for the saturated hydraulic conductivity of the upper and lower peat layer in the order of 10^{-3} and 10^{-4} (m s^{-1}), respectively, in Arctic and subarctic environments. These orders of magnitude are used in the calibration scheme presented in Section 4.2. Soil porosity measured by Quinton (1997, p. 59) shows that the active porosity in the upper organic layer ranges from 0.75 to 0.85 and for the lower organic layer ranges between 0.5 and 0.8. The porosity of the mineral soil layer was measured by Carey and Woo (2005) in a subarctic basin, with an average value of 0.5. In this study, we set the porosity of the upper and lower peat, and mineral soil at 0.8, 0.8 and 0.5, respectively. The thickness of the upper organic layer was estimated at 10 cm and the lower organic layer between 30 and 40 cm (c.f. calibration section), as presented by Quinton and Marsh (1999). Mineral soil thickness is more uncertain; however, its water storage potential depends on the thaw depth.

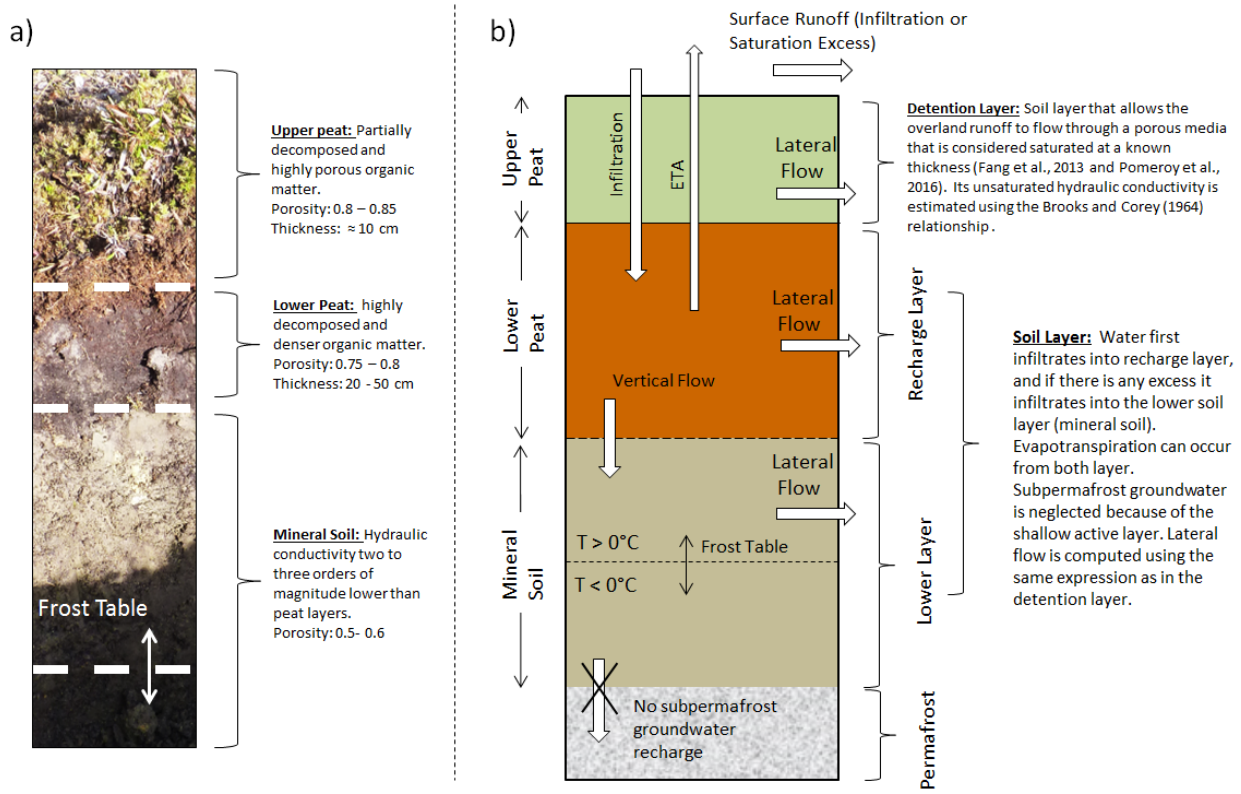

Figure 3.4 a) General soil profile characterization and flow paths for a tundra-dominated landscape in an Arctic environment. Soil layers values taken from Quinton and Marsh (1999) in Siksik Creek Basin (55 km northeast of Inuvik, NWT). Soil profile picture was taken from a soil pit in the Ogilvie Mountains, Km Post 152 Dempster Highway (65°4'0.8" N, 138°14'46.1" W). b) Conceptual representation with three layers used in CRHM to simulate soil moisture transport and storage.

The velocity at which water moves vertically from the upper recharge layer to the lower layer was estimated using Darcy's law and the Brooks and Corey (1964) relationship for unsaturated hydraulic conductivity, which depends on the saturated hydraulic conductivity, the pore size distribution index and the degree of saturation of the soil. The pore size distribution for peat was estimated at 5.6, as presented by Zhang et al. (2010) for a subarctic basin (Scotty Creek Peat Plateau) in the Northwest Territories. Lateral flow was simulated using the same method, but with a correction for the ground slope. Subsurface flow routing between HRUs was simulated using Clark's hydrograph (Clark, 1945), which is based on a lag and a storage coefficient estimated through calibration.

3.3.4.1.4 Permafrost thaw and freeze

Ten sub-surface layers with a uniform thickness of 10 cm were used to simulate ground freeze/thaw in the first metre, and ten more layers with a uniform thickness of 20 cm were used for the lower two metres. The top four layers represent the upper and lower peat layers with a porosity of 0.8, a thermal conductivity for dry unfrozen peat of 0.06 W m^{-1} K^{-1}, a frozen saturated hydraulic conductivity of 1.9 W m^{-1} K^{-1} and a saturated unfrozen thermal conductivity of 0.5 W m^{-1} K^{-1} (Woo, 2012, p. 48). The mineral soil layer was represented by the remaining 16 layers with a porosity of 0.5, a thermal conductivity for dry unfrozen mineral soil of 0.25 W m^{-1} K^{-1} (Woo, 2012, p. 48), a frozen saturated hydraulic conductivity of 1.8 W m^{-1} K^{-1} (Johansen, 1975, p. 222) and a saturated unfrozen thermal conductivity of 1.2 W m^{-1} K^{-1} (Farouki, 1981, p. 104).

3.3.4.1.5 Evapotranspiration

Evapotranspiration was simulated using the Penman-Monteith (Monteith, 1981) algorithm, except for Open Water and Wetland HRUs, for which the Priestley and Taylor (Priestley and Taylor, 1972) method was used. Average shrub height was estimated at 1.75 m based on field observations and the range presented by Marsh et al. (1997) of 0.5 to 3 m, whereas the average taiga and forest height was estimated at 6 and 8 m, respectively, also based on field observations. Winter Leaf Area Index (LAI) for both Shrub and Forest HRU was set to 0.25 and 1.2 m^2 m^{-2} (Pomeroy et al., 1999). Eugster et al. (2000) compiled a series of land-atmosphere energy exchange parameters for different vegetation types in Arctic environments, including the maximum canopy conductance. From these values, the stomata resistance parameters for the Penman Monteith model were set. For low Arctic tundra under wet non-coastal conditions, Eugster et al. (2000) present values from 76 to 147 s m^{-1}, whereas for tundra shrubs in the low Arctic, values from 150 to 153 s m^{-1} are given. For non-closed spruce forest in an open subarctic environment, a value of 90 s m^{-1} is presented by Eugster et al. (2000). Based on the values compiled by Eugster et al. (2000), the minimum stomata resistance values of 76, 150, 90 and 90 s m^{-1} were set for Tundra, Tundra Shrub, Taiga and Forest HRU, respectively. Ground heat flux for evapotranspiration during the ground thaw season was estimated at 18% and 16% of net radiation based on the observations presented by Rouse (1984) for tundra and forest, respectively.

3.3.4.2 Calibration

The majority of the parameters required to run the model were set either from field observations or other studies in the region. However, parameters related to subsurface and surface hydraulics and storage were unknown or highly uncertain (see Table 3.6). The Dynamically Dimensioned Search algorithm (DDS) from Tolson and Shoemaker (2007) was implemented to automatically estimate these parameters by maximizing the Nash and Sutcliffe (1970) coefficient. DDS has been

implemented in other cold regions hydrology modelling studies (Dornes et al., 2008; Rasouli et al., 2014). Daily records from 1995 to 2004 were used for calibration and from 2006 to 2009 for validation (no streamflow records are available for 2005).

3.3.5 Model sensitivity and uncertainty analysis

The new state-of-the-art Global Sensitivity Analysis framework (VARS) presented by Razavi and Gupta (2016a, 2016b) was used to assess the sensitivity of streamflow performance, using the Nash-Sutcliffe coefficient, to parameter uncertainty. The following six parameters were used in the analysis, selected from an informal evaluation of their uncertainty and model process sensitivity to their values: (1) Leaf Area Index ('LAI' $m^2 m^{-2}$), (2) Maximum Canopy Snow Load Capacity ('Sbar' kg m^{-2}), (3) Minimum Stomata Resistance ('rcs' s m^{-1}), (4) Saturated Hydraulic Conductivity ('Ks' m s^{-1}), (5) Soil Recharge Layer Capacity ('Soil Recharge' mm) and Vegetation Height ('Ht' m). Parameter ranges used for the analysis are presented in Table 3.4 and are based on values from the literature for this region and field observations. The saturated hydraulic conductivity of the upper and lower peat layers was varied, such that the lower peat layer hydraulic conductivity was always one order of magnitude smaller than the upper layer, in order to avoid a lower peat layer with a greater hydraulic conductivity, which is contrary to observations in the region and soil development principles (Carey and Woo, 2001; Quinton and Marsh, 1999). The VARS framework uses a sampling strategy called "star based" as it requires a number of "stars" to sample parameter combinations. In this study 20 stars were used, resulting in 1,100 combinations; this was considered appropriate for this application (S. Razavi, personal communication, 2016).

As a secondary goal, the uncertainty of the mean annual mass balance associated with these parameters was also assessed using the same "star-based" sampling strategy used for the sensitivity analysis. This means that 1,100 parameters scenarios were run and the mass balance was computed for each parameter scenario.

Table 3.4 Parameter range for the VARS sensitivity analysis

Parameters		**Tundra**	**Shrubs**	**Closed Shrubs**	**Taiga**	**Forest**
Leaf Area Index* (m^2 m^{-2})	Upper Limit	n/a	0.3	0.6	0.96	1.44
	Lower Limit	n/a	0.2	0.4	0.64	0.96
Vegetation Height* (m)	Upper Limit	0.24	2.1		7.2	9.6
	Lower Limit	0.36	1.4		4.8	6.4
Maximum Canopy Snow Load Capacity* (kg m^{-2})	Upper Limit	n/a	0.6		7.08	
	Lower Limit	n/a	0.4		4.72	
Stomata Resistance* (s m^{-1})	Upper Limit	91.2	180		108	
	Lower Limit	60.8	120		72	
Saturated Hydraulic Conductivity of the Upper Organic Layer (m s^{-1})	Upper Limit	1E-01				
	Lower Limit	1E-05				
Saturated Hydraulic Conductivity of the Lower Organic Layer (m s^{-1})	Upper Limit	1E-02				
	Lower Limit	1E-06				
Soil Recharge (mm)	Upper Limit	500				
	Lower Limit	300				

*The upper and lower limit is defined as a ±20% from the original value.

3.4 Results and discussion

3.4.1 Precipitation correction and temporal disaggregation

Corrected mean monthly precipitation and temperature for the period between 1980 and 2009 is presented in Figure 3.5. Corrected mean annual precipitation is 327 mm yr^{-1}, as opposed to the 240.6 mm yr^{-1} from ECCC Climate Normals, resulting in an increase of roughly 36%. This is

consistent with wind undercatch corrections suggested for northern Canada by Pomeroy and Goodison (1997) and more recent corrections by Pan et al. (2016) for relatively open sites. Validation of the temporal disaggregation of precipitation is presented in Table 3.5. The disaggregation approach successfully represents the main statistics, where the greatest errors are found for skewness and autocorrelation lag-1 (around 13.2% and 15.5%, respectively). Therefore, this method is considered valid for this region, as the assumption of a fractal behaviour in the frequency distribution function of the weight factors (Güntner et al., 2001) was met (not shown here).

Table 3.5 Comparison of statistics between observed and disaggregated hourly precipitation

Statistics (2005 – 2014)	**Mean hourly precipitation (mm)**	**Variance (mm^2)**	**Skewness (.)**	**Probability of Dry Hour (.)**	**Autocorrelation Lag-1 (.)**
Observed	0.025	0.053	34.92	0.935	0.309
Microcanonical Model	0.025	0.051	39.62	0.916	0.36
Bias Error (%)	0%	3.8%	-13.2%	2.0%	-15.5%

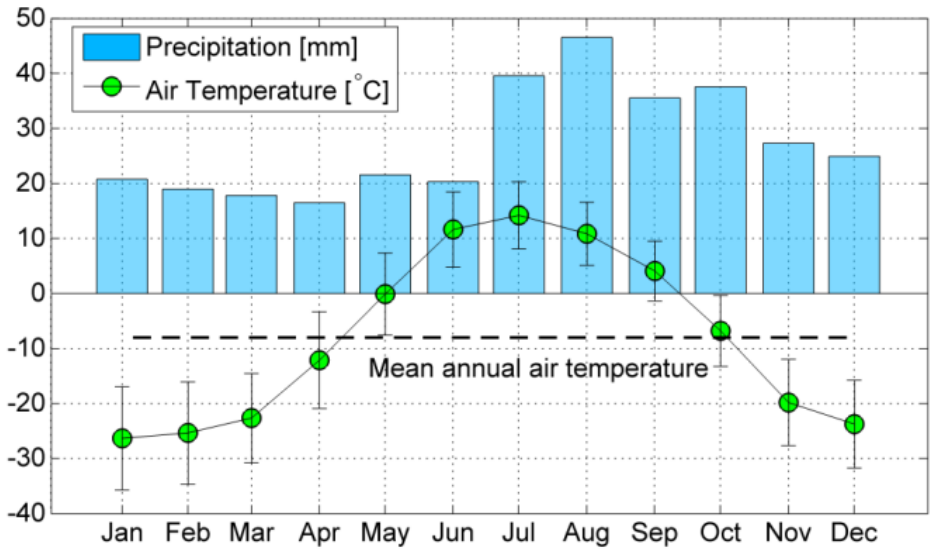

Figure 3.5 Wind-corrected precipitation and air temperature based on Inuvik Airport, Inuvik Climate and Inuvik Upper Air MSC stations - period from 1980 to 2010. Temperature error bar corresponds to the standard deviation.

3.4.2 Model calibration and validation

Parameter ranges used for calibration and their optimum values after 1,000 iterations using the DDS algorithm are presented in Table 3.6. Saturated hydraulic conductivity for the upper and lower peat layer show similar values, both close to $1x10^{-3}$ m s^{-1}. The conceptual nature of routing parameters (storage and lag) precludes a detailed interpretation of the values obtained through calibration; however, a consistent result is the higher subsurface lag and storage associated with forest, which is likely due to its larger contributing area. Also, open water and wetland have consistent small surface lag and storage parameter, which is in agreement with the faster response expected from a saturated surface.

Table 3.6 Parameters and ranges used in the DDS calibration algorithm. 1,000 iterations were performed.

Parameter	**Land Cover**	**Optimization Range**	**DDS Optimum value**
Subsurface Routing Storage (days)	Tundra	0 - 10	0.99
	Shrubs		0.3
	Forest		9.9
	Wetland		9.7
Subsurface Routing Lag (hours)	Tundra	0 - 100	2.8
	Shrubs		32.3
	Forest		98.9
	Wetland		0.25
Surface Routing Storage (days)	Tundra	0 – 10	9.9
	Shrubs		0.01
	Forest		9.8
	Wetland		0.1
	Open Water		0.1

Parameter	Land Cover	Optimization Range	DDS Optimum value
Surface Routing Lag (hours)	Tundra	0 – 100	12.3
	Shrubs		0.2
	Forest		0.1
	Wetland		0.02
	Open Water		0.8
Maximum Recharge Layer Capacity (mm)	All (but Open Water)	300 – 500	325
Saturated Hydraulic Conductivity ($m\ s^{-1}$)	Upper Peat	$[1 – 9.9] \times 10^{-3}$	1.04×10^{-3}
	Lower Peat	$[1 – 9.9] \times 10^{-4}$	9.88×10^{-4}
Maximum Snow Water Storage Capacity in Detention Layer (mm)	All	0 – 100	1.1
Depression Storage (mm)	Wetland	0 – 200	17

Simulated and observed hydrographs for the calibration and validation periods are presented in Figure 3.6a and Figure 3.6b, respectively. Nash-Sutcliffe (NS) coefficients for the calibration and validation periods are both 0.41, whereas mean BIAS is 6.8% and 9.1%, respectively. Snowmelt runoff largely dominates the hydrograph; therefore, it is important to capture the timing and magnitude of snowmelt. Peak streamflow timing is generally well represented by the model, as well as the recession limb of the hydrograph. Streamflow from rainfall-runoff events is less frequent and significantly smaller than streamflow from snowmelt events.

Great inter-annual variability in simulated streamflow performance is observed, as years with NS up to 0.79 and down to negative values exist; similar results are observed for the model BIAS. This indicates problems with the modelled streamflows, which may be due to field-observed parameter uncertainty, model structure (e.g. HRU discretization) and weather forcing data uncertainty; however, this can also be partially explained by the significant uncertainty in streamflow observations, particularly in the magnitude of peak streamflows, as acknowledged by WSC. The quality of observed streamflow is significantly impacted by the formation of ice in the stream cross section, producing a variable cross section that makes the use of previously defined

rating curves problematic. Drifted snow in channels can also cause uncertainty in streamflow measurements, particularly at the beginning of the melt season. The model was compared to observed streamflow for all the years with data, including those with acknowledged great uncertainty.

Figure 3.6c and Figure 3.6d present the probability distribution of daily streamflow and the cumulative mean daily streamflow for simulated and observed streamflow, respectively, during the period 1995 to 2009 (excluding 2005). The probability distribution of simulated daily streamflow shows relatively good agreement with observation; however, low exceedance probability streamflows are slightly underestimated due to difficulties in simulating peak flows in 2000, 2001 and 2006. Cumulative mean daily streamflow shows an adequate performance, particularly during snowmelt (days of the year between 120 and 160); however, the model slightly overestimates streamflow during summer.

Figure 3.7 presents a comparison between simulated and observed Snow Water Equivalent (SWE). Simulated SWE shows an adequate performance, especially during the accumulation period; although for some years, such as 2005, SWE is underestimated. Errors in simulating maximum snow accumulation are probably associated with uncertainty in the precipitation records and local snow redistribution processes that may be over-simplified in the model or not well represented along the snow survey transect due to local site and scale differences. Overall, the model presents relatively good agreement with observations, especially when considering the uncertainties aforementioned and the complex environment, and therefore, it is deemed suitable for further analysis.

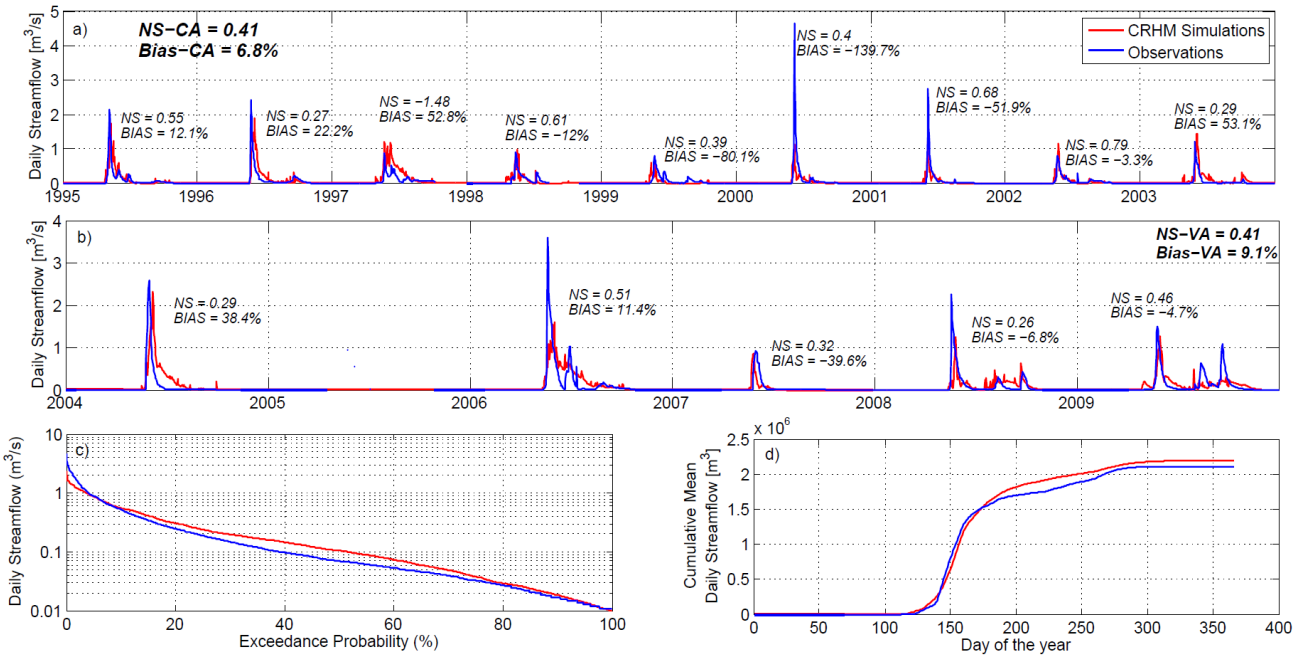

Figure 3.6 a) and b) Daily streamflow for the calibration (CA) and validation (VA) periods, respectively. Nash-Sutcliffe (NS) and Bias are presented for each water year and each full period (bold). No streamflow records are available for the year 2005. c) Daily observed and simulated streamflow frequency distribution using a Weibull distribution and d) cumulative observed and simulated mean daily streamflow. c) and d) use data from CA and VA period (1995 to 2009).

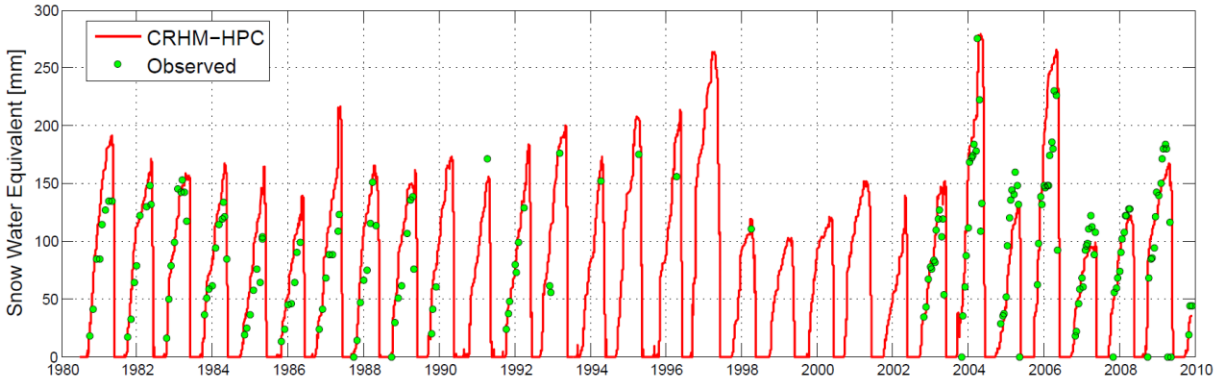

Figure 3.7 Observed from a snow survey transect versus simulated snow water equivalent at the Lower Shrub HRU.

3.4.3 Snow accumulation, melt, and redistribution

Figure 3.8 presents simulated average annual HRUs winter mass fluxes between 1982 and 2009. The Wetland HRU is not shown, as the winter mass fluxes are very similar to the Lower Shrubs HRU. The mass fluxes included are cumulative drift out/in, cumulative sublimation from the snow surface, cumulative blowing snow sublimation, cumulative canopy interception and sublimation, and daily SWE. SWE exhibits a substantial variability amongst HRUs, with maximum accumulation values from 67 mm for the Upper Tundra up to 475 mm for the Upper Drift/Gully HRU. The great variability in SWE is due to blowing snow redistribution and sublimation in the upper basin and snow interception and sublimation from canopy. Higher wind speeds in the upper elevations, together with poorly vegetated tundra, allow significant sublimation and transport of blowing snow. As shown in the upper left panel in Figure 3.8, blowing snow in the Upper Tundra HRU starts in early October and sublimates up to 76 mm yr^{-1} by the end of the winter; this is 40% of the average snowfall. Blowing snow transport redistributes 35 mm yr^{-1} to the Upper Shrubs HRU. Blowing snow redistribution in the lower basin is much smaller, as can be seen in the lower right panel in Figure 3.8; only 114 mm yr^{-1} is transported to the Lower Drift/Gully HRU, as compared to 316 mm yr^{-1} transported to the Upper Drift/Gully HRU. This difference is explained by the distinct wind regimes simulated by Walmsley's windflow model (c.f. Section 3.1.2), resulting in wind speeds being 55% higher in the upper basin. Sublimation from canopy interception also plays an important role in the snow mass balance, particularly in the Forest and Taiga HRUs, for which 88 and 25 mm yr^{-1} are sublimated, respectively. Sublimation of intercepted snow also occurs from Lower Shrubs, Closed Shrubs and Wetland HRUs; however, these values are small, at 4 to 7 mm yr^{-1}, as the maximum canopy snow interception load and LAI are significantly smaller (c.f. Section 3.4.1) than those found in the forested sites. Snow surface sublimation has a lower spatial variability, with values ranging from 20 to 35 mm yr^{-1} across the basin. The processes result in great spatial variability in SWE, which is also reflected in the snowcovered area during the ablation period. Snowcover in the Upper Gully/Drift HRU lasts until late June, three to four more weeks than in other HRUs. End of the winter mass fluxes are summarized in Table 3.7.

Winter snow processes in HPC have been previously studied by Pomeroy and Marsh (1997) for the 1992-1993 season, which despite the short period of analysis, provided detailed SWE field observation and analysis. Figure 12 in Pomeroy and Marsh (1997) shows observed average SWE from snow survey transects of 55, 135, 145, 150, 405 and 155 mm for the Upland Tundra, Lowland Tundra, Shrubs Tundra, Taiga, Drift and Forest, respectively. The CRHM-AHM simulations for the same time period of time show values of 100, 170, 190, 160, 470 and 70 mm of SWE for the HRUs representing those locations. Overall, the CRHM-AHM overestimates the values observed by Pomeroy and Marsh; however, it captures the spatial variability observed by them. Also, it should be noted that the CRHM-AHM model represents the average value within a HRU, and the observations represent a transect through only part of the HRU.

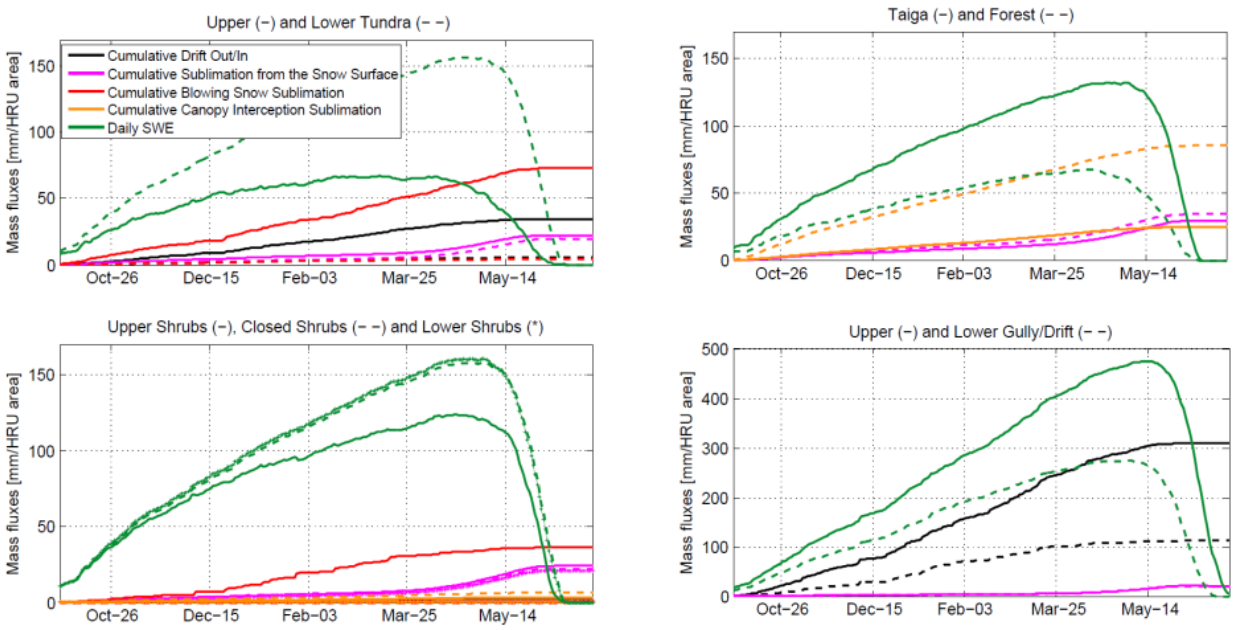

Figure 3.8 HRU-scale mean snow fluxes for the period between 1982 and 2009. Snow Water Equivalent (SWE) is presented as daily values, whereas other fluxes are presented as cumulative values. Drift in Tundra and Shrub HRUs are losses ("Out"), whereas for the Gully/Drift HRUs it represents a gain of snow ("In"). Note that a different scale is used for the Gully/Drift HRU (lower-right panel).

Table 3.7 Mean winter mass fluxes for each HRU.

Hydrological Response Unit	**End-of-the-winter SWE (mm)**	**Blowing snow transport* (mm yr^{-1})**	**Blowing snow sublimation (mm yr^{-1})**	**Sublimation from canopy interception (mm yr^{-1})**	**Sublimation from the snow surface (mm yr^{-1})**
Upper Tundra	67	-35	76	0	23
Lower Tundra	157	-6	4	0	20
Upper Sparse Tundra Shrubs	124	-3	37	4	24
Lower Sparse Tundra Shrubs	160	-1	1	0	21
Closed Shrubs	158	0	0	7	22
Taiga	132	0	0	25	30
Forest	68	0	0	88	35
Upper Gully/Drift	475	316	0	4	20
Lower Gully/Drift	275	114	0	4	20

*Positive value is associated with blowing snow added to the HRU whereas a negative value represents a loss from the HRU.

3.4.4 Active layer development

Figure 3.9a presents the average development of the active layer from June to September between 1982 and 2009 for a selection of representative HRUs, namely, Upper Tundra, Lower Shrubs, Forest and Upper Gully/Drift. Mean Active Layer Thickness (ALT) varies from roughly 0.55 m for the Upper Gully/Drift HRU up to 0.85 m for the Forest HRU; however, values in any individual year can exceed 0.8 and 1.1 m, respectively. The main factors controlling the ALT are ice content, the volumetric water content of the unfrozen soil layers, which impact the heat transfer from the ground surface to the frozen ground, and the surface freeze/thaw index (degree-day); the latter has a direct relationship with air temperature and timing of snowcover depletion. As discussed in

Section 3.4.3, the Upper Gully/Drift holds snowcover longer than other HRUs, delaying initiation of the snow-free period, reducing the surface thaw-index and thus the ALT. Conversely, the snowpack in the Upper Tundra HRU is the first to melt, allowing a greater thaw-index; however, other factors such as lower volumetric water content (resulting in a lower thermal conductivity) and net radiation restrict further ground thawing when compared with Lower Shrubs and Forest HRUs. Overall, simulations of the development of the ALT show similar behaviour for all HRUs; however, spatial variability exists and it is important that the CRHM-AHM model was able to capture it. Figure 3.9b presents a comparison between observed temperature at the organic layer (1 – 8 cm below the surface; Marsh et al., 2000) in a single location surrounded by Taiga forest and simulated surface temperature at the Lower Shrubs HRU (also surrounded by Taiga forest) during 1999. During the simulated snowcovered period, simulations failed to represent ground surface temperatures accurately, which is likely due to the lack of capability in the model to simulate snow meltwater percolation to the ground surface via preferential flow paths (Marsh and Pomeroy, 1999; Marsh and Woo, 1984a) and refreezing of meltwater on top of the frozen soils (Pomeroy et al., 1998). In addition, during the snowcover season, CRMH-AHM simulates ground temperature using the lower layer temperature and depth as estimated by SNOBAL, which can be problematic for shallow snowpacks (Debeer and Pomeroy, 2009); in this case a snowpack of less than 30 cm is simulated during this period. On the other hand, a more adequate representation of ground temperature is achieved during the simulated snow-free period. During this period the diurnal cycle of ground temperature is well represented, as well as its main trend; however, a slight overestimation is observed. Figure 3.9c presents a comparison between observed and simulated thawing/freezing fronts using observed soil temperature data at 10, 20, 30 and 45 cm depth in HPC (Marsh et al., 2000). Observations show that ground thaw begins in mid-May (14), whereas simulations show a 13-day later start of May 27, which is partly explained by delay in the snowmelt simulations (Figure 3.9b). By July 22, observations show a thaw depth of at least 45 cm whilst simulations predict ground thaw to be 49 cm. The lack of observations deeper than 45 cm precludes a more detailed analysis of deeper ground thaw simulations. The initiation of the ground freeze is well represented by the model (September 28); however, observations show that 20 cm below the surface, the soil is already at 0°C on that date, a much faster response compared to simulations. During November the simulated ground freeze advanced faster than observed, with the freezing front reaching 60 cm when observations showed 45 cm. Figure 3.9d presents a comparison showing good agreement between measured ALT at Havikpak Creek by the Geological Survey of Canada (Smith et al., 2009) and simulations. Mean bias is 12% and the mean of the residuals is 7.5 cm, showing a slight overestimation by the model, which may be due to the model's neglect of sensible heat (Kurylyk and Hayashi, 2016). Uncertainties when comparing point measurements against HRU areal averages, along with the assumptions of the permafrost model may explain part of the disagreement between observed and simulated ALT. These analyses suggest that the new XG-algorithm implemented in the CRHM platform is capable of providing adequate simulations of ALT over a continuous permafrost environment.

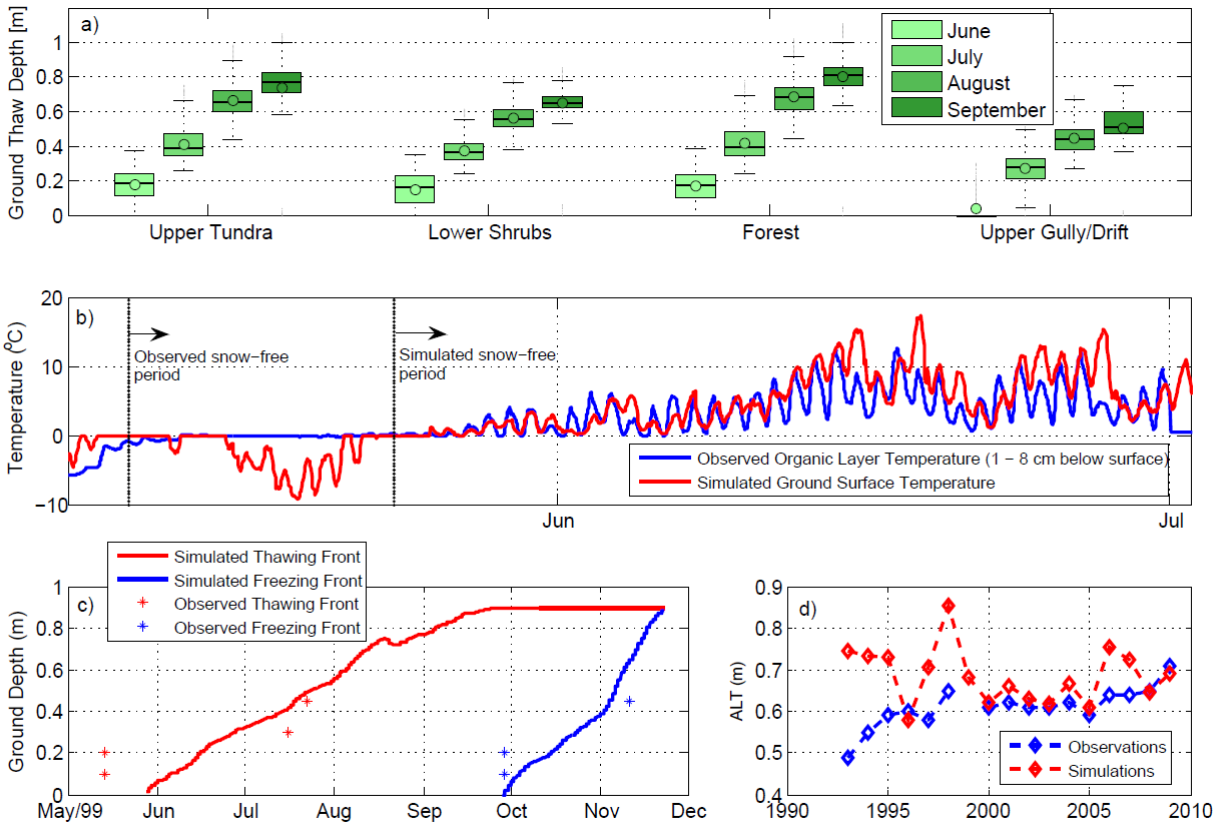

Figure 3.9: a) Active layer thickness for different HRUs during the thawing season. The box centre line represents the 50th percentile, and the lower and upper box edges the 25th and 75th percentiles, respectively. The edge of the line outside the box represent the range of possible values not considered as outlier (dots outside this range), and the circle represents the average value. b) Observed versus simulated ground temperature for the period between May and June 1999. c) Simulated versus observed thawing and freezing fronts for the period between May and June 1999. d) Simulated versus observed active layer thickness (ALT).

3.4.5 Water fluxes and storage

Figure 3.10 presents the average annual water fluxes between 1982 and 2009 for all HRUs (except open water) aggregated by landcover classes, namely, tundra (Upper and Lower Tundra HRU), shrub (Upper, Lower and Closed Shrub HRU), forest (Taiga and Forest HRU), drift (Upper and Lower Gully/Drift HRU) and wetland (Wetland HRU). Standard deviation is included as a shade around the average values to illustrate inter-annual variability. Water fluxes for rainfall, snowfall, evapotranspiration, sublimation, surface runoff and subsurface runoff are presented as cumulative values, whereas SWE is presented as daily values. Surface runoff represents the excess of infiltration and depression storage, not including incoming surface runoff from upstream areas, whereas subsurface runoff includes subsurface runoff from upstream areas. For example, the

average subsurface runoff in wetlands reaches up to 1,750 mm yr^{-1}, which would be impossible with a mean annual precipitation of 329 mm without the subsurface input from upstream areas. This demonstrates the necessity of an approach that routes water from HRU to HRU to calculate the water balance of wetlands in this low precipitation environment. Clearly, snowmelt runoff is the main mechanism by which surface runoff is produced; nevertheless, surface runoff from rainfall-runoff events during summer also contributes but with a much smaller fraction that varies between landcover from roughly 4% to 10% of the total surface runoff. In consequence, and as expected, a close relationship exists between the end-of-the-winter SWE and the total surface runoff for all the landcover classes, as frozen ground conditions during spring restrict meltwater infiltration.

Evapotranspiration (ET) exhibits great spatial variability. ET from gullies that are covered with snowdrifts shows the lowest annual cumulative values (96 mm), which can be explained by the three to four weeks shorter snow-free season due to the deeper snowpack. Tundra and shrub ET shows a similar behaviour, with average annual values of 117 and 107 mm, respectively; however, the tundra ET exhibits greater inter-annual variability with an annual standard deviation of 23 mm, as opposed to the 10 mm found for shrub ET. Forest and wetland ET present the largest cumulative annual values, at 164 and 218 mm, respectively; both landcovers show similar inter-annual variability with an annual standard deviation of 17 and 23 mm, respectively.

Sublimation, as presented in Figure 3.10, is the aggregated value of blowing snow sublimation, canopy interception sublimation and sublimation from the snow surface. Annual sublimation in wetlands and gullies with drifts is lowest at 23 mm, which is mostly composed of sublimation from the snow surface, as blowing snow sublimation is suppressed and canopy interception sublimation is very small (c.f. Table 3.7). Tundra and shrubs also present similar annual sublimation losses of 40 and 32 mm, respectively; however, in this case, blowing snow sublimation is quite important. For example, blowing snow sublimation from the Upper Tundra HRU is 76 mm yr^{-1}. The largest sublimation loss is 123 mm yr^{-1} and is associated with the Forest HRU, where sublimation from canopy interception is large (33 mm yr^{-1}). Inter-annual variability of annual sublimation ranges between 6 and 9 mm which, for the gully with snowdrifts, tundra and shrubs represents about 29%, 23% and 22% of the mean annual sublimation, respectively; whereas for forests this is only 15%.

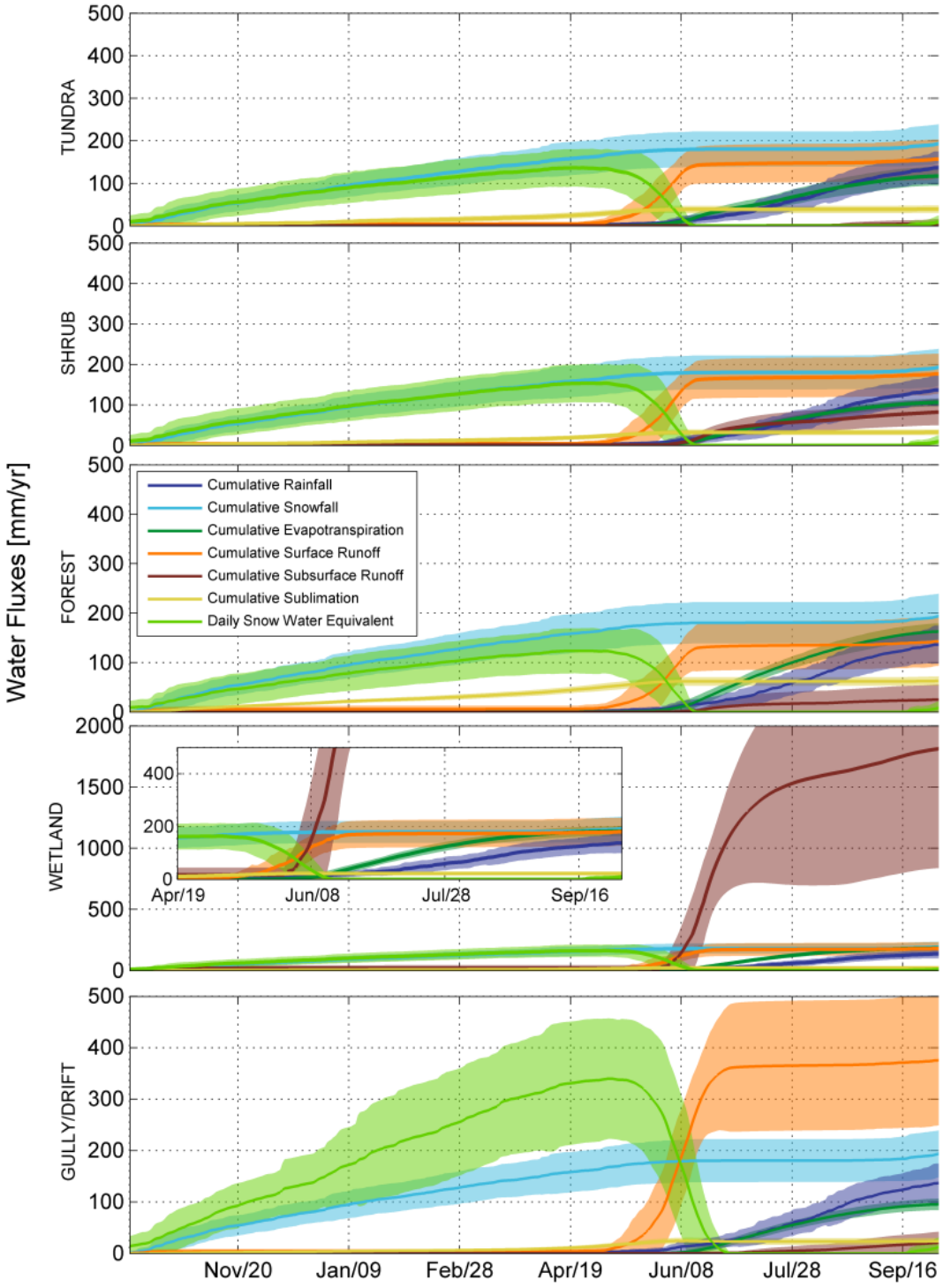

Figure 3.10: Line represents the annual mean of daily cumulative water fluxes and daily snow water equivalent for each landcover class and the shadow represents the standard deviation from 1982 to 2009. The water year is defined as starting from October 1. Note that a different scale is used for the Wetland (mid-right panel); however, the inset has the same scale as the other panels.

Table 3.8 presents HPC modelled seasonal and mean annual water fluxes for the period between 1982 and 2009. Annual precipitation is 329 mm, of which 58% is snowfall and 42% is rainfall, giving a rainfall ratio of 0.42. Mean annual evapotranspiration (ET), including evaporation of intercepted rain, is 156 mm (47% of mean annual precipitation), of which 135 mm (87%) occurs during summer. Mean annual streamflow is 127 mm, resulting in an average runoff ratio of 0.39. The difference in storage includes soil moisture, depression storage and SWE. On average, the interannual difference in storage was positive, at 2 mm $year^{-1}$, meaning a greater value at the end of the period. Seasonal values were much larger, with winter gains of 129 mm yr^{-1} due to the accumulation of snow, and summer losses of -63 mm yr^{-1}, mostly due to the decrease of soil moisture driven by evapotranspiration and the remaining SWE in the ground. Mean annual sublimation is 47 mm, which includes blowing snow sublimation, canopy interception sublimation and sublimation from the snow surface; this value represents roughly 14% of annual precipitation and 25% of the mean annual snowfall.

Marsh et al. (2004) calculated mean annual fluxes for HPC for the period between 1992 and 2000, using a water balance approach based on observations and the Priestley and Taylor (Priestley and Taylor, 1972) method to estimate ET for the entire basin. This ET estimation method contrasts to that applied here, where it was restricted to wetlands with water available at the surface all summer. Table 1 in Marsh et al. (2004) presents values for rainfall, snowfall, streamflow, ET and the residual of the water balance of 135, 148, 110, 134 and 37 mm, respectively. The source of meteorological data is not the same, as Marsh et al. (2004) used specialized data collected by ECCC's National Water Research Institute (NWRI) that was not available to this study, as opposed to ECCC's MSC dataset used in the present study. Also of note is that the period of analysis is not the same; however, there is overlap. Differences exist in the estimation of mean rainfall and snowfall, which could be due to the source of the meteorological dataset, the bias-correction approach used for wind-undercatch or the method used to partition rain and snow (Marsh et al. (2004) used a simple 0°C threshold, whereas this study used a psychrometric energy balance approach). Consequently, differences in annual precipitation, ET and streamflow of 46, 22 and 17 mm, respectively, are found. Interestingly, the residual of the water balance presented by Marsh et al. (2004) (37 mm) is close to the sublimation estimated with the CRHM-AHM model (47 mm), with a difference of 10 mm. The latter emphasizes the need to include sublimation calculations in cold regions studies, to reduce the uncertainty associated with water balance simulations, which has been identified by previous studies (Johansson et al., 2015; Pomeroy et al., 1997). Although values from the present study and those by Marsh et al. (2004) are not the same, they agree in that ET is the greatest loss of water in the basin, followed by streamflow, which is mostly composed of snowmelt runoff. Zhuravin (2004) presented a water balance study for the Kontakovi Creek Basin in East Siberia, which has similar features as HPC; a drainage area (21.2 km^2) underlined by continuous permafrost, and a mix of tundra, shrubs and forest landcover. Results from Zhuravin (2004) showed that streamflow is the dominant mass flux, followed by ET (including sublimation losses), with values of 73 and 34% with respect to the mean annual precipitation, with an error estimated at -7%. Differences with the water balance shown in this study can be attributed to the

larger area covered by tundra at the Kontakovi Basin (>30%) and the steeper slope (40%), which reduce evapotranspiration, as tundra transpires less than forest, and a steeper slope reduces surface and subsurface water retention, enhancing runoff generation.

Table 3.8: Mean annual water fluxes at a basin scale for the water years between 1982 and 2009. First two years are used to spin-up the model.

Mean Mass Fluxes (mm yr^{-1})	**Winter: Oct-Apr**	**Spring: May**	**Summer: Jun-Aug**	**Fall: Sep**	**Annual**
Rain	2	8	106	21	137
Snow	162	13	3	14	192
Evapotranspiration	1	6	135	14	156
Streamflow	4	43	74	6	127
Δ Storage*	129	-63	-79	13	2
Blowing Snow Sublimation	4	0	0	0	4
Canopy Interception Sublimation	16	1	0	1	18
Sublimation from the Snow Surface	17	8	0	0	25
Blowing snow transport within the basin	2	0	0	0	2

*Difference between final and initial soil moisture, depression storage and snow water equivalent. There is a 3 mm yr^{-1} error in the mass balance closure (<1%).

3.4.6 Model sensitivity and uncertainty

Figure 3.11a) shows the result from VARS using values from the Integrated Variogram Across a Range of Scale (IVARS) between 0 - 50% of the parameter range, as suggested in the VARS-Tool Manual for a single global sensitivity metric. This result reveals that vegetation height ('Ht') is the parameter that impacts simulated streamflow performance the most; therefore, a reliable estimation of vegetation height and potential changes due to a changing environment is advised for future applications. This result is explained as vegetation height impacts vegetation snow interception efficiency, affecting the end-of-the-winter SWE and, therefore, snowmelt runoff. The parameter 'Sbar' is second in the ranking, supporting the great impact that canopy interception and sublimation have in the model and the need to reliably represent this physical process. The ranking is followed by 'Ks', 'Soil Recharge', 'LAI' and 'rcs' in decreasing order.

The results from the mass balance uncertainty and the values from the model with the original set of parameters (c.f. Section 3.4.), are presented in Figure 3.11b. Sublimation from blowing snow and at the snow surface shows very little uncertainty $<\pm 0.5$ and ± 2 mm yr^{-1}, respectively, which is somewhat expected, as blowing snow has a small contribution to the basin mass balance and sublimation at the snow surface is not directly affected by any of the parameters used in the analysis; however, it is impacted by fluctuations in snow accumulation due to changes in snow interception. Minimum and maximum values for streamflow, evapotranspiration and sublimation from canopy interception are 95 - 157 mm yr^{-1}, 131 - 168 mm yr^{-1} and 11 - 44 mm yr^{-1}. Greater range is observed for streamflow, as this represents the combined overall uncertainty from the other mass fluxes. This analysis is interesting, as it shows the range of potential variability the mean annual mass balance has, which is intended to provide the readers with an estimation of the model uncertainty.

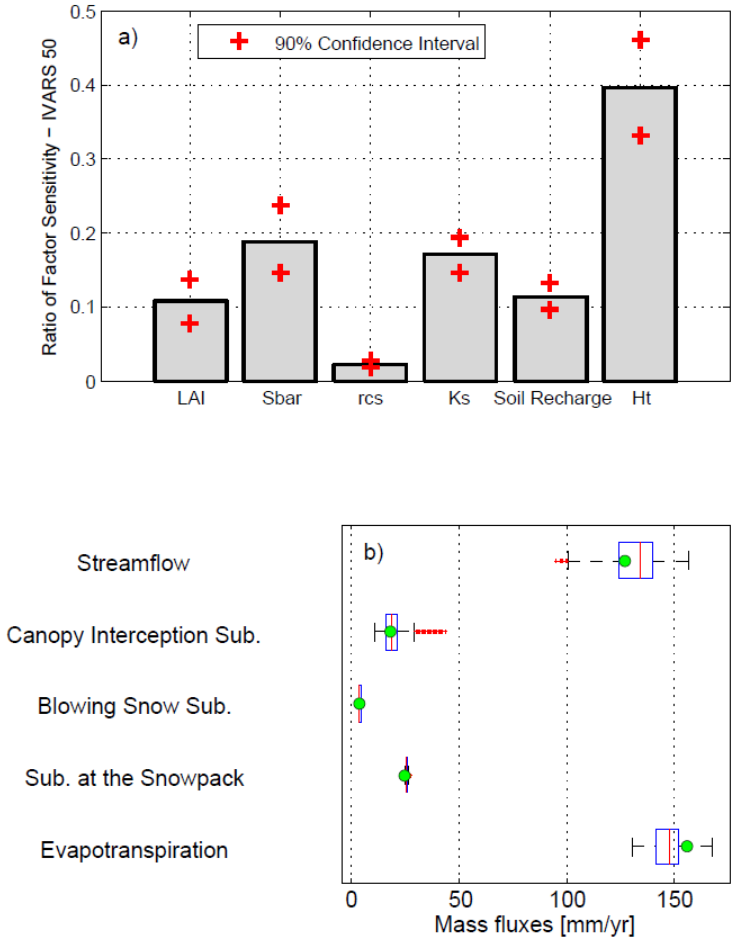

Figure 3.11: a) Ratio of Factor sensitivity using IVARS 50. b) Annual mass fluxes sensitivity to parameter uncertainty. Bars correspond to the maximum and minimum values, the box are the percentile 25th and 75th, and the red line is the percentile 50th. The green circle shows the mass fluxes associated with the control run. The term "Sub." refers to sublimation.

3.5 Conclusions

A physically based Arctic Hydrological Model created using the CRHM platform, coupling the atmosphere-snowpack-surface-subsurface energy and mass fluxes for a small basin underlain by permafrost in the taiga-tundra transition was implemented over a 28-year period and validated using field data. The model showed an adequate performance against continuous daily streamflow, discontinuous SWE and continuous but short records of ground surface temperature and ground freeze/thaw. Problems in capturing the timing and intensity of snowmelt peak flows may be partially associated with the formation of snow dams in the upper basin valleys that were not simulated by the model; however, significant uncertainties in streamflow observation due to ice

formation in the cross section also exist. The simulated snow water equivalent distribution and active layer thickness were also compared with observations presented by Pomeroy and Marsh (1997), Marsh et al. (2000) and the Geological Survey of Canada, all showing good agreement.

Mean active layer thickness simulations range from about 0.5 m to 0.9 m, depending on volumetric water content of the soil and the date at which the ground is snow-free; therefore, blowing snow sinks such as upland gullies, which may hold snow up to three to four weeks longer, exhibit the shallower active layer. Evapotranspiration in Havikpak Creek represents the largest mass flux, accounting for roughly 47% of the mean annual precipitation, whereas streamflow accounts for approximately 39%. Sublimation represents about 14% of the mean annual precipitation, of which approximately 53% comes from sublimation from the snow surface, 38% from canopy interception and 9% from blowing snow. Although blowing snow is not very important for basin scale mass balances, at the local upland tundra it comprises up to 33% of its water loss. The sensitivity analysis revealed that from the set of parameters considered, routing parameters were not included as they were not measured and were calibrated; vegetation height is the parameter that most influences the model streamflow performance, as it has a significant impact on canopy interception and thus, a good estimation of its value is advised. The uncertainty analysis shows that uncertainty in estimates of sublimation from blowing snow and at the snow surface is relatively small (<2 mm yr^{-1}). Streamflow shows the largest range of uncertainty (95 - 157 mm yr^{-1}) as this represents the combined effect of the uncertainty from the other mass fluxes.

The effect of the complex interaction between observed trends in climate (Vincent et al., 2015) and shrub cover (Lantz et al., 2013) on future hydrology of Arctic basins, particularly in the Tundra-Taiga transition region, is inherently uncertain. As a new tool to address this question, CRHM-AHM can be used to analyse and predict these changes under future climate and vegetation scenarios for HPC or other basins in subarctic and Arctic environments. The main advantages of using this model are that it includes all the key and complex physical processes found in this type of environment in a relatively simple and efficient way that can be easily duplicated for other basins. Future research aims to investigate past trends and future hydrology for the region using the Arctic Hydrology Model.

CHAPTER 4

Recent changes to the hydrological cycle of an Arctic basin at the tundra-taiga transition

Wetland around Havikpak Creek, Northwest Territories, September 8, 2014.

Abstract

The impact of transient changes in climate and vegetation on the hydrology of small Arctic headwater basins has not been investigated, particularly in the tundra-taiga transition region. This study uses weather and land cover observations and a cold regions hydrological model to investigate historical changes in modelled hydrological processes driving the streamflow response of a small Arctic basin at the treeline. The physical processes found in this environment and explicit changes in vegetation extent and density were simulated and validated against observations of streamflow discharge, snow water equivalent and active layer thickness. Mean air temperature and all-wave irradiance have increased by 3.7°C and 8.4 W m^{-2}, respectively, while precipitation has decreased 48 mm (10%) since 1960. Two modelling scenarios were created to separate the effects of changing climate and vegetation on hydrological processes. Results show that over 1960-2016 most hydrological changes were driven by climate changes, such as decreasing snowfall, evapotranspiration, deepening active layer thickness, earlier snowcover depletion, and diminishing annual sublimation and soil moisture. However, changing vegetation has a significant impact on decreasing blowing snow redistribution and sublimation, counteracting the impact of decreasing precipitation on streamflow, demonstrating the importance of including transient changes in vegetation on long-term hydrological studies. Streamflow dropped by 38 mm as a response to the 48 mm decrease in precipitation, suggesting a small degree of hydrological resiliency. These results represent the first detailed estimate of hydrological changes occurring in small Arctic basins, and can be used as a reference to inform other studies of Arctic climate change impacts.

This manuscript has been modified for inclusion in this thesis. It was originally published as:

Krogh, S. and J. Pomeroy, 2018: Recent Changes to the hydrological cycle of an Arctic basin at the tundra-taiga transition, *Hydrology and Earth System Sciences*, https://doi.org/10.5194/hass-22-1-2018.

Author contributions:

SK and JP designed the study. SK performed the simulations and the statistical analyses and prepared the manuscript with contributions from JP to the manuscript structure, readability and analysis and discussion of the results.

4.1 Introduction

Rapid warming in the Arctic (Hansen et al., 2010; Przybylak *et al.*, 2010; Wanishsakpong *et al.*, 2016) has produced significant environmental changes (Hinzman et al., 2005), such as decreasing snowcover duration (Brown et al., 2010) and permafrost thaw (Liljedahl et al., 2016). A reduced snowcover period can result in smaller, slower snowmelt, larger evapotranspiration losses and reduced sublimation losses from cold regions headwater basins (Pomeroy et al., 2015b; Rasouli et al., 2015). Permafrost thaw can impact regional and local hydrology by increasing surface and subsurface connectivity, and baseflow (Connon et al., 2014; Liljedahl et al., 2016; Walvoord and Kurylyk, 2016). Increases in vegetation cover and density have been observed and are especially pronounced near the tundra-taiga ecozone transition (Lantz et al., 2013; Myers-Smith et al., 2011; Sturm et al., 2001; Tape et al., 2006; Xu et al., 2013); however, the impact on the hydrology of these transition Arctic basins is poorly understood. These environmental changes will likely continue in the future, representing challenges for water resources managers and engineers throughout the Arctic.

Precipitation trends over the Arctic are highly uncertain due to a sparse monitoring network (Serreze et al., 2003) and difficulties in measuring snowfall in windswept environments (Goodison et al., 1998; Pan et al., 2016). Nevertheless, positive and negative trends have been calculated for the largest Arctic river basins (Walsh, 2005, table 6.12) and throughout the Arctic (Whitfield et al., 2004). Over northern Canada, an overall increasing trend in annual precipitation has been observed (DeBeer et al., 2016; Vincent et al., 2015); however, there is great spatial variability and uncertainty due to the low-density observational network (Milewska and Hogg, 2001). Mean annual temperatures in northwestern Canada have increased more than anywhere else in Canada by roughly 3 – 3.5 °C between 1948 and 2012 (Vincent et al., 2015); moreover, mean winter temperatures show the largest increase of up to 6.5 °C (DeBeer et al., 2016).

Arctic vegetation has changed in response to warmer temperatures (Hinzman et al., 2005; Martin et al., 2017; Myers-Smith and Hik, 2018). The tundra-taiga treeline in Alaska, U.S.A., has advanced between 80 to 100 m in the last 200 years (Suarez et al., 1999). Payette and Filion (1985) studied white spruce (picea glauca) expansion into northern Quebec, Canada, and found that the treeline has not changed substantially over the past centuries; however, below the treeline, its density has increased. On the other hand, both shrub coverage and density have increased in the Arctic. Lantz *et al.* (2013) reported that between 1972 and 2004, shrub density and cover have increased substantially in the upland tundra east of the Mackenzie River Delta of northwestern Canada. Similar results were found by Tape et al. (2006) in northern Alaska and pan-Arctic. Overall, these previous studies observed that the Arctic treeline has not undergone a substantial change over the last century, but shrub expansion is ubiquitous near the Arctic treeline in North America. Wildfires can rapidly modify vegetation cover and are important to nutrient cycling, biodiversity, and control of pathogens and pests (Bond and Keeley, 2005). Warmer temperatures and longer dry seasons are increasing vulnerability to wildfire (Romero-Lankao et al., 2014),

resulting in increased frequency and duration of wildfires since the mid-1980s (Westerling et al., 2006; Williamson et al., 2009). Changes in vegetation are important, as they have been shown to control snow redistribution (Ellis et al., 2013; Essery and Pomeroy, 2004; Ménard et al., 2014; Pomeroy and Brun, 2001) and energy fluxes (Ménard et al., 2012; Pomeroy et al., 2006; Sturm et al., 2000).

Many studies have looked at observed changes in large northward flowing river basins. There is an increase in annual discharge from large river basins to the Arctic Ocean (McClelland et al., 2006; Overeem and Syvitski, 2010; Peterson et al., 2002; Rood et al., 2017; Yang et al., 2002), a decrease in river ice thickness (Peterson et al., 2002) and an earlier river/lake ice break-up dates (Janowicz, 2010; Prowse et al., 2011). However, most of these large river basins have their headwaters and primary zones of runoff generation well below the Arctic Circle; and therefore are not necessarily representative of changes in the Arctic hydrological cycle. As limited observations are available in the Arctic, model outputs have also been used to investigate change. Increasing trends were found in simulated monthly evapotranspiration and streamflow for the Mackenzie River Basin, Canada (Yip et al., 2012) and in simulated Arctic soil temperature and active layer thickness (Oelke et al., 2004), and decreasing trends were found in simulated Arctic snow accumulation and snowcover duration (Liston and Hiemstra, 2011). López-Moreno *et al.* (2016) analyzed simulated historical trends in the snow processes of a small basin above the Arctic treeline in Svalbard, using a physically based cold regions hydrological model that accounted for blowing snow redistribution and energy balance snowmelt. They found that simulated snow accumulation, snowcovered season and days with snowfall decreased significantly, driven by a significant increase in air temperature. No study has looked at changes in Arctic hydrological processes from headwater basins that originate near the Arctic treeline, nor has the relationship between changes in hydrological processes due to climate and vegetation change been investigated.

Using hydrological models to simulate the hydrological cycle can compensate for an inability to observe it due to ungauged basins (Pomeroy et al., 2013b) and decline in the coverage of Arctic monitoring networks (Laudon et al., 2017). Previous studies acknowledged the need for robust cold regions hydrological models to simulate Arctic hydrology (Quinton and Carey, 2008; Woo et al., 2008), particularly due to the complex interaction between subsurface and surface mass and energy fluxes (Kane et al., 1991; Krogh et al., 2017; Z. Zhang et al., 2000). Physical processes that must be accounted for include: snow accumulation and melt (Marsh *et al.*, 2010), snow interception and sublimation from forest canopies (Hedstrom and Pomeroy, 1998; Pomeroy et al., 1998; Schmidt and Gluns, 1991), blowing snow sublimation and redistribution (Pomeroy et al., 1997; Schmidt, 1982), evapotranspiration (Wessel and Rouse, 1994), infiltration into frozen and unfrozen soils (Gray et al., 2001; Kane, 1980; Kane and Stein, 1983), water flow through snowpack (Colbeck, 1972; Marsh and Woo, 1984a, 1984b), ground freeze and thaw (Juminikis, 1977), surface and subsurface flow (Quinton and Gray, 2001; Quinton and Marsh, 1999), groundwater (Cederstrom et al., 1953) and streamflow routing (Woo and Sauriol, 1980). The Cold Regions

Hydrological Model (CRHM) platform was used to create the Arctic Hydrology Model (AHM) configuration (CRHM-AHM) by Krogh *et al.* (2017). This spatially distributed and physically based model includes the key hydrological processes found at the Arctic treeline, such as blowing snow, snow and rain interception, sublimation, snowmelt, flow through snow, infiltration to frozen and unfrozen soils, evapotranspiration, runoff as overland flow and subsurface flow through organic terrain, frozen ground dynamics including active layer thaw, groundwater flow and streamflow routing. CRHM-AHM was shown to properly represent the winter and summer hydrology of this environment with minimal calibration of some uncertain routing and storage parameters (Krogh et al., 2017). A great advantage of this model is its flexibility and potential to be adapted for simulation of other Arctic basins.

The aim of this study is to understand, diagnose and quantify the long-term hydrological changes of a small Arctic treeline basin, including transient changes over a multidecadal period, using the CRHM-AHM model. The study addresses the following research questions: what hydrological changes are caused by individual transient changes in climate and vegetation? What are the coupled hydrological impacts of changes in climate and vegetation; does transient vegetation change enhance or dampen climate change? Does Arctic hydrology show resiliency to the impacts of climate change? To address these questions, the study compares three observation-driven hydrological modelling scenarios: (1) observed climate change and constant vegetation cover, (2) observed transient changes in vegetation with climate held constant and (3) observed changes in climate and vegetation.

4.2 Study site

Havikpak Creek (HPC) with an area of 16.4 km^2 is located east of Inuvik, Northwest Territories, Canada (Figure 4.1), near the tundra-taiga transition. HPC is in the continuous permafrost region, with an elevation rising from 60 m.a.s.l. in the southwest to 240 m.a.s.l. in the northeast. This basin was selected as it has a history of process-based hydrological studies, which provides a good understanding of dominating hydrological processes, has long-term meteorological records and has been part of important international initiatives, such as the Mackenzie GEWEX study (MAGS). HPC is also within the domain of the NASA Arctic-Boreal Vulnerability Experiment (ABoVE; https://above.nasa.gov/), which aims to better understanding the vulnerability and resiliency of Arctic boreal ecosystems, and therefore, its great relevance.

Estimates of mean annual temperature and precipitation between 1981 and 2010 at Inuvik, using observations at the Meteorological Service of Canada weather station (Climate ID: 2202570) by Environment and Climate Change Canada (ECCC), are -8.2 °C and 240.6 mm, respectively (http://climate.weather.gc.ca/climate_normals/index_e.html). However, Krogh *et al.* (2017) showed that the corrected mean annual precipitation between 1980 and 2009 at Inuvik, based on the Adjusted and Homogenized Canadian Climate Dataset (AHCCD; Mekis and Vincent, 2011) and additional local weather stations, is 327 mm. Differences between precipitation estimates

published by ECCC and Krogh *et al.* (2017) are due to Krogh's use of the AHCCD dataset with its corrections of snowfall wind undercatch and trace events. Such large adjustments to corrected precipitation are not uncommon at high latitudes in Canada and can influence trend detection (Pomeroy and Goodison, 1997). Using corrected data, 59% of the mean annual precipitation is snowfall; however, peak monthly precipitation occurs as rainfall in August (~45 mm; Krogh *et al.*, 2017). Snow accumulation typically starts in mid-September, with peak accumulation at the end of April or beginning of May, and snowmelt lasts until early- to mid-June (Krogh et al., 2017). The streamflow regime of Havikpak Creek is measured by the Water Survey of Canada and is characterized by a rapid increase due to snowmelt in May and June, during which the annual peak streamflow occurs (1-4 $m^3 s^{-1}$), followed by decreasing streamflow interrupted by sporadic summer peaks due to intense rainfall (Krogh et al., 2017). No streamflow was observed during winter.

In 1992, HPC was predominantly covered by Black Spruce (*Picea mariana*) forest (50.0%) followed by Alder shrubs (31.7%), short grass, moss and lichen tundra (11.6%) and open water (6.7%) (Krogh et al., 2017). However, as shrubs colonize the tundra (Lantz et al., 2013) these percentages have changed. No changes in forest cover have been reported, though investigations into this are understood to be underway. A slight "greening" of the region has been detected through NDVI analysis of Landsat satellite imagery, but not attributed to specific vegetation changes (Ju and Masek, 2016). Soils in HPC are characterized by a top layer (roughly 10 cm) of decomposed and highly porous organic matter (upper peat), followed by a highly decomposed and denser organic layer underneath (lower peat), estimated between 20 to 50 cm thick on top of a mineral soil layer (Krogh et al., 2017). No soil changes have been reported. For a detailed description regarding HPC climate, landcover, soils, weather and hydrometric stations, the reader is referred to Krogh *et al.* (2017).

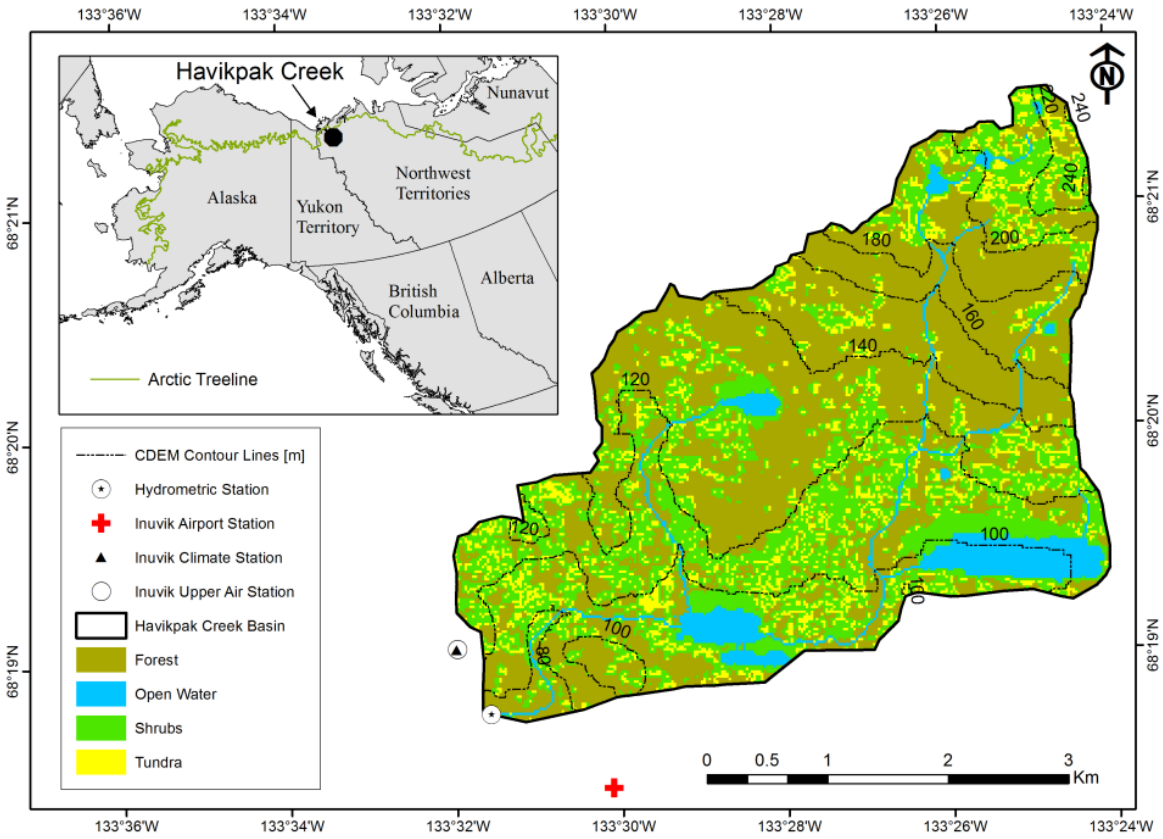

Figure 4.1: Havikpak Creek Basin including elevation contour lines (based on the Canadian Digital Elevation Map – 20m), the location of weather and hydrometric stations, and the 1992 landcover map based on Krogh et al. (2017). Inset plot shows the location of the study site within North America and the approximate location of the Arctic treeline.

4.3 Data

Reconstructed weather time series used in this study are based on a combination of observations, adjusted and homogenized time series from the AHCCD dataset (station ID: 2202578; Mekis and Vincent, 2011), ERA-40 (Uppala et al., 2005) and ERA-Interim (Dee et al., 2011) reanalysis over the period 1960-2016. Reanalysis data has been used in the past to complement meteorological observations for hydrological studies (e.g. Krogh et al., 2015). Six hourly-timestep variables were used to drive CRHM-AHM (see Section 4.4.1): precipitation, air temperature, relative humidity, wind speed, and incoming short- and long-wave radiation (Figure 4.2). Data used for model validation consist of observed daily streamflow (Section 0). A reconstructed vegetation cover map, topographic information and a site visit informed the spatial model configuration.

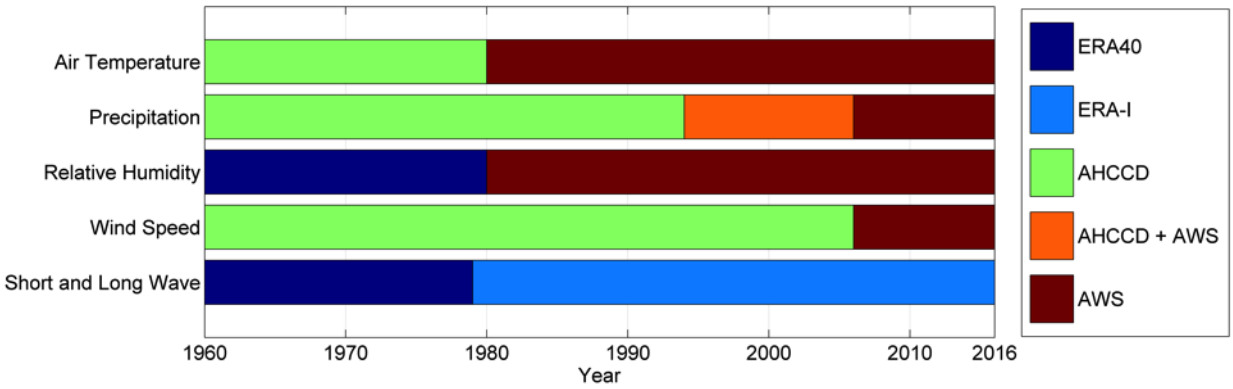

Figure 4.2: Data source for each of the weather variables during the period 1960-2016. AWS: Automatic Weather Stations. AHCCD: Adjusted and Homogenized Canadian Climate Data. ERA-I: ERA-Interim.

4.3.1 Air temperature

Daily minimum, maximum and mean temperatures from the AHCCD dataset are available from 1957 to 2014. Hourly temperature is available from Inuvik Airport from 1980 to 2016 and from Inuvik Climate from 2003 to 2016. To generate a uniform time series of hourly temperature, the following steps were followed: (1) minimum and maximum from AHCCD dataset (1957-2014) were used to generate hourly temperature by fitting a sinusoidal function, as presented by Chow and Levermore (2007; Equation 6); (2) hourly temperature measured by the Inuvik Airport station (1980-2016) was used to correct hourly temperature from the AHCCD dataset (1960-1980) through a linear regression model ($R^2 = 0.97$); and (3) Inuvik Airport hourly data was used for the period 1980-2016.

4.3.2 Precipitation

Daily precipitation from the AHCCD dataset for the period 1960-2006 is available; however, after 1994, several gaps were found. Precipitation measurements from the AHCCD at Inuvik were all made by observers and are considered reliable. After 1994, automatic systems were sometimes used to improve the corrections from snow ruler measurements (Mekis and Vincent, 2011). For measurements from 1994 to 2007, a combination of AHCCD and the local ECCC automatic weather stations: Inuvik Climate, Inuvik Upper Air and Inuvik Airport, was used. From 2007 onward, the Inuvik Climate station (automatic) was the only station recording precipitation. The automatic station snowfall data was corrected for wind undercatch using the expression presented by (Smith, 2008) for the Alter-shielded Geonor solid precipitation gauge. A specific snowfall correction had to be applied between October and March for the water years 2010 to 2012, as winter precipitation from the Inuvik Climate precipitation gauge was not found to be credible.

Observed snow accumulation (snow water equivalent, SWE) in sheltered sites and observed streamflow suggest that snowfall measured during these years was grossly underestimated. The ratio between measured end-of-the-winter SWE (April 1) and cumulative snowfall in 2011, 2012 and 2013 was 2.6, 1.7 and 2.5, respectively (after wind undercatch corrections); the ratio associated with the other years with both SWE and streamflow data (2003 to 2015) show values around 1. A solution to this problem was proposed and implemented by Pomeroy *et al.* (1997) at a nearby location (Trail Valley Creek) and consists of estimating 'true' winter snowfall from late season snow surveys in a small glade within a forest. Pomeroy *et al.* (1997) argued that the wind and sun sheltered, and cold conditions of the site ensured that the snow on the ground in the glade was not redistributed, sublimated or melted, and was therefore equal to the cumulative snowfall. SWE measurements used in this study have the same conditions as those found by Pomeroy *et al.* (1997) (i.e. sheltered site with mild winds and cold environment), and therefore, their approach was used to estimate 'true' snowfall.

To disaggregate daily into hourly precipitation, the same procedure used in Krogh *et al.* (2017) was followed. This employs the microcanonical cascade model presented by Güntner et al. (2001). This disaggregation technique assumes that the probability distribution function of the weights factors, defined as the ratio between a lower and upper disaggregation level (e.g. 12 hr and 24 hr), from the different disaggregation levels (e.g. 3, 6, 12 and 24 hr) is constant, and it was obtained aggregating hourly precipitation records. The reader is referred to Güntner et al. (2001) and Krogh *et al.* (2017) for further details of this methodology and the particular application to Inuvik precipitation dataset, respectively.

4.3.3 Relative humidity

Relative humidity was calculated using six-hourly air temperature and dew point temperature from ERA-40 for the period 1960-2002, using the expression from Lawrence (2005). A linear interpolation was then used to calculate hourly values. ERA-40 values from 1960-1980 were corrected using a linear relationship for the period 1980-2002 between hourly ERA-40 and measured relative humidity at Inuvik Airport (R^2 = 0.7). Finally, hourly corrected values from ERA-40 were used from 1960-1980 and observed values from 1980 to 2016. Relative humidity was not permitted to exceed 100% in this estimation.

4.3.4 Wind speed

Hourly 10-metre height wind speed from the AHCCD dataset and Inuvik Airport station for the period 1960-2006 and 2006-2016 were used, respectively.

4.3.5 Short- and long-wave irradiance

Short- and long-wave irradiance were not measured and so were obtained from the ERA-40 (Uppala *et al.*, 2005; 1960-2002) and ERA-Interim (Dee *et al.*, 2011; 1979-2016) atmospheric model reanalyses at three-hr time steps. A linear interpolation was used to obtain hourly values for each dataset. The ERA-Interim is a more advanced reanalysis, and has shown small biases in Arctic environments (Lindsay et al., 2014), so it was used as "true" incoming radiation and ERA-40 outputs were corrected to match the ERA-Interim. The overlapping period between ERA-40 and ERA-Interim is 1979-2002 (23 years); this period was used to bias-correct ERA-40 over 1960-1979 using the quantile mapping technique. Quantile mapping is a statistical approach used in hydrometeorological studies to bias correct weather variables times from atmospheric models against measurements (e.g. Boé *et al.*, 2007); it corrects each quantile by matching the empirical cumulative distribution functions. The irradiance time series created uses the bias-corrected ERA-40 for 1960-1979 and ERA-I for 1979-2016.

4.3.6 Streamflow

Daily streamflow discharge at HPC was observed and estimated at the hydrometric station (ID: 10LC017) by the ECCC Water Survey of Canada (WSC). This station is downstream from the Havikpak Creek crossing with the Dempster Highway and its drainage area defines the basin for modelling purposes. Discharge estimates for this station start in 1995 and are available to 2015; however, the year 2005 is not available. Measuring small stream discharge in the Arctic is challenging and problems or uncertainties associated with the estimates are acknowledged in the metadata provided by the ECCC through the Environment Canada Data Explorer. The main issues in the hydrometric record are due to the presence of ice and snow in the cross section during snowmelt including peak streamflows, as ice and snow cause substantial variability in rating curves and make streamflow and water stage measurements quite difficult.

4.3.7 Vegetation cover and shrub density

The vegetation cover map and shrub density used in this study are based on the map and values presented by Krogh *et al.* (2017) from 1992, and the changing shrub cover and density rates presented by Lantz *et al.* (2013) for a larger region that includes Havikpak Creek. Lantz *et al.* (2013) showed that between 1972 and 2004 (32 years) shrub cover increased by 15% (±3.6) and shrub density increased by 68% (±24.1), in average. These average rates were recalculated to an annual basis, resulting in rates of 0.47 % yr^{-1} and 2.13 % yr^{-1} for shrub cover and density increases, respectively. To reconstruct times series of vegetation cover and shrub density, the average rates presented by Lantz *et al.* (2013) were used to linearly extrapolate forwards and backwards from the values used in Krogh *et al.* (2017), creating a time series of vegetation cover and shrub density

from 1960 to 2016. As shrubs colonize the tundra, any increase in shrub cover is compensated by a decrease in the tundra cover, maintaining a constant drainage area. It is unclear when shrubs expansion in the Arctic began (Tape et al., 2006), mostly because satellite images started to be available in the 70's, limiting our understanding of vegetation changes to the 70's onward.

The HPC forest was held constant in this study, as there are no published studies quantifying forest cover or density change in the region. However, we acknowledge that there are ongoing investigations about changes in forest structure in the region. Greening of the NDVI is not directly attributable to forest change and could be due documented shrubification. There are no recorded wildfires in Havikpak Creek during the study period as it is close to the airport and so fire suppression by local authorities is very effective.

4.4 Methodology

4.4.1 Hydrological modelling

The Cold Regions Hydrological Modelling platform (CRHM) is a process-based and spatially distributed hydrological modelling-system with a flexible modular structure that allows the selection of different hydrological processes from an extensive library to create a customized hydrological model. Most of the modules available in the CRHM have a strong physical basis, with particular emphasis on, but not restricted to, cold region processes. The CRHM Arctic Hydrology Model configuration (CRHM-AHM) developed and verified by Krogh et al. (2017) includes the following hydrological processes: forest canopy interception, sublimation and evaporation, snow-melt and snow accumulation, evapotranspiration, blowing snow redistribution and sublimation, ground freeze and thaw, water flow through snowpack and organic terrain, infiltration into frozen and unfrozen soils, soil moisture storage and flow, surface water flow and streamflow routing. The model was run over October 1960 to October 2016 on an hourly basis. A four-year spin-up period was used by repeating the years 1960-1963.

CRHM uses Hydrological Response Units (HRUs; Flügel, 1995) as the spatial unit of discretization for application of the continuity equation to compute mass and energy fluxes. In the CRHM-AHM, HPC basin was discretized into 11 HRUs initially classified by land cover: tundra, sparse shrubs, close shrubs, taiga, forest, wetland, and open water. To include the different near-surface wind regimes observed by Pomeroy and Marsh (1997) over the basin, the tundra and sparse shrubs HRUs were each split into an upper and lower HRU to reflect stronger wind regimes in the hilly, higher elevation, upper basin. To simulate the long lasting snow drifts found in steep gullies and around small lakes, a Gully/Drift HRU was created following the criteria from Pomeroy and Marsh (1997). The physiographic characteristics of the HRUs used in the CRHM-AHM applied in HPC are as in Krogh et al. (2017, Table 2).

The parameterization of the CRHM-AHM followed the Deduction-Induction-Abduction approach (DIA; Pomeroy et al., 2013a) by first using field information (e.g. slope and vegetation cover) parameters from previous studies in Havikpak Creek and other research basins with similar hydrological regimes and physical processes to set parameters, and then calibrating against streamflow a few subsurface and surface hydraulic and storage parameters for which there was poor understanding. The CRHM-AHM represents the snow, permafrost and streamflow regimes of Havikpak Creek well when compared to observations (Krogh *et al.*, 2017).

4.4.2 Modelling scenarios

Three modelling scenarios representing only historical climate change (ΔC), only historical vegetation change (ΔV) and both historical climate and vegetation change (ΔCV) were developed to examine the hydrological impacts of changes in HPC since 1960 and are described below.

4.4.2.1 Model Scenario 1 (MS1): changing climate and constant vegetation

This scenario uses the reconstructed climate time series presented in Section 4.3 for the period 1960-2016 with a constant vegetation cover and density representative of the year 1988, which is the average vegetation cover of the modelling period.

4.4.2.2 Model Scenario 2 (MS2): constant climate and changing vegetation

This scenario uses a "normal" water year in terms of precipitation and temperature to generate the stationary climate. The mean annual (October to September) precipitation and temperature for the period October/1960 to October/2015 is 332 mm and -8.2 °C, respectively. To select a "normal" water year, the residual between mean annual precipitation and air temperature for the entire period (1960-2016) was calculated to select water year with the minimum combined residual. This was the water year 1962-1963 as the mean annual precipitation and temperature were 327 mm and -8.0 °C, respectively. Seasonal representability was also investigated by looking at the standard deviation of the absolute difference between mean monthly values and the 1962-1963 water year monthly values, resulting in a 10 mm and 1.1 °C for precipitation and temperature, respectively, suggesting that 1962-1963 is a good representation of the monthly variations. Given the importance of snowmelt to streamflow in the Arctic, winter precipitation (October to April) was compared; for 1962-1963 it was 194 mm, and on average over the period it was 166 mm, suggesting that this "normal" year is somewhat snowier than average.

This scenario includes transient changes in vegetation using the vegetation cover and density time series as described in Section 4.3. The increase in shrub cover was proportionally applied to the Upper and Lower Sparse Shrubs HRUs, whereas the area of the Wetland and Gully/Drift HRUs were kept constant as their delineation does not depend on the shrub covered area, but on wetland

and topographic criteria (Krogh et al., 2017). To implement this transient change, the model was run annually and the shrub cover and density parameters were incremented every November 1. Figure 4.3 presents the change in area for the Sparse Shrubs and Tundra HRUs during the modelling period, and the year 1992, which is the vegetation cover used by Krogh *et al.* (2017).

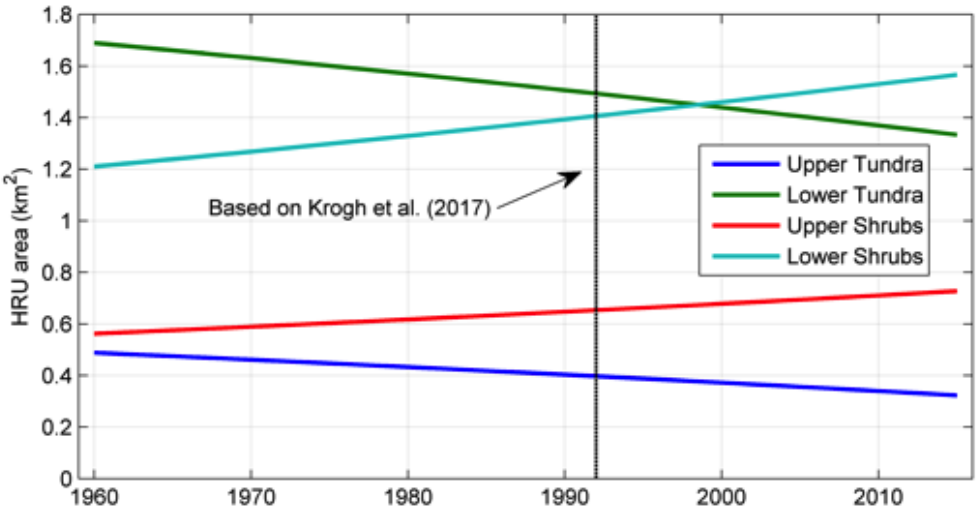

Figure 4.3: Annual changes in the Tundra and Shrubs HRUs area used in the CRHM-AHM model.

4.4.2.3 Model Scenario 3 (MS3): changing vegetation and climate

This scenario includes changing climate and transient vegetation as presented for the scenarios ΔC and ΔV, and represents the hydrology of Havikpak Creek as realistically as possible.

4.4.2.4 Transferring initial conditions

In ΔV and ΔCV, the CRHM-AHM was run annually to permit the updating of vegetation parameters at the end of the hydrological year; therefore, final conditions from one year needed to be transferred to the next, and updated with the change in the HRU area. To transfer the initial condition of a given state variable "S" (e.g. volumetric soil moisture or snow water equivalent) from the year (t) and HRU1 (S_1^t) to the next year and HRU2 (S_2^{t+1}), the following relationship can be obtained through mass conservation, assuming that area is transferred from HRU1 (Tundra) to HRU2 (Sparse Shrub):

$$S_2^{t+1} = \frac{A_2^t * S_2^t + (A_1^{t+1} - A_1^t) * S_1^t}{A_2^{t+1}} \qquad \textit{Equation 4-1}$$

$$S_1^{t+1} = S_1^t \qquad \textit{Equation 4-2}$$

.

Equation 4-1 and *Equation 4-2* were used to pass on soil moisture, soil recharge and snow water equivalent state variables from year to year as HRU areas changed.

4.4.3 Trend and change point analysis

The non-parametric Mann-Kendall test (Kendall, 1975; Mann, 1945) was used to perform trend analysis on simulated hydrological variables and observed weather data using a significance threshold of $p \leq 0.05$. The Mann-Kendall test has been extensively used to analyse linear trends in hydrological datasets (e.g. Burn and Hag Elnur, 2002; Hamed, 2008; Yip *et al.*, 2012), proving better results than other methods (Hess et al., 2001). As recommended by Hamed and Rao (1998) time series autocorrelation was removed before performing the Mann-Kendall test to eliminate the detection of false trends. The trend of slopes was calculated using Sen (1968) based on Kendall's rank correlation τ. Variables presented as a percentage of annual precipitation (i.e. rainfall and snowfall ratios) were log transformed ($y = \log (x / (1-x))$ first. Single change point in the time series were detected using the R-Package "changepoint" version 2.2.2 (Killick et al., 2016) based upon Hinkley (1970). These two techniques (Mann-Kendall and change point analysis) were used together as they complement each other and can be used to look at changes in different ways. For example, the detection of significant trends using Mann-Kendall depends on the arbitrary significance threshold, whereas the change point analysis assumes that the time series is normally distributed. Although both techniques have their own limitations they are both equally legitimate, resulting in potentially two different results, such a time series with no statistically significant trend but a detectable mean change point.

4.4.4 Teleconnections

To determine the influence of climatological teleconnections on hydrometeorological conditions in HPC, basin-scale mass fluxes were correlated to five climatic indexes representing large scale circulation features over 1960-2016: (1) Arctic oscillation (AO; Thompson and Wallace, 1998), (2) North Atlantic Oscillation (NAO; Hurrell *et al.*, 2001), (3) North Pacific Index (NPI; Trenberth and Hurrell, 1994), (4) Southern Oscillation Index (SAO; Rasmusson *et al.*, 1982) and (5) Pacific Decadal Oscillation (PDO; Mantua and Hare, 2002). These climatic indexes have been used to investigate teleconnections in Arctic and subarctic environments (Bonsal et al., 2006; Déry and Wood, 2004; Serreze et al., 2002). Teleconnections analysis was restricted to ΔCV as this scenario fully represents observed change in HPC.

4.5 Results

4.5.1 Meteorological trends

Figure 4.4 shows point changes and trends in seasonal and water year (October to September) precipitation for the period October 1960 - October 2016. Seasons were defined based on local hydrology: winter is from October to April when the snowpack forms and redistributes, spring is May when most snowmelt occurs, summer is from June to August and is a season of rainfall, soil thaw and minimal snowmelt, and fall is September when the active layer of the grounds starts to refreeze and precipitation shifts to snowfall. No trends were found for seasonal or annual precipitation, except spring, which had a significant and decreasing trend of -2.7 mm decade^{-1}. Conversely to the trend analysis, the change point analysis shows changes at most seasons and annually. Winter, spring and summer precipitation decreases from 187 to 160 mm, 25 to 13 mm, and 146 to 108 mm, respectively; whereas, fall precipitation increases from 16 to 34 mm. Annual precipitation decreases from 369 to 321 mm (48 mm) at the water year 1972 (Table 4.3). Analysis of the number of days with precipitation above the thresholds 1, 2, 5, 10 and 25 mm day^{-1} showed a decreasing trend for events greater than 1, 2 and 5 mm day^{-1} with a slope of -3.8, -1.7 and -0.7 days decade^{-1}, respectively. There are no changes in measurements methods associated with these changes.

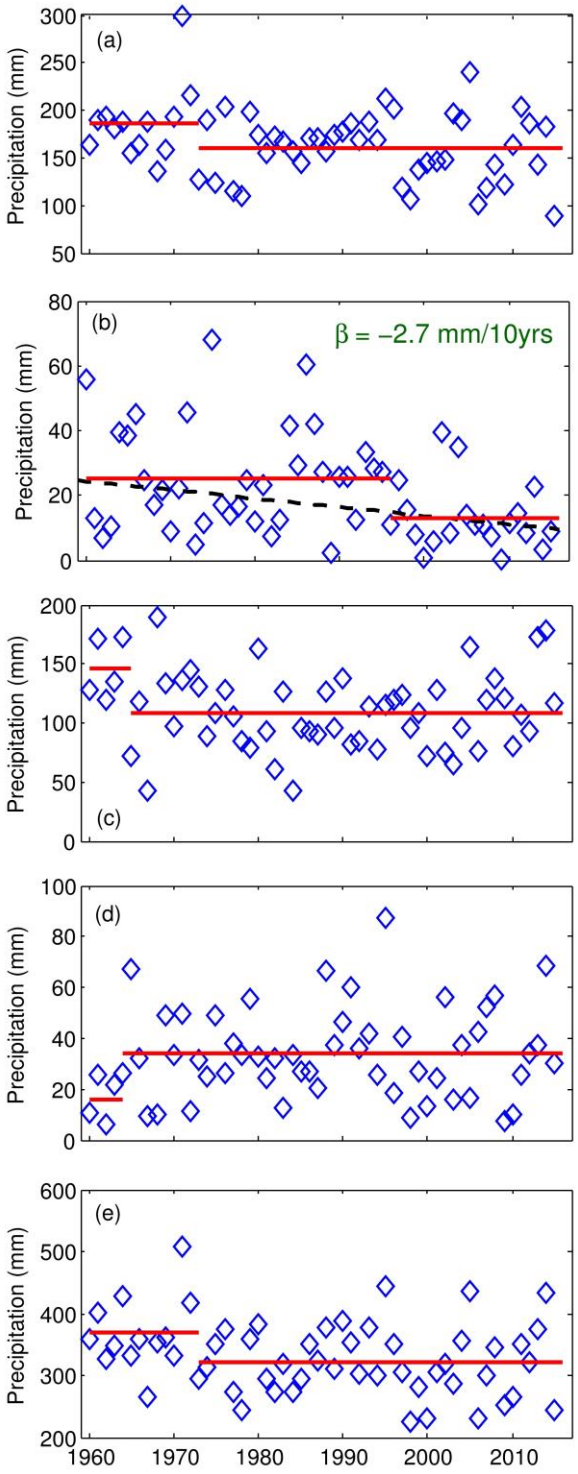

Figure 4.4: Observed seasonal and annual precipitation for each water year (October-September) from 1960 to 2015. (a) Winter (Oct-Apr), (b) spring (May), (c) summer (Jun-Aug), (d) fall (Sep) and (e) annual. Slope (β) is shown in mm decade^{-1} for statistically significant trends at the p≤0.05 significance threshold. Solid red line shows the annual change point.

Figure 4.5 shows seasonal and annual changes points and trends for minimum, maximum and mean daily air temperature. Increasing trends for mean air temperature were found annually and in every season, with the largest positive trend of 0.9 °C decade^{-1} in winter. Maximum air temperatures increased significantly annually and in summer, at 0.3 °C decade^{-1} in both cases. Winter, spring and fall maximum air temperatures did not show significant trends. Minimum air temperatures increased rapidly annually and in winter, at 1.4 °C decade^{-1} in both cases. Spring, summer and fall minimum annual temperatures did not show significant trends. Change point analysis showed that these trends are reflected by an increase in mean annual temperature during the water year 1992, from -9.1 to -7.1 °C (Table 4.3). Seasonally the change point analysis shows warming at all seasons but in summer and fall for minimum and mean temperature, respectively. Table 4.1 presents the changes in temperature for the period 1960-2016 for variables with statistically significant trends. The 8 °C increase in annual and winter minimum temperatures and 3.2 °C increase in annual (5.2 °C winter) mean temperatures over 56 years are remarkable and amongst the highest recorded on Earth.

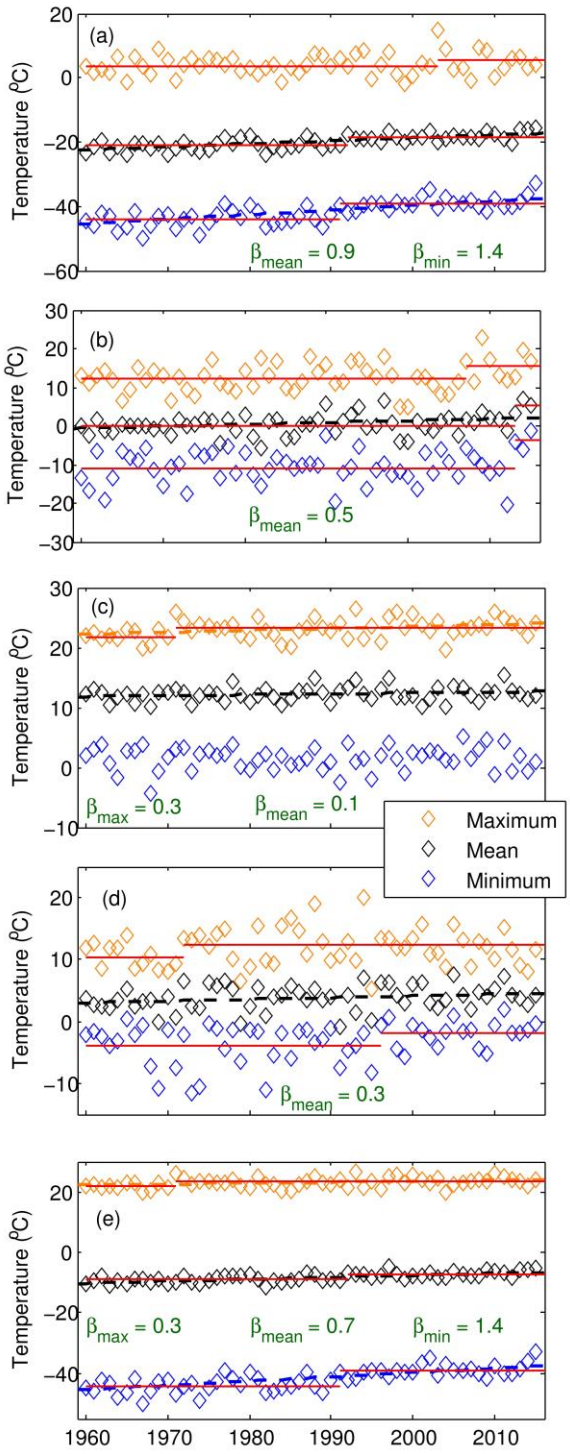

Figure 4.5: Observed seasonal and annual maximum, mean and minimum temperature for each water year (October-September) calculated from mean daily temperature, between 1960 and 2015. (a) Winter (Oct-Apr), (b) spring (May), (c) summer (Jun-Aug), (d) fall (Sep) and (e) annual. The dashed line is the linear regression using Sen (1968). Slope (β) in °C

Table 4.1: Changes in precipitation and temperature for the period 1960-2016 and statistically significant trends at the p≤0.05 significance threshold using Mann-Kendall test. Changes in precipitation as percentage with respect to 1960 are also presented.

Period	**Precipitation (mm)**	**Minimum Temperature (°C)**	**Mean Temperature (°C)**	**Maximum Temperature (°C)**
Winter	-	8.0	5.2	-
Spring	-15.1 (27%)	-	2.7	-
Summer	-	-	0.8	1.8
Fall	-	-	1.6	-
Annual	-	8.0	3.7	1.8

Table 4.2 presents the statistically significant trends for the other meteorological forcing variables used by CRHM-AHM at seasonal and annual scales. Mean annual short-wave irradiance has been decreasing by -1.4 W m^{-2} $decade^{-1}$ driven by decreases in spring and summer, whilst mean annual long-wave irradiance has been increasing by 2.9 W m^{-2} $decade^{-1}$ with greater increases in summer and fall than in winter and spring. Mean annual all-wave irradiance (short- and long-wave irradiance) has been increasing by 1.5 W m^{-2} $decade^{-1}$; however, summer all-wave irradiance has been decreasing by -2.9 W m^2 $decade^{-1}$. Mean annual wind speed did not change and relative humidity has been increasing by 0.8 % $decade^{-1}$. Table 4.3 shows the change point analysis for the atmospheric variables forcing CRHM-AHM. Mean annual short- and long-wave irradiance have change points in the water year 1969, from 112 to 104 and 230 to 242 W m^{-2}, whereas all-wave irradiance has a change point in 1997, from 344 to 348 W m^{-2}. Mean annual relative humidity has a change point in the water 2013, from 69 to 75%. No change point was found for mean annual wind speed. Three wind speed thresholds representing non-blowing snow (2 m s^{-1}), light drifting (6 m s^{-1}) and strong blizzards (12 m s^{-1}) were analyzed. Significant decreases in the hours of events larger than 2 and 6 m s^{-1} were found at -71 and -23 events $decade^{-1}$. The number of hourly events with strong blizzards showed no significant trend.

Table 4.2: Slope for statistically significant weather trends at the p≤0.05 significance threshold using Mann-Kendall test.

Period	**Shortwave Irradiance (W m^{-2} $decade^{-1}$)**	**Longwave Irradiance (W m^{-2} $decade^{-1}$)**	**Allwave Irradiance (W m^{-2} $decade^{-1}$)**	**Wind speed (m s^{-1} $decade^{-1}$)**	**Relative Humidity (% $decade^{-1}$)**
Winter	0.8	2.8	3.9	-	0.6
Spring	-4.3	2.4	-	-	-
Summer	-6	3.3	-2.9	-0.1	1.4
Fall	-	3.7	2.4	-	1.2
Annual	-1.4	2.9	1.5	-	0.8

Table 4.3: Mean change point analysis of the atmospheric forcing variables.

Atmospheric Variable	**Mean Annual Change**	**Year**
Precipitation (mm)	369 to 321	1972
Air Temperature (°C)	-9.1 to -7.1	1992
Short-wave Irradiance (W m^{-2})	112 to 104	1969
Long-wave Irradiance (W m^{-2})	230 to 242	1969
All-wave Irradiance (W m^{-2})	344 to 348	1997
Wind Speed (m s^{-1})	N/A	N/A
Relative Humidity (%)	69 to 75	2013

4.5.2 Updated CRHM-AHM validation

The 1995 to 2015 Nash-Sutcliffe Efficiency (NSE) and mean bias were found to be 0.40 and 6%, respectively; suggesting that the model's streamflow performance is consistent with that showed by Krogh *et al.* (2017), and changing vegetation dynamic parameterization has a small impact on the short-term model's streamflow performance.

4.5.3 Trends comparison between modelling scenarios

4.5.3.1 Sub-basin scale

Figure 4.6 presents trends in annual (water year) evapotranspiration and sublimation for various HRUs. Evapotranspiration (ET) refers to the actual wetted surface and canopy intercepted rain evaporation and plant transpiration as calculated by Penman-Monteith (P-M) and Priestley-Taylor (P-T; wetlands and lakes) methods (Krogh et al., 2017), but restricted by not only stomatal conductance in P-M but also by available storage of intercepted rainfall, ponded surface water and soil moisture content and the soil moisture withdrawal curve in CHRM. ET in ΔC and ΔCV has been significantly decreasing by 2 and 5 mm decade^{-1} for some HRUs, whereas in ΔV it has been increasing from HRU#3 (Upper Gully/Drift). Evaporation from canopy rainfall interception has been decreasing by up to 2 mm decade^{-1} in ΔC and ΔCV for most HRUs, but has no trend in ΔV where only vegetation increases. Soil moisture- restricted and -unrestricted ET from P-M and P-T equations has virtually the same trends, except from Taiga Forest (HRU#5), suggesting that soil moisture content has had little effect in ET. Blowing snow sublimation has a decreasing trend in the Upper and Lower Shrub HRUs for ΔV and ΔCV where vegetation increases, with the largest trend in the upper basin (~-14 mm decade^{-1}). Decreasing blowing snow sublimation by 3 mm decade^{-1} was found in the Upper Tundra HRU for ΔC and ΔCV. Sublimation from canopy intercepted snow has a decreasing trend for all of the vegetated HRUs in ΔC and ΔCV, with the largest trend in the Forest HRU (roughly 6 mm decade^{-1}). Sublimation at the snow surface has a decreasing trend in the Forest (HRU#6) in ΔC and ΔCV (~-1 mm decade^{-1}), whereas in ΔV it has an increasing trend in the Upper Gully/Drift (HRU#3) and decreasing in the Upper Shrub HRU. Annual sublimation, defined as the sum of the previous three sublimation terms, has a decreasing trend in ΔV for the Upper and Lower Shrubs and Upper Gully/drift (about 2 to 3 mm decade^{-1}, respectively). In ΔC and ΔCV it has a decreasing trend in the forested HRUs and Lower Shrub HRU, driven by the decreasing sublimation from canopy interception, which is the dominant sublimation term over the basin (Krogh et al., 2017). Blowing snow redistribution, defined as the divergence between incoming and outgoing blowing snow transport, decreased in the Upper and Lower Gully/Drift HRU for all scenarios, between -20 and -45 mm decade^{-1} in the upper basin and -10 and -20 in the lower basin.

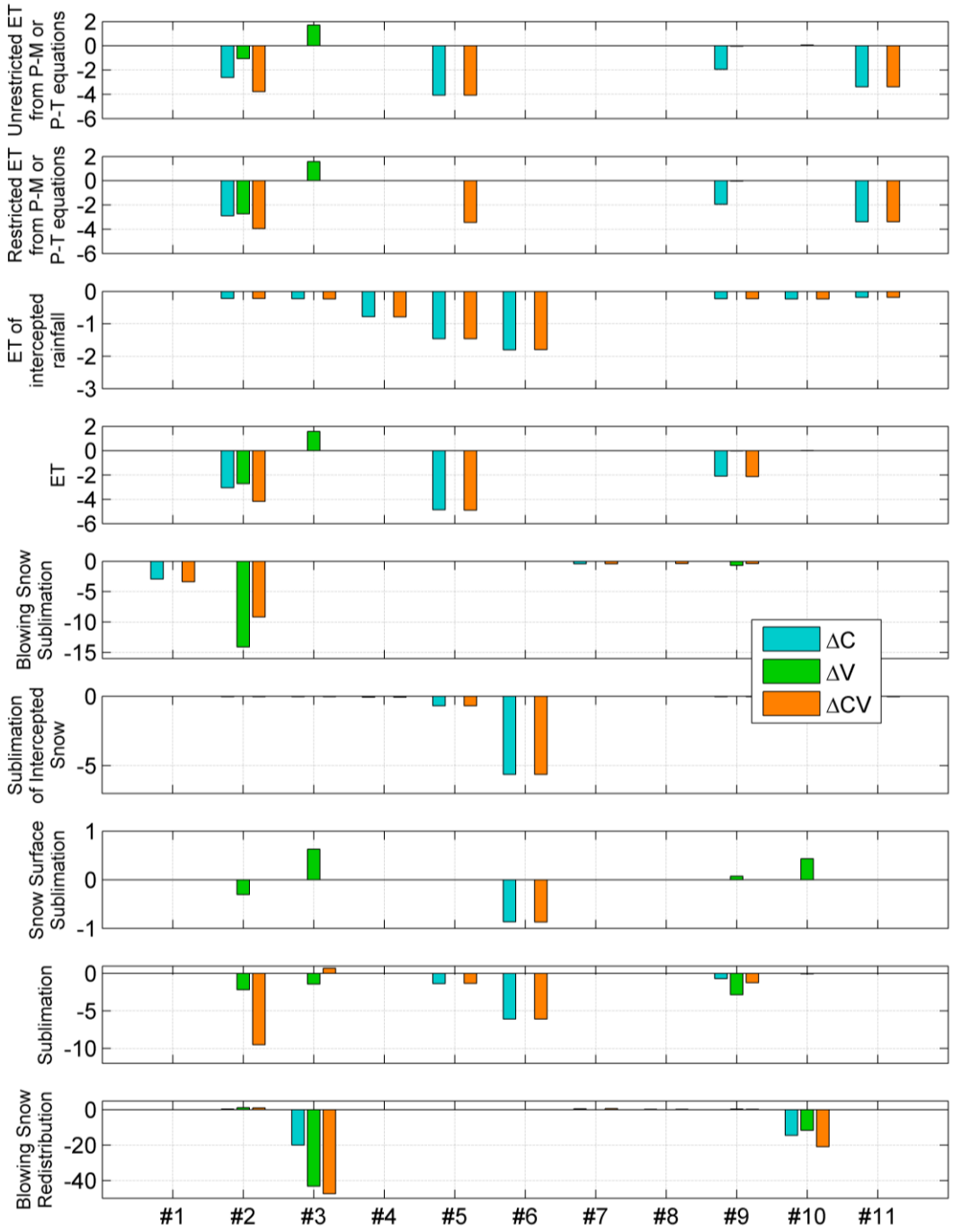

Figure 4.6: Units in mm decade^{-1}.Scenario comparison of significant trends ($p \leq 0.05$) for selected mass fluxes at an HRU-scale. X-axis as follows: Upper Tundra (#1), Upper Sparse Shrubs (#2), Upper Gully-Drift (#3), Close Shrubs (#4), Taiga Forest (#5), Forest (#6), Lower Tundra (#7), Open Water (#8), Lower Sparse Shrubs (#9), Lower Gully-Drift (#10) and Wetland (#11).

Figure 4.7 present a series of trends related to snowcover and ground freeze/thaw. Maximum SWE for ΔC decreased in some HRUs, with the largest trend in the Lower Sparse Shrub HRU (-17 mm decade^{-1}), whereas for ΔCV the largest decreasing trend was found in the Upper Sparse Shrub HRU (-54 mm decade^{-1}). Maximum SWE for ΔV showed increasing and decreasing trends in the Sparse Shrub and Gully/Drift HRUs, respectively, with the largest changes found in the upper basin. Note that increasing vegetation cover and density hampered blowing snow transport from Sparse Shrub towards Gully/Drift HRUs (Figure 4.6). The snowcover depletion date for ΔC and ΔCV advanced in almost all HRUs, around -1 and -3 days decade-1, whereas for ΔV, both advancing and retreating were found in the Upper Sparse Shrub and Upper Gully/Drift, respectively. Snowcover duration for ΔC and ΔCV declined for some HRUs (around -1 and -3 days decade^{-1}), whereas for ΔV, both extension and decline was found in the Upper Sparse Shrub and Gully/Drift HRUs (roughly 1 and -1 days decade^{-1}). Ground thaw initiation had similar changes as the snowcover depletion timing, which is expected as ground thaw typically starts once the ground is snow-free and temperatures are above 0°C. Active layer thickness (ALT) for ΔC and ΔCV deepened throughout the basin at between 2 and 5 cm decade^{-1}, whereas for ΔV it deepened in the Upper Sparse Shrub and Gully/Drift HRUs (<2 cm decade^{-1}). Snow ablation rate, here defined as the ratio between the maximum SWE and the number of days between maximum SWE and the depletion of snowcover, decreased for ΔC and ΔCV in some HRUs by between -0.1 and -1.5 mm day^{-1} decade^{-1}, whereas for ΔV it increased in the Sparse Shrub and decreased in the Gully/Drift HRUs.

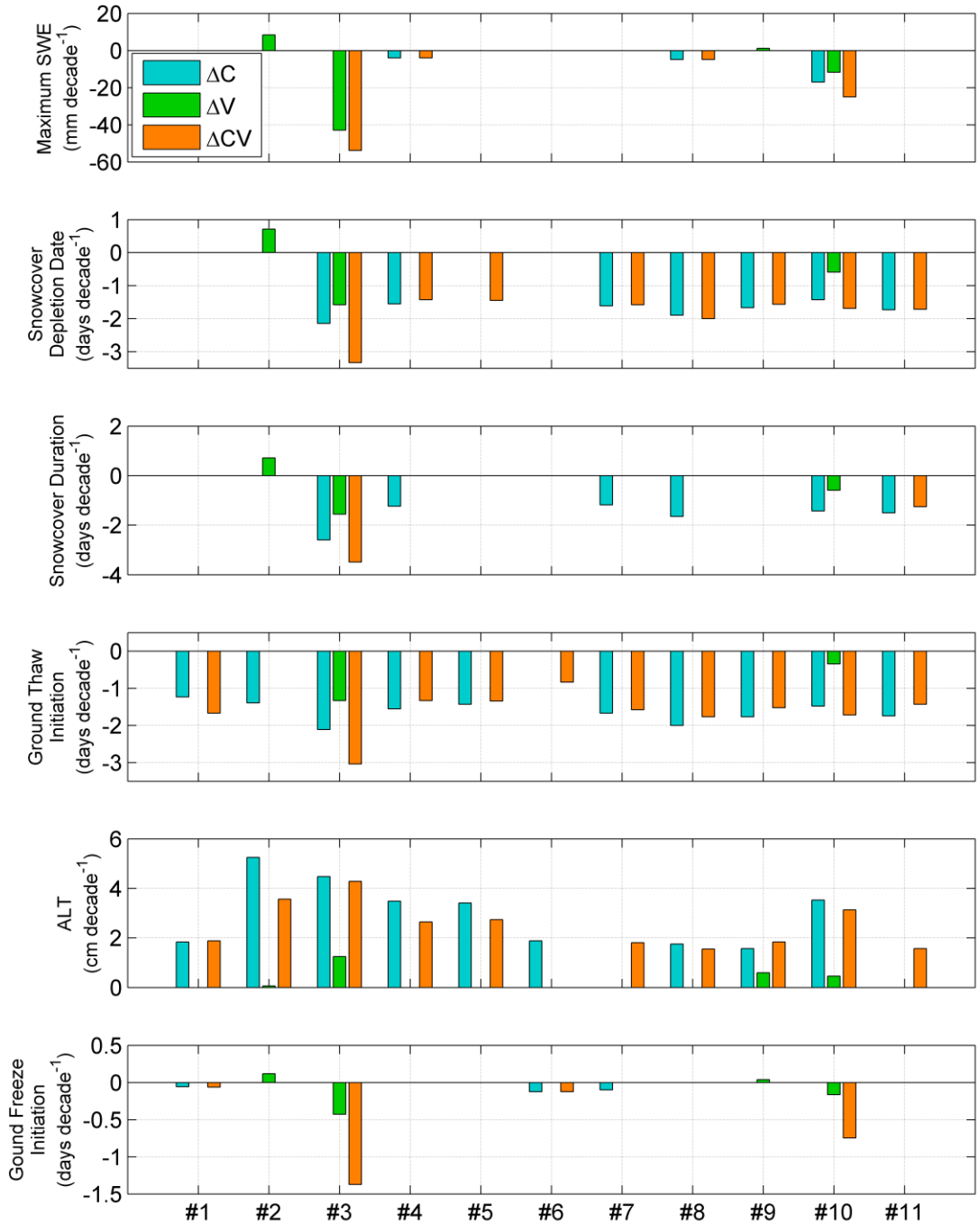

Figure 4.7: Comparison of significant trends ($p \leq 0.05$) for snow and ground freeze/thaw related variables at an HRU-scale for the three scenarios. Note that trends for snowcover depletion date, snowcover duration and ground thaw initiation are in dates, and for maximum SWE, ALT and snow ablation are in rates. X-axis as follows: Upper Tundra (#1), Upper Sparse Shrubs (#2), Upper Gully-Drift (#3), Close Shrubs (#4), Taiga Forest (#5), Forest (#6), Lower Tundra (#7), Open Water (#8), Lower Sparse Shrubs (#9), Lower Gully-Drift (#10) and Wetland (#11). ALT: Active Layer Thickness. SWE: Snow Water Equivalent.

4.5.3.2 Basin scale

The primary annual mass flux trends from the three modelling scenarios are presented in Figure 8 at the basin scale. No trend was found for annual rainfall depths; however, a decreasing trend of -7.8 mm decade^{-1} was found for snowfall depths in ΔC and ΔCV. The rainfall ratio (rainfall divided by total precipitation) exhibited no trend. Annual sublimation losses decreased by -1.3, -0.7 and -1.8 mm decade^{-1} in scenarios ΔC, ΔV and ΔCV, respectively. The sublimation trend in ΔC was driven by decreasing sublimation from canopy interception, likely due to decreasing snowfall. Decreasing sublimation in the ΔV scenario was driven by decreasing blowing snow sublimation caused by expanding and densifying tundra shrubs, whereas for the ΔCV scenario, both drove sublimation trends. Annual ET losses decreased by -2.5 mm decade^{-1} in ΔCV, in contrast to the trend to increase by 0.06 mm decade^{-1} for ΔV, driven by positive trends in all ET components. ET in ΔC showed no trend. Decreasing ET in ΔCV was driven by a decreasing trend in evaporation of rain intercepted in the canopy. To investigate the potential impact of changes in stomata resistance on evapotranspiration, trends in mean annual stomata resistance were also calculated. For both scenarios with changing climate (ΔC and ΔCV), no trend was found; however, for the changing vegetation-only scenario (ΔV) a positive trend of 1.6 s m^{-1} decade^{-1} was found, which agrees with the small increase in ET found for this scenario. Annual streamflow shows an increasing trend of 0.6 mm decade^{-1} only for ΔV, likely due to the increasing snow accumulation at some HRUs (Figure 4.6) as a result of reduced blowing snow transport.

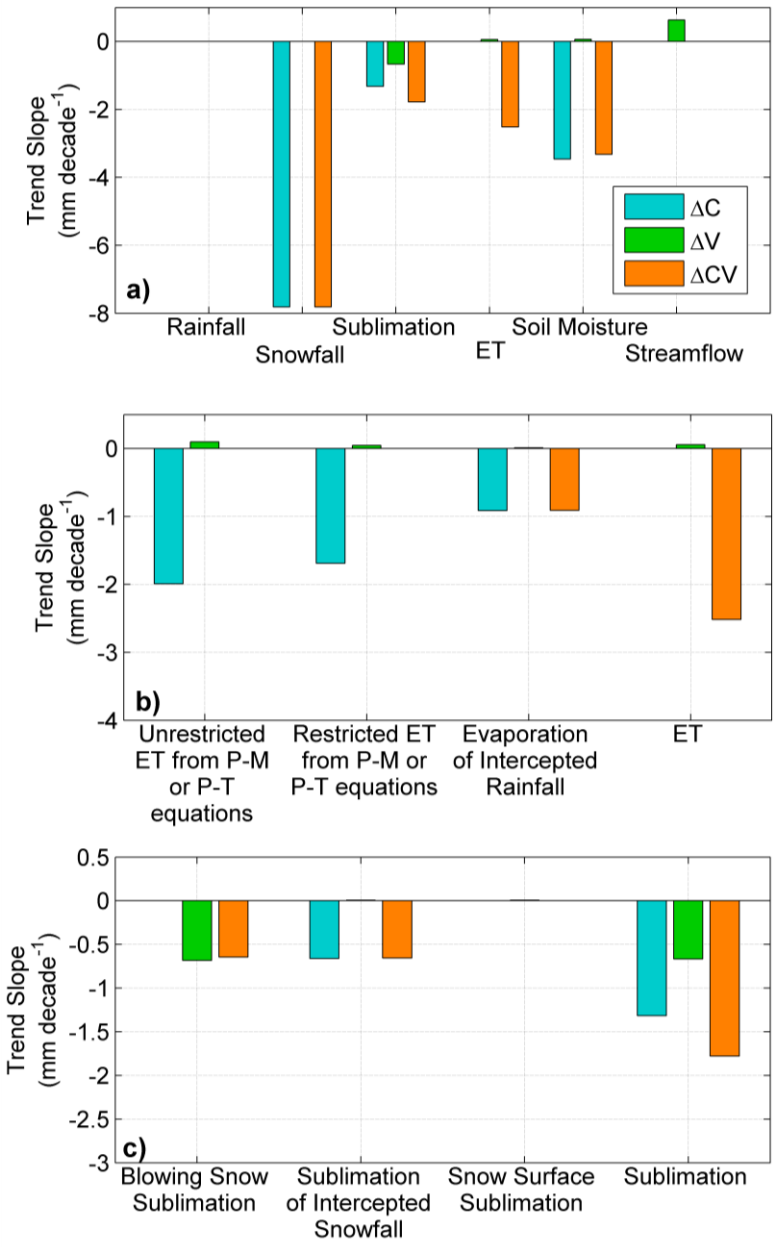

Figure 4.8: Comparison of basin-scale annual mass fluxes trends ($p \leq 0.05$) over the water years from 1960 to 2015, for the three scenarios. a) Main mass fluxes. b) Evapotranspiration components. c) Sublimation components.

Table 4.4 presents the change point analysis for selected annual mass fluxes at the basin scale for the three scenarios. Rainfall shows an increase from 131 to 196 mm in 2013, whereas snowfall decreases from 211 to 169 mm in 1997. Similarly to the trend analysis, sublimation shows a decrease in all the modelling scenarios, from 39 to 28 mm, 37 to 35 mm, and 42 to 36 mm, for ΔC, ΔV and ΔCV, respectively. ET, which showed no significant trend for ΔC, presents a decreasing change point from 160 to 144 for ΔC, driven by the dryer conditions. ET for ΔV shows no change

point, despite the small significant trend in ET (0.06 mm decade^{-1}). For the combined scenario (ΔCV) ET shows a decrease change point in 1977 from 160 to 144 mm, driven by dryer conditions and the decrease in radiative energy for ET (all-wave irradiance). Streamflow for ΔC has a decreasing change point from 180 to 140 mm in 1973, despite the lack of significant trend (Figure 4.8). For ΔV, streamflow has a small increase from 133 to 135 mm in 1992, which somewhat counteracts the effect of changing climate (180 to 140 mm), resulting in a smaller change from 178 to 140 mm in 1973 for ΔCV.

Table 4.4: Change point analysis for selected annual basin-scale mass fluxes for the three modelling scenario

Mass Fluxes	**ΔC: Δ Climate-only**		**ΔV: Δ Vegetation-only**		**ΔCV: Δ Climate and Vegetation**	
	Mean Change (mm)	**Year**	**Mean change (mm)**	**Year**	**Mean Change (mm)**	**Year**
Rainfall	131 to 196	2013	N/A	N/A	131 to 196	2013
Snowfall	211 to 169	1997	N/A	N/A	211 to 169	1997
Sublimation	39 to 28	2013	37 to 35	1988	42 to 36	1980
ET	160 to 144	1977	N/A	N/A	160 to 144	1977
Soil Moisture	80 to 48	1968	N/A	N/A	82 to 49	1968
Streamflow	180 to 140	1973	133 to 135	1992	178 to 140	1973

4.5.4 Streamflow regime change

The ΔCV scenario most comprehensively represents historical change in climate and vegetation in the Havikpak Creek Basin; therefore, it was used to estimate and diagnose changes in streamflow. Figure 4.9 presents annual time series of variables associated with annual streamflow and peak streamflow for the water years between 1960 and 2015. These time series are: annual streamflow volume (Figure 4.9a), annual peak daily streamflow discharge (Figure 4.9b), date (day of the year, DOY) of peak discharge (Figure 4.9c), the DOY of the centre of mass (50% of volume passed) of streamflow discharge (Figure 4.9d) and daily streamflow discharge associated with different exceedance probabilities: 5%, 25%, 50%, 75% and 95% using a Weibull distribution function (Figure 4.9e). The Weibull distribution was used as it shown to successfully represent daily streamflow probability distribution (not shown). The DOY of peak daily annual streamflow and the DOY of streamflow's centre of mass decreased by -1.8 and 1.2 days decade^{-1}, respectively. This finding is consistent with the earlier snow depletion date shown in Figure **4.7**. The abnormally high value for the DOY peak daily annual streamflow and of streamflow's centre of mass (Figure 4.9c and d; DOY = 226, mid-August) for the water year 1968 is associated with a water year with abnormally high rainfall-runoff compared to snowmelt runoff. No trends were found in monthly streamflow volumes for each month between May and October (not shown), except for September, which decreased at about -47.1 m^3 decade^{-1}.

Figure 4.10 presents the mean daily streamflow discharge for observed streamflow (1995-2015) and the three modelling scenarios over the period 1960-2016. The ΔC and ΔCV scenarios show very similar mean hydrographs; with streamflow discharge starting in mid-April reaching the peak discharge at 0.7 m^3 s^{-1} in June 8 and ending by mid-November. The ΔV scenario presents a much different mean discharge response, which is not surprising as meteorological drivers largely control the mean conditions and these were kept constant in this scenario. Under this scenario (ΔV), streamflow starts in mid-May reaching the peak discharge at 1.7 m^3 s^{-1} in May 22, and it ends in mid-August, having a much shorter discharge season. The current mean hydrological regime, discussed in detail by Krogh et al. (2017), shows an earlier peak flow compared with the long-term ΔC or ΔCV scenarios, which is consistent with the reduction in the date of peakflow presented in Figure 4.9c. Also, larger late-fall streamflow discharge is present under current conditions.

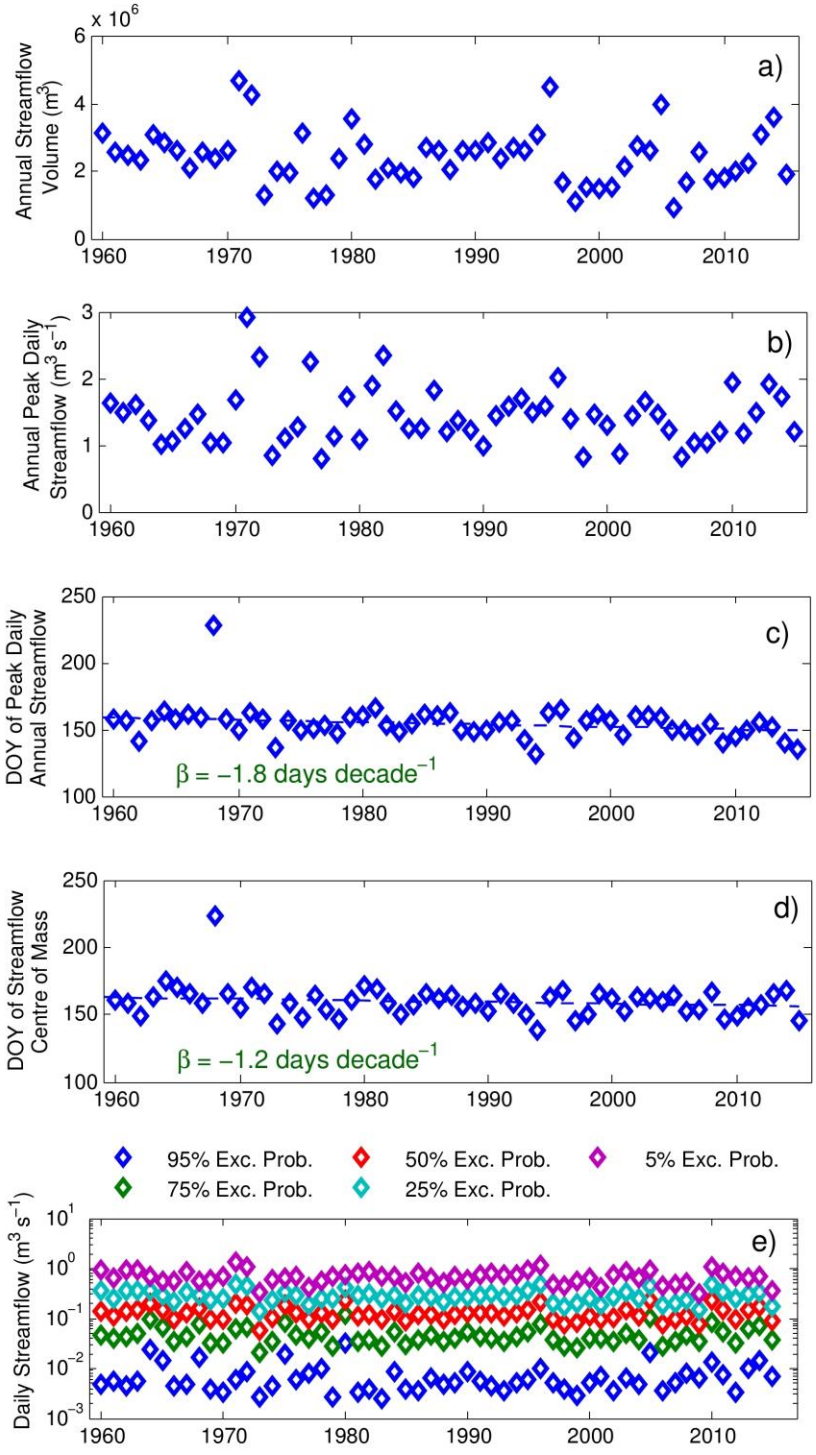

Figure 4.9: a) Annual streamflow volume. b) Annual peak daily streamflow. c) Day of the Year (DOY) of peak daily streamflow. d) Day of the Year (DOY) of streamflow volume discharge centre of mass. e) Streamflow discharge associated for various exceedance probabilities. X-axis of all subplots is the water year starting in October.

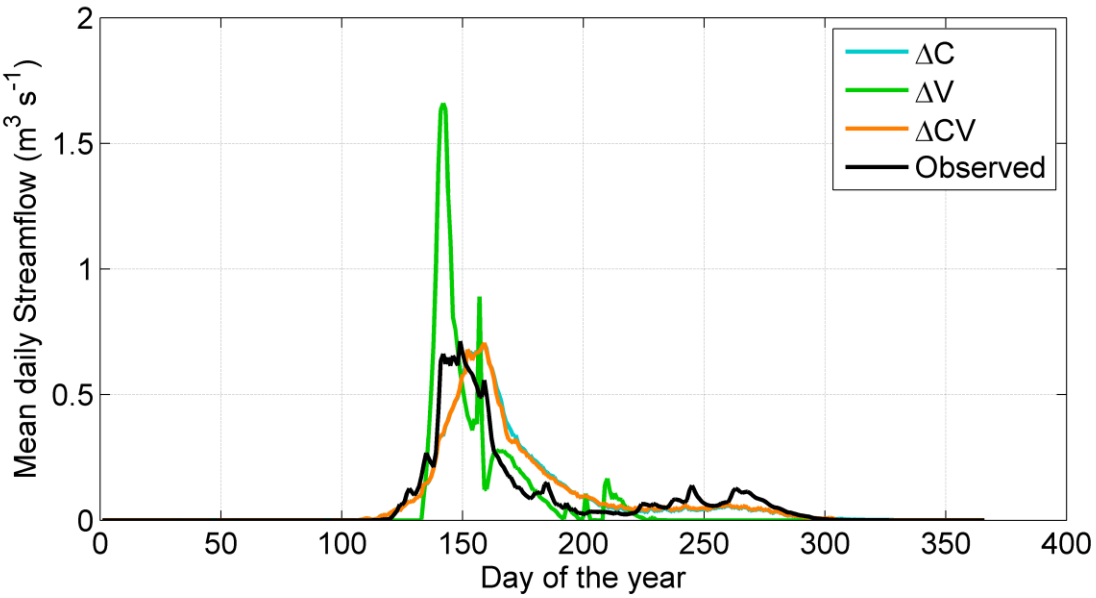

Figure 4.10: Mean annual hydrograph for the observed streamflow (1995-2015), and the three modelling scenarios: changing climate-only (ΔC), changing vegetation-only (ΔV) and changing climate and vegetation (ΔCV). Note the overlapping between the ΔC and ΔCV scenarios.

4.5.5 Teleconnections

Table 4.5 lists Pearson correlations coefficients between annual basin scale mass fluxes and five climatic indices. Statistically significant correlation coefficients with p-values ≤ 0.05 are in bold. Significant correlations were found between some mass fluxes and North Pacific Index (NPI), Southern Oscillation Index (SOI) and Pacific Decadal Oscillation (PDO); however, even significant Pearson coefficients were relatively low (<0.4), suggesting that large-scale climatic oscillations do not have an important effect on Havikpak Creek Basin hydrology. The same analysis on a seasonal scale provided similarly low correlation coefficients (not shown).

Table 4.5: Pearson correlation coefficient between basin-scale mass fluxes and climatic indexes, using water year values (October-September). Correlation coefficients with p-value ≤0.05 are in bold.

Climatic Index	**AO**	**NAO**	**NPI**	**SOI**	**PDO**
Rainfall	0.134	0.002	0.207	-0.007	-0.110
Snowfall	-0.013	0.151	0.116	-0.168	0.022
Precipitation	0.075	0.114	0.219	-0.130	-0.054
Sublimation	-0.021	0.125	0.256	0.185	**-0.340**
Blowing Snow Sublimation	0.044	0.020	**0.336**	0.200	**-0.397**
Snowpack Sublimation	-0.049	0.077	0.108	0.203	-0.249
Sublimation of Intercepted Snowfall	-0.014	0.172	0.143	-0.071	-0.058
Restricted ET from P-M or P-T equations	0.161	-0.200	0.253	**0.268**	**-0.332**
Evaporation from Canopy Interception	-0.034	0.125	-0.017	-0.078	0.061
ET	0.156	-0.183	0.250	0.256	**-0.323**
Soil Moisture	-0.010	-0.158	0.191	-0.065	-0.073
Streamflow	-0.002	0.062	0.083	-0.262	0.141

4.6 Discussion

4.6.1 Changing climate

The increasing air temperature trends at Inuvik found in this study (Figure 4.5) qualitatively agree with those trends found by other studies using gridded data products (DeBeer et al., 2016; Vincent et al., 2015). Inuvik winters have warmed to the greatest degree; minimum and mean air temperature have increased by 8.0 and 5.2 °C, respectively, over 1960-2016. No temporal trend in precipitation was found at Inuvik (Figure 4.4), except for decrease in the spring (-2.7 mm decade^{-1}; Figure 4.4); however, the change point analysis showed an important decrease in year 1972 from 369 to 321 mm yr^{-1} for the mean annual precipitation (Table 4.3). Vincent *et al.* (2015) investigated long-term trends in precipitation records over Canada for the period between 1948 and 2012 using the gridded and spatially interpolated CANGRD dataset (Rapaic *et al.*, 2015). For the region around Havikpak Creek Vincent *et al.* (2015) showed significant spatial variability with a small

increase of less than 10% in annual precipitation. The CANGRD dataset is a spatially interpolated 50 km product that is based on the AHCCD dataset and has shown problems when compared against weather station data, particularly north of 60° N (Milewska and Hogg, 2001). Different trends found in this study and Vincent *et al.* (2015) can be explained by interpolation errors in the CANGRD dataset and the different period of analysis. This suggests that careful assessment of regional climate product needs to be performed when looking at individual sites, particularly in the Arctic where there are few stations.

As presented in Section 4.3.2, the precipitation time series was produced using mostly the AHCCD dataset and corrected records from automated weather stations (AWS) for wind undercatch, producing a discontinuity in the time series in the mid-90s. Although uncertainty exists in the precipitation records, there is a relatively high confidence in the accuracy of precipitation, supported by the typically low wind speed limiting wind undercatch losses, the meticulous quality control and corrections used in the AHCCD dataset (Mekis and Vincent, 2011), the well-established wind-undercatch correction used for the AWS snow gauge, and the snow surveys from small clearing with minimal snow distribution and sublimation that allows a good estimation of seasonal snowfall. Comparing this precipitation dataset with another nearby station is challenging, as it there is no station with similar long-term records close to Inuvik. Nevertheless, the impacts of such uncertainty on the presented results are expected to be small and should not change the core discussions and conclusions of this study.

Mean annual short-wave irradiance from combined ERA-40 and ERA-I decreased by -1.4 W m^{-2} $decade^{-1}$ (Table 4.2) or -7.4% over 1960-2016 with respect to 1960. Other studies have also found that measured solar irradiance in the Arctic has decreased. For example, Weston *et al.* (2007) found a decreasing trend in solar irradiance at two Canadian Arctic sites: Alert and Resolute Bay, Nunavut Territory, for the period 1964-2002 and 1957-2003, respectively. They argued that decreases in short-wave irradiance are driven by changes in atmospheric composition, such as aerosols and greenhouse gases, producing a decreasing in the calculated daily Clearness Index. However, ERA-I irradiance model calculation (Saunders et al., 1999) does not include the effect of aerosols scattering, but it does include the effect of greenhouse gasses, such as water vapour and carbon monoxide. Mean annual long-wave irradiance shows an increasing trend of 2.9 W m^{-2} $decade^{-1}$ (Table 4.2) 7.3% over 1960-2016 with respect to 1960. This result agrees with global observations showing an increase in long-wave radiation (Ohmura, 2009), particularly over the Canadian Arctic, for which observed net long-wave is also increasing (Weston et al., 2007), and is consistent with an increase in cloud cover and/or water vapour in the atmosphere with resulting increasing atmospheric emissivity and/or increasing air temperatures. The annual modelled all-wave irradiance is increasing by 2.6%, but with seasonal variations. Winter all-wave irradiance has been increasing by 10% providing more energy to snowmelt and sublimation, whereas summer all-wave irradiance has been decreasing by 3%, which decreases the energy for ET and ground thaw.

4.6.2 Changes to hydrological cycle

Precipitation phase shifted from snowfall to rainfall in the scenarios including climate change (ΔC and ΔCV; Figure 4.8) by 22.7% from 1960 to 2016, this was driven by the increase in mean annual air temperature of 3.7 °C (Table 4.1). Snowcover duration decreased for ΔC (some HRUs; Figure 4.7), whereas for ΔV both decreased and increased over the HRUs; however, the ΔCV resulted in a shortened snow season (most HRUs). This shortening was mostly driven by changing climate with reduced snowfall and snow redistribution to drifts by wind. Similarly to the snow season duration, the snowcover depletion date for ΔCV decreased between 8 and 17 days over 1960-2016 (Figure 4.7), with the greatest decrease in the Upper Gully/Drift HRU, due to decreasing blowing snow redistribution and hence peak SWE. As peak streamflow in HPC is dominated by snowmelt events, these changes are consistent with the 10 day advance in peak streamflow date. Peak SWE decreased between 12 and 33% in the ΔC, whereas for ΔV it increased in the Sparse Shrub HRUs by 3 to 30% and decreased in the Gully/Drift HRUs by 22 to 40%, respectively. The ΔCV scenario resulted in diminishing peak SWE by 12 to 50%, due to the combination of decreasing snowfall and blowing snow redistribution from Sparse Shrubs to Gully/Drift HRUs. Snow ablation rates for ΔC decreased by 0.3 to 1.1% over 1960-2016, whereas for ΔV decreased in the Sparse Shrub HRUs by 0.1 to 0.4% and increases by 0.31 to 0.4% in the Gully/Drift HRUs. Changes in snow ablation rates due to a warmer climate have been investigated in other cold regions. Rasouli *et al.* (2014) and Pomeroy et al. (2015) modelled snow hydrology in mountain basins in Yukon and Alberta, Canada, respectively, and attributed the lower snow ablation rates under climate change to an earlier snowmelt season, occurring when lower solar radiation inputs are available. Using snow accumulation records in western U.S.A., Musselman *et al.* (2017) reached a similar conclusion. López-Moreno et al. (2012) also found a reduction in ablation rates in the Spanish Pyrenees under a scenario of warmer temperatures. However, here some snow ablation rates increased for ΔV, suggesting climatic factor are not the only control in ablation rates, but that vegetation dynamics can compensate or even reverse trends in ablation rates due to changing climate.

Sublimation decreased in ΔC by 23%, due to a decrease in sublimation of intercepted snow by 19%. Factors decreasing sublimation of intercepted snow are warmer temperatures, causing accelerated snow unloading from the canopy, and decreasing snowfall. Sublimation for ΔV decreased by 10%, due to blowing snow sublimation dropping by 44%, mostly in the upper basin. Decreasing blowing snow in this scenario is driven by shrub densification, increasing the aerodynamic roughness height and wind speeds required to initiate blowing snow transport. Shrub densification intensified the effect of changing climate on sublimation, decreasing sublimation by 29% over the study period. ET was found not to change in the changing climate-only scenario; however, the ET of intercepted rainfall and soil moisture-restricted ET from the P-M or P-T equations decreased by 51 and 6%, respectively. This is explained by the different inter-annual variability of the two ET terms hampering the individual trends; nevertheless, the change point

analysis of mean annual ET shows a decrease of 16 mm yr^{-1} in 1977 (9.5% with respect to 1960 for ΔC and ΔCV), consistently with the simulated trends of each ET component. ET for ΔV increased by a marginal 0.2%, due to the 1.5% increase in soil moisture content and 0.8% increase in ET of intercepted rainfall due to shrub expansion. The combined effect of changing climate and vegetation decreased ET by 8.5%, driven largely by changing climate. Decreasing summer all-wave irradiance (3%) and soil moisture content (19%) were driving decreasing ET in the scenario with combined climate and vegetation changes.

Active layer thickness (ALT) for ΔC increased by 11 to 28 cm over 1960-2016 for most HRUs, caused by the earlier snow depletion date (8 to 11 days) and ground thaw initiation (6 to 11 days), and warmer ground-surface temperatures due to warmer air temperatures. ALT increased up to 6 cm for ΔV in some HRUs, driven by the earlier snowcover depletion date (3 to 8) and ground thaw initiation (2 to 6 days). The effect of changing vegetation dampened the deepening in ALT found in ΔC scenario for most HRUs; nevertheless, in the ΔCV scenario, ALT increased by 11 to 22 cm.

Annual Streamflow volume from HPC has dropped by 38 mm (21%) whilst annual precipitation has dropped by 48 (13%) mm since 1960. We argue that the 10 mm (21%) difference between the decrease in precipitation and streamflow discharge from HPC suggest a small degree of hydrological resiliency, here defined as the capacity of a basin to actively counteract the impact of changes in weather on streamflow discharge, which is explained by the declining ET and sublimation. This result emphasizes the need for a full physically based representation of the hydrological cycle in models so that the processes driving this streamflow resiliency can be used to diagnose its function.

4.6.3 Havikpak Creek basin changes versus other Arctic studies

The ΔCV scenario best represents historical change in Havikpak Creek Basin; therefore, it is used to compare with other Arctic studies. Snowcover depletion dates in HPC accelerated between 1.5 and 3.2 days $decade^{-1}$ (Figure 4.7), which are higher than the average trend presented by Liston and Hiemstra (2011) for the entire Arctic (-1.28 days $decade^{-1}$), but smaller than their largest trend in the Arctic (-9.89 days $decade^{-1}$). The maximum ALT depth increased by 1.8 to 4.2 cm $decade^{-1}$ (Figure 4.7), which is smaller than the average trend of 4.7 cm $decade^{-1}$ modelled by Oelke *et al.* (2004) over the Mackenzie River Basin. Differences in ALT change simulations can be due to: (1) differences in the model's spatial representation, Oelke et al. used grids of 25 km, with which small-scale features are not well represented; (2) differences in the ground freeze/thaw method algorithm, Oelke et al. use a one-dimensional heat conduction (i.e. lateral flow is neglected); and (3) the driving meteorology used by Oelke et al. was the NCEP/NCAR reanalysis, which has shown some problems in representing Arctic climate (Serreze et al., 1998; Serreze and Hurst, 2000). However, the average permafrost conditions of the Mackenzie River Basin (MRB) are thinner and warmer compared with those in HPC, and so average changes in ALT are expected to be larger for the MRB than for HPC.

Annual streamflow volume at HPC has dropped (Table 4.4); unfortunately there are no long-term studies of small streams that originate in the Arctic to compare this result with. There are studies showing increasing large river basin streamflow into the Arctic Ocean (McClelland et al., 2006; Overeem and Syvitski, 2010; Peterson et al., 2002; Rood et al., 2017; Yang et al., 2002). However, a significant portion of the runoff in these basins originates south of the Arctic Circle (e.g. the Mackenzie and the Lena River basins in Canada and Russia, respectively), and therefore these trends are not representative of changes in Arctic hydrology. Previous studies have argued that the increase in the streamflow of large rivers flowing into the Arctic is driven by increasing baseflow due to permafrost thaw and increasing precipitation. However, HPC annual precipitation and streamflow have both dropped and the earlier shifts in the hydrograph are inconsistent with such mechanism. Instead, baseflow during the end of the summer is minimal, streamflow has been decreasing during September, and no winter flow has been observed. Only a few similarities can be found between results of studies of large river basins flowing to the Arctic and HPC, such increasing ALT and accelerating snow-free date; however, most processes, such as evapotranspiration and streamflow depend on the local scale interaction between several physical processes, which are undergoing distinct changes that are not evident in rivers flowing into the Arctic. Therefore, the results of studies of these large river basins should not be confused with the results for an Arctic hydrology study.

This study considered changing climate and transient vegetation change separately to identify their individual effects; nevertheless, they are strongly coupled in the historical record. Warming temperatures are well correlated with shrub growth (Myers-Smith et al., 2011), which has a positive feedback to atmospheric heating by decreasing surface albedo, generating greater sensible heat flux to the atmosphere (Pomeroy et al., 2006) and a negative feedback by consuming more atmospheric CO_2 (Myers-Smith et al., 2011). The modelling scenario experiments here revealed that most simulated trends in the water balance are attributable to changes in climate; however, the effect of transient vegetation as expressed in shrub expansion and densification, was shown to further reduce blowing snow redistribution and sublimation, which intensified climate change-driven trends produced by the reduced snow accumulation. This emphasizes the need to included transient vegetation changes in hydrological simulations, which is typically neglected in hydrological models. Reliable rates of change in vegetation species, height and density need to be available for this purpose; therefore, comprehensive studies investigating these changes in other transitioning environments are needed.

4.7 Conclusion

This study diagnosed changes in the hydrology of a small Arctic basin in the tundra-taiga transition using a spatially distributed and physically based hydrological model. It considered both transient climate and vegetation changes for the first time. There was no evidence for intensification of the hydrological cycle as instead, most processes slowed. In the changing climate-only scenario, statistically significant changes were found for diminishing snow accumulation, sublimation, blowing snow redistribution, snowcover duration, snow ablation rate, and evapotranspiration, deepening active layer thickness, and earlier snowcover depletion and ground thaw initiation. These, along with warming temperatures, declining summer net radiation and declining precipitation, resulted in diminished annual streamflow volume of 40 mm over the 56 years. However, the decline in streamflow did not match the larger decline in precipitation (48 mm), providing some evidence of resilience to climate change, as despite rising temperatures, both evapotranspiration and sublimation dropped with declining precipitation and this attenuated the streamflow volume decline. Transient vegetation changes further decreased blowing snow sublimation by reducing blowing snow transport. The combination of changing climate and transient vegetation change resulted in annual streamflow volume dropping by 38 mm over 56 years – a change that is not substantially different from that due to climate change alone. These results suggest that historical changes in vegetation and a degree of hydrological resiliency have not compensated for the effects of climate change on the hydrological regime of Havikpak Creek. They provide the first estimates of long-term change for a drainage basin located completely within the Arctic Circle, and demonstrate the large, complex and recent hydrological changes that have occurred, which can be used as a reference to inform other studies of Arctic climate change impacts.

Chapter 5

Impact of future climate and vegetation on the hydrology of an Arctic basin at the tundra-taiga transition

Boreal forest and lake in northwestern Canada, Dempster Highway, September 7, 2014.

Abstract

The rapidly warming Arctic is experiencing permafrost degradation and shrub expansion. Future climate projections show a clear increase in mean annual temperature and increasing precipitation in the Arctic; however, the impact of these changes on hydrological cycling in Arctic headwater basins is poorly understood. This study investigates the impact of climate change, as represented by simulations using a high-resolution atmospheric model under a pseudo-global-warming configuration, and projected changes in vegetation, using a spatially distributed and physically based Arctic hydrological model, on a small headwaters basin at the tundra-taiga transition in northwestern Canada. Climate projections under the RCP8.5 emission scenarios show a 6.1 °C warming, 38% increase in annual precipitation and a 19 W m^{-2} increase in all-wave annual irradiance over the 21st C. Hydrological modelling results suggest a dramatic shift in hydrological processes with maximum peak snow accumulation increasing by 70%, snowcover duration shortening by 26 days, active layer deepening by 0.25 m, evapotranspiration increasing by 18% and sublimation decreasing by 9%. This results in an intensification of the hydrological regime by doubling discharge volume, a 130% increase in spring runoff, and earlier and larger peak streamflow. Most hydrological changes were found to be driven by climate change; however, increasing vegetation cover and density reduced blowing snow redistribution and sublimation, and increased evaporation from intercepted rainfall. This study provides the first detailed investigation of projected changes in climate and vegetation on the hydrology of an Arctic headwater basin, and so it is expected to help inform larger scale climate impact studies in the Arctic.

This manuscript has been modified for inclusion in this thesis. It was originally submitted as:

Krogh, S. and J. Pomeroy, 2018: Impact of future climate and vegetation on the hydrology of an Arctic basin at the tundra-taiga transition, *Journal of Hydrometeorology*.

Author contributions:

SK and JP designed the study. SK performed the simulations and analyses and prepared the manuscript with contributions from JP to the manuscript structure, readability and analysis and discussion of the results.

5.1 Introduction

Recent changes in Arctic climate (Wanishsakpong et al., 2016; Whitfield et al., 2004), vegetation (Xu et al., 2013) and other environmental functions (Hinzman et al., 2005) motivate the investigation of future Arctic hydrology. Streamflow discharge is typically the variable of interest when assessing hydrological changes under climate change scenarios (e.g. Mendoza et al. 2015; Arheimer and Lindström 2014); however, changes in other variables such as permafrost thaw (Woo et al., 2007), subsurface water storage and flow (Walvoord et al., 2012) and snow accumulation and cover (Liston and Hiemstra, 2011), are also of great interest. An improved understanding of hydrological change is necessary to more effectively adapt and mitigate the potential impacts of climate change; however, given the complexity of the environment and the uncertainty associated with climate projection, this has represented a great scientific challenge.

Arctic climate projections from Global Climate Models (GCMs) can vary drastically between different CO_2 emission scenarios and models; however, most simulations agree in a warmer and wetter Arctic by the end of the century (Kattsov et al., 2005). Due to problems with GCMs in representing regional or local surface weather, higher resolution (tens of km) Regional Climate Models (RCMs) are used to dynamically downscale GCMs over large domains such as the NARCCAP (Mearns et al., 2009) and ENSEMBLES (Hewitt, 2004) projects; however, large scale RCMs still fail to represent surface weather, particularly precipitation and particularly in areas with complex topography, deep convection or extreme events (Prein et al., 2015). Further downscaling is needed to drive hydrological models. Downscaling techniques are classified into statistical and dynamical approaches, the former using empirical relationships between observed and simulated climate of varying complexity, and the latter requiring the implementation of a high resolution climate model (Fowler et al., 2007; Maraun et al., 2010). Statistical downscaling has the advantages of being relatively easy to implement and computationally inexpensive, allowing the realization of multiple scenarios, whereas dynamical downscaling is computationally intensive and challenging to implement. However, dynamical downscaling has the important advantage of producing physically connected or consistent weather variables, as opposed to most statistical approaches (Fowler et al., 2007). This is viewed as critical for cold regions (Pomeroy et al., 2015a), as the lack of physical realism in relationships amongst driving meteorological variables restricts the implementation of statistical downscaling in hydrological studies using physically based cold regions hydrological models. Such models can fail when there is inconsistency in the atmospheric forcing. Given the abrupt rise in computational power over the last decades, dynamical downscaling at high spatial resolutions is now available (Liu et al., 2017; Pieri et al., 2015). Recent studies have argued that performing dynamically downscaled using Convection Permitting Models (CPMs, spatial resolution < 4 km) is required to properly represent changes in extreme precipitation events (Kendon et al., 2017; Prein et al., 2015) that are hydrologically important. The convergence of computational capability and realisation of model need has encouraged the use of dynamical downscaling as opposed to statistical downscaling for both historical and future scenarios.

Shrub expansion and densification have been well documented in the Arctic, particularly near the treeline (Lantz et al., 2013; Myers-Smith et al., 2011). However, there are no published studies investigating changes in the forest structure (i.e. density, height and extension) in detail, particularly over northwestern Canada. Sniderhan and Baltzer (personal communication, January 31, 2018) argued that in the recent decades a significant increase in the forest basal area produced by infilling of trees below the treeline near Inuvik, Northwest Territories, Canada, has occurred; although this study has not been published yet, it provides the first evidence of changes in forest structure in the western Canadian Arctic. Payette and Filion (1985) found that white spruce treeline in northern Quebec, has not substantially changed over the past centuries, whereas Suarez et al (1999) found that the tundra-taiga treeline in Alaska advanced northward between 80 to 100 m north over the last 200 years. Gamache and Payette (2004) studied black spruce height near the Arctic treeline in eastern Canada and found that height growth has not significantly changed. Trends in greening and browning have been studied in Canada and Alaska using remote sensing and the Normalized Difference Vegetation Index (NDVI), showing an spatially heterogeneous response but a clear greening trend in northwestern Canada and north Alaska (Ju and Masek, 2016); however, this was not attributed to changes in specific species and is likely driven by reported shrub expansion and densification. Zhang et al. (2013) investigated Arctic vegetation projections under future climate conditions and showed an overall shrubification of the tundra; however, virtually no change in the tundra-taiga transition in the northwestern Canadian Arctic was found.

Arctic hydrological processes needed to calculate basin hydrology below or at the treeline include: snow accumulation and melt, sublimation and unloading of intercepted snow from forest canopy, blowing snow redistribution and sublimation, evapotranspiration, infiltration into frozen and unfrozen soils, ground freeze and thaw, water flow through snowpack, surface and subsurface flow, groundwater and streamflow routing (Kane et al., 1991; Pomeroy et al., 2008). These processes have been included in the spatially distributed and physically based Arctic Hydrology Model (AHM) developed by Krogh et al. (2017) using the Cold Regions Hydrological Modelling platform (CRHM; Pomeroy et al. 2007). Krogh et al. (2017) verified CRHM-AHM using streamflow, snowpack and active layer measurements from Havikpak Creek Basin, a small Arctic basin near the tundra-taiga transition in northwestern Canada. This model was later used by Krogh and Pomeroy (2018) to diagnose recent changes (1960-2016) to the hydrology of Havikpak Creek, including transient changes in climate and vegetation for the first time.

The purpose of this study is to investigate the effect of future climate and vegetation changes on the hydrological processes of a small Arctic treeline basin underlain by continuous permafrost. These steps were followed to pursue this goal: (1) climate projections from a high-resolution climate model under a convection-permitting configuration were compared to surface observations and used to force the CRHM-AHM under historical and future conditions; (2) vegetation projections based on observed rates of changes were used to parameterize land cover for the

CRHM-AHM; (3) climate and hydrological projections were analyzed and discussed; and (4) a sensitivity analysis examined the impact of vegetation change on the basin water balance.

5.2 Study site

Havikpak Creek Basin (HPC; Figure 5.1), located in the Northwest Territories, Canada, was selected as it has a history of hydrological process studies (Jones et al., 1999; Marsh et al., 2002; Pomeroy and Marsh, 1996), hydrological modelling applications (Krogh et al. (2017) and Krogh and Pomeroy (2018)) and is located near the tundra-taiga transition, where changes in vegetation are anticipated and may impact the hydrology. HPC is a small basin with a 16.4 km^2 drainage area, that is underlain by continuous permafrost and covered primarily by taiga forest (>50%), with large areas of open tundra, shrubs, wetlands and open water. HPC mean annual precipitation and temperature from 1980 to 2010 are 327 mm and -8.2 °C (Krogh et al., 2017), resulting in long winters (October to April) and relatively dry conditions. Soils at HPC are characterized by an upper layer of permeable organic peat, composed of decomposed vegetation, lichen and moss, followed by a lower peat layer over a relatively impermeable mineral soil layer. The peat and sometimes part of the mineral soil layers can thaw seasonally. A detailed description of HPC, including soil characteristics, meteorology and other characteristics are presented and discussed by Krogh et al. (2017).

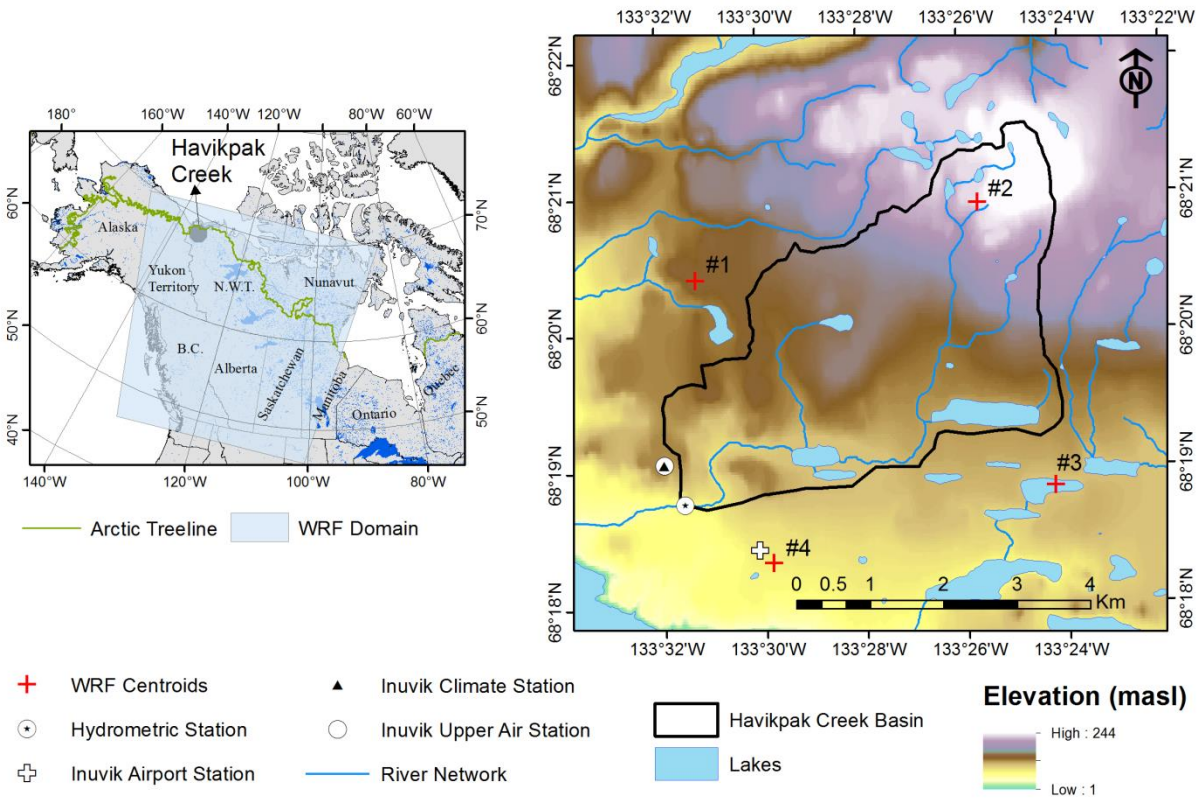

Figure 5.1: Left panel shows Havikpak Creek location within North America and the domain of the regional climate model (Section 5.3.3), including the Arctic treeline. Right panel shows Havikpak Creek basin, elevation map, the location of weather and hydrometric stations, lakes, river network and the closest centroids of the grid points from the regional climate model.

5.3 Data

5.3.1 Automated weather stations

An hourly and long-term meteorological time series for Havikpak Creek was reconstructed by Krogh and Pomeroy (2018) for the period 1960-2016, including precipitation, temperature, wind speed, relative humidity and short- and long-wave irradiance, based on a combination of in-situ meteorological observations, the Adjusted and Homogenized Canadian Climate Dataset (AHCCD; Mekis and Vincent, 2011) at the Inuvik station (ID: 2202578), and the ERA-Interim (Dee et al., 2011) and ERA-40 atmospheric reanalyses (Uppala et al., 2005). The automated weather stations used were the Inuvik Climate, the Inuvik Airport and the Inuvik Upper Air (Figure 5.1), all maintained by Environment and Climate Change Canada (ECCC). For details about the time series reconstruction the readers are referred to Krogh and Pomeroy (2018).

5.3.2 Streamflow

Daily streamflow records at the Havikpak Creek station (ID: 10LC017) have been measured by the ECCC Water Survey of Canada (WSC) since 1995. The hydrometric station is located downstream from the Havikpak Creek crossing with the Dempster Highway (Figure 5.1). Arctic stream gauging is challenging, particularly in small creeks due to the presence of ice and snow in the cross section during the spring snowmelt runoff, during which the annual peak streamflow discharge and the majority of the annual discharge volume typically occurs (Kane et al., 1991; Krogh et al., 2017; Marsh and Pomeroy, 1996; Woo, 1986). These problems and the associated uncertainty in the observations are acknowledged in the metadata provided by ECCC through the Environment Canada Data Explorer.

5.3.3 Atmospheric model: The Weather Research and Forecasting (WRF) model

5.3.3.1 Historical simulations

The Weather Research and Forecasting (WRF; Skamarock et al., 2008) model is a state-of-the-art numerical weather prediction (NWP) and atmospheric modelling system developed by a group of US government agencies lead by the National Center for Atmospheric Research (NCAR). WRF (version 3.4.1) was run at a convection-permitting resolution of 4-km over western Canada for the period 2000-2013 (Yanping et al., 2016), covering the Mackenzie and South Saskatchewan River basins. The initial and lateral boundary conditions used were six-hourly time series from the ERA-Interim reanalysis (Dee et al., 2011) at a 0.7° spatial-resolution, surface states and fluxes from the Noah-MP (Niu et al., 2011) land-surface scheme, and the year 2000 was used to spin-up the model. Main benefits of these runs are: (1) the large extent of the spatial domain, (2) the decadal period, (3) the high-resolution topographic representation and the (4) convection-permitting configuration. The last two have shown to greatly improve summer and winter precipitation representation, as opposed to climate models using cumulus parameterizations with lower spatial resolution (Brisson et al., 2016; Fosser et al., 2015; Prein et al., 2015; Rasmussen et al., 2014, 2011), providing more robust precipitation projections under future climate scenarios (Kendon et al., 2017, 2014). The outputs from this run used in this study are 2D hourly time series at the ground surface of precipitation, air temperature, wind speed, specific humidity, and shortwave and longwave irradiance.

5.3.3.2 Future simulations

The Pseudo-Global-Warming (PGW) approach (Schär et al., 1996; Hara et al., 2008; Kawase et al., 2009; Rasmussen et al., 2011, 2014; Liu et al., 2016) was used to produce future weather

simulations (Yanping et al., 2016). The PGW approach adds a mean monthly perturbation to the ERA-Interim initial and lateral boundary condition to the period 2000 – 2013. The mean monthly perturbations are calculated as the difference between the 25-year monthly values from the 1975-1999 and 2075-2099 periods, using the historical and future models ensemble from the CMIP5 model intercomparison experiment (Taylor et al., 2012), under the RCP8.5 high greenhouse gas concentration scenario (Riahi et al., 2011), resulting in an equivalent 2086 – 2099 period. Two benefits of the PGW approach are: the reduction of uncertainty caused by the interannual variability and the reduction of model bias contained in the Global Circulation Model projections (Kawase et al., 2008), and the main disadvantage is that it does not allow for future interannual variability. Previous studies have used PGW to quantify hydrological changes under futures climate scenarios (Ma et al., 2010; Mendoza et al., 2016).

5.4 Method

Figure 5.2 presents the modelling flowchart that summarizes the methodology used in this study. The first modelling stage comprises historical hydrological simulations using bias-corrected simulated weather from WRF. Historical runs are validated against daily observed streamflow discharge. Future simulations use the bias-corrected simulated weather from WRF-PGW with vegetation projections based on observed rates of growth. Finally, the sensitivity of the future mass balance to projected changes in vegetation is performed.

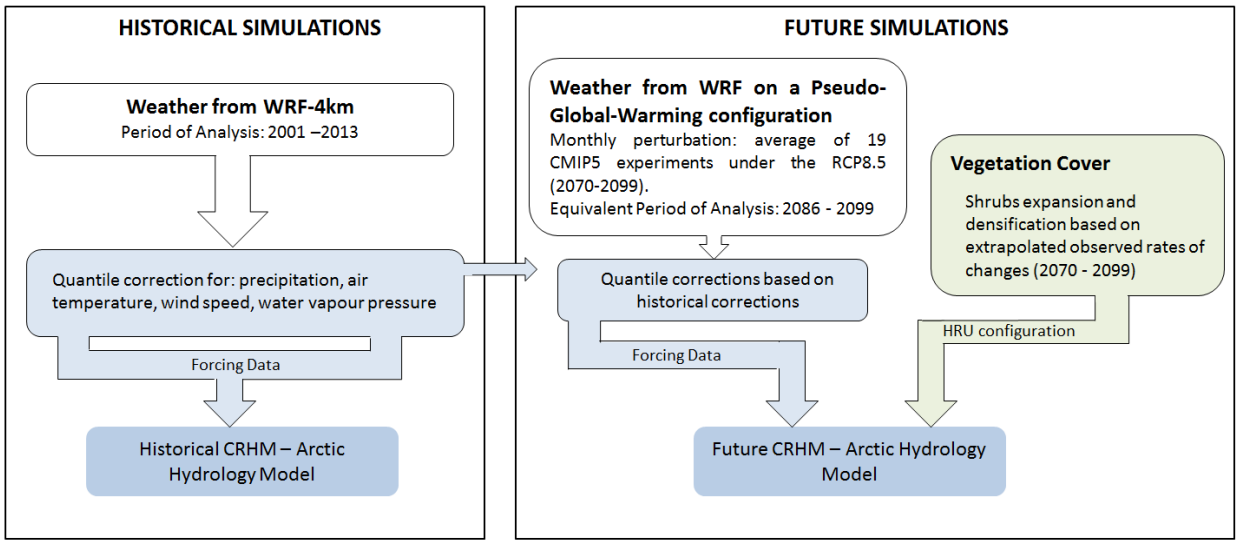

Figure 5.2: Modelling flowchart

5.4.1 WRF bias correction

WRF simulated weather was bias-corrected to generate forcing data that is as representative as possible of observed records. Despite the great improvement that high resolution Regional Climate

Models (RCMs) at convection permitting scales have achieved in representing local surface weather (Kendon et al., 2017; Prein et al., 2015), bias-correction is still required for hydrological studies. Bias correction techniques typically focus on correcting mean, variance and higher moments, depending on the complexity of the approach. Methods referred as Quantile mapping bias corrections, which bias-correct all the quantiles of the simulated time series distribution, have been proven to outperform simpler approaches that correct only the mean or variance, particularly in the context of hydrological modelling applications (Chen et al., 2013).

This study uses the univariate quantile mapping correction (QDM) from the R package MBC (https://CRAN.R-project.org/package=MBC), which uses the quantile delta-mapping algorithm described by Cannon et al. (2015). Quantile mapping correction was performed to hourly precipitation, air temperature, wind speed and water vapour pressure, using the observed weather time series presented by Krogh and Pomeroy (2018). Air temperature was divided into two periods: (1) spring (April-May) and (2) non-spring (June-March) for quantile mapping correction in order to compensate for the larger WRF cold bias that was during spring. Precipitation was also divided into two periods: (1) winter and (2) summer using the 0°C mean temperature threshold. The separation between summer and winter was important to properly represent cumulative snowfall and extreme rainfall events as accurately as possible. Wind speed correction was performed to the full period as no further classification was required. Water vapour pressure correction was required to properly calculate relative humidity following the Clausius-Clapeyron relationship. Quantile correction was performed to the entire period, and then relative humidity was calculated based on corrected air temperature, water vapour pressure, and the Buck formula (Buck, 1981) to compute the saturated water vapour with respect to water and ice. Relative humidity was not allowed to exceed 100%.

5.4.2 Hydrological model

The hydrological model used in this study is the Arctic Hydrology Model (AHM; Krogh et al., 2017) developed with the Cold Regions Hydrological Modelling platform (CRHM; Pomeroy et al., 2007). The CRHM-AHM is a physically based and spatially distributed hydrological model that includes the following key physical processes found in Arctic environment: blowing snow redistribution and sublimation, snowmelt energy balance, sublimation/evaporation of canopy intercepted snowfall/rainfall, soil moisture storage and flow, evapotranspiration, infiltration into frozen and unfrozen ground, flow through organic terrain and snowpack, ground freeze and thaw, surface runoff and streamflow routing. The formulations used to represent each of these hydrological processes are described in detail by Krogh et al. (2017). The model uses Hydrological Response Units (HRU; Flügel, 1995) to spatially discretize HPC based on land cover classes, elevation and topographic features such as gullies and snowdrifts. This discretization resulted in 11 HRUs: upper and lower tundra, upper and lower sparse shrubs, upper and lower gully/drift, close shrubs, taiga forest, forest, wetland and open water. CRHM-AHM is run forced by hourly

precipitation, air temperature, wind speed, relative humidity, and shortwave and longwave irradiance.

The parameterization of the CRHM-AHM model was carried out following the Deduction-Induction-Abduction approach, which tends to avoid calibration (DIA; Pomeroy et al., 2013a). Most parameters used in the CRHM-AHM were taken from field observations (e.g. vegetation cover, slope and aspect), previous process studies in HPC and other basins with similar hydrological behaviour, such as Wolf Creek Basin (Rasouli et al., 2014) and Trail Valley Creek Basin (Marsh and Pomeroy, 1996). A few uncertain subsurface and surface hydraulic and storage parameters were calibrated against observed daily streamflow using the automated Dynamically Dimensioned Search algorithm (DDS; Tolson and Shoemaker, 2007). Parameters used in the CRHM-AHM are detailed by Krogh et al. (2017). CRHM-AHM validation against daily streamflow, snow accumulation and active layer thickness at Havikpak Creek was described by Krogh et al. (2017), showing an adequate representation of all of these variables. Krogh and Pomeroy (2018) presented an updated streamflow validation for the CRHM-AHM model including the most recent years. The readers are referred to Krogh et al. (2017) for a full description of the CRHM-AHM model configuration, validation and sensitivity analysis to key parameters.

5.4.2.1 Historical modelling

The CRHM-AHM was run for the period January 2001 – October 2013 using the corrected weather time series from the four closest WRF centroids to HPC (Figure 5.1). To select the most suitable WRF centroid, simulated streamflow from each run was compared against observed streamflow, for which centroid #1 provided the best simulation, and therefore, it was used for all the analyses. Note that there were small differences amongst weather from the different centroids, resulting in very small differences between the four streamflow simulations and, therefore, the impact of the centroid selection is expected to be minimal for the analysis and discussion presented in this study.

Shrubs extension and density characteristics were taken as the average for the years 2001 to 2013 based on the extrapolated rates presented by Krogh and Pomeroy (2018), which are based on observations made by Pomeroy and Marsh (1997) and the increasing shrub cover and density presented by Lantz et al. (2013). The vegetation characteristics used in for the historical modelling are presented in Table 5.1.

Subsurface and surface hydraulic and storage parameters calibrated by Krogh et al. (2017) were used for this simulation; nevertheless, the uncertainty introduced by this new weather time series was investigated by performing another automated calibration with the DDS algorithm.

5.4.2.2 Future modelling

Future hydrological modelling include both climate and vegetation projections. Climate projections are those from the bias-corrected WRF-PGW for the equivalent period of 2087 to 2099. The year 2086 was used as a spin-up period for the climate model. Vegetation projections assume that the observed rates of changing shrub cover and density from Lantz et al (2013) remains the same in the future, as no other projections are available. To include the "new" sparse shrubs in the CRHM-AHM, two new HRUs were added: the upper and lower "new" sparse shrubs, resulting in a model with 13 HRUs. Projected area, stem density and leaf area index (LAI) for the projected HRUs are presented in Table 5.1. Vegetation height of the new sparse shrubs was estimated to be 0.8 m, which corresponds to roughly half of the estimated average height of current sparse shrubs at HPC (Krogh et al., 2017) and reflects that these plants are colonizing previous tundra-covered surfaces.

No significant changes in Arctic latitudinal treeline are expected by the end of the century in northwestern Canada (Zhang et al., 2013), also previous studies have shown that tree expansion has not change substantially over the past centuries in eastern Canada (Payette and Filion, 1985); however, variable greening and browning of the Canadian boreal forest has been found (Sulla-Menashe et al., 2018). There are no quantitative projections of forest height, density or extension available and, therefore, the forested HRUs were held constant in the future model configuration.

Table 5.1: Vegetation cover and density for the historical (2001-2013) and future (2087-2099) modelling periods.

HRU	Historical Modelling			Future Modelling		
	Area (km^2)	**Stem density (# m^{-2})**	**LAI (m^2 m^{-2})**	**Area (km^2)**	**Stem density (# m^{-2})**	**LAI (m^2 m^{-2})**
Upper Tundra	0.35	N/A	N/A	0.11	N/A	N/A
Upper Sparse Shrubs	0.7	0.4	0.25	0.7	0.9	0.5
"New" Upper Sparse Shrubs	N/A	N/A	N/A	0.24	0.3	0.25
Close Shrubs	2.6	1	0.5	2.6	1	0.7
Lower Tundra	1.4	N/A	N/A	0.9	N/A	N/A
Lower Sparse Shrubs	1.5	0.4	0.25	1.5	0.9	0.5
"New" Lower Sparse Shrubs	N/A	N/A	N/A	0.5	0.3	0.25

5.4.3 Statistical mean change analysis

Projected mean annual changes between historical and future simulations for several water fluxes and state variables (e.g. annual streamflow discharge and active layer thickness) were tested using

the non-parametric Wilcoxon rank test (Wilcoxon, 1945) with a significance threshold of $p \leq 0.05$. The Wilcoxon test assumes that the two series are independent and continuous.

5.5 Results

5.5.1 WRF validation

Bias-corrected weather simulated by WRF for the period 2001-2013 was validated against observed records at HPC. Figure 5.3a presents a comparison of annual cumulative precipitation between observed, raw and bias-corrected WRF historical data. Raw WRF mean bias was only 8 mm yr^{-1}, demonstrating very good performance of WRF; nevertheless, this bias was removed after applying the quantile mapping correction of daily precipitation, which also improved the representation of high precipitation events (Figure 5.3b). These events are important as they typically occur during summer and can produce important rainfall-runoff responses. Figure 5.3c presents the Q-Q plot between observed and bias-corrected WRF precipitation, in which the high precipitation events are well represented. Despite the good representation of mean precipitation and its quantiles, bias-corrected WRF has mixed performance representing the variability of annual precipitation. For example, precipitation was overestimated by roughly 80 mm in 2004 and underestimated by 60 mm in 2007. Figure 5.3d compares monthly observed, raw and bias corrected WRF air temperature. An overall cold bias of 2.7 °C was found for the raw WRF. Despite the cold bias, seasonal temperatures and quantiles (Figure 5.3e) were well represented by raw WRF. After bias correction of hourly temperature, WRF air temperatures agreed well with observations and the cold bias was removed (Figure 5.3f). 10-m hourly wind speed (not shown) simulated by WRF overestimated surface observations by an average of 1.5 m s^{-1}; this was removed after bias correction. Calculated relative humidity from WRF bias-corrected water vapour pressure and air temperature represented observed mean and quantiles well (not shown).

Table 5.2 presents a comparison between observed and bias-corrected WRF daily precipitation for wet and dry spells. A wet (dry) spell is defined as any period with at least three consecutive days with precipitation above (below) 0.1 mm $days^{-1}$. Observed mean annual number of dry and wet spells is 28 and 14, respectively, whereas simulated mean annual number of dry and wet spells is 30 and 13, respectively. The mean annual length of dry spells is 8.9 and 8.1 days for observation and simulations, respectively, whereas the mean length of wet spells is 5.4 and 5.5 days for observations and simulations, respectively. This suggests that the overall representation of simulated daily precipitation is consistent with the observed patterns of dry and wet periods, which is critical to properly represent the hydrological cycle.

Table 5.2: Dry/Wet spells comparison between observed and simulated daily precipitation. A threshold of 0.1 mm day^{-1} was used for the analysis.

	Dry spells		**Wet Spells**	
	Observations	**Simulations**	**Observations**	**Simulations**
Mean annual number of dry/wet spells	28	30	14	13
Mean annual length of dry/wet spells (days)	8.9	8.1	5.4	5.5

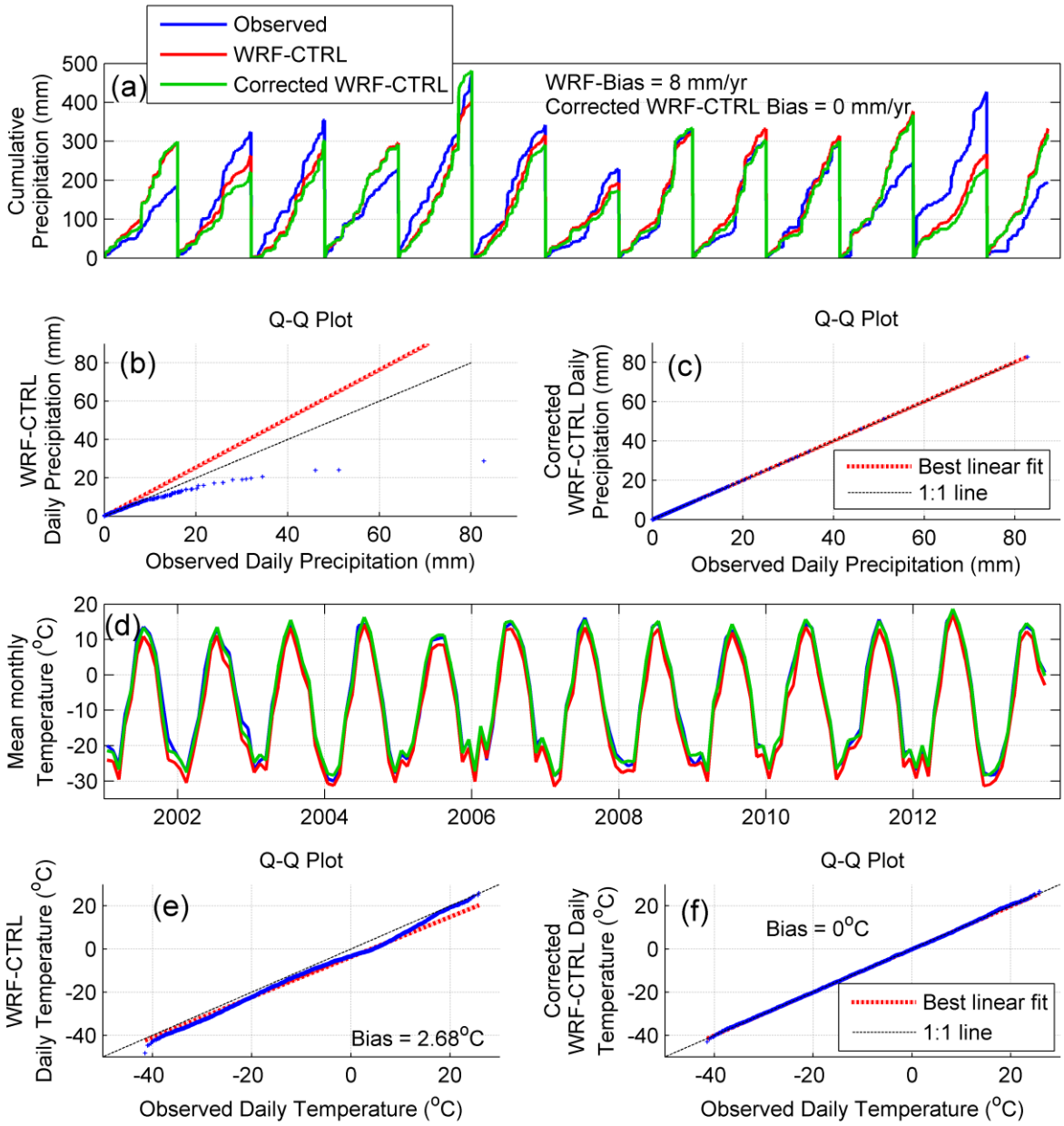

Figure 5.3: (a) Cumulative annual precipitation comparison. (b) Quantile-quantile plot between observes daily precipitation and raw WRF daily precipitation. (c) Same as (b) but using bias-corrected daily WRF precipitation. (d) Mean monthly air temperature comparison. (e) Quantile-quantile plot between observed daily air temperature and raw WRF daily air temperature. (f) Same as (e) but using bias-corrected WRF daily air temperature. All the data correspond to the 2001-2013 period.

5.5.2 Projected changes in weather

Figure 5.4 presents mean daily time series of projected changes using bias-corrected WRF simulations of air temperature, cumulative precipitation, wind speed and relative humidity, and raw WRF simulations of shortwave and longwave irradiance; mean annual changes are also included in bold when they are statistically significant ($p \leq 0.05$). Table 5.3 presents seasonal and annual changes for the same variables presented in Figure 5.4 and the all-wave irradiance. A significant warming of 6.1°C in mean annual air temperature is projected by the WRF-PGW, particularly during winter and spring, for which an increase of 6.8 and 7.1°C, respectively, is indicated. The date at which temperature reaches 0°C is projected to occur roughly 2 weeks earlier in spring, whereas the date at which temperature drops below freezing is delayed by 16 days in fall. Cumulative precipitation significantly increased by 117 mm yr^{-1} or 38% with respect to the historical period, with the largest seasonal increase in winter (October to April, 94.3 mm). A negligible increase in mean annual wind speed of about 0.1 m s^{-1} is projected. The simulated mean annual increase in relative humidity is about 4%, with the largest increases in winter of about 10%. Shortwave irradiance decreased annually by 2.1 W m^{-2}; however, a small increase of roughly 2.5 W m^{-2} was found in summer, whereas longwave irradiance significantly increased by 21.2 W m^{-2} annually, with the largest seasonal increase in winter of 22.8 W m^{-2}. The total change in all-wave

irradiance is an annual increase of 19 W m^{-2}, which is consistent throughout the year except in spring, during which a small decrease of 3.4 W m^{-2} was projected.

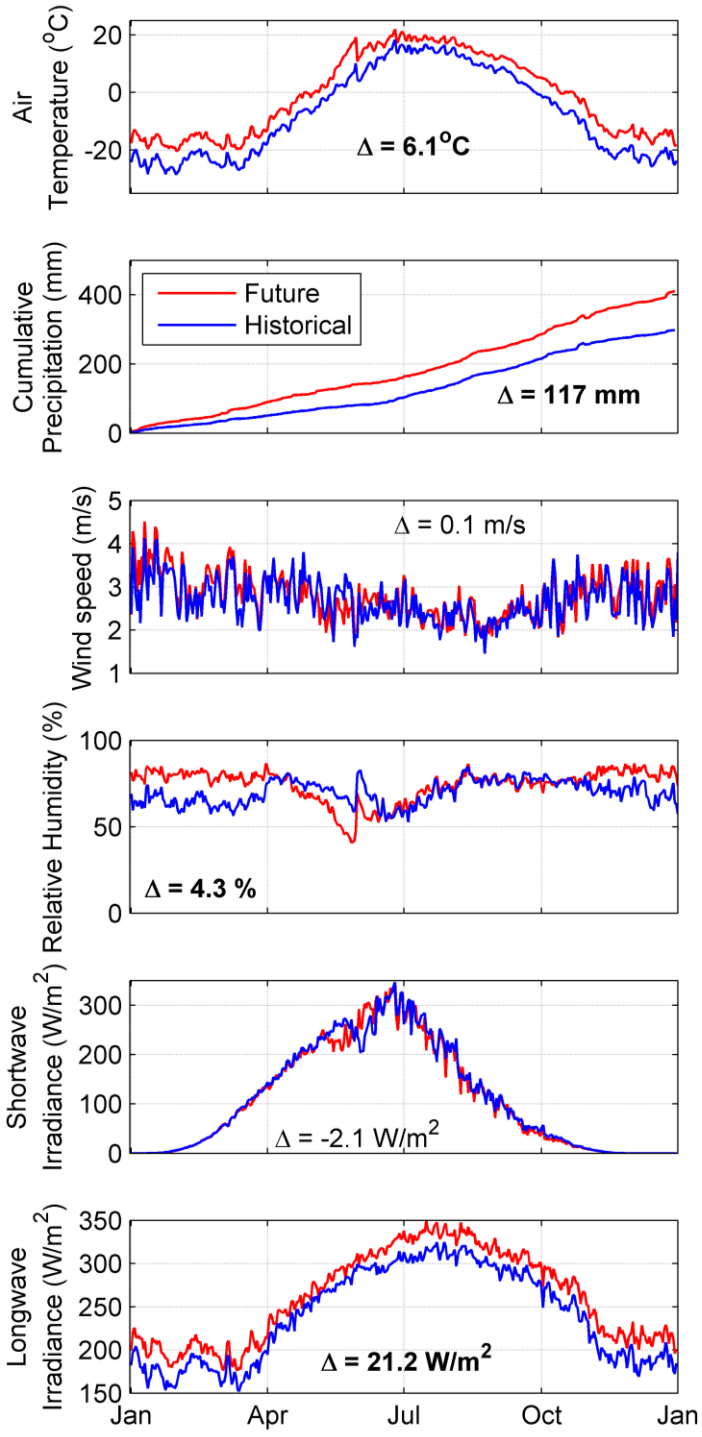

Figure 5.4: Mean daily projected changes in weather time series for historical (2001-2013) and future (2087-2099) periods. Precipitation is presented as cumulative mean daily values. Mean annual change (Δ = Future-Historical) is bold when statistically significant ($p \leq 0.05$).

Table 5.3: Seasonal and annual weather changes between the historical (2011-2013) and future (2087-2099) scenarios.

Atmospheric Variables	**Winter (October-April)**	**Spring (May)**	**Summer (August - July)**	**Fall (September)**	**Annual**
Air Temperature (°C)	6.8	7.1	4.4	4.9	6.1
Precipitation (mm)	94.3	13.2	6.3	3.1	117
Wind Speed ($m\ s^{-1}$)	0.2	-0.3	0.1	0.1	0.1
Relative Humidity (%)	9.7	-13.3	-0.5	-1.9	4.3
Shortwave Irradiance ($W\ m^{-2}$)	-1.5	-16.4	2.5	-5.6	-2.1
Longwave Irradiance ($W\ m^{-2}$)	22.8	13	21	19.9	21.2
All-wave Irradiance ($W\ m^{-2}$)	21.3	-3.4	23.5	14.3	19.1

5.5.3 Hydrological model performance

Krogh et al. (2017) and Krogh and Pomeroy (2018) showed that the CRHM-AHM model simulates daily streamflow, snow accumulation from snow survey and active layer thickness adequately when forced with observed meteorology. The CRHM-AHM performance using the parameters from Krogh et al. and the corrected WRF meteorology was investigated to determine its fitness for purpose in this study. The Nash-Sutcliffe Efficiency coefficient (NSE) and mean bias using observed and simulated daily streamflow resulted in 0.44 and -16%, respectively, for the period 2002 to 2012. These results are consistent with those presented by Krogh et al. (2017) and Krogh

and Pomeroy (2018), suggesting a consistent representation of Havikpak Creek hydrology. Nevertheless, to assess the sensitivity of the model to this new forcing data, a few surface and subsurface storage and flow parameters calibrated by Krogh et al. (2017) were re-calibrated using corrected WRF data and the NSE as objective function. Automatic calibration was carried out performing 500 model iterations for the period 2002-2008 (six years) using the Dynamically Dimensioned Search algorithm (DDS; Tolson and Shoemaker, 2007), and the period 2009-2012 (three years) for validation. The result of the parameters re-calibration and the one performed by Krogh et al. is presented in Table A1 (Appendix). NSE and mean bias for the period entire 2002-2012 period using corrected WRF was 0.45 and -18%, respectively, suggesting a marginal improvement in NSE and a deterioration of mean bias. Figure 5.5 shows a comparison between observed streamflow (blue), simulated streamflow using parameters from Krogh et al. (2017) (red) and simulated streamflow using re-calibrated parameters (green). Annual streamflow discharge (Figure 5.5a) is underestimated in five years; the largest difference in 2008 was likely due to an underestimation of precipitation in late 2007 (Figure 5.3) reducing snow accumulation and subsequent snowmelt runoff. Simulated mean monthly streamflow (Figure 5.5b) represents some of the observed seasonality, in particular the rise in May streamflow, but underestimated the rise in the end of the summer streamflow. Flow duration curves (Figure 5.5c) show similar results to those presented by Krogh et al (2017); a good overall agreement with some errors in representing high flows. Cumulative streamflow shows that simulations rise slightly earlier than observations (Figure 5.5d), and correctly simulate the rate of increase in rising discharge, but underestimate spring discharge volumes. Overall, the CRHM-AHM showed consistent streamflow response with those presented by Krogh et al. (2017); however, a larger bias was found, likely due to the imperfect inter-annual variability of corrected WRF precipitation. Differences between CRHM-AHM simulations using the few calibrated parameters from Krogh et al. (2017) or the ones re-calibrated for this study showed only marginal differences; therefore, the parameter values presented by Krogh et al. (2017) are used as they produce a slight smaller mean bias and are presumed to be more realistic, as they were derived using observed weather.

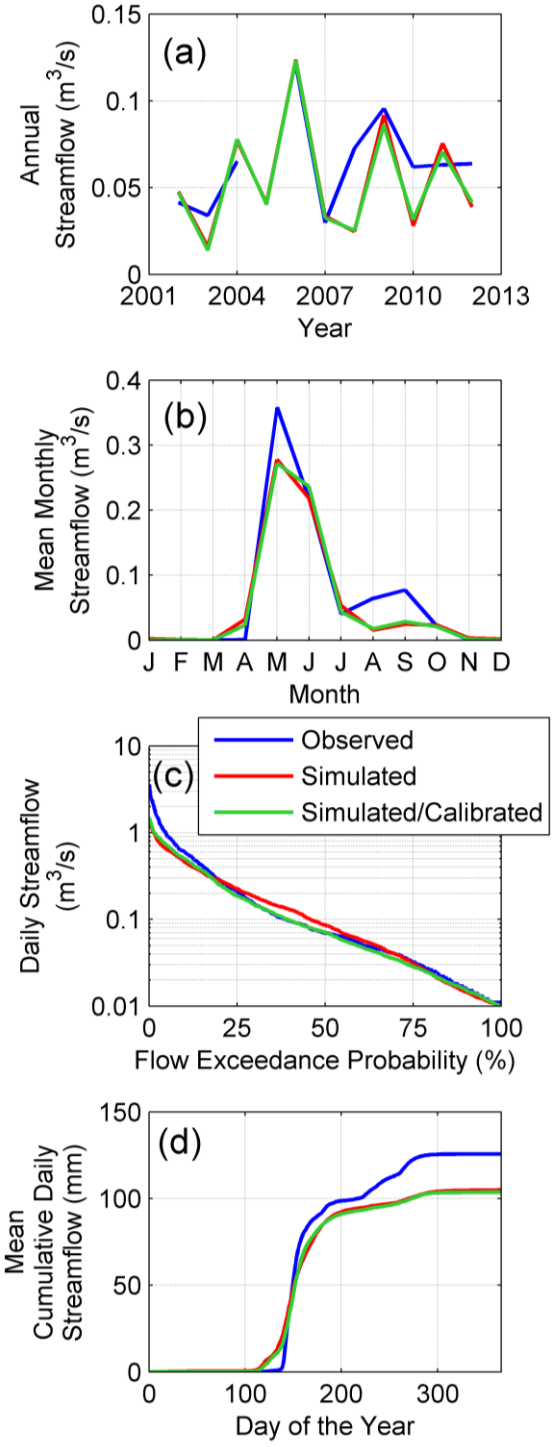

Figure 5.5: Observed versus simulated streamflow for the period 2002-2012. (a) Annual streamflow discharge volume, (b) mean monthly streamflow discharge, (c) flow duration curve and (d) mean cumulative streamflow discharge. There are no streamflow records in 2005.

5.5.4 Changes in snow accumulation and cover

Figure 5.6 presents historical and future mean and standard deviation of daily snow water equivalent (SWE) for the HPC basin and four representative land cover classes. Basin scale peak SWE is projected to increase in 80 mm and occur at the same day of the year (April 19). Snowcover duration is projected to shorten by 26 days, as there is a 15 days delay in the initiation of snow accumulation and 11 days earlier snowcover depletion (Table 5.4). Due to the larger peak SWE and the earlier snowcover depletion date, the snow ablation rate increased significantly from 1.8 to 3.5 mm day^{-1}. An increase in peak SWE for most land covers of 67-83 mm was found (Figure 5.6), mostly due to the increasing snowfall and warmer conditions that dampened redistribution or interception and hence sublimation. Peak SWE in the Gully/Drift decreased by 164 mm due to suppression of blowing snow redistribution due to warmer temperatures and increasing shrub density. The smaller increase in peak SWE in the dense forest compared to the taiga forest is due to the dense forest's higher interception capacity, which allows for higher sublimation losses.

Table 5.4: Snow distribution and melt at the basin scale

Variable	**Historical**	**Future**	**Difference**
Peak SWE (mm)	115	184	80
Date of Peak SWE	April 19	April 19	0 days
Snow accumulation start date	September 11	September 26	15 days
Snowcover depletion date	June 21	June 10	-11 days
Snowcover duration (days)	283	257	-26
Average snow ablation rate (mm day^{-1})	1.8	3.5	1.5

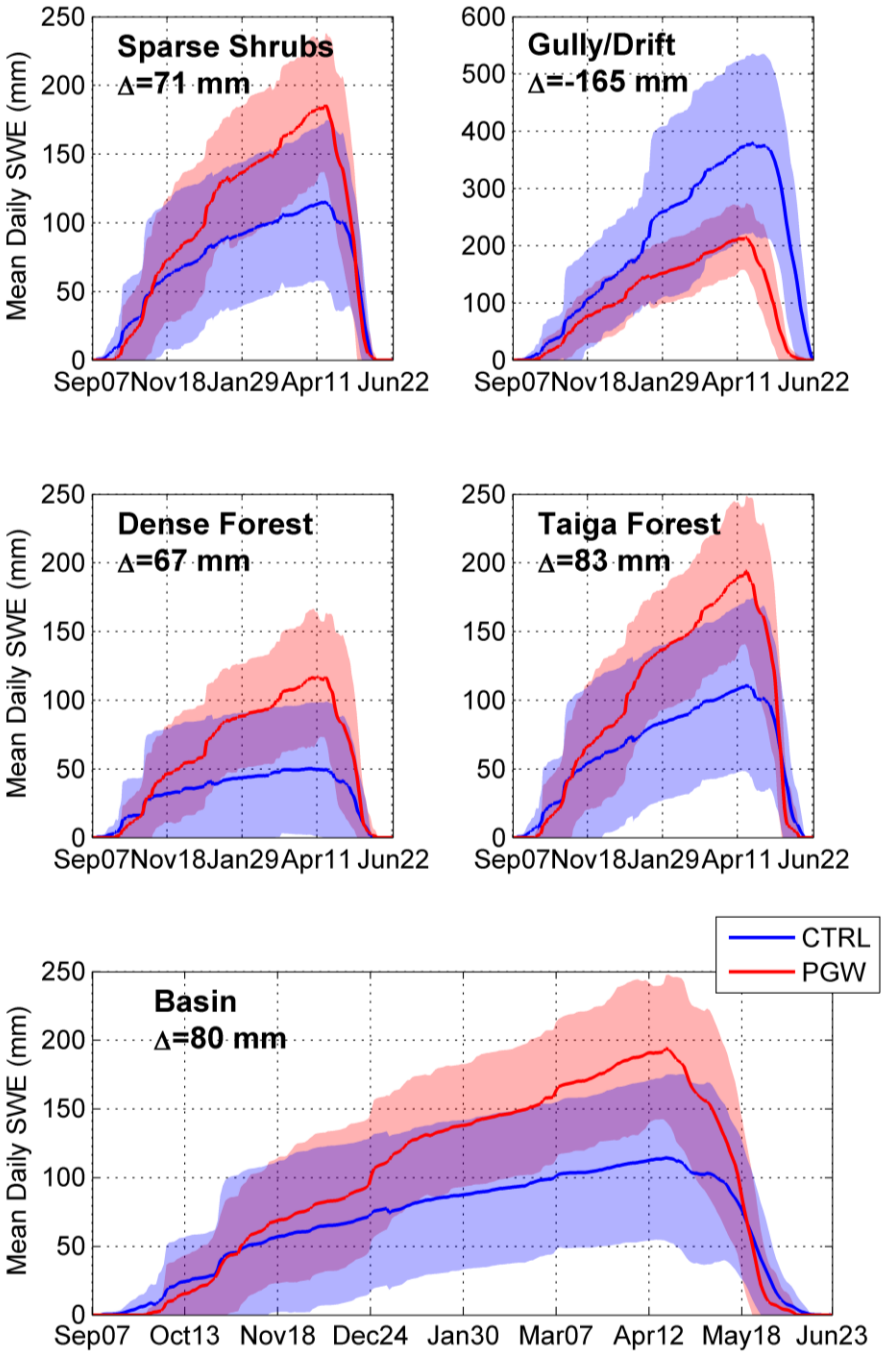

Figure 5.6: Mean (solid line) and standard deviations (shade) of historical (2001-2013) and future (2087-2099) daily snow water equivalent (SWE) for selected land cover and basin average. Significant changes between future and historical peak SWE simulations at the $p \leq 0.05$ significance thresholds are bold.

5.5.5 Changes in active layer thickness

Figure 5.7 shows changes associated with the active layer thickness (ALT) for selected land cover and the basin average. The basin average ALT is projected to increase by 0.25 m, thawing from approximately 0.96 down to 1.21 m in the future. Spatial heterogeneities amongst land cover types were found in the increased ALT, ranging from roughly 0.2 to 0.35 m between the historical and future scenarios. The 26 days increase in the snow-free season and increased air temperature can explain the deepening ALT depth (Table 5.4). Ground thaw initiation started roughly 5 days earlier in future simulations, shifting from May 22 to May 17 for the historical and future scenarios, respectively, consistently with the earlier depletion of snowcover. Ground freeze initiation is delayed by 17 days in the future, driven by the two weeks later initiation of snowcover. Average thawing rates increased in the future from 0.78 to 0.83 cm day^{-1}, driven by the longer thawing season and the warmer air temperatures.

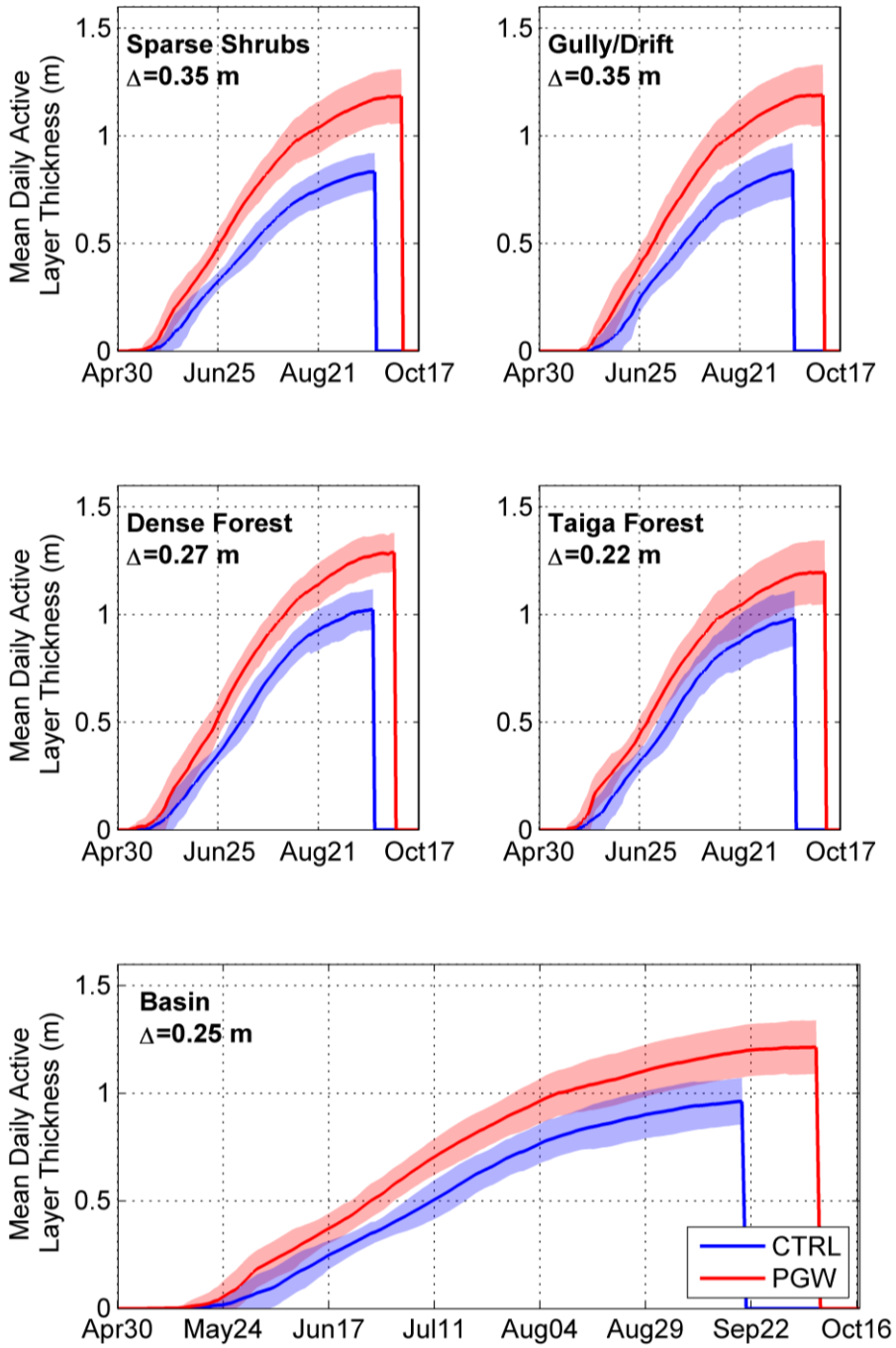

Figure 5.7: Mean (solid line) and standard deviation (shade) of the daily active layer thickness comparison between the historical (2001-2013) and future (1987-2099) scenarios. Significant changes between future and historical ALT simulations at the $p \leq 0.05$ significance thresholds are bold.

5.5.6 Changes in the mass fluxes

Figure 5.8 shows mean annual cumulative fluxes for the historical and future scenarios at the basin scale. Historically, snowfall was the largest precipitation component with 172 mm (57% of mean annual precipitation), whereas rainfall contributed 133 mm (43%). Future partitioning between rainfall and snowfall shows the largest increase, 63 mm, going towards rainfall (Figure 5.8a), whereas snowfall increased by only 54 mm (Figure 5.8b). Despite this disproportionate increase, snowfall remains the largest precipitation component in the future with 53% of the mean annual precipitation. The largest increase in rainfall compared with snowfall is due to the 6.1 °C of warming. That rainfall did not increase further for such a substantial temperature increase is because much of the snowfall fell in very cold periods that remained capable of producing snowfall in the future. Figure 5.8c shows that ET increased by 27 mm in the future, which along with the 117 mm increase in mean annual precipitation results in a reduction of the evaporation ratio (ET/Precipitation) from 0.49 to 0.42. Increased ET is the result of the warmer and wetter conditions, and the larger all-wave irradiance (Table 5.3). The three components of sublimation: sublimation of snow intercepted on forest canopies, blowing snow sublimation and sublimation from the snow surface are presented in Figure 5.8d, Figure 5.8e and Figure 5.8f, respectively. Slightly higher mean sublimation rates from intercepted snowfall were found; however, cumulative intercepted sublimation dropped by 1 mm, which is not a substantial change but when compared with the 54 mm increase in snowfall it results in a decrease from 11% to 8% of the mean annual snowfall. Decreasing total sublimation from intercepted snowfall is explain by the shortening of the snowfall season permitting snow interception on the canopy and warming air temperatures that induce more rapid and earlier unloading of canopy snow. Total blowing snow sublimation increased by 2 mm due to the increased snowfall, which to some degree overcame the impact of shrub expansion and densification has in restricting blowing snow redistribution. Daily rates of sublimation at the snow surface remain virtually the same; however, cumulative surface sublimation decreased by 6 mm due to the shortening of the snowcover season. The cumulative sublimation decreased by 5 mm, with a substantial drop in the sublimation ratio to snowfall from 34% to 23% (Figure 5.8g).

Mean annual soil moisture increased by roughly 7 mm (Figure 5.8h), which is attributed to the increased soil storage capacity associated with deeper ALT (Figure 5.7) allowing more moisture in early winter when ET is minimal, as well as the increase in precipitation that was not matched by a proportionate increase in ET or sublimation. Larger rates of soil recharge were found at the beginning of the summer; however, these were somewhat compensated by the faster soil moisture depletion projected by mid-summer, resulting in virtually the same minimum soil moisture. The same minimum soil moisture in historical and future simulations is likely due to the storage in deeper layers of the soil (mineral soil), which have very low permeability and can hold moisture for longer periods of time. A significant increase in streamflow discharge volume by roughly 100 mm was projected (Figure 5.8i), suggesting that most of the increased precipitation (117 mm) is

translated into streamflow. More details about changes in the streamflow regime are presented in the next section.

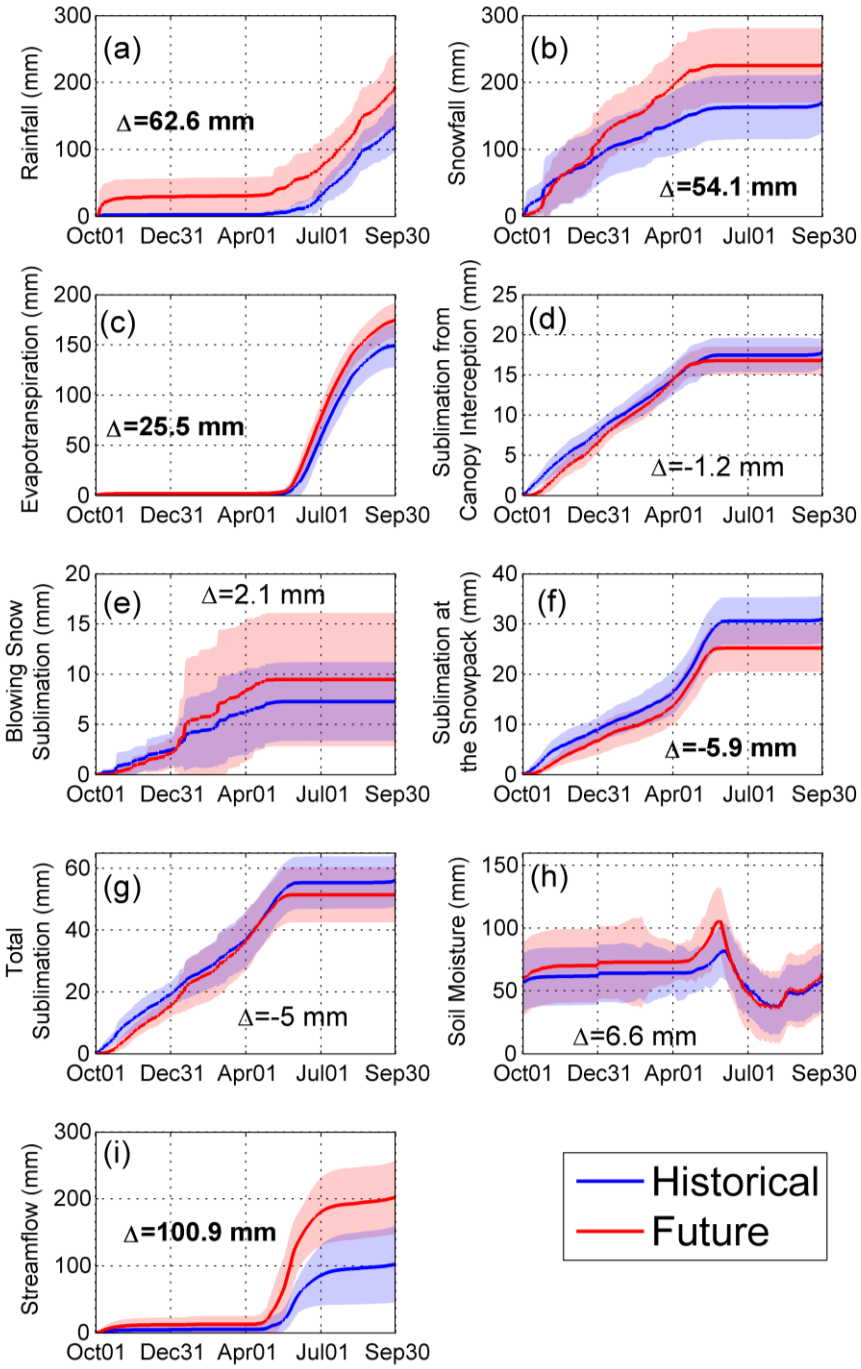

Figure 5.8: Comparison of mean basin scale mass fluxes between the historical (2001-2013) and future (2087-2099) periods. Mass fluxes are presented as cumulative of mean daily values, except for soil moisture that is shown as the mean daily values. Mean annual change (Δ = Future-Historical) is bold when statistically significant ($p \leq 0.05$).

5.5.7 Changes in the hydrological regime

Figure 5.9 presents a comparison between historical and future mean monthly streamflow discharge (Figure 5.9a), flow duration curve (Figure 5.9b), mean daily streamflow (Figure 5.9c) and mean cumulative daily streamflow (Figure 5.9d). Mean monthly streamflow shows a significant peak in spring runoff, which increased by roughly 130%, from 0.28 to 0.65 $m^3 s^{-1}$ and a much smaller increase in fall flows. The flow duration curve shows an increase in daily streamflow discharge for most of the exceedance probabilities, particularly for low exceedance probabilities, which indicate extreme events. For example, the 1, 5 and 10% exceedance probability, associated with return periods of 100, 20 and 10 years, increased by 0.6, 0.3 and 0.25 $m^3 s^{-1}$, respectively. Mean streamflow discharge (Figure 5.9c) initiates about a week earlier in the future, consistently with earlier snow depletion, whereas the end of the streamflow discharge is delayed by 6 days. The mean annual peak flow changed from 0.9 to 1.6 $m^3 s^{-1}$, whereas the date at which it occurs advanced by a week from May 22 to May 15. Runoff ratio increased by 45% from 0.33 to 0.48.

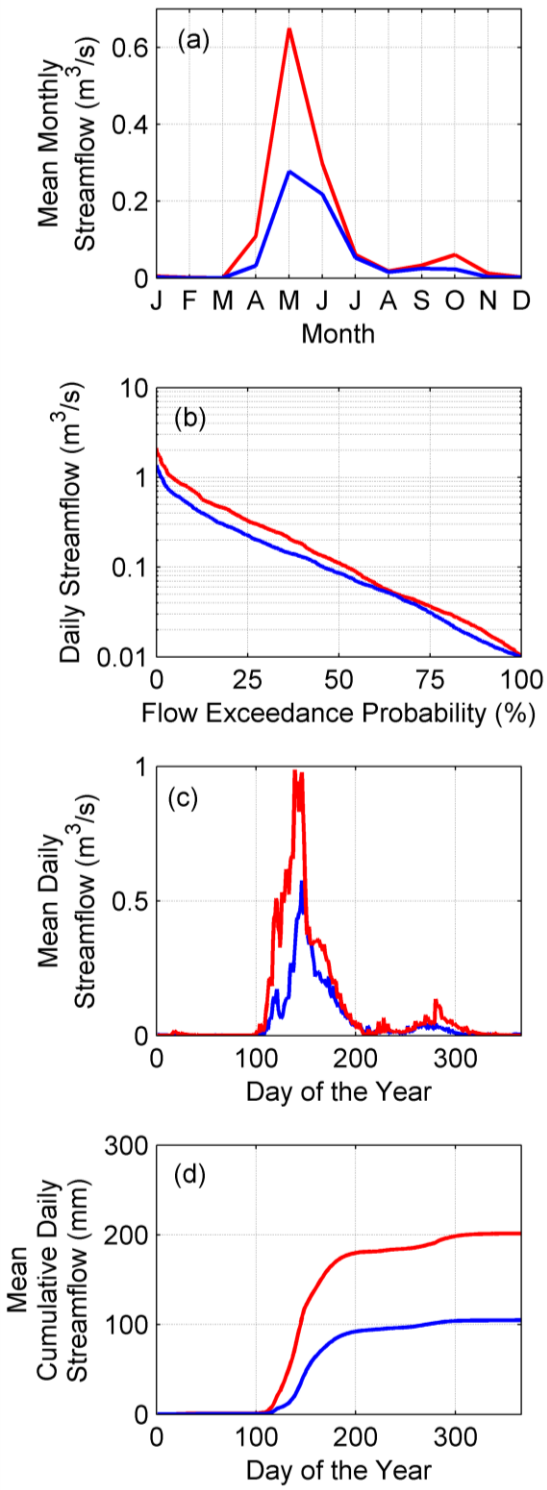

Figure 5.9: Streamflow comparison between historical (2001-2013) and future (1987-2099). (a) Mean monthly streamflow. (b) Flow duration curve. (c) Mean daily streamflow discharge. (d) Mean cumulative daily streamflow discharge.

5.5.8 Mass balance sensitivity to projected vegetation changes

To explore uncertainty and assess the mass balance sensitivity to the projected changes in vegetation characteristics, 1,296 vegetation scenarios were created (Table 5.5). Values in parenthesis in Table 5.5 show the values used in the future model configurations described in Section 5.4.2.2, and N/A values (not applicable) are used for parameters that are not subject to the sensitivity analysis. These scenarios assumed that vegetation height in those HRUs with previously existing shrubs: Close Shrubs, Gully/Drift and Wetland, remain the same, as there is no evidence of increasing shrubs height in the region. Scenarios of shrub expansion range from a slight increase in shrub cover to a complete shrubification of the tundra. Changes in forest LAI are included to assess the potential impact of increasing forest density on the mass balance.

Table 5.5: Parameters range for the vegetation projection sensitivity analysis. In parenthesis the projection used in the deterministic future scenario (Section 5.4.2.2) using an estimate from extrapolating observed rates of growth is presented. N/A: not applicable, it is used when no changes were performed in the sensitivity analysis.

HRU	**Area (km^2)**	**Stem Density (# m^{-2})**	**Vegetation Height (m)**	**LAI (m^2 m^{-2})**
Upper Tundra	0.01 – 0.34 (0.11)	N/A	N/A	N/A
Lower Tundra	0.01 – 1.39 (0.89)	N/A	N/A	N/A
Upper New Sparse Shrubs	0.01 – 0.34 (0.24)	0.1 – 0.6 (0.4)	0.1 – 1.5 (0.8)	0.1 – 0.4 (0.25)
Lower New Sparse Shrubs	0.01 – 1.39 (0.51)	0.1 – 0.6 (0.4)	0.1 – 1.5 (0.8)	0.1 – 0.4 (0.25)
Upper Old Sparse Shrubs	N/A	0.4 – 1 (0.9)	N/A	0.25 – 0.7 (0.5)
Lower Old Sparse Shrubs	N/A	0.4 – 1 (0.9)	N/A	0.25 – 0.7 (0.5)
Close Shrubs	N/A	N/A	N/A	0.5 – 1.0 (0.8)
Gully/Drift	N/A	0.4 – 1 (0.9)	N/A	0.25 – 0.7 (0.5)

HRU	Area (km^2)	Stem Density (# m^{-2})	Vegetation Height (m)	LAI (m^2 m^{-2})
Wetland	N/A	0.4 – 1 (0.9)	N/A	0.25 – 0.7 (0.5)
Dense Forest	N/A	N/A	N/A	1.2 – 2.0 (1.2)
Taiga Forest	N/A	N/A	N/A	0.8 – 1.5 (0.8)

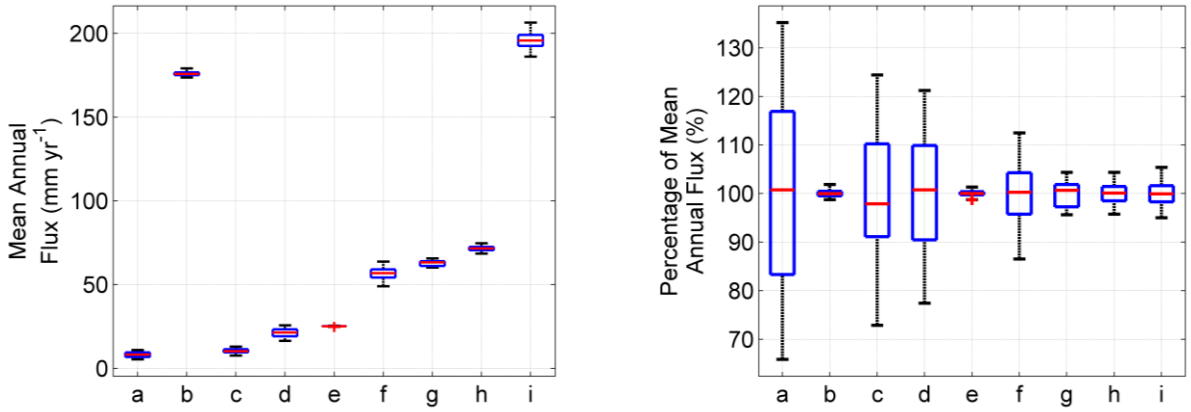

Figure 5.10: Left panel shows a box plot for selected mean annual hydrological fluxes calculated for the 1,296 future vegetation scenarios. Right panel shows the same plot but as a percentage of each mean annual flux. a) ET from intercepted rainfall, b) evapotranspiration, c) blowing snow sublimation, d) sublimation of intercepted snowfall, e) sublimation at the snow surface, f) total sublimation, g) soil moisture, h) snow water equivalent and i) streamflow discharge.

The water balance sensitivity to changes in projected vegetation scenarios is presented in Figure 5.10. The left panel in Figure 5.10 shows that the overall sensitivity of the water balance to vegetation change is relatively small for most mass fluxes. The hydrological flux with the largest absolute sensitivity is streamflow (i), ranging from 186 to 206 mm yr^{-1} (runoff ratio between 0.47 and 0.52), followed by total sublimation (f) and sublimation of intercepted snowfall (d) ranging from 49 to 64 mm yr^{-1} and 16 to 26 mm yr^{-1}, respectively. The right panel in Figure 5.10 shows the relative sensitivity of vegetation projections with respect to each mass flux as calculated with the vegetation projection presented in Section 5.4.2.2. The largest relative sensitivity is associated with evaporation from intercepted rainfall (a), which ranges between 66 and 135%; this was expected as the forest covers the majority of the basin and, therefore, changes to forest LAI will have a substantial impact on basin-scale losses from intercepted rainfall. The second largest relative change is associated with blowing snow sublimation (c), which ranges between 73 and

124%; this is explained as shrub expansion and densification reduces the snowpacks from which blowing snow can occur and increases the wind speed threshold required to initiate blowing snow. The third largest relative sensitivity is from sublimation of intercepted snowfall (d), which ranges between 77 and 121% due to the direct relationship between changes in forest LAI and canopy interception capacity. The relatively large sensitivity to these two sublimation terms ((c) and (d)) drive the sensitivity to total sublimation (f), which ranges between 87 and 112%. The other mass fluxes show a relative low sensitivity (<±10%), in which evapotranspiration (b) and sublimation at the snow surface (e) have the lowest sensitivity of all with roughly ±1%.

5.6 Discussion

Historical climate simulations using WRF at 4 km generally represented precipitation well at Inuvik with a small mean bias of 8 mm yr^{-1} or 3%, and a good agreement in the number and mean length of dry and wet spells (Table 5.2); however, the largest summer rainfall events were somewhat underestimated. These errors were greatly reduced with the quantile mapping bias correction (Figure 5.3). The good representation of precipitation and the physical connection between weather variables encourage the use of dynamically downscaled, high resolution atmospheric models to force physically based hydrological models, as opposed to using statistical downscaling techniques that do not guarantee a physical consistency such as the covariance amongst weather variables. The value of high resolution atmospheric models to represent precipitation has been noted by other studies (Cai et al., 2018; Kendon et al., 2017; Prein et al., 2015). A cold bias in simulated temperature of 2.7 °C was found and corrected, which has also been found in other Arctic studies using high resolution atmospheric models. For example, Cai et al. (2018) dynamically downscaled ERA-Interim using polar WRF (Hines et al., 2011) at a 10 km spatial resolution over Alaska, and found a mean cold bias of 1.4 °C.

Dynamically downscaled weather using a pseudo global warming (PGW) approach under the RCP8.5 scenario produces significantly warmer (6.1°C) and wetter (117 mm yr^{-1} or 39% increase) conditions (Table 5.3), small changes in wind speed and relative humidity, and an overall increase in all-wave irradiance (19 W m^{-2}). The largest projected changes in weather are associated with air temperature and precipitation. These results are consistent with, but slightly larger than estimations from the Polar WRF forced by the Community Earth System Model 1.0 (CESM1.0) under the RCP8.5 scenario in northern Alaska (Cai et al., 2018), which shows an increase of 5°C in the mean air temperature and 100 mm or 25% in the mean annual precipitation. Overland et al. (2013) investigated seasonal average changes in Artic surface air temperature projections using CMIP5 ensembles mean under the RCP8.5 and RCP4.5 scenario (Thomson et al., 2011), and found a roughly 2°C difference between RCP8.5 (5°C) and RCP4.5 (3°C) projections. There are inherent uncertainties in climate projection due to CO_2 emission scenarios, model structure and parameters, and intrinsic internal variability (Hodson et al., 2013); however, to include all the sources of uncertainties is computationally very expensive (e.g. Liu et al. (2016)), particularly when applying high resolution climate models over large domains (i.e. regional or continental). Due to this

restriction, this study addressed only one climate projection; however, the strength of this approach lies in a robust representation of weather changes (Kendon et al., 2017) and the physical consistency between the atmospheric variables, which allows a detailed investigation of hydrological changes using physically based hydrological models.

Large hydrological changes under changing climate and vegetation were projected to the end of the century. An increase of 80 mm or 70% in peak SWE, a shortening in 26 days or 9% or the snowcovered period and a doubling in the snow ablation rate from 1.8 to 3.5 mm day^{-1} are projected (Table 5.4). These changes are driven by the increase in snowfall by 54 mm yr^{-1} or 31% and the warmer temperatures. Callaghan et al. (2011) analyzed changes in Arctic SWE and snow cover duration using global climate models (GCMs) from CMIP3 for the 2050 period, and found a smaller increase in peak SWE of up to 15% for most of the Arctic and a larger decrease in snowcover duration of 10-20%. However, large scale GCMs cannot properly resolve snow accumulation processes in environments with complex topography or where snow redistribution is important. López-Moreno et al. (2012), Musselman et al. (2017), Pomeroy et al., (2015b) and Rasouli et al. (2014) found decreasing snowmelt rates with climate warming in the western US, Spain and southwestern and sub-arctic Canada – in contrast to the accelerating melt rates found further north in this Arctic study location. The results suggest that the impact of warming on melt rates cannot be generalized and a detail analysis that includes the snow processes driving snow accumulation and melt need to be considered.

One of the consequences of a shorter snowcover season is the earlier exposure of bare ground, triggering ground thaw 5 days earlier, and delaying the initiation of ground freeze by 17 days, resulting in a 22 days longer ground thaw season, increased ground thaw rates and a 0.25 m thicker active layer. Woo et al. (2007) projected a similar 0.3 m increase in the active layer thickness under the A2 scenario by 2100 for two Arctic sites with a 0.2 m peat cover. Increasing ground thaw rates and the larger peak SWE, allowed more infiltration producing faster soil moisture recharge during spring; however, soil moisture depletion in the highly porous peat layer was also fast, resulting in virtually the same minimum soil moisture content by late summer (Figure 5.8). Later in the fall, due to wetter and warmer conditions, soil moisture content increased by roughly 8 mm, resulting in an average increase of about 7 mm in the annual soil moisture content. Total sublimation was projected to slightly decrease by 5 mm or 9% mostly driven by the shortening of the snowcovered period and warmer temperatures dampening the sublimation from canopy-intercepted snowfall. The combined effect of these projected changes resulted in a significant increase of 100 mm or 100% in streamflow volume, mostly due to the doubling of spring runoff (Figure 5.9) driven by the 80 mm increase in peak SWE, but also by increasing fall runoff. Note that the 117 mm increase in annual precipitation and the 6°C warming did not produce a particularly large increase in ET (26 mm or 18%); in fact, it decreased the evaporative index from 0.49 to 0.42. Similarly, the sublimation ratio dropped from 34 to 23%. However, the wetter and warmer conditions produced a substantial increase in spring runoff. Capturing this particular hydrological behaviour is critical in cold regions, where the hydrological regime is dominated by snowmelt, as misrepresenting the

timing and magnitude of precipitation can produce a completely different hydrological response (e.g. larger ET and less streamflow if precipitation increase shifts to the summer); this encourages the use of dynamical downscaling approaches. Having the appropriate hydrological processes represented realistically in the model is also important - the drop in ratios of sublimation and ET were critical to the increase in runoff ratio and required including canopy resistance, interception of rainfall and snowfall and blowing snow transport processes in the model.

Krogh and Pomeroy (2018) analysed historical change at Havikpak Creek using the CRHM-AHM over 1960 – 2016, showing some discrepancies between the historical trends and the future projections presented in this study. Decreasing historical annual trends in ET (2.5 mm decade^{-1}), soil moisture (3 mm decade^{-1}) and blowing snow sublimation (0.6 mm decade^{-1}), and a negative change point in streamflow volume from 180 to 140 mm in 1968, oppose the projected increase in annual ET (26 mm), soil moisture (7 mm), blowing snow sublimation (2 mm) and streamflow discharge (100 mm) for the end of this century. These discrepancies are due to the large increase in precipitation projected for the future (40%) as opposed to the declining precipitation found in the historical period (change point in 1972 from 369 to 321 mm yr^{-1}). Nevertheless, similarities also exist. For example, earlier snowcover depletion and peak streamflow, delayed ground freeze and snowcover initiation, and thicker active layer were found in both the historical change analysis and this study. These processes are mostly controlled by changes in air temperature, which explains consistencies between historical trends and future projections, as both analyses included a significant increase in mean air temperature.

To the best of the author's knowledge, there are only three studies that have investigated the impact of climate change in Arctic headwater basins. The first study by Hinzman and Kane (1992) in Imnavait Creek, Alaska, USA, used the HBV model and defined three scenarios of climate change by increasing observed temperature in 4°C and precipitation by 0 and ±15%; however, these simulations were performed over a one year period, limiting the generalization of the results. The second and third studies by Pohl et al. (2007) in Trail Valley Creek, Northwest Territories, and Lewis and Lamoureux (2010) in the West watershed, Melville Island, Canadian Arctic Archipelago, respectively, used WATFLOOD and a similar approach to generate climate change scenarios for the end of the century; however, the mean changes in temperature and precipitation were informed by different GCMs and emission scenarios. Both studies showed results that are in the same direction as those presented in this study, such as increasing runoff volume and evaporation, and earlier spring runoff and peak streamflow; however, their analysis is limited by the use of calibrated empirical relationships to simulate evapotranspiration and snow ablation that could fail under future climate conditions. Importantly, snow redistribution and sublimation processes were not included despite their demonstrated importance in this environment (Liston et al., 2002; Pomeroy and Li, 2000; Pomeroy et al., 1997), and no permafrost calculations or changes in vegetation were included. Those shortcomings have been addressed in this study, producing simulations that are expected to be more robust under future conditions. However, limitations in this study arise from the use of a single future climate – a necessary feature of PGW research due

to computational costs. Future studies should aim to include a larger number of future climate projections to incorporate some of the uncertainty produced by different emission scenarios and model structure. The physical consistency between climate variables provided by dynamically downscaled, high-resolution atmospheric models provided an advantage in driving physically based hydrological models such as the one used in this study – this advantage should not be abandoned in pursuit of representing uncertainty from climate models by adopting statistical downscaling. A potential solution to producing high resolution and long term ensembles of future climate is the use of hybrid approaches combining dynamical and statistical downscaling such as the one presented by Walton et al. (2015), or implementing atmospheric models with intermediate complexity that require significantly less computational resources such as ICAR (Gutmann et al., 2016). In either case, the physical consistency between the standard weather variable required to drive physically based hydrological models in cold regions (i.e. air temperature, precipitation, wind speed, relative humidity and irradiance) has to be carefully assessed.

5.7 Conclusion

This study presented the implementation of a spatially distributed and physically based Arctic hydrological model (CRHM-AHM) forced with historical and future dynamically downscaled weather from a high resolution (4 km) atmospheric model (WRF) under a pseudo-global-warming (WRF) configuration, as well as projections of vegetation changes. A small mean bias in simulated precipitation (3%) and an adequate representation of the number and mean length of the dry and wet spells was found; however, bias correction using quantile mapping technique was implemented to remove the bias and better represent extreme precipitation events. A cold bias of 2.7 °C was also found and removed using the same technique. Future weather at HPC showed much warmer (6.1 °C) and wetter (40%) conditions, which produced several hydrological changes. These changes include an intensification of the hydrological regime by increasing spring runoff by 130%, producing earlier (one week) and larger (77%) peak streamflow, increasing peak snow accumulation (70%), shortening of the snowcover duration (26 days), increasing the melt rate (94%), thickening of the active layer thickness (0.25 m), increasing ET (18%) and decreasing sublimation (9%). These projected changes are strongly conditioned to projected changes in climate; however, projected increase in shrub cover and density also play an important role in annual ET from intercepted rainfall and blowing snow redistribution and sublimation, as revealed by the sensitivity analysis performed to changes in vegetation characteristics. Overall the hydrological processes shifted from controls exerted by cold regions processes towards summer processes, though the future basin remains a snow and permafrost dominated cold regions basin despite the impacts of climate change.

The high-resolution WRF run provided physically consistent weather time series that did not require further downscaling and drove realistic hydrological model responses that did not require model calibration when compared with observed streamflow discharge at Havikpak Creek. This suggests that atmospheric modelling at 4 km resolution provides suitable driving weather for small

scale hydrological modelling in environments with relatively low topographic gradients, as the one found in the delta of the Mackenzie River. Therefore, future climate from WRF under the PGW configuration is expected to be robust and suitable for hydrological applications; however, the main limitation of this approach remain the large computational and human resources required, currently restricting the number of future projections to one simulation. This limitation is expected improve over time as computing power increases, new hybrid approaches that use both dynamical and statistical downscaling are developed or atmospheric models with intermediate complexity improve their performance. This study provides the first detailed investigation of projected changes in climate and vegetation on the hydrology of and hydrological processes operating in an Arctic headwater basin, which is expected to help inform other Arctic climate impact studies.

Chapter 6

Conclusions

Tombstone Mountains, Km 85, Dempster Highway, Yukon Territory, September 6, 2014.

6.1 Concluding remarks

This thesis presented research that diagnosed and predicted changes to the hydrological cycling of an Arctic headwater basin under scenarios of changing climate and vegetation. Key aspects of the methodology implemented in this study include: (1) coupling of the key hydrological processes found in Arctic environments in a single modelling framework, such as ground freeze and thaw, snow redistribution by wind, snowmelt, canopy interception of snowfall and rainfall, and sublimation of intercepted, surface and blowing snow, which are not typically found in hydrological models; (2) the inclusion of explicit transient vegetation changes for the first time in a hydrological model; and (3) the evaluation and application of a dynamically downscaled, high-resolution (4 km) regional climate simulation under historical and future conditions to predict changes to hydrological cycling by the end of the century. The results, analysis and the new methodology presented in this study are expected to be relevant for policy makers, water managers and engineers interested in cold regions hydrology, particularly near the Arctic treeline, as key aspects of Arctic hydrology have been analysed and discussed for the first time, adding to a better understanding of the Arctic.

The main conclusions regarding the specific objectives proposed in Chapter 1 are presented below.

Objective 1: Determine the temporal and spatial variability, and interactions of the states and fluxes of the hydrological cycle within an Arctic basin.

The first step to accomplish this goal was to develop the first physically based hydrological model specific for Arctic environments (CRHM-AHM) that couples all the key hydrological processes during winter and summer. The CRHM-AHM was tested at two weather station sites (Chapter 2) and at a watershed scale (Chapter 3), all sites underlined by permafrost. The novelty of this model lies in the coupling of an algorithm that represents ground freeze and thaw, with the subsurface flow and storage fluxes previously included in the CRHM platform. The CRHM-AHM properly represented ground thaw timing and magnitude at both single-point and watershed scales; this has been previously shown to be a key control in subsurface water flow and storage, as it increases storage capacity and impacts the location of the water table and the hydraulic conductivity (Quinton and Gray, 2003). The Arctic hydrology model also showed to properly represent long-term snow accumulation and melt processes from snow survey records and daily streamflow discharge (Chapter 3), the latter being particularly challenging in such a remote and cold environment.

The application of the CRHM-AHM to Havikpak Creek (HPC) basin revealed the mean annual conditions, the interactions between physical processes and mass fluxes controlling its hydrology, and how they vary over time and space. Precipitation is dominated by snowfall; however, peak monthly precipitation typically occurs during summer (August) and it can be associated with rainfall-runoff events. Due to the cold conditions found in this environment, long winters from

October to April are common and, therefore cold region hydrological processes are very important. Snow accumulation and redistribution are key processes over this period. Great spatial variability in peak snow accumulation and snow cover duration was found due to blowing snow redistribution from the tundra to sparse shrubs, gullies and snowdrifts, and interception and sublimation from the forest canopy, demonstrating the importance of including such physical processes. Properly capturing snow accumulation is critical to represent snowmelt runoff, which is the most important hydrological event, but also due to the long-lasting and deeper snowpack in gullies and snowdrift that can provide runoff later on the year supporting low streamflow periods. Evapotranspiration was shown to be the largest mass flux component of HPC's hydrology, comprising almost half of the water losses, which was found to be particularly large at the wetlands. Active layer thickness was found to vary within HPC, which was largely controlled by two factors: (1) the volumetric water content in the soil as it increases the soil's thermal conductivity and (2) the end of snow ablation, which is strongly couple with the initiation of ground thaw. Diagnosing and understanding these interactions is critical to quantifying the effect of changes in climate and vegetation on the hydrology of Arctic basins.

Objective 2: Diagnose the historical hydrological responses to changing climate and vegetation in an Arctic basin.

Chapter 4 discussed in detail the historical changes (1960-2016) produced individually by changing climate and vegetation, and their combined effect at Havikpak Creek basin. Observed warming and reduction in annual precipitation produced several environmental changes, such as decreasing streamflow, earlier peak streamflow, decreasing evapotranspiration (ET) and sublimation, and increasing active layer thickness. Some of these changes can be expected; however, changes in ET and streamflow are not easily diagnosed due to their complex nature. For example, ET depends not only on temperature and precipitation, but also on stomata resistance, net radiation, wind speed, relative humidity and soil moisture storage in the rooting zone, which in turn have a complex interaction with other physical processes. Using simple temperature-index models to estimate ET, under significant warming, will likely provide a wrong (opposite) estimate of changing ET, which is the most important water loss. This highlights the importance of using hydrological models that include a physical representation of the key processes driving Arctic hydrology. The effect of changing vegetation is not as important as changing climate; however, it has important impacts and so it is critical to include this in models. Changing vegetation reduces blowing snow transport and thus sublimation, allowing more snow to accumulate by the end of the winter, and therefore, more water available as snowmelt runoff. This process dampened the effect of decreasing streamflow discharge from changing climate, thus, slightly increasing HPC's hydrological resiliency, and demonstrating the need to include observed rates of vegetation changes in Arctic hydrological models, something historically neglected that was investigated and quantified for the first time in this study. Historical changes in the hydrological processes of HPC revealed that climate and vegetation changes are decelerating its hydrological response, mostly driven by the decrease in observed mean annual precipitation.

Objective 3: Quantify future hydrological changes due to projected changes in climate and vegetation in an Arctic basin.

The first challenge to accomplish this goal was generating a plausible and physically consistent climate prediction that can be used to force the CRHM-AHM. A dynamically downscaled, convection-permitting and high-resolution climate model (4 km) was able to realistically represent observed climate at Inuvik after bias correction. This demonstrated its suitability to realistically represent future climate under a pseudo-global-warming (PGW) configuration using the RCP8.5 scenario. Significant hydrological changes were projected, such as increasing streamflow discharge and snow accumulation, thickening of the ALT, increasing ET and peak streamflow, and larger snow ablation rates, opposing the historical trends found in Chapter 4. Proportional losses to sublimation and ET diminished under the future climate, indicating strong streamflow sensitivity to increased precipitation. This suggests that under sufficient climate change (much warmer and wetter conditions), the historical trend towards the deceleration of the hydrological regime of HPC will reverse; however, hydrological states controlled by changes in air temperature such as active layer thickness and snowcover depletion and duration will continue to change in the same direction.

Given the large amount of computational resources required to run high resolution RCMs, only one climate scenario was studied; however, the PGW was generated using an ensemble of climate projections and, therefore, it is expected to be representative of the mean conditions projected by RCP8.5. Furthermore, as RCP8.5 is the scenario that projects the largest climatic changes, compared with RCP2.6, RCP4.5 and RCP6.0, the hydrological projections presented in Chapter 5 should be interpreted as the largest expected hydrological changes expected in this century. The sensitivity analysis of changing vegetation projections to the future water balance revealed a relatively low sensitivity to changing shrub expansion and densification, and forest infilling, which is explained as the large changes in climate are dominating the future hydrological response. However, under scenario of moderate climate changes (e.g. RCP2.6), changes in vegetation are expected to play a more significant role, especially in regions where advances of the taiga treeline may occur. This is the first study looking at climate and vegetation changes in Arctic headwater basins in detail and using state-of-the-art climate projections; therefore, it is expected to provide guidance to coming studies assessing future hydrological changes in Arctic environments.

6.2 Concluding discussion

6.2.1 Diagnosing Arctic hydrology

Arctic hydrology is different from other regions as continuous permafrost plays a significant role controlling subsurface energy and mass fluxes, and cold temperatures result in a hydrological regime dominated by snow-processes, such as snow redistribution, sublimation, snow

accumulation and snow melt. Moreover, due to the Arctic's remoteness and the sparse population, the number of research studies found in this region is considerably lower than those in warmer regions, making Arctic hydrology a challenging and interesting topic for research. To diagnose Arctic hydrology it is essential to have a comprehensive understanding of the hydrological processes controlling the water cycling, and, as presented in Chapter 1 (Section 1.2.1), there is a relatively consolidated understanding of the key hydrological processes in Arctic regions. This thesis presented the development of a spatially distributed and physically based hydrological model suitable for Arctic regions using the Cold Regions Hydrological Model platform (CRHM; Pomeroy et al. 2007), and its application at two new weather station sites for a period limited to two and three seasons (Chapter 2), and at a watershed scale in Havikpak Creek basin (Chapter 3) for 28 years, all in northwestern Canada. The application and verification in Havikpak Creek included long-term records of snow accumulation, daily streamflow, ground surface temperature and active layer thickness, whereas the two weather station sites validated a single-point model application for ground surface temperature, ground thaw and snow water equivalent under relatively warmer conditions than those from found at Havikpak Creek. What is unique about the CRHM-AHM is that it includes all the key hydrological processes typically found in Arctic headwater basins, such as snowmelt and accumulation energy balance, blowing snow redistribution and sublimation, sublimation and evaporation from canopy intercepted snowfall and rainfall, infiltration into frozen and unfrozen soils, flow through snowpack and organic terrain, ground freeze and thaw, subsurface water flow and storage, evapotranspiration and streamflow routing, using mostly parameterizations with strong physical basis. Previous hydrological models for Arctic headwater basins lack the representation of some of this processes, such as blowing snow redistribution and sublimation, canopy interception of snowfall and rainfall and ground freeze and thaw, or simple unrealistic parameterizations, such as the degree-day index for snowmelt, were used; therefore, the CRHM-AHM is a more comprehensive model that allows the investigation of the interactions between these processes under different conditions for the first time. A key strength of CRHM-AHM is its flexibility as it can be modified and applied to other Arctic basins. For example, groundwater contribution at Havikpak Creek was considered to be minimal as it is underlined by ice-rich continuous permafrost limiting the sub- and supra-permafrost groundwater exchange, and no streamflow has been observed during winter; however, other basins may have groundwater contributions that can be easily included in the model.

The hydrological regime of Havikpak Creek is dominated by snowmelt runoff during spring and early summer, as can be deduced from observed streamflow records; however, sub-basin and interannual variability of mass and energy fluxes have not been investigated. The 28-year (1982-2009) simulation showed that from the 329 mm mean annual precipitation input, 47% is lost to evapotranspiration, 39% forms streamflow discharge and 14% sublimates. Great spatial variability was found for most of these mass fluxes. For example, mean annual evapotranspiration at the tundra sites is about 117 mm, whereas at the wetland it is 218 mm and at the forested sites it is 164 mm. Surface runoff generation (Figure 3.10) is strongly correlated with snowmelt as frozen ground restricts infiltration producing large snowmelt runoff events, whereas subsurface runoff is

generally much smaller, except at the wetlands where subsurface runoff is very significant. Due to the importance of the end-of-the-winter SWE, capturing snow processes that determine SWE is critical in modelling Arctic basins such as Havikpak Creek. Snowfall is the largest water input to the watershed, representing about 59% of mean annual precipitation. From the annual snowfall about 25% (47 mm) is lost by sublimation, which is composed of sublimation from the snowpack surface (25 mm), sublimation of intercepted snowfall (18 mm) and blowing snow sublimation (4 mm). Blowing snow redistribution is also a key process within Havikpak, as it redistributes snow from the wind-swept Tundra HRUs to the Gully/Drift HRUs (Figure 3.8), forming large snowdrifts whose meltwaters support summer streamflow.

The change analysis presented in Chapter 4 revealed interesting results about the effect of changing climate and vegetation on the hydrology of HPC that have never been investigated before. The 56-year analysis showed that since 1960 precipitation has decreased at Inuvik from 369 to 321 (13%), mean annual temperature has increased by 3.7 °C and all-wave irradiance has decreased by 4 W m^{-2}. These climatological changes in addition to changes in vegetation characteristics, particularly shrub expansion and densification, have produced several hydrological changes over the 56-year period. The scenarios analysis presented in Chapter 4 revealed that most hydrological changes in HPC are dominated by changing climate, such as decreasing streamflow, soil moisture, snowfall, peak SWE, ET and snowcover duration, and increasing active layer thickness; however, changing vegetation increases the wind speed threshold required to initiation blowing snow events, therefore, reducing blowing snow redistribution and sublimation. Changes in shrub characteristics showed to dampened the effect of decreasing precipitation on HPC hydrological regime, as lower sublimation from increasing shrubs increases peak SWE. This result in a slight increase of hydrological resiliency for HPC, demonstrating the importance of including transient vegetation in long-term hydrological models, something typically neglected. Observed and simulated changes in climate, vegetation and hydrology provide useful insights on potential future hydrological changes under plausible scenarios of changing climate and vegetation, as observed patterns may continue in the future.

6.2.2 Predicting Arctic hydrology

Predicting Arctic hydrology was the ultimate goal of this thesis and it is presented in Chapter 5. Future climatological projections are inherently uncertain as they are derived from a variety of greenhouse gas concentration scenarios and different global climate models that are subject to large uncertainties. This study tackled this problem by using a pseudo-global-warming approach, using the average response of 19 GCMs under the RCP8.5 scenario to perturb a high resolution RCM (WRF; 4 km). Although this approach does not explicitly account for the uncertainty associated with climate projections and model structure, it does provide mean climate projections that are physically consistent between the atmospheric variables (e.g. shortwave irradiance and precipitation), which is critical for driving physically based hydrological models. This physical

consistency cannot be guaranteed through statistical downscaling of climate model outputs and, therefore, it is a key component of this study. Due to computational and technical personal requirements to perform the high-resolution climate simulations, only one future scenario was assessed. Although this is a limitation of the study, it is also one of its main strength, as no previous study has looked at future changes in the interaction between hydrological processes of Arctic headwater basins using a physically based approach before, representing a step forward in predicting future Arctic hydrology. Historical climate simulations successfully represented observed weather with a small bias in annual precipitation (3%) and good representation of the mean number and length of wet and dry spells (Table 5.2), which is hydrologically very important. An overall cold bias was found (2.7 °C); however, a strong correlation exists (Figure 5.3), and the bias could be easily removed using quantile-mapping techniques. Other atmospheric variables were properly represented as well, such as relative humidity and wind speed. Future climate projections show much warmer (6.1 °C) and wetter conditions (40%), increased all-wave irradiance through increasing long-wave, and small changes in wind speed and relative humidity. The largest temperature changes are projected to occur during winter and spring reducing the period with air temperatures above 0 °C in about one month, and rainfall and snowfall are projected to increase by 63 and 54 mm, respectively.

In terms of future vegetation changes, shrub expansion and densification are expected to continue along with forest infilling, as warmer and wetter conditions provide longer growing seasons and ground thaw allows deeper roots development; however, the exact rate of this growth is uncertain, as there are other controlling factors, such as herbivory and forest fires. This study extrapolated observed rates of shrub growth from a previous study in the region (Lantz et al., 2013), and included a sensitivity of changes in this rate of growth to the future water cycling; from slight increases to a complete shrubification of the tundra, showing an overall small sensitivity to the absolute mean water fluxes, but a larger sensitivity to relatively changes in water fluxes such as evaporation from intercepted rain, blowing snow sublimation, sublimation from intercepted snowfall and total sublimation (Figure 5.10). This exercise allowed concluding that although including vegetation changes is important, as shown in Chapter 4, if significant climate change occurs, then plausible scenario of changing shrub characteristics become less relevant in the overall hydrological response.

Under these scenarios of climate and vegetation changes for the end of the century (2086-2099), several hydrological changes are projected. The hydrological regime of Havikpak Creek will intensify, as spring (May) runoff increases by 130%, mean annual streamflow volume doubles, and earlier and larger peak streamflow are projected. Increasing snowfall impacts snow processes at Havikpak Creek by increasing mean peak SWE in 80 mm, shortening snowcover duration in 26 days and increasing snow ablation rates by 83%. Other predicted changes include increasing ET by 26 mm, decreasing sublimation by 5 mm and increasing active layer thickness by 0.25 m. The small change in sublimation is the result of compensating processes, in one hand annual blowing snow sublimation increases slightly (2 mm) due to larger snowfall events and deeper snowpacks,

but on the other hand sublimation from intercepted snowfall and sublimation at the snowpack surface decrease (-1 and -6, respectively) due to the shorter snowfall and snowcovered periods, resulting in a small decrease in total sublimation. Overall, large changes in the hydrological cycling of Arctic headwater basins can be expected under these scenarios of changing climate and vegetation. These changes can have significant effect in the future. For example, larger peak streamflow may damage highway infrastructure designed for historical conditions, producing floods and overwhelming bridges and culverts. Changes in the snowcover season will have an impact in the atmospheric energy balance due to changing surface albedo, producing a positive feedback with climate change. Permafrost thaw can damage building foundations, deteriorate road stability and change natural landscape (e.g. drunken forests, ice wedge degradation). All of this has already been observed in the Inuvik region. Therefore, the great importance of investigating future Arctic hydrology, so that authorities, engineers, researchers and communities can be better informed in their search for sustainable adaptation measures.

The results, analysis and methodology used to diagnose the past and predict future Arctic hydrology in this thesis are expected to allow a deeper understanding of the hydrological controls of Arctic basins under observed and potential scenarios of change. Hopefully, Arctic researchers will find guidance in this research as they seek to improve the understanding of Arctic hydrology or to understand potential impacts of climate and vegetation changes near the Arctic treeline.

6.3 Outlook

An important focus of this study was the development and validation of a hydrological model suitable for Arctic environments, which were achieved by implementing and improving the Cold Regions Hydrological Model platform (CRHM), particularly by incorporating a ground freeze and thaw algorithm that represents heat conduction and latent heat exchange. However, further improvements to existing algorithms or in the incorporation of new algorithms representing physical and/or biological processes, not currently included, should be explored in future applications. For example, the effect of shrub canopy on sub-canopy energetics, particularly on shortwave irradiance, should be implemented, as it has been shown to have a significant effect in the energy balance and snowmelt (Menard et al., 2014; Pomeroy et al., 2006). Relatively simple models such as the one presented by Bewley et al. (2007), based on shrub geometry, can be explored. The bending of shrub branches produced by intercepted snowfall and the later spring-up produced by wet snow metamorphism and changing branches elasticity due to warmer temperatures (Menard et al., 2012) and its effect on surface albedo (Sturm et al., 2005) should be included. For example, aspects of the full shrub model presented by Ménard et al. (2012) could be included in the future. Another complex process that can occur in Arctic headwater basins is the formation of snow dams in the river channel. Woo and Sauriol (1980) investigated this process for the first time, and since, it has been acknowledged as a source of great uncertainty in streamflow routing due to the delay effect that it has on streamflow (Kane et al., 1991; Z. Zhang et al., 2000); however, no study has explicitly incorporated its effect. This is likely a key area for improvement

in Arctic basins to generate more reliable peak streamflow predictions. An improvement of winter ground surface temperature simulations should be pursued in the future, as current approaches based on the snowpack's thermal conductivity and depth, tend to underestimate it. This is not a significant source of error for Havikpak Creek as cold conditions guarantee the full refreeze of the active layer; however, in southern regions with discontinuous permafrost, it could potentially become an issue representing ground freeze-up and subsurface flow, or under sufficient global warming.

Due to the Arctic's remoteness and cold conditions, the availability of quality and long-term meteorological data is uncommon and, therefore, the implementation of a long-term and physically based hydrological model, such as the one implemented in this thesis, is very challenging. Currently, thanks to great improvements in computational resources and climate simulations, there are a number of products that can be used to overcome problems related with data scarcity. Atmospheric reanalyses have been used to inform hydrological models on poorly gauged regions (Krogh et al., 2015); however, they still lack of a reliable representation of precipitation. High resolution and long-term dynamical downscaling using RCMs forced with reanalysis (Cai et al., 2018; Liu et al., 2017; Pieri et al., 2015) provide more reliable weather estimates to perform hydrological analyses, as they offer all the required data, such as precipitation, air temperature, relative humidity, wind speed, and incoming longwave and shortwave radiation. However, locally observed weather is still a critical source of information to validate or bias correct datasets from high resolution RCMs, as they might misrepresent some key weather variables, which reflect in the poor hydrological simulations. This is particularly problematic, as the number of high-latitude research basins has been declining in last decades (Laudon et al., 2017); this trend needs to be reversed to produce more accurate predictions in Arctic regions.

A key step towards a better understanding and quantification of future hydrology is the access to robust climate projections that can be verified under historical conditions. Hydrologically, precipitation is the variable of main concern and the most difficult to properly represent by atmospheric models. Features such as precipitation intensity, frequency and duration are critical, as well as the number and length of wet/dry spells. This study showed that some of these features are well represented by a state-of-the-art RCM at relatively small scales, opening new opportunities for hydrological studies. Other atmospheric variables such as relative humidity, wind speed, and radiative fluxes, were found to perform well in northwestern Canada, whereas air temperature showed a cold bias that can be removed using observed records. Air temperature bias from RCMs can be improved using spectral nudging techniques, which function in a similar way to data assimilation (Rummukainen, 2010). Deriving future climate projection based on high resolution models that can explicitly resolve convection (<4 km; Prein et al., 2015) is becoming a more common practice, and some studies have argued that they are more suitable as then can represent changes in atmospheric features such as precipitation patterns (e.g. intensity) and wind gusts (Kendon et al., 2017, 2014). These changes cannot be properly captured by statistical downscaling techniques. Although using high resolution RCMs to project future climate looks

very promising, there is still one issue that needs to be addressed, this is the quantification of uncertainty in climate projections. This is typically tackled by using different RCMs driven by a variety of GCMs; however, the large amount of computational resources and technical personal required to run high resolution RCMs prevent the realization of multiple runs. This could be improved by implementing hybrid approaches that combine dynamical downscaling techniques to understanding local atmospheric dynamics, which can be then used to guide statistical downscaling, such as the approach proposed by Walton et al. (2015). Although not an ideal solution, this can help improving uncertainty quantification as computational improvements allow for a full set of high resolution RCM ensembles in the future. A second solution is the implementation of atmospheric models with intermediate complexity that require significantly less computational resources, which can be used to generate ensemble predictions over large domains, such as the one proposed by Gutmann et al. (2016); however, the accuracy and reliability of this approach needs to be further investigated and verified.

Another area of improvement is the generation of scenarios of changing vegetation in Arctic regions as vegetation plays a key hydrological role in winter and summer hydrological processes. Zhang et al. (2013) and Pearson et al. (2013) investigated changes in vegetation by the end of the 21st century, which is a step forward a better understating of future vegetation dynamic. This need to be further investigated and aim for an ensemble of potential scenarios of vegetation changes to be included in hydrological models. Moreover, the feedback between vegetation and climate changes needs to be explored and explicitly included in a single framework allowing a more comprehensive understanding of future conditions in the Arctic.

References

Abbott, M.B., Bathurst, J.C., Cunge, J.A., O'Connell, P.E., Rasmussen, J., 1986a. An introduction to the European Hydrological System — Systeme Hydrologique Europeen, "SHE", 1: History and philosophy of a physically-based, distributed modelling system. J. Hydrol. 87, 45–59. doi:10.1016/0022-1694(86)90114-9

Abbott, M.B., Bathurst, J.C., Cunge, J.A., O'Connell, P.E., Rasmussen, J., 1986b. An introduction to the European Hydrological System — Systeme Hydrologique Europeen, "SHE", 2: Structure of a physically-based, distributed modelling system. J. Hydrol. 87, 61–77. doi:10.1016/0022-1694(86)90115-0

Aksamit, N.O., Pomeroy, J.W., 2016. Near-Surface Snow Particle Dynamics from Particle Tracking Velocimetry and Turbulence Measurements during Alpine Blowing Snow Storms.

Cryosph. Discuss. 1–25. doi:10.5194/tc-2016-95

Aksamit, N.O., Pomeroy, J.W., 2017. The Effect of Coherent Structures in the Atmospheric Surface Layer on Blowing-Snow Transport. Boundary-Layer Meteorol. 1–23. doi:10.1007/s10546-017-0318-2

Aksamit, N.O., Pomeroy, J.W., 2018. Scale Interactions in Turbulence for Mountain Blowing Snow. J. Hydrometeorol. 19, 305–320. doi:10.1175/JHM-D-17-0179.1

Annandale, J.G., Jovanovic, N.Z., Benade, N., Allen, R.G., 2002. Software for missing data error analysis of Penman-Monteith reference evapotranspiration. Irrig. Sci. 21, 57–67. doi:10.1007/s002710100047

Arheimer, B., Lindström, G., 2014. Climate impact on floods – changes of high-flows in Sweden for the past and future (1911–2100). Hydrol. Earth Syst. Sci. Discuss. 11, 7551–7584. doi:10.5194/hessd-11-7551-2014

Ayers, H.D., 1959. Influence of Soil Profile and Vegetation Characteristic on Net Rainfall Supply to Runoff, in: Spillway Design Floods: Proceeding of Hydrology Symposium No. 1, National Research Council of Canada. pp. 198–205.

Bailey, W.G., Oke, T.R., Rouse, W.R., 1997. The Surface Climates of Canada. McGill-Queen's University Press.

Bartelt, P., Lehning, M., 2002. A physical SNOWPACK model for the Swiss avalanche warning: Part I: numerical model. Cold Reg. Sci. Technol. 35, 123–145. doi:10.1016/S0165-232X(02)00074-5

Beilman, D.W., Vitt, D.H., Halsey, L.A., 2001. Localized Permafrost Peatlands in Western Canada: Definition, Distributions, and Degradation. Arctic, Antarct. Alp. Res. 33, 70. doi:10.2307/1552279

Beltaos, S., 1983. River Ice Jams: Theory, Case Studies, and Applications. J. Hydraul. Eng. 109, 1338–1359. doi:10.1061/(ASCE)0733-9429(1983)109:10(1338)

Beltaos, S., Prowse, T., 2009. River-ice hydrology in a shrinking cryosphere. Hydrol. Process. 23, 122–144. doi:10.1002/hyp.7165

Beven, K., 1997. TOPMODEL: A critique. Hydrol. Process. 11, 1069–1085. doi:10.1002/(SICI)1099-1085(199707)11:9<1069::AID-HYP545>3.0.CO;2-O

Beven, K., 2001. Dalton Medal Lecture: How Far Can We Go In Distributed Hydrological Modelling? Hydrol. Earth Syst. Sci. 5, 1–12.

Beven, K., Freer, J., 2001. A dynamic TOPMODEL. Hydrol. Process. 15, 1993–2011. doi:10.1002/hyp.252

Beven, K., Kirkby, M., Schofield, N., Tagg, A., 1984. Testing a physically-based flood forecasting

model (TOPMODEL) for three U.K. catchments. J. Hydrol. 69, 119–143. doi:10.1016/0022-1694(84)90159-8

Bewley, D., Pomeroy, J.W., Essery, R.L.H., 2007. Solar Radiation Transfer Through a Subarctic Shrub Canopy. Arctic, Antarct. Alp. Res. 39, 365–374. doi:10.1657/1523-0430(06-023)[BEWLEY]2.0.CO;2

Blaney, H.F., Criddle, W.D., 1962. Determining Consumptive Use and Irrigation Water Requirements. Agricultural Research Service, USDA.

Boé, J., Terray, L., Habets, F., Martin, E., 2007. Statistical and dynamical downscaling of the Seine basin climate for hydro-meteorological studies. Int. J. Climatol. 27, 1643–1655. doi:10.1002/joc.1602

Bond, W.J., Keeley, J.E., 2005. Fire as a global 'herbivore': the ecology and evolution of flammable ecosystems. Trends Ecol. Evol. 20, 387–394. doi:10.1016/j.tree.2005.04.025

Bonsal, B.R., Prowse, T.D., Duguay, C.R., Lacroix, M.P., 2006. Impacts of large-scale teleconnections on freshwater-ice break/freeze-up dates over Canada. J. Hydrol. 330, 340–353. doi:10.1016/j.jhydrol.2006.03.022

Boughton, W., 1989. A review of the USDA SCS curve number method. Aust. J. Soil Res. 27, 511. doi:10.1071/SR9890511

Bowen, I.S., 1926. The Ratio of Heat Losses by Conduction and by Evaporation from any Water Surface. Phys. Rev. 27, 779–787. doi:10.1103/PhysRev.27.779

Brisson, E., Weverberg, K. Van, Demuzere, M., 2016. How well can a convection ‐ permitting climate model reproduce decadal statistics of precipitation, temperature and cloud characteristics ? Clim. Dyn. 47, 3043–3061. doi:10.1007/s00382-016-3012-z

Brohan, P., Kennedy, J.J., Harris, I., Tett, S.F.B., Jones, P.D., 2006. Uncertainty estimates in regional and global observed temperature changes: A new data set from 1850. J. Geophys. Res. Atmos. 111, 1–21. doi:10.1029/2005JD006548

Brooks, R., Corey, A., 1964. Hydraulic properties of porous media. Hydrology Papers, Colorado State University.

Brown, R., Derksen, C., Wang, L., 2010. A multi-data set analysis of variability and change in Arctic spring snow cover extent, 1967–2008. J. Geophys. Res. 115, D16111. doi:10.1029/2010JD013975

Buck, A.L., 1981. New Equations for Computing Vapor Pressure and Enhancement Factor. J. Appl. Meteorol. doi:10.1175/1520-0450(1981)020<1527:NEFCVP>2.0.CO;2

Burn, D.H., Hag Elnur, M.A., 2002. Detection of hydrologic trends and variability. J. Hydrol. 255, 107–122. doi:10.1016/S0022-1694(01)00514-5

Cai, L., Alexeev, V.A., Arp, C.D., Jones, B.M., Liljedahl, A.K., Gädeke, A., 2018. The Polar WRF Downscaled Historical and Projected Twenty-First Century Climate for the Coast and Foothills of Arctic Alaska. Front. Earth Sci. 5, 1–15. doi:10.3389/feart.2017.00111

Callaghan, T. V., Johansson, M., Brown, R.D., Groisman, P.Y., Labba, N., Radionov, V., Barry, R.G., Bulygina, O.N., Essery, R.L.H., Frolov, D.M., Golubev, V.N., Grenfell, T.C., Petrushina, M.N., Razuvaev, V.N., Robinson, D.A., Romanov, P., Shindell, D., Shmakin, A.B., Sokratov, S.A., Warren, S., Yang, D., 2011. The changing face of arctic snow cover: A synthesis of observed and projected changes. Ambio 40, 17–31. doi:10.1007/s13280-011-0212-y

Cannon, A.J., Sobie, S.R., Murdock, T.Q., 2015. Bias correction of GCM precipitation by quantile mapping: How well do methods preserve changes in quantiles and extremes? J. Clim. 28, 6938–6959. doi:10.1175/JCLI-D-14-00754.1

Cannon, A.J., Whitfield, P.H., 2002. Downscaling recent streamflow conditions in British Columbia, Canada using ensemble neural network models. J. Hydrol. 259, 136–151. doi:10.1016/S0022-1694(01)00581-9

Carey, K.L., 1973. Icings developed from surface water and ground water. Corps of Engineers, U.S. Army, Hanover, New Hampshire.

Carey, S.K., Quinton, W.L., Goeller, N.T., 2007. Field and laboratory estimates of pore size properties and hydraulic characteristics for subarctic organic soils. Hydrol. Process. 21, 2560–2571. doi:10.1002/hyp.6795

Carey, S.K., Woo, M., 2001. Spatial variability of hillslope water balance, Wolf Creek basin, subarctic Yukon. Hydrol. Process. 15, 3113–3132. doi:10.1002/hyp.319

Cederstrom, D.J., Johnston, P.M., Subitzky, S., 1953. Occurrence and development of ground water in permafrost regions. Geological Survey Circular 275, Washington, D. C.

Cey, E.E., Rudolph, D.L., 2009. Field study of macropore flow processes using tension infiltration of a dye tracer in partially saturated soils. Hydrol. Process. 1779, 1768–1779. doi:10.1002/hyp

Changwei, X., Gough, W.A., 2013. A Simple Thaw-Freeze Algorithm for a Multi-Layered Soil using the Stefan Equation. Permafr. Periglac. Process. 24, 252–260. doi:10.1002/ppp.1770

Chen, J., Brissette, F.P.F.P., Chaumont, D., Braun, M., 2013. Finding appropriate bias correction methods in downscaling precipitation for hydrologic impact studies over North America. Water Resour. Res. 49, 4187–4205. doi:10.1002/wrcr.20331

Choi, W., Kim, S.J., Rasmussen, P.F., Moore, A.R., 2009. Use of the North American Regional Reanalysis for hydrological modelling in Manitoba. Can. Water Resour. J. 34, 17–36. doi:10.4296/cwrj3401017

Chow, D., Levermore, G.J., 2007. New algorithm for generating hourly temperature values using

daily maximum, minimum and average values from climate models. Build. Serv. Eng. Res. Technol. 28, 237–248. doi:10.1177/0143624407078642

Chow, V. Te, Maidment, D.R., Mays, L.W., 1994. Hidrologia Aplicada, Spanish. ed. McGraw-Hill Interamericana S.A., Santafe de Bogoto, Colombia.

Ciarapica, L., Todini, E., 2002. TOPKAPI: a model for the representation of the rainfall-runoff process at different scales. Hydrol. Process. 16, 207–229. doi:10.1002/hyp.342

Clark, C.O., 1945. Storage and the Unit Hydrograph. Transections, ASCE 110, 1419–1446.

Clark, M.P., Nijssen, B., Lundquist, J.D., Kavetski, D., Rupp, D.E., Woods, R. a, Freer, J.E., Gutmann, E.D., Wood, A.W., Brekke, L.D., Arnold, J.R., Gochis, D.J., Rasmussen, R.M., 2015. A unified approach for process-based hydrologicmodeling: 1. Modeling concept. Water Resour. Res. 51, 1–17. doi:10.1002/2015WR017200.A

Colbeck, S.C., 1972. A Theory of Water Percolation in Snow. J. Glaciol. 11, 369–385. doi:10.3189/S0022143000022346

Colbeck, S.C., 1975. A theory for water flow through a layered snowpack. Water Resour. Res. 11, 261–266. doi:10.1029/WR011i002p00261

Colbeck, S.C., 1979. Water flow through heterogeneous snow. Cold Reg. Sci. Technol. 1, 37–45. doi:10.1016/0165-232X(79)90017-X

Collins, M., Knutti, R., Arblaster, J., Dufresne, J.-L., Fichefet, T., Friedlingstein, P., Gao, X., Gutowski, W.J., Johns, T., Krinner, G., Shongwe, M., Tebaldi, C., Weaver, A.J., Wehner, M., 2013. Long-term Climate Change: Projections, Commitments and Irreversibility, in: Intergovernmental Panel on Climate Change (Ed.), Climate Change 2013 - The Physical Science Basis. Cambridge University Press, Cambridge, pp. 1029–1136. doi:10.1017/CBO9781107415324.024

Connon, R.F., Quinton, W.L., Craig, J.R., Hayashi, M., 2014. Changing hydrologic connectivity due to permafrost thaw in the lower Liard River valley, NWT, Canada. Hydrol. Process. 28, 4163–4178. doi:10.1002/hyp.10206

Davie, T., 2008. Fundamentals of Hydrology, Second Edition, Second. ed. Taylor & Francis.

DeBeer, C.M., Wheater, H.S., Carey, S.K., Chun, K.P., 2016. Recent climatic, cryospheric, and hydrological changes over the interior of western Canada: A review and synthesis. Hydrol. Earth Syst. Sci. 20, 1573–1598. doi:10.5194/hess-20-1573-2016

Dee, D.P., Uppala, S.M., Simmons, A.J., Berrisford, P., Poli, P., Kobayashi, S., Andrae, U., Balmaseda, M.A., Balsamo, G., Bauer, P., Bechtold, P., Beljaars, A.C.M., van de Berg, L., Bidlot, J., Bormann, N., Delsol, C., Dragani, R., Fuentes, M., Geer, A.J., Haimberger, L., Healy, S.B., Hersbach, H., Hólm, E. V., Isaksen, L., Kållberg, P., Köhler, M., Matricardi, M., McNally, a. P., Monge-Sanz, B.M., Morcrette, J.-J., Park, B.-K., Peubey, C., de Rosnay, P., Tavolato, C., Thépaut, J.-N., Vitart, F., 2011. The ERA-Interim reanalysis: configuration and

performance of the data assimilation system. Q. J. R. Meteorol. Soc. 137, 553–597. doi:10.1002/qj.828

Del Genio, A.D., Kovari, W., Yao, M.-S., Jonas, J., 2005. Cumulus Microphysics and Climate Sensitivity. J. Clim. 18, 2376–2387. doi:10.1175/JCLI3413.1

Déry, S.J., Wood, E.F., 2004. Teleconnection between the Arctic Oscillation and Hudson Bay river discharge. Geophys. Res. Lett. 31, 2–5. doi:10.1029/2004GL020729

Déry, S.J., Wood, E.F., 2005. Decreasing river discharge in northern Canada. Geophys. Res. Lett. 32, L10401. doi:10.1029/2005GL022845

Déry, S.J., Yau, M.K., 1999. A Bulk Blowing Snow Model. Boundary-Layer Meteorol. 93, 237–251. doi:10.1023/A:1002065615856

Dingman, S., 2002. Physical Hydrology, Second Edi. ed. Waveland Press, Inc.

Dingman, S.L., 1966. Characteristics of summer runoff from a small watershed in central Alaska. Water Resour. Res. 2, 751–754. doi:10.1029/WR002i004p00751

Ellis, C.R., Pomeroy, J.W., Brown, T., MacDonald, J., 2010. Simulation of snow accumulation and melt in needleleaf forest environments. Hydrol. Earth Syst. Sci. 14, 925–940. doi:10.5194/hess-14-925-2010

Ellis, C.R., Pomeroy, J.W., Link, T.E., 2013. Modeling increases in snowmelt yield and desynchronization resulting from forest gap-thinning treatments in a northern mountain headwater basin. Water Resour. Res. 49, 936–949. doi:10.1002/wrcr.20089

Endrizzi, S., Quinton, W.L., Marsh, P., 2011. Modelling the spatial pattern of ground thaw in a small basin in the arctic tundra. Cryosph. Discuss. 5, 367–400. doi:10.5194/tcd-5-367-2011

Essery, R., Li, L., Pomeroy, J., 1999. A distributed model of blowing snow over complex terrain. Hydrol. Process. 13, 2423–2438. doi:10.1002/(SICI)1099-1085(199910)13:14/15<2423::AID-HYP853>3.0.CO;2-U

Essery, R.L.H., Pomeroy, J.W., 2004. Vegetation and Topographic Control of Wind-Blown Snow Distributions in Distributed and Aggregated Simulations for an Arctic Tundra Basin. J. Hydrometeorol. 5, 735–744. doi:https://doi.org/10.1175/1525-7541(2004)005<0735:VATCOW>2.0.CO;2

Flügel, W.-A., 1995. Delineating hydrological response units by geographical information system analyses for regional hydrological modelling using PRMS/MMS in the drainage basin of the River Bröl, Germany. Hydrol. Process. 9, 423–436. doi:10.1002/hyp.3360090313

Fosser, G., Khodayar, S., Berg, P., 2015. Benefit of convection permitting climate model simulations in the representation of convective precipitation. Clim. Dyn. 45–60. doi:10.1007/s00382-014-2242-1

Fowler, H.J., Blenkinsop, S., Tebaldi, C., 2007. Linking climate change modelling to impacts studies: recent advances in downscaling techniques for hydrological modelling. Int. J. Climatol. 27, 1547–1578. doi:10.1002/joc

Fox, J.D., 1992. Incorporating freeze-thaw calculations into a water balance model. Water Resour. Res. 28, 2229–2244. doi:10.1029/92WR00983

Frauenfeld, O.W., Zhang, T., Mccreight, J.L., 2007. Northern Hemisphere freezing/thawing index variations over the twentieth century. Int. J. Climatol. 27, 47–63. doi:10.1002/joc.1372

Freeze, R.A., 1972. Role of subsurface flow in generating surface runoff: 1, Base flow contributions to channel flow. Water Resour. Res. 8, 609–623. doi:10.1029/WR009i002p00491

Gachon, P., Dibike, Y., 2007. Temperature change signals in northern Canada : convergence of statistical downscaling results using two driving GCMs. Int. J. Climatol. 27, 1623–1641. doi:10.1002/joc

Gamache, I., Payette, S., 2004. Height growth response of tree line black spruce to recent climate warming across the forest-tundra of eastern Canada. J. Ecol. 92, 835–845. doi:10.1111/j.0022-0477.2004.00913.x

Garnier, B.J., Ohmura, A., 1970. The evaluation of surface variations in solar radiation income. Sol. Energy 13, 21–34. doi:10.1016/0038-092X(70)90004-6

Goodison, B.E., Louie, P.Y., Yang, D., 1998. WMO Solid Precipitation Measurement Intercomparison. Report No. 67, World Meteorological Organization.

Gordon, C., Cooper, C., Senior, C.A., Banks, H., Gregory, J.M., Johns, T.C., Mitchell, J.F.B., Wood, R.A., 2000. The simulation of SST, sea ice extents and ocean heat transports in a version of the Hadley Centre coupled model without flux adjustments. Clim. Dyn. 16, 147–168. doi:10.1007/s003820050010

Granger, R.J.J., Gray, D.M.M., 1989. Evaporation From Natural Nonsaturated Surfaces. J. Hydrol. 111, 21–29. doi:10.1016/0022-1694(89)90249-7

Gray, D.M., Granger, R.J., Landine, P.G., 1986. Modelling snowmelt infiltration and runoff in a prairie environment, in: Proceeding of the Symposium: Cold Regions Hydrology. American water Resources Association, Maryland, pp. 427–438.

Gray, D.M., Landine, P.G., 1987. Albedo model for shallow prairie snow covers. Can. J. Earth Sci. 24, 1760–1768. doi:10.1139/e87-168

Gray, D.M., Landine, P.G., 1988. An energy-budget snowmelt model for the Canadian Prairies. Can. J. Earth Sci. 25, 1292–1303. doi:10.1139/e88-124

Gray, D.M., Landine, P.G., Granger, R.J., 1985. Simulating infiltration into frozen Prairie soils in streamflow models. Can. J. Earth Sci. 22, 464–472. doi:10.1139/e85-045

Gray, D.M., Toth, B., Zhao, L., Pomeroy, J.W., Granger, R.J., 2001. Estimating areal snowmelt infiltration into frozen soils. Hydrol. Process. 15, 3095–3111. doi:10.1002/hyp.320

Güntner, A., Olsson, J., Calver, A., Gannon, B., 2001. Cascade-based disaggregation of continuous rainfall time series: the influence of climate. Hydrol. Earth Syst. Sci. 5, 145–164. doi:10.5194/hess-5-145-2001

Gutmann, E., Barstad, I., Clark, M., Arnold, J., Rasmussen, R., 2016. The Intermediate Complexity Atmospheric Research Model (ICAR). J. Hydrometeorol. 17, 957–973. doi:10.1175/JHM-D-15-0155.1

Hamed, K.H., 2008. Trend detection in hydrologic data: The Mann-Kendall trend test under the scaling hypothesis. J. Hydrol. 349, 350–363. doi:10.1016/j.jhydrol.2007.11.009

Hamed, K.H., Rao, A.R., 1998. A modified Mann-Kendall trend test for autocorrelated data. J. Hydrol. 204, 182–196. doi:10.1016/S0022-1694(97)00125-X

Hansen, J., Ruedy, R., Sato, M., Lo, K., 2010. Global Surface Temperature Change. Rev. Geophys. 48, RG4004. doi:10.1029/2010RG000345

Hara, M., Yoshikane, T., Kawase, H., Kimura, F., 2008. Estimation of the Impact of Global Warming on Snow Depth in Japan by the Pseudo-Global-Warming Method. Hydrol. Res. Lett. 64, 61–64. doi:10.3178/HRL.2.61

Harder, P., Pomeroy, J.W., 2013. Estimating precipitation phase using a psychrometric energy balance method. Hydrol. Process. 27, 1901–1914. doi:10.1002/hyp

Harris, S.A., French, H.. M., Heginbottom, J.A., Johnston, G.H., 1988. Glossary of Permafrost and Related Ground-Ice Terms. Technical Memorandum No. 142, National Research Council of Canada, Ottawa, Ontario, Canda.

Hayashi, M., Goeller, N., Quinton, W.L., Wright, N., 2007. A simple heat-conduction method for simulating the frost-table depth in hydrological models. Hydrol. Process. 21, 2610–2622. doi:10.1002/hyp.6792

Hedstrom, N.R., Pomeroy, J.W., 1998. Measurements and modelling of snow interception in the boreal forest. Hydrol. Process. 12, 1611–1625. doi:https://doi.org/10.1002/(SICI)1099-1085(199808/09)12:10/11<1611::AID-HYP684>3.0.CO;2-4

Herndon, E.M., 2018. Permafrost slowly exhales methane. Nat. Clim. Chang. 8, 273–274. doi:10.1038/s41558-018-0129-6

Hess, A., Iyer, H., Malm, W., 2001. Linear trend analysis: a comparison of methods. Atmos. Environ. 35(30), 5211–5222. doi:10.1016/S1352-2310(01)00342-9

Hewitt, C.D., 2004. Ensembles-based predictions of climate changes and their impacts. Eos, Trans. Am. Geophys. Union 85, 566–566. doi:10.1029/2004EO520005

Hines, K.M., Bromwich, D.H., Bai, L.-S., Barlage, M., Slater, A.G., 2011. Development and Testing of Polar WRF. Part III: Arctic Land*. J. Clim. 24, 26–48. doi:10.1175/2010JCLI3460.1

Hinkley, D. V, 1970. Inference About the Change-Point in a Sequence of Random Variables. Biometrika 57, 1–17. doi:10.2307/2334932

Hinzman, L.D., Bettez, N.D., Bolton, W.R., Chapin, F.S., Dyurgerov, M.B., Fastie, C.L., Griffith, B., Hollister, R.D., Hope, A., Huntington, H.P., Jensen, A.M., Jia, G.J., Jorgenson, T., Kane, D.L., Klein, D.R., Kofinas, G., Lynch, A.H., Lloyd, A.H., McGuire, a. D., Nelson, F.E., Oechel, W.C., Osterkamp, T.E., Racine, C.H., Romanovsky, V.E., Stone, R.S., Stow, D. a., Sturm, M., Tweedie, C.E., Vourlitis, G.L., Walker, M.D., Walker, D. a., Webber, P.J., Welker, J.M., Winker, K.S., Yoshikawa, K., 2005. Evidence and Implications of Recent Climate Change in Northern Alaska and Other Arctic Regions. Clim. Change 72, 251–298. doi:10.1007/s10584-005-5352-2

Hinzman, L.D., Kane, D.L., 1991. Snow hydrology of a headwater Arctic basin: 2. Conceptual analysis and computer modeling. Water Resour. Res. 27, 1111–1121. doi:10.1029/91WR00261

Hinzman, L.D., Kane, D.L., 1992. Potential Response of an Arctic Watershed During a Period of Global Warming. J. Geophys. Res. 97, 2811–2820. doi:10.1029/91JD01752

Hock, R., 2003. Temperature index melt modelling in mountain areas. J. Hydrol. 282, 104–115. doi:10.1016/S0022-1694(03)00257-9

Hodson, D.L.R., Keeley, S.P.E., West, A., Ridley, J., Hawkins, E., Hewitt, H.T., 2013. Identifying uncertainties in Arctic climate change projections. Clim. Dyn. 40, 2849–2865. doi:10.1007/s00382-012-1512-z

Horton, R.E., 1933. The role of infiltration in the hydrological cycle. EOS, Trans. Am. Geophys. Union 14, 446–460.

Hurrell, J.W., 2001. CLIMATE: The North Atlantic Oscillation. Science (80-.). 291, 603–605. doi:10.1126/science.1058761

Janowicz, J.R., 2008. Apparent recent trends in hydrologic response in permafrost regions of northwest Canada. Hydrol. Res. 39, 267. doi:10.2166/nh.2008.103

Janowicz, J.R., 2010. Observed trends in the river ice regimes of northwest Canada. Hydrol. Res. 41, 462–470. doi:10.2166/nh.2010.145

Janowicz, J.R., Gray, D.M., Pomeroy, J.W., 1997. Snowmelt and Runoff in a Subarctic Mountain Basin, in: Hydro-Ecology Workshop on the Arctic Environmental Strategy. pp. 303–320.

Jarvis, N.J., 2007. A review of non-equilibrium water flow and solute transport in soil macropores: Principles, controlling factors and consequences for water quality. Eur. J. Soil Sci. 58, 523–546. doi:10.1111/j.1365-2389.2007.00915.x

Jarvis, P.G., 1976. The Interpretation of the Variations in Leaf Water Potential and Stomatal Conductance Found in Canopies in the Field. Philos. Trans. R. Soc. B Biol. Sci. 273, 593–610. doi:10.1098/rstb.1976.0035

Jones, H.G., Pomeroy, J.W., Davies, T.D., Tranter, M., Marsh, P., 1999. CO2 in Arctic snow cover: Landscape form, in-pack gas concentration gradients, and the implications for the estimation of gaseous fluxes. Hydrol. Process. 13, 2977–2989. doi:10.1002/(SICI)1099-1085(19991230)13:18<2977::AID-HYP12>3.0.CO;2-#

Jorgenson, M.T., Shur, Y.L., Pullman, E.R., 2006. Abrupt increase in permafrost degradation in Arctic Alaska. Geophys. Res. Lett. 33, 2–5. doi:10.1029/2005GL024960

Ju, J., Masek, J.G., 2016. The vegetation greenness trend in Canada and US Alaska from 1984-2012 Landsat data. Remote Sens. Environ. 176, 1–16. doi:10.1016/j.rse.2016.01.001

Juminikis, A.R., 1977. Thermal Geotechnics. Rutgers University Press, New Brunswick, New Jersey.

Kalnay, E., Kanamitsu, M., Kistler, R., Collins, W., Deaven, D., Gandin, L., Iredell, M., Saha, S., White, G., Woollen, J., Zhu, Y., Leetmaa, A., Reynolds, R., Chelliah, M., Ebisuzaki, W., Higgins, W., Janowiak, J., Mo, K.C., Ropelewski, C., Wang, J., Jenne, R., Joseph, D., 1996. The NCEP/NCAR 40-Year Reanalysis Project. Bull. Am. Meteorol. Soc. 77, 437–471. doi:10.1175/1520-0477(1996)077<0437:TNYRP>2.0.CO;2

Kane, D.L., 1980. Snowmelt infiltration into seasonally frozen soils. Cold Reg. Sci. Technol. 3, 153–161. doi:10.1016/0165-232X(80)90020-8

Kane, D.L., 1981. Physical mechanics of aufeis growth. Can. J. Civ. Eng. 8, 186–195. doi:10.1139/l81-026

Kane, D.L., Hinzman, L.D., Benson, C.S., Everett, K.R., 1989. Hydrology of Imnavait Creek, an arctic watershed. Ecography (Cop.). 12, 262–269. doi:10.1111/j.1600-0587.1989.tb00845.x

Kane, D.L., Hinzman, L.D., Benson, C.S., Liston, G.E., 1991. Snow hydrology of a headwater arctic basin, 1. Physical measurements and process studies. Water Resour. Res. 27, 1099–1109. doi:10.1029/91WR00262

Kane, D.L., Stein, J., 1983. Water movement into seasonally frozen soils. Water Resour. Res. 19, 1547–1557. doi:10.1029/WR019i006p01547

Kapur, A., Zhang, C., Zavala-Garay, J., Hendon, H.H., 2011. Role of stochastic forcing in ENSO in observations and a coupled GCM. Clim. Dyn. 38, 87–107. doi:10.1007/s00382-011-1070-9

Kattsov, V.M., Källén, E., Cattle, H.P., Christensen, J., Drange, H., Hanssen-bauer, I., Jóhannesen, T., Karol, I., Räisänen, J.J., Svensson, G., Vavulin, S., Chen, D., Polyakov, I., Rinke, A., 2005. Future Climate Change : Modeling and Scenarios for the Arctic, in: Symon, C., Arris, L., Heal, B. (Eds.), Arctic Climate Impact Assessment. Cambridge University Press, New

York, pp. 99–150.

Kavetski, D., Kuczera, G., Franks, S.W., 2003. Semidistributed hydrological modeling: A "saturation path" perspective on TOPMODEL and VIC. Water Resour. Res. 39, 1246. doi:10.1029/2003WR002122

Kawase, H., Yoshikane, T., Hara, M., Ailikun, B., Kimura, F., Yasunari, T., 2008. Downscaling of the Climatic Change in the Mei-yu Rainband in East Asia by a Pseudo Climate Simulation Method. Sci. Online Lett. Atmos. 4, 73–76. doi:https://doi.org/10.2151/sola.2008-019

Kawase, H., Yoshikane, T., Hara, M., Kimura, F., Yasunari, T., Ailikun, B., Ueda, H., Inoue, T., 2009. Intermodel variability of future changes in the Baiu rainband estimated by the pseudo global warming downscaling method. J. Geophys. Res. 114, 1–14. doi:10.1029/2009JD011803

Kendall, M.G., 1975. Rank Correlation Methods, 4th Editio. ed. Charles Griffin, London.

Kendon, E.J., Ban, N., Roberts, N.M., Fowler, H.J., Roberts, M.J., Chan, S.C., Evans, J.P., Fosser, G., Wilkinson, J.M., 2017. Do convection-permitting regional climate models improve projections of future precipitation change? Bull. Am. Meteorol. Soc. 98, 79–93. doi:10.1175/BAMS-D-15-0004.1

Kendon, E.J., Roberts, N.M., Fowler, H.J., Roberts, M.J., Chan, S.C., Senior, C.A., 2014. Heavier summer downpours with climate change revealed by weather forecast resolution model. Nat. Clim. Chang. 4, 570–576. doi:10.1038/nclimate2258

Killick, R., Haynes, K., Eckley, I., Fearnhead, P., Lee, J., 2016. Methods for Changepoint Detection. https://cran.r-project.org/web/packages/changepoint/changepoint.pdf.

Klene, A.E., Nelson, F.E., Shiklomanov, N.I., Hinkel, K.M., 2001. The N-Factor in Natural Landscapes: Variability of Air and Soil-Surface Temperatures, Kuparuk River Basin, Alaska, U.S.A. Arctic, Antarct. Alp. Res. 33, 140. doi:10.2307/1552214

Knoblauch, C., Beer, C., Liebner, S., Grigoriev, M.N., Pfeiffer, E.-M., 2018. Methane production as key to the greenhouse gas budget of thawing permafrost. Nat. Clim. Chang. 8, 309–312. doi:10.1038/s41558-018-0095-z

Kouwen, N., 1988. WATFLOOD: a Micro-Computer Based Flood Forecasting System Based on Real-Time Weather Radar. Can. Water Resour. J. 13, 62–77. doi:10.4296/cwrj1301062

Krogh, S.A., Pomeroy, J.W., 2018. Recent changes to the hydrological cycle of an Arctic basin at the tundra–taiga transition. Hydrol. Earth Syst. Sci. 22, 3993–4014. doi:10.5194/hess-22-3993-2018

Krogh, S.A., Pomeroy, J.W., Marsh, P., 2017. Diagnosis of the hydrology of a small Arctic basin at the tundra-taiga transition using a physically based hydrological model. J. Hydrol. 550, 685–703. doi:10.1016/j.jhydrol.2017.05.042

Krogh, S.A., Pomeroy, J.W., McPhee, J., 2015. Physically Based Mountain Hydrological Modeling Using Reanalysis Data in Patagonia. J. Hydrometeorol. 16, 172–193. doi:10.1175/JHM-D-13-0178.1

Kurylyk, B.L., Watanabe, K., 2013. The mathematical representation of freezing and thawing processes in variably-saturated, non-deformable soils. Adv. Water Resour. 60, 160–177. doi:10.1016/j.advwatres.2013.07.016

Lachenbruch, A.H., Marshall, B. V., 1986. Changing Climate: Geothermal Evidence from Permafrost in the Alaskan Arctic. Science (80-.). 234, 689–696. doi:10.1126/science.234.4777.689

Lantz, T.C., Marsh, P., Kokelj, S. V., 2013. Recent Shrub Proliferation in the Mackenzie Delta Uplands and Microclimatic Implications. Ecosystems 16, 47–59. doi:10.1007/s10021-012-9595-2

Laudon, H., Spence, C., Buttle, J., Carey, S.K., McDonnell, J.J., McNamara, J.P., Soulsby, C., Tetzlaff, D., 2017. Save northern high-latitude catchments. Nat. Geosci. 10, 324–325. doi:10.1038/ngeo2947

Lawrence, M.G., 2005. The relationship between relative humidity and the dewpoint temperature in moist air: A simple conversion and applications. Bull. Am. Meteorol. Soc. 86, 225–233. doi:10.1175/BAMS-86-2-225

Leroux, N.R., Pomeroy, J.W., 2017. Modelling capillary hysteresis effects on preferential flow through melting and cold layered snowpacks. Adv. Water Resour. 107, 250–264. doi:10.1016/j.advwatres.2017.06.024

Lewis, T., Lamoureux, S.F., 2010. Twenty-first century discharge and sediment yield predictions in a small high Arctic watershed. Glob. Planet. Change 71, 27–41. doi:10.1016/j.gloplacha.2009.12.006

Li, Y., Kurkute, S., Asong, E., Chen, L., 2016. The western Canada high resolution WRF simulation, in: Changing Cold Region Network (CCRN), Special Observation and Analysis Period (SOAP). Saskatoon, Saskatchewan.

Liljedahl, A.K., Boike, J., Daanen, R.P., Fedorov, A.N., Frost, G. V., Grosse, G., Hinzman, L.D., Iijma, Y., Jorgenson, J.C., Matveyeva, N., Necsoiu, M., Raynolds, M.K., Romanovsky, V.E., Schulla, J., Tape, K.D., Walker, D.A., Wilson, C.J., Yabuki, H., Zona, D., 2016. Pan-Arctic ice-wedge degradation in warming permafrost and its influence on tundra hydrology. Nat. Geosci. 9, 312–318. doi:10.1038/ngeo2674

Lindsay, R., Wensnahan, M., Schweiger, A., Zhang, J., 2014. Evaluation of Seven Different Atmospheric Reanalysis Products in the Arctic*. J. Clim. 27, 2588–2606. doi:10.1175/JCLI-D-13-00014.1

Ling, F., Zhang, T., 2004. A numerical model for surface energy balance and thermal regime of the active layer and permafrost containing unfrozen water. Cold Reg. Sci. Technol. 38, 1–15.

doi:10.1016/S0165-232X(03)00057-0

Liston, G.E., Hiemstra, C.A., 2011. The changing cryosphere: Pan-Arctic snow trends (1979-2009). J. Clim. 24, 5691–5712. doi:10.1175/JCLI-D-11-00081.1

Liston, G.E., Mcfadden, J.P., Sturm, M., Pielke, R. a., 2002. Modelled changes in arctic tundra snow, energy and moisture fluxes due to increased shrubs. Glob. Chang. Biol. 8, 17–32. doi:10.1046/j.1354-1013.2001.00416.x

Liston, G.E., Sturm, M., 1998. A snow-transport model for complex terrain. J. Glaciol. 44, 498–516. doi:10.3189/S0022143000002021

Liu, C., Ikeda, K., Rasmussen, R., Barlage, M., Newman, A.J., Prein, A.F., Chen, F., Chen, L., Clark, M., Dai, A., Dudhia, J., Eidhammer, T., Gochis, D., Gutmann, E., Kurkute, S., Li, Y., Thompson, G., Yates, D., 2017. Continental-scale convection-permitting modeling of the current and future climate of North America. Clim. Dyn. 49, 71–95. doi:10.1007/s00382-016-3327-9

López-Moreno, J.I., Boike, J., Sanchez-Lorenzo, A., Pomeroy, J.W., 2016. Impact of climate warming on snow processes in Ny-Ålesund, a polar maritime site at Svalbard. Glob. Planet. Change 146, 10–21. doi:10.1016/j.gloplacha.2016.09.006

López-Moreno, J.I., Pomeroy, J.W., Revuelto, J., Vicente-Serrano, S.M., 2012. Response of snow processes to climate change: spatial variability in a small basin in the Spanish Pyrenees. Hydrol. Process. 27, 2637–2650. doi:10.1002/hyp.9408

Ma, X., Yoshikane, T., Hara, M., Wakazuki, Y., Takahashi, H.G., Kimura, F., 2010. Hydrological response to future climate change in the Agano River basin, Japan. Hydrol. Res. Lett. 4, 25–29. doi:10.3178/hrl.4.25

Mackay, J.R., 1980. The origin of hummocks, western Arctic coast, Canada. Can. J. Earth Sci. 17, 996–1006. doi:10.1139/e80-100

Magnuson, J.J., Robertson, D.M., Benson, B.J., Wynne, R.H., Livingstone, D.M., Arai, T., Assel, R.A., Barry, R.G., Card, V., Kuusisto, E., Granin, N.G., Prowse, T.D., Steward, K.M., Vuglinski, V.S., 2000. Historical Trends in Lake and River Ice Cover in the Northern Hemisphere. Science (80-.). 289, 1743–1746. doi:10.1126/science.289.5485.1743

Male, D.H., Granger, R.J., 1981. Snow surface energy exchange. Water Resour. Res. 17, 609–627. doi:10.1029/WR017i003p00609

Manabe, S., Bryan, K., Spelman, M.J., 1975. A Global Ocean-Atmosphere Climate Model. Part I. The Atmospheric Circulation. J. Phys. Oceanogr. 5, 3–29. doi:10.1175/1520-0485(1975)005<0003:AGOACM>2.0.CO;2

Mann, H.B., 1945. Nonparametric Test against Trend. Econometrica 13, 245–259. doi:http://dx.doi.org/10.2307/1907187

Mantua, N.J., Hare, S.R., 2002. The Pacific Decadal Oscillation. J. Oceanogr. 58, 35-44, doi:10.1023/A:1015820616384

Maraun, D., Wetterhall, F., Ireson, A.M., 2010. Precipitation downscaling under climate change: recent developments to bridge the gap between dynamical models and the end user. Rev. … 48, 1–34. doi:10.1029/2009RG000314.1.INTRODUCTION

Marks, D., Kimball, J., Tingey, D., Link, T., 1998. The sensitivity of snowmelt processes to climate conditions and forest cover during rain-on-snow: a case study of the 1996 Pacific Northwest flood. Hydrol. Process. 12, 1569–1587. doi:10.1002/(SICI)1099-1085(199808/09)12:10/11<1569::AID-HYP682>3.0.CO;2-L

Marks, D., Link, T., Winstral, A., Garen, D., 2001. Simulating snowmelt processes during rain-on-snow over a semi-arid mountain basin. Ann. Glaciol. 32, 195–202. doi:10.3189/172756401781819751

Marsh, P., Bartlett, P., MacKay, M., Pohl, S., Lantz, T., 2010. Snowmelt energetics at a shrub tundra site in the western Canadian Arctic. Hydrol. Process. 24, 3603–3620. doi:10.1002/hyp.7786

Marsh, P., Onclin, C., Neumann, N., 2002. Water and energy fluxes in the lower Mackenzie valley, 1994/95. Atmosphere-Ocean 40, 245–256. doi:10.3137/ao.400211

Marsh, P., Pomeroy, J.W., 1996. Meltwater fluxes at an Arctic forest-tundra site. Hydrol. Process. 10, 1383–1400. doi:10.1002/(SICI)1099-1085(199610)10:10<1383::AID-HYP468>3.0.CO;2-W

Marsh, P., Woo, M.-K., 1984a. Wetting front advance and freezing of meltwater within a snow cover: 1. Observations in the Canadian Arctic. Water Resour. Res. 20, 1853–1864. doi:10.1029/WR020i012p01865

Marsh, P., Woo, M.-K., 1984b. Wetting front advance and freezing of meltwater within a snow cover: 2. A simulation model. Water Resour. Res. 20, 1865–1874. doi:10.1029/WR020i012p01865

Marti, O., Braconnot, P., Dufresne, J.-L., Bellier, J., Benshila, R., Bony, S., Brockmann, P., Cadule, P., Caubel, a., Codron, F., Noblet, N., Denvil, S., Fairhead, L., Fichefet, T., Foujols, M. -a., Friedlingstein, P., Goosse, H., Grandpeix, J.-Y., Guilyardi, E., Hourdin, F., Idelkadi, a., Kageyama, M., Krinner, G., Lévy, C., Madec, G., Mignot, J., Musat, I., Swingedouw, D., Talandier, C., 2009. Key features of the IPSL ocean atmosphere model and its sensitivity to atmospheric resolution. Clim. Dyn. 34, 1–26. doi:10.1007/s00382-009-0640-6

Martin, A.C., Jeffers, E.S., Petrokofsky, G., Myers-Smith, I.H., Macias-fauria, M., 2017. Shrub growth and expansion in the Arctic tundra: an assessment of controlling factors using an evidence-based approach. Environ. Res. Lett. 12, 085007. doi:10.1088/1748-9326/aa7989

Mason, P.J., Sykes, R.I., 1979. Flow over an isolated hill of moderate slope. Q. J. R. Meteorol. Soc. 105, 383–395. doi:10.1002/qj.49710544405

Masui, T., Matsumoto, K., Hijioka, Y., Kinoshita, T., Nozawa, T., Ishiwatari, S., Kato, E., Shukla, P.R., Yamagata, Y., Kainuma, M., 2011. An emission pathway for stabilization at 6 Wm-2radiative forcing. Clim. Change 109, 59–76. doi:10.1007/s10584-011-0150-5

Maurer, E.P., O'Donnell, G.M., Lettenmaier, D.P., Roads, J.O., 2001. Evaluation of the land surface water budget in NCEP/NCAR and NCEP/DOE reanalyses using an off-line hydrologic model. J. Geophys. Res. Atmos. 106, 17841–17862. doi:10.1029/2000JD900828

McClelland, J.W., Déry, S.J., Peterson, B.J., Holmes, R.M., Wood, E.F., 2006. A pan-arctic evaluation of changes in river discharge during the latter half of the 20th century. Geophys. Res. Lett. 33, 2–5. doi:10.1029/2006GL025753

Mearns, L., Gutowski, W., Richard, J., Leung, R., McGinnis, S., Nunes, A., Quan, Y., 2009. A regional climate change assessment program for North America. Eos Trans. AGU 90, 2008–2009. doi:10.1029/2009EO360002.

Mekis, É., Vincent, L.A., 2011. An Overview of the Second Generation Adjusted Daily Precipitation Dataset for Trend Analysis in Canada. Atmosphere-Ocean 49, 163–177. doi:10.1080/07055900.2011.583910

Ménard, C.B., Essery, R., Pomeroy, J., Marsh, P., Clark, D.B., 2012. A shrub bending model to calculate the albedo of shrub-tundra. Hydrol. Process. 28, 341–351. doi:10.1002/hyp.9582

Ménard, C.B., Essery, R., Pomeroy, J.W., 2014. Modelled sensitivity of the snow regime to topography, shrub fraction and shrub height. Hydrol. Earth Syst. Sci. 18, 2375–2392. doi:10.5194/hess-18-2375-2014

Mendoza, P.A., Clark, M.P., Mizukami, N., Gutmann, E.D., Arnold, J.R., Brekke, L.D., Rajagopalan, B., 2016. How do hydrologic modeling decisions affect the portrayal of climate change impacts? Hydrol. Process. 30, 1071–1095. doi:10.1002/hyp.10684

Mendoza, P.A., Clark, M.P., Mizukami, N., Newman, A.J., Barlage, M., Gutmann, E.D., Rasmussen, R.M., Rajagopalan, B., Brekke, L.D., Arnold, J.R., 2015. Effects of Hydrologic Model Choice and Calibration on the Portrayal of Climate Change Impacts. J. Hydrometeorol. 16, 762–780. doi:10.1175/JHM-D-14-0104.1

Mesinger, F., DiMego, G., Kalnay, E., Mitchell, K., Shafran, P.C., Ebisuzaki, W., Jović, D., Woollen, J., Rogers, E., Berbery, E.H., Ek, M.B., Fan, Y., Grumbine, R., Higgins, W., Li, H., Lin, Y., Manikin, G., Parrish, D., Shi, W., 2006. North American Regional Reanalysis. Bull. Am. Meteorol. Soc. 87, 343–360. doi:10.1175/BAMS-87-3-343

Michalakes, J., Duchia, J., Gill, D., Henderson, T., Klemp, J., Skamarock, W., Wang, W., 2005. The Weather Research and Forecast model: software architecture and performance, in: Use of High Performance Computing in Meteorology. WORLD SCIENTIFIC, pp. 156–168. doi:10.1142/9789812701831_0012

Milewska, E., Hogg, W.D., 2001. Spatial representativeness of a long-term climate network in Canada. Atmosphere-Ocean 39, 145–161. doi:10.1080/07055900.2001.9649671

Monin, A.S., Obukhov, A.M., 1954. Basic laws of turbulent mixing in the surface layer of the atmosphere, in: Proceesings of Geophysiclas Institute, National Academy of Science, SSSR. pp. 163–187.

Monteith, J.L., 1981. Evaporation and surface temperature. Q. J. R. Meteorol. Soc. 107, 1–27. doi:10.1002/qj.49710745102

Music, B., Caya, D., 2007. Evaluation of the Hydrological Cycle over the Mississippi River Basin as Simulated by the Canadian Regional Climate Model (CRCM). J. Hydrometeorol. 8, 969–988. doi:10.1175/JHM627.1

Musselman, K.N., Clark, M.P., Liu, C., Ikeda, K., Rasmussen, R., 2017. Slower snowmelt in a warmer world. Nat. Clim. Chang. 7, 214–219. doi:10.1038/nclimate3225

Myers-Smith, I.H., Forbes, B.C., Wilmking, M., Hallinger, M., Lantz, T., Blok, D., Tape, K.D., Macias-Fauria, M., Sass-Klaassen, U., Lévesque, E., Boudreau, S., Ropars, P., Hermanutz, L., Trant, A., Collier, L.S., Weijers, S., Rozema, J., Rayback, S.A., Schmidt, N.M., Schaepman-Strub, G., Wipf, S., Rixen, C., Ménard, C.B., Venn, S., Goetz, S., Andreu-Hayles, L., Elmendorf, S., Ravolainen, V., Welker, J., Grogan, P., Epstein, H.E., Hik, D.S., 2011. Shrub expansion in tundra ecosystems: dynamics, impacts and research priorities. Environ. Res. Lett. 6, 045509. doi:10.1088/1748-9326/6/4/045509

Myers-Smith, I.H., Harden, J.W., Wilmking, M., Fuller, C.C., McGuire, A.D., Chapin, F.S., 2008. Wetland succession in a permafrost collapse: interactions between fire and thermokarst. Biogeosciences 5, 1273–1286. doi:10.5194/bg-5-1273-2008

Myers-Smith, I.H., Hik, D.S., 2018. Climate warming as a driver of tundra shrubline advance. J. Ecol. 106, 547–560. doi:10.1111/1365-2745.12817

New, M., Todd, M., Hulme, M., Jones, P., 2001. Precipitation measurements and trends in the twentieth century. Int. J. Climatol. 21, 1889–1922. doi:10.1002/joc.680

Niu, G.Y., Yang, Z.L., Mitchell, K.E., Chen, F., Ek, M.B., Barlage, M., Kumar, A., Manning, K., Niyogi, D., Rosero, E., Tewari, M., Xia, Y., 2011. The community Noah land surface model with multiparameterization options (Noah - MP): 1 . Model description and evaluation with local - scale measurements. J. Geophys. Res. 116, 1–19. doi:10.1029/2010JD015139

Oelke, C., Zhang, T., Serreze, M.C., 2004. Modeling evidence for recent warming of the Arctic soil thermal regime. Geophys. Res. Lett. 31, 4–7. doi:10.1029/2003GL019300

Ohmura, A., 2009. Observed decadal variations in surface solar radiation and their causes. J. Geophys. Res. 114, D00D05. doi:10.1029/2008JD011290

Osterkamp, T.E., Romanovsky, V.E., 1999. Evidence for warming and thawing of discontinuous permafrost in Alaska. Permafr. Periglac. Process. 10, 17–37. doi:10.1002/(SICI)1099-1530(199901/03)10:1<17::AID-PPP303>3.0.CO;2-4

Overeem, I., Syvitski, J.P.M., 2010. Shifting discharge peaks in arctic rivers, 1977–2007. Geogr.

Ann. Ser. A, Phys. Geogr. 92, 285–296. doi:10.1111/j.1468-0459.2010.00395.x

Overland, J.E., Wang, M., Walsh, J.E., Stroeve, J.C., 2013. Future Arctic climate changes : Adaptation and mitigation time scales. Earth's Futur. 2, 68–74. doi:10.1002/2013EF000162.Received

Pan, X., Yang, D., Li, Y., Barr, A., Helgason, W., Hayashi, M., Marsh, P., Pomeroy, J., Janowicz, R.J., 2016. Bias corrections of precipitation measurements across experimental sites in different ecoclimatic regions of western Canada. Cryosphere 10, 2347–2360. doi:10.5194/tc-10-2347-2016

Parviainen, J., Pomeroy, J.W., 2000. Multiple-scale modelling of forest snow sublimation: initial findings. Hydrol. Process. 14, 2669–2681. doi:10.1002/1099-1085(20001030)14:15<2669::AID-HYP85>3.0.CO;2-Q

Payette, S., 2004. Accelerated thawing of subarctic peatland permafrost over the last 50 years. Geophys. Res. Lett. 31, L18208. doi:10.1029/2004GL020358

Payette, S., Filion, L., 1985. White spruce expansion at the tree line and recent climatic change. Can. J. For. Res. 15, 241–251. doi:10.1139/x85-042

Pearson, R.G., Phillips, S.J., Loranty, M.M., Beck, P.S.A., Damoulas, T., Knight, S.J., Goetz, S.J., 2013. Shifts in Arctic vegetation and associated feedbacks under climate change. Nat. Clim. Chang. 3, 673–677. doi:10.1038/nclimate1858

Peterson, B.J., Holmes, R.M., McClelland, J.W., Vorosmarty, C.J., Lammers, R., Shiklomanov, A.I., Shiklomanov, I.A., Rahmstorf, S., 2002. Increasing River Discharge to the Arctic Ocean. Science (80-.). 298, 2171–2173. doi:10.1126/science.1077445

Philip, J.R., 1957. The theory of infiltration: 1. The infiltration equation and its solution. Soil Sci. 84, 257-264, doi:10.1097/00010694-195709000-00010

Pieri, A.B., von Hardenberg, J., Parodi, A., Provenzale, A., 2015. Sensitivity of Precipitation Statistics to Resolution, Microphysics, and Convective Parameterization: A Case Study with the High-Resolution WRF Climate Model over Europe. J. Hydrometeorol. 16, 1857–1872. doi:10.1175/JHM-D-14-0221.1

Pohl, S., Marsh, P., Bonsal, B.R., 2007. Modeling the impact of climate change on runoff and annual water balance of an arctic headwater basin. Arctic 60, 173–186. doi:10.14430/arctic242

Pomeroy, J.W., Bernhardt, M., Marks, D., 2015a. Research network to track alpine water. Nature 521, 32–32. doi:10.1038/521032c

Pomeroy, J.W., Bewley, D.S., Essery, R.L.H., Hedstrom, N.R., Link, T., Granger, R.J., Sicart, J.E., Ellis, C.R., Janowicz, J.R., 2006. Shrub tundra snowmelt. Hydrol. Process. 20, 923–941. doi:10.1002/hyp.6124

Pomeroy, J.W., Brun, E., 2001. Physical Properties of Snow, Snow Ecology: an Interdisciplinary Examination of Snow-covered Ecosystems. Cambridge University Press.

Pomeroy, J.W., Fang, X., Marks, D.G., 2016. The cold rain-on-snow event of June 2013 in the Canadian Rockies - characteristics and diagnosis. Hydrol. Process. 30, 2899–2914. doi:10.1002/hyp.10905

Pomeroy, J.W., Fang, X., Rasouli, K., 2015b. Sensitivity of snow processes to warming in the Canadian Rockies. 72nd East. Snow Conf. Sherbrooke, Quebec, Canada 22–33.

Pomeroy, J.W., Fang, X., Shook, K., Whitfield, P.H., 2013a. Predicting in Ungauged Basins using Physical Principles Obtained using The Deductuve, Inductive, and Abductive Reasoning Approach, in: Putting Prediction in Ungauged Basins into Practice. Canadian Water Resources Association (CWRA) and the International Association of Hydrological Sciences (IAHS), pp. 41–62.

Pomeroy, J.W., Goodison, B.E., 1997. Winter and Snow, in: Bailey, W.G., Oke, T.R., Rouse, W.R. (Eds.), The Surface Climates of Canada. McGill-Queen's University Press, pp. 68–100.

Pomeroy, J.W., Gray, D.M., 1990. Saltation of snow. Water Resour. Res. 26, 1583–1594. doi:10.1029/WR026i007p01583

Pomeroy, J.W., Gray, D.M., Brown, T., Hedstrom, N.R., Quinton, W.L., Granger, R.J., Carey, S.K., 2007. The cold regions hydrological model: a platform for basing process representation and model structure on physical evidence. Hydrol. Process. 21, 2650–2667. doi:10.1002/hyp.6787

Pomeroy, J.W., Gray, D.M., Landine, P.G., 1993. The Prairie Blowing Snow Model: characteristics, validation, operation. J. Hydrol. 144, 165–192. doi:10.1016/0022-1694(93)90171-5

Pomeroy, J.W., Gray, D.M., Marsh, P., 2008. Studies on snow redistribution by wind and forest, snow-covered area depletion, and frozen soil infiltration in northern and western Canada, in: Woo, M. (Ed.), Cold Region Atmospheric and Hydrologic Studies, the Mackenzie GEWEX Experience, Vol. 2: Hydrologic Processes. Springer, pp. 81–96.

Pomeroy, J.W., Li, L., 2000. Prairie and Arctic areal snow cover mass balance using a blowing snow model. J. Geophys. Res. Atmos. 105, 26619–26634. doi:10.1029/2000JD900149

Pomeroy, J.W., Male, D.H., 1992. Steady-state suspension of snow. J. Hydrol. 136, 275–301. doi:10.1016/0022-1694(92)90015-N

Pomeroy, J.W., Marsh, P., 1997. The application of remote sensing and a blowing snow model to determine snow water equivalent over northern basins, in: Kite, G.W., Pietroniro, A., Pultz, T.J. (Eds.), Applications of Remote Sensing in Hydrology: NHRI Symposium No. 17. Saskatoon, SK, pp. 253–270.

Pomeroy, J.W., Marsh, P., Gray, D.M., 1997. Application of a distributed blowing snow model to

the Arctic. Hydrol. Process. 11, 1451–1464. doi:10.1002/(SICI)1099-1085(199709)11:11<1451::AID-HYP449>3.0.CO;2-Q

Pomeroy, J.W., Parviainen, J., Hedstrom, N., Gray, D.M., 1998. Coupled modelling of forest snow interception and sublimation. Hydrol. Process. 12, 2317–2337. doi:10.1002/(SICI)1099-1085(199812)12:15<2317::AID-HYP799>3.0.CO;2-X

Pomeroy, J.W., Schmidt, R.A., 1993. The Use of Fractal Geometry in Modelling Intercepted Snow Accumulation and Sublimation, in: 50th Eastern Snow Conference 61st Western Snow Conference.

Pomeroy, J.W., Spence, C., Whitfield, P.H., Spence, C., 2013b. Putting Prediction in Ungauged Basins into Practice. Canadian Water Resources Association.

Pomeroy, J.W., Toth, B., Granger, R.J., Hedstrom, N.R., Essery, R.L.H., 2003. Variation in Surface Energetics during Snowmelt in a Subarctic Mountain Catchment. J. Hydrometeorol. 4, 702–719. doi:10.1175/1525-7541(2003)004<0702:VISEDS>2.0.CO;2

Prein, A.F., Langhans, W., Fosser, G., Ferrone, A., Ban, N., Keller, M., Tölle, M., Gutjahr, O., Feser, F., Brisson, E., 2015. A review on regional convection-permitting climate modeling: Demonstrations, prospects, and challenges. Rev. Geophys. 53, 323–361. doi:10.1002/2014RG000475

Priestley, C.H.B., Taylor, R.J., 1972. On the Assessment of Surface Heat Flux and Evaporation Using Large-Scale Parameters. Mon. Weather Rev. 100, 81–92. doi:10.1175/1520-0493(1972)100<0081:OTAOSH>2.3.CO;2

Prowse, T., Alfredsen, K., Beltaos, S., Bonsal, B., Duguay, C., Korhola, A., McNamara, J., Pienitz, R., Vincent, W.F., Vuglinsky, V., Weyhenmeyer, G.A., 2011. Past and future changes in Arctic lake and river ice. Ambio 40, 53–62. doi:10.1007/s13280-011-0216-7

Prueger, J.H., Kustas, W.P., 2005. Aerodynamic Methods for Estimating Turbulent Fluxes, in: Micrometeorology in Agricultural Systems. USDA-ARS / UNL Faculty, pp. 407–436.

Przybylak, R., Vízi, Z., Wyszyński, P., 2010. Air temperature changes in the Arctic from 1801 to 1920. Int. J. Climatol. 30, 791–812. doi:10.1002/joc.1918

Quinton, W.L., Carey, S.K., 2008. Towards an energy-based runoff generation theory for tundra landscapes. Hydrol. Process. 22, 4649–4653. doi:10.1002/hyp.7164

Quinton, W.L., Carey, S.K., Goeller, N.T., 2004. Snowmelt runoff from northern alpine tundra hillslopes: major processes and methods of simulation. Hydrol. Earth Syst. Sci. 8, 877–890. doi:10.5194/hess-8-877-2004

Quinton, W.L., Gray, D.M., 2001. Estimating subsurface drainage from organic- covered hillslopes underlain by permafrost : toward a combined heat and mass flux model, in: Sixth IAHS Scientific Assmble. Maastricht, Netherlands.

Quinton, W.L., Gray, D.M., 2003. Subsurface drainage from organic soils in permafrost terrain : the major factors to be represented in a runoff model, in: Proceedings of the Eighth International Conference on Permafrost. Davos, Switzerland, p. 6.

Quinton, W.L., Gray, D.M., Marsh, P., 2000. Subsurface drainage from hummock-covered hillslopes in the Arctic tundra. J. Hydrol. 237, 113–125. doi:10.1016/S0022-1694(00)00304-8

Quinton, W.L., Marsh, P., 1999. A conceptual framework for runoff generation in a permafrost environment. Hydrol. Process. 13, 2563–2581. doi:10.1002/(SICI)1099-1085(199911)13:16<2563::AID-HYP942>3.0.CO;2-D

Raddatz, R.L., Papakyriakou, T.N., Swystun, K. a., Tenuta, M., 2009. Evapotranspiration from a wetland tundra sedge fen: Surface resistance of peat for land-surface schemes. Agric. For. Meteorol. 149, 851–861. doi:10.1016/j.agrformet.2008.11.003

Rapaić, M., Brown, R., Markovic, M., Chaumont, D., 2015. An Evaluation of Temperature and Precipitation Surface-Based and Reanalysis Datasets for the Canadian Arctic, 1950–2010. Atmosphere-Ocean 53, 283–303. doi:10.1080/07055900.2015.1045825

Rasmussen, R., Ikeda, K., Liu, C., Gochis, D., Clark, M., Dai, A., Gutmann, E., Dudhia, J., Chen, F., Barlage, M., Yates, D., Zhang, G., 2014. Climate Change Impacts on the Water Balance of the Colorado Headwaters: High-Resolution Regional Climate Model Simulations. J. Hydrometeorol. 15, 1091–1116. doi:10.1175/JHM-D-13-0118.1

Rasmussen, R., Liu, C., Ikeda, K., Gochis, D., Yates, D., Chen, F., Tewari, M., Barlage, M., Dudhia, J., Yu, W., Miller, K., Arsenault, K., Grubišić, V., Thompson, G., Gutmann, E., 2011. High-resolution coupled climate runoff simulations of seasonal snowfall over Colorado: A process study of current and warmer climate. J. Clim. 24, 3015–3048. doi:10.1175/2010JCLI3985.1

Rasmusson, E.M., Carpenter, T.H., 1982. Variations in Tropical Sea Surface Temperature and Surface Wind Fields Associated with the Southern Oscillation/El Niño. Mon. Weather Rev. doi:10.1175/1520-0493(1982)110<0354:VITSST>2.0.CO;2

Rasouli, K., Pomeroy, J.W., Janowicz, J.R., Carey, S.K., Williams, T.J., 2014. Hydrological sensitivity of a northern mountain basin to climate change. Hydrol. Process. 28, 4191–5208. doi:10.1002/hyp.10244

Rasouli, K., Pomeroy, J.W., Marks, D.G., 2015. Snowpack sensitivity to perturbed climate in a cool mid-latitude mountain catchment. Hydrol. Process. 29, 3925–3940. doi:10.1002/hyp.10587

Razavi, S., Gupta, H. V., 2016a. A new framework for comprehensive, robust, and efficient global sensitivity analysis: 1. Theory. Water Resour. Res. 52, 423–439. doi:10.1002/2015WR017558

Razavi, S., Gupta, H. V., 2016b. A new framework for comprehensive, robust, and efficient global

sensitivity analysis: 2. Application. Water Resour. Res. 52, 440–455. doi:10.1002/2015WR017559

Riahi, K., Rao, S., Krey, V., Cho, C., Chirkov, V., Fischer, G., Kindermann, G., Nakicenovic, N., Rafaj, P., 2011. RCP 8.5-A scenario of comparatively high greenhouse gas emissions. Clim. Change 109, 33–57. doi:10.1007/s10584-011-0149-y

Roeckner, E., Bäuml, G., Bonaventura, L., Brokopf, R., Esch, M., Giorgetta, M., Hagemann, S., Kirchner, I., Kornblueh, L., Manzini, E., Rhodin, A., Schlese, U., Schulzweida, U., Tompkins, A., 2003. ECHAM5: Model description. Max Planck Intitute for Meteorology, Hamburg.

Romano, N., Brunone, B., Santini, A., 1998. Numerical analysis of one-dimensional unsaturated flow in layered soils. Adv. Water Resour. 21, 315–324. doi:10.1016/S0309-1708(96)00059-0

Romero-Lankao, P., Smith, J.B., Davidson, D.J., Diffenbaugh, N.S., Kinney, P.L., Kirshen, P., Kovacs, P., Villers-Ruiz, L., 2014. North America, in: Barros, V.R., Field, C.B., Dokken, D.J., Mastrandrea, M.D., Mach, K.J., Bilir, T.E., Chatterjee, M., Ebi, K.L., Estrada, Y.O., Genova, R.C., Girma, B., Kissel, E.S., Levy, A.N., MacCracken, S., Mastrandrea, P.R., White, L.L. (Eds.), Climate Change 2014: Impacts, Adaptation, and Vulnerability. Part B: Regional Aspects. Contribution of Working Group II to the Fifth Assessment Report of the Intergovernmental Panel of Climate Change. Cambridge University Press, Cambridge, United Kingdom and New York, NY, USA, pp. 1439–1498.

Rood, S.B., Kaluthota, S., Philipsen, L.J., Rood, N.J., Zanewich, K.P., 2017. Increasing discharge from the Mackenzie River system to the Arctic Ocean. Hydrol. Process. 31, 150–160. doi:10.1002/hyp.10986

Rouse, W.R., 1984. Microclimate at Arctic Tree Line 3. The Effects of Regional Advection on the Surface Energy Balance of Upland Tundra. Water Resour. Res. 20, 74–78. doi:10.1029/WR020i001p00074

Rouse, W.R., Eaton, A.K., Petrone, R.M., Boudreau, L.D., Marsh, P., Griffis, T.J., 2003. Seasonality in the Surface Energy Balance of Tundra in the Lower Mackenzie River Basin. J. Hydrometeorol. 4, 673–679. doi:10.1175/1525-7541(2003)004<0673:SITSEB>2.0.CO;2

Rummukainen, M., 2010. State-of-the-art with regional climate models. Wiley Interdiscip. Rev. Chang. 1, 82–96. doi:10.1002/wcc.008

Saha, S., Moorthi, S., Pan, H.-L., Wu, X., Wang, J.J., Nadiga, S., Tripp, P., Kistler, R., Woollen, J., Behringer, D., Liu, H., Stokes, D., Grumbine, R., Gayno, G., Hou, Y.-T., Chuang, H.-Y., Juang, H.-M.H., Sela, J., Iredell, M., Treadon, R., Kleist, D., Van Delst, P., Keyser, D., Derber, J., Ek, M., Meng, J., Wei, H., Yang, R., Lord, S., Van Den Dool, H., Kumar, A., Wang, W., Long, C., Chelliah, M., Xue, Y., Huang, B., Schemm, J.-K., Ebisuzaki, W., Lin, R., Xie, P., Chen, M., Zhou, S., Higgins, W., Zou, C.-Z., Liu, Q., Chen, Y., Han, Y., Cucurull, L., Reynolds, R.W., Rutledge, G., Goldberg, M., 2010. The NCEP Climate Forecast System Reanalysis. Bull. Am. Meteorol. Soc. 91, 1015–1057. doi:10.1175/2010BAMS3001.1

Samani, N., Kompani-Zare, M., Barry, D.A., 2004. MODFLOW equipped with a new method for the accurate simulation of axisymmetric flow. Adv. Water Resour. 27, 31–45. doi:10.1016/j.advwatres.2003.09.005

Saunders, R., Matricardi, M., Brunel, P., 1999. An improved fast radiative transfer model for assimilation of satellite radiance observations. Q. J. R. Meteorol. Soc. 125, 1407–1425. doi:10.1002/qj.1999.49712555615

Schär, C., Frei, C., Lüthi, D., Davies, H.C., 1996. Surrogate climate-change scenarios for regional climate models. Geophys. Res. Lett. 23, 669–672. doi:10.1029/96GL00265

Schmidt, R.A., 1981. Estimates of threshold windspeed from particle sizes in blowing snow. Cold Reg. Sci. Technol. 4, 187–193. doi:10.1016/0165-232X(81)90003-3

Schmidt, R.A., 1982. Properties of blowing snow. Rev. Geophys. 20, 39–44. doi:10.1029/RG020i001p00039

Schmidt, R.A., 1991. Sublimation of snow intercepted by an artificial conifer. Agric. For. Meteorol. 54, 1–27. doi:10.1016/0168-1923(91)90038-R

Schmidt, R.A., Gluns, D.R., 1991. Snowfall interception on branches of three conifer species. Can. J. For. Res. 21, 1262–1269. doi:10.1139/x91-176

Schramm, I., Boike, J., Bolton, W.R., Hinzman, L.D., 2007. Application of TopoFlow, a spatially distributed hydrological model, to the Imnavait Creek watershed, Alaska. J. Geophys. Res. 112, G04S46. doi:10.1029/2006JG000326

Scinocca, J.F., McFarlane, N. a., Lazare, M., Li, J., Plummer, D., 2008. Technical Note: The CCCma third generation AGCM and its extension into the middle atmosphere. Atmos. Chem. Phys. 8, 7055–7074. doi:10.5194/acp-8-7055-2008

Semenova, O., Lebedeva, L., Vinogradov, Y., 2013. Simulation of subsurface heat and water dynamics, and runoff generation in mountainous permafrost conditions, in the Upper Kolyma River basin, Russia. Hydrogeol. J. 21, 107–119. doi:10.1007/s10040-012-0936-1

Sen, P.K., 1968. Estimates of the regression coefficient based on Kendall's Tau. J. Am. Stat. Assoc. 63, 1379–1389. doi:10.2307/2285891

Serreze, M.C., Bromwich, D.H., Clark, M.P., Etringer, A.J., Zhang, T., Lammers, R., 2002. Large-scale hydro-climatology of the terrestrial Arctic drainage system. J. Geophys. Res. 108, 8160. doi:10.1029/2001JD000919

Serreze, M.C., Clark, M.P., Bromwich, D.H., 2003. Monitoring Precipitation over the Arctic Terrestrial Drainage System: Data Requirements, Shortcomings, and Applications of Atmospheric Reanalysis*. J. Hydrometeorol. 4, 387–407. doi:10.1175/1525-7541(2003)4<387:MPOTAT>2.0.CO;2

Serreze, M.C., Hurst, C.M., 2000. Representation of Mean Arctic Precipitation from NCEP–

NCAR and ERA Reanalyses. J. Clim. 13, 182–201. doi:10.1175/1520-0442(2000)013<0182:ROMAPF>2.0.CO;2

Serreze, M.C., Key, J.R., Box, J.E., Maslanik, J.A., Steffen, K., 1998. A new monthly climatology of global radiation for the arctic and comparisons with NCEP-NCAR reanalysis and ISCCP-C2 fields. J. Clim. 11, 121–136. doi:10.1175/1520-0442(1998)011<0121:ANMCOG>2.0.CO;2

Sicart, J.E., Pomeroy, J.W., Essery, R.L.H., Bewley, D., 2006. Incoming longwave radiation to melting snow: observations, sensitivity and estimation in northern environments. Hydrol. Process. 20, 3697–3708. doi:10.1002/hyp

Singh, P., Spitzbart, G., Hübl, H., Weinmeister, H.., 1997. Hydrological response of snowpack under rain-on-snow events: a field study. J. Hydrol. 202, 1–20. doi:10.1016/S0022-1694(97)00004-8

Sivapalan, M., 2003. Prediction in ungauged basins: a grand challenge for theoretical hydrology. Hydrol. Process. 17, 3163–3170. doi:10.1002/hyp.5155

Skamarock, W.C., Klemp, J.B., Dudhi, J., Gill, D.O., Barker, D.M., Duda, M.G., Huang, X.-Y., Wang, W., Powers, J.G., 2008. A Description of the Advanced Research WRF Version 3, NCAR Technical Report. Boulder, Colorado, USA. doi:10.5065/D6DZ069T

Sloan, C.E., van Everdingen, R.O., 1988. Region 28, Permafrost region, in: The Geology of North America. The Geological Society of America, Colorado.

Smith, C., 2008. Correcting the wind bias in snowfall measurements made with a Geonor T-200B precipitation gauge and alter wind shield, in: CMOS Bulletin SCMO. pp. 162–167.

Smith, C.A.S., Meikle, J.C., Roots, C.F., 2004. Ecoregions of the Yukon Territory: Biophysical properties of Yukon landscape. Summerland, British Columbia.

Sturm, M., Douglas, T., Racine, C., Liston, G.E., 2005. Changing snow and shrub conditions affect albedo with global implications. J. Geophys. Res. 110, 1–13. doi:10.1029/2005JG000013

Sturm, M., Holmgren, J., McFadden, J.P., Liston, G.E., Chapin, F.S., Racine, C.H., 2001a. Snow–Shrub Interactions in Arctic Tundra: A Hypothesis with Climatic Implications. J. Clim. 14, 336–344. doi:10.1175/1520-0442(2001)014<0336:SSIIAT>2.0.CO;2

Sturm, M., Racine, C., Tape, K., 2001b. Increasing shrub abundance in the Arctic. Nature 411, 546–547. doi:10.1038/35079180

Suarez, F., Binkley, D., Kaye, M.W., Stottlemyer, R., 1999. Expansion of forest stands into tundra in the Noatak National Preserve, northwest Alaska. Écoscience 6, 465–470. doi:10.1080/11956860.1999.11682538

Sulla-Menashe, D., Woodcock, C.E., Friedl, M.A., 2018. Canadian boreal forest greening and browning trends: an analysis of biogeographic patterns and the relative roles of disturbance

versus climate drivers. Environ. Res. Lett. 13, 014007. doi:10.1088/1748-9326/aa9b88

Szeto, K.K., 2002. Moisture recycling over the Mackenzie basin. Atmosphere-Ocean 40, 181–197. doi:10.3137/ao.400207

Tape, K., Sturm, M., Racine, C., 2006. The evidence for shrub expansion in Northern Alaska and the Pan-Arctic. Glob. Chang. Biol. 12, 686–702. doi:10.1111/j.1365-2486.2006.01128.x

Taylor, K.E., Stouffer, R.J., Meehl, G.A., 2012. An Overview of CMIP5 and the Experiment Design. Bull. Am. Meteorol. Soc. 3, 485–498. doi:10.1175/BAMS-D-11-00094.1

Thompson, D.W.J., Wallace, J.M., 1998. The Arctic Oscillation signature in the wintertime geopotential height and temperature fields. Geophys. Res. Lett. 25, 1297–1300. doi:10.1029/98GL00950

Thomson, A.M., Calvin, K. V., Smith, S.J., Kyle, G.P., Volke, A., Patel, P., Delgado-Arias, S., Bond-Lamberty, B., Wise, M.A., Clarke, L.E., Edmonds, J.A., 2011. RCP4.5: a pathway for stabilization of radiative forcing by 2100. Clim. Change 109, 77–94. doi:10.1007/s10584-011-0151-4

Thornthwaite, C.W., 1948. An Approach toward a Rational Classification of Climate. Geogr. Rev. 38, 55–94. doi:10.2307/210739

Tolson, B.A., Shoemaker, C.A., 2007. Dynamically dimensioned search algorithm for computationally efficient watershed model calibration. Water Resour. Res. 43, W01413. doi:10.1029/2005WR004723

Trenberth, K.E., Hurrell, J.W., 1994. Decadal atmosphere-ocean variations in the Pacific. Clim. Dyn. 9, 303–319. doi:10.1007/BF00204745

Uppala, S.M., Kallberg, P.W., Simmons, A.J., Andrae, U., Bechtold, V.D.C., Fiorino, M., Gibson, J.K., Haseler, J., Hernandez, A., Kelly, G.A., Li, X., Onogi, K., Saarinen, S., Sokka, N., Allan, R.P., Andersson, E., Arpe, K., Balmaseda, M.A., Beljaars, A.C.M., Berg, L. Van De, Bidlot, J., Bormann, N., Caires, S., Chevallier, F., Dethof, A., Dragosavac, M., Fisher, M., Fuentes, M., Hagemann, S., Hólm, E., Hoskins, B.J., Isaksen, L., Janssen, P.A.E.M., Jenne, R., Mcnally, a. P., Mahfouf, J.-F., Morcrette, J.-J., Rayner, N. a., Saunders, R.W., Simon, P., Sterl, A., Trenberth, K.E., Untch, A., Vasiljevic, D., Viterbo, P., Woollen, J., 2005. The ERA-40 re-analysis. Q. J. R. Meteorol. Soc. 131, 2961–3012. doi:10.1256/qj.04.176

Valente, F., David, J.S., Gash, J.H.C., 1997. Modelling interception loss for two sparse eucalypt and pine forests in central Portugal using reformulated Rutter and Gash analytical models. J. Hydrol. 190, 141–162. doi:10.1016/S0022-1694(96)03066-1

van Vuuren, D.P., Stehfest, E., den Elzen, M.G.J., Kram, T., van Vliet, J., Deetman, S., Isaac, M., Goldewijk, K.K., Hof, A., Beltran, A.M., Oostenrijk, R., van Ruijven, B., 2011. RCP2.6: Exploring the possibility to keep global mean temperature increase below 2°C. Clim. Change 109, 95–116. doi:10.1007/s10584-011-0152-3

van Wijngaarden, W.A., 2014. Temperature trends in the Canadian arctic during 1895–2014. Theor. Appl. Climatol. 120, 609–615. doi:10.1007/s00704-014-1202-3

Vincent, L. a., Mekis, É., 2006. Changes in Daily and Extreme Temperature and Precipitation Indices for Canada over the Twentieth Century. Atmosphere-Ocean 44, 177–193. doi:10.3137/ao.440205

Vincent, L.A., Zhang, X., Brown, R.D., Feng, Y., Mekis, E., Milewska, E.J., Wan, H., Wang, X.L., 2015. Observed Trends in Canada's Climate and Influence of Low-Frequency Variability Modes. J. Clim. 28, 4545–4560. doi:10.1175/JCLI-D-14-00697.1

Viswanathan, M., 1984. Recharge characteristics of an unconfined aquifer from the rainfall-water table relationship. J. Hydrol. 70, 233–250. doi:10.1016/0022-1694(84)90124-0

Vitt, D.H., Halsey, L. a., Zoltai, S.C., 2000. The changing landscape of Canada's western boreal forest: the current dynamics of permafrost. Can. J. For. Res. 30, 283–287. doi:10.1139/cjfr-30-2-283

Voldoire, a., Sanchez-Gomez, E., Salas y Mélia, D., Decharme, B., Cassou, C., Sénési, S., Valcke, S., Beau, I., Alias, a., Chevallier, M., Déqué, M., Deshayes, J., Douville, H., Fernandez, E., Madec, G., Maisonnave, E., Moine, M.-P., Planton, S., Saint-Martin, D., Szopa, S., Tyteca, S., Alkama, R., Belamari, S., Braun, a., Coquart, L., Chauvin, F., 2012. The CNRM-CM5.1 global climate model: description and basic evaluation. Clim. Dyn. 40, 2091–2121. doi:10.1007/s00382-011-1259-y

Wagener, T., Boyle, D.P., Lees, M.J., Wheater, H.S., Gupta, H. V., Sorooshian, S., 2001. A framework for development and application of hydrological models. Hydrol. Earth Syst. Sci. 5, 13–26. doi:10.5194/hess-5-13-2001

Wallace, J.M., Hobbs, P. V., 2006. Atmospheric Science, an Introductory Survey, Second. ed. Elsevier Inc.

Walmsley, J.L., Taylor, P.A., Keith, T., 1986. A simple model of neutrally stratified boundary-layer flow over complex terrain with surface roughness modulations (MS3DJH/3R). Boundary-Layer Meteorol. 36, 157–186. doi:10.1007/BF00117466

Walsh, J.E., 2005. Cryosphere and Hydrology, in: Symon, C., Arris, L., Heal, B. (Eds.), Arctic Climate Impact Assessment - Scientific Report. Cambridge University Press, pp. 183–242.

Walton, D.B., Sun, F., Hall, A., Capps, S., 2015. A hybrid dynamical-statistical downscaling technique. Part I: Development and validation of the technique. J. Clim. 28, 4597–4617. doi:10.1175/JCLI-D-14-00196.1

Walvoord, M.A., Kurylyk, B.L., 2016. Hydrologic impacts of thawing permafrost - a review. Vadose Zo. J. 15, 1–20. doi:10.2136/vzj2016.01.0010

Walvoord, M.A., Voss, C.I., Wellman, T.P., 2012. Influence of permafrost distribution on groundwater flow in the context of climate-driven permafrost thaw: Example from Yukon

Flats Basin, Alaska, United States. Water Resour. Res. 48, 1–17. doi:10.1029/2011WR011595

Wanishsakpong, W., McNeil, N., Notodiputro, K.A., 2016. Trend and pattern classification of surface air temperature change in the Arctic region. Atmos. Sci. Lett. 17, 378–383. doi:10.1002/asl.668

Wessel, D.A., Rouse, W.R., 1994. Modelling evaporation from wetland tundra. Boundary-Layer Meteorol. 68, 109–130. doi:10.1007/BF00712666

Westerling, A.L., Hidalgo, H.G., Cayan, D.R., Swetnam, T.W., 2006. Warming and Earlier Spring Increase Western U.S. Forest Wildfire Activity. Science (80-.). 313, 940 LP-943. doi:10.1126/science.1128834

Weston, S.T., Bailey, W.G., McArthur, L.J.B., Hertzman, O., 2007. Interannual solar and net radiation trends in the Canadian Arctic. J. Geophys. Res. Atmos. 112, 1–8. doi:10.1029/2006JD008000

Whitfield, P.H., 2012. Floods in future climates: a review. J. Flood Risk Manag. 5, 336–365. doi:10.1111/j.1753-318X.2012.01150.x

Whitfield, P.H., Hall, A.W., Cannon, A.J., 2004. Changes in the Seasonal Cycle in the Circumpolar Arctic, 1976-95: Temperature and Precipitation. ARCTIC 57, 80–93. doi:10.14430/arctic485

Wilby, R.., Dawson, C.., Barrow, E.., 2002. Sdsm — a Decision Support Tool for the Assessment of Regional Climate Change Impacts. Environ. Model. Softw. 17, 145–157. doi:10.1016/S1364-8152(01)00060-3

Wilcoxon, F., 1945. Individual Comparisons by Ranking Methods. Biometrics Bull. 1, 80–83. doi:10.2307/3001968

Williams, J.R., Waller, R.M., 1966. Ground water occurrence in permafrost regions of Alaska, in: 1st International Conference on Permafrost. Lafayette, pp. 159–164.

Williams, T.J., Pomeroy, J.W., Janowicz, J.R., Carey, S.K., Rasouli, K., Quinton, W.L., 2015. A radiative-conductive-convective approach to calculate thaw season ground surface temperatures for modelling frost table dynamics. Hydrol. Process. 29, 3954-3965. doi:10.1002/hyp.10573

Williamson, T., Colombo, S., Duinker, P., Gray, P., Hennessey, R., Houle, D., Johnston, M., Ogden, A., Spittlehouse, D., 2009. Climate change and Canada's forests: from impacts to adaptation. Sustainable Forest Management Network and Natural Resources Canada, Canadian Forest Service, Northern Forestry Centre ed., Edmonton, AB.

Woo, M.-K., 1986. Permafrost hydrology in North America 1. Atmosphere-Ocean 24, 201–234. doi:10.1080/07055900.1986.9649248

Woo, M.-K., 2012. Permafrost Hydrology. Springer Berlin Heidelberg, Berlin, Heidelberg.

doi:10.1007/978-3-642-23462-0

Woo, M.-K., Kane, D.L., Carey, S.K., Yang, D., 2008. Progress in permafrost hydrology in the new millennium. Permafr. Periglac. Process. 19, 237–254. doi:10.1002/ppp.613

Woo, M.-K., Sauriol, J., 1980. Channel Development in Snow-Filled Valleys, Resolute, N. W. T., Canada. Geogr. Ann. Ser. A, Phys. Geogr. 62, 37–56. doi:10.1080/04353676.1980.11879998

Woo, M.-K., Xia, Z., 1995. Suprapermafrost groundwater seepage in gravelly terrain, resolute, NWT, Canada. Permafr. Periglac. Process. 6, 57–72. doi:10.1002/ppp.3430060107

Woo, M., 2008. Cold Region Atmospheric and Hydrologic Studies. The Mackenzie GEWEX Experience. Volume 2: Hydrological Processes. Springer Berlin Heidelberg, Berlin, Heidelberg. doi:10.1007/978-3-540-73936-4

Woo, M., Guan, X.J., 2006. Hydrological Connectivity and Seasonal Storage Change of Tundra Ponds in a Polar Oasis Environment , Canadian High Arctic. Permafr. Periglac. Process. 323, 309–323. doi:10.1002/ppp

Woo, M., Heron, R., Marsh, P., 1982. Basal Ice in High Arctic Snowpacks. Arct. Alp. Res. 14, 251. doi:10.2307/1551157

Woo, M., Mollinga, M., Smith, S.L., 2006. Simulating Active Layer Thaw in a Boreal Environment. Géographie Phys. Quat. 60, 9–17. doi:10.7202/016361ar

Woo, M., Mollinga, M., Smith, S.L., 2007. Climate warming and active layer thaw in the boreal and tundra environments of the Mackenzie Valley. Can. J. Earth Sci. 44, 733–743. doi:10.1139/e06-121

Woo, M., Steer, P., 1982. Occurrence of surface flow on arctic slopes , southwestern Cornwallis Island. Can. J. Earth Sci. 19, 2368–2377. doi:10.1139/e82-206

Woo, M.K., Arain, M.A., Mollinga, M., Yi, S., 2004. A two-directional freeze and thaw algorithm for hydrologic and land surface modelling. Geophys. Res. Lett. 31, 1–4. doi:10.1029/2004GL019475

Xu, L., Myneni, R.B., Chapin III, F.S., Callaghan, T. V., Pinzon, J.E., Tucker, C.J., Zhu, Z., Bi, J., Ciais, P., Tømmervik, H., Euskirchen, E.S., Forbes, B.C., Piao, S.L., Anderson, B.T., Ganguly, S., Nemani, R.R., Goetz, S.J., Beck, P.S.A., Bunn, A.G., Cao, C., Stroeve, J.C., 2013. Temperature and vegetation seasonality diminishment over northern lands. Nat. Clim. Chang. 3, 581–586. doi:10.1038/nclimate1836

Yang, D., Kane, D.L., Hinzman, L.D., Zhang, X., Zhang, T., Ye, H., 2002. Siberian Lena River hydrologic regime and recent change. J. Geophys. Res. Atmos. 107, 1–10. doi:10.1029/2002JD002542

Yip, Q.K.Y., Burn, D.H., Seglenieks, F., Pietroniro, A., Soulis, E.D., 2012. Climate Impacts on Hydrological Variables in the Mackenzie River Basin. Can. Water Resour. J. 37, 209–230.

doi:10.4296/cwrj2011-899

Zhang, W., Miller, P.A., Smith, B., Wania, R., Koenigk, T., Döscher, R., 2013. Tundra shrubification and tree-line advance amplify arctic climate warming: Results from an individual-based dynamic vegetation model. Environ. Res. Lett. 8, 1–12. doi:10.1088/1748-9326/8/3/034023

Zhang, X., Hogg, W.D., Mekis, É., 2001. Spatial and Temporal Characteristics of Heavy Precipitation Events over Canada. J. Clim. 14, 1923–1936. doi:10.1175/1520-0442(2001)014<1923:SATCOH>2.0.CO;2

Zhang, X., Vincent, L.A., Hogg, W.D., Niitsoo, A., 2000. Temperature and precipitation trends in Canada during the 20th century. Atmosphere-Ocean 38, 395–429. doi:10.1080/07055900.2000.9649654

Zhang, Z., Kane, D.L., Hinzman, L.D., 2000. Development and application of a spatially-distributed Arctic hydrological and thermal process model (ARHYTHM). Hydrol. Process. 14, 1017–1044. doi:10.1002/(SICI)1099-1085(20000430)14:6<1017::AID-HYP982>3.0.CO;2-G

Zhao, L., Gray, D.M., 1997. A parametric expression for estimating infiltration into frozen soils. Hydrol. Process. 11, 1761–1775. doi:10.1002/(SICI)1099-1085(19971030)11:13<1761::AID-HYP604>3.0.CO;2-O

Zhao, L., Gray, D.M., 1999. Estimating snowmelt infiltration into frozen soils. Hydrol. Process. 13, 1827–1842. doi:10.1002/(SICI)1099-1085(199909)13:12/13<1827::AID-HYP896>3.0.CO;2-D

Zhao, L., Gray, D.M., Male, D.H., 1997. Numerical analysis of simultaneous heat and mass transfer during infiltration into frozen ground. J. Hydrol. 200, 345–363. doi:10.1016/S0022-1694(97)00028-0

Appendix

Table A1 presents the results from the model re-calibration performed in Chapter 5. This table supports the result that demonstrates the robustness of the CRHM-AHM streamflow simulation, as recalibration using weather from WRF, as opposed to observations, did not significantly impact the performance of simulated streamflow.

Table A1: Parameters optimization comparison between those presented by Krogh et al. (2017) and the re-calibration experiment using corrected WRF as forcing data.

Parameter	**Land Cover**	**Optimization Range**	**Optimum value from Krogh et al. (2017)**	**Current optimum value**
Subsurface Routing Storage (days)	Tundra	0 - 10	0.99	0.3
	Shrubs		0.3	9.9
	Forest		9.9	2.5
	Wetland		9.7	9.9
Subsurface Routing Lag (hours)	Tundra	0 - 100	2.8	10.7
	Shrubs		32.3	98.8
	Forest		98.9	99.0
	Wetland		0.25	74.6
Surface Routing Storage (days)	Tundra	0 – 10	9.9	9.9
	Shrubs		0.01	0.25
	Forest		9.8	1.9
	Wetland		0.1	0.2
	Open Water		0.1	0.85

Parameter	**Land Cover**	**Optimization Range**	**Optimum value from Krogh et al. (2017)**	**Current optimum value**
Surface Routing Lag (hours)	Tundra	0 – 100	12.3	98.9
	Shrubs		0.2	2.5
	Forest		0.1	0.12
	Wetland		0.02	98.0
	Open Water		0.8	0.17
Maximum Recharge Layer Capacity (mm)	All (but Open Water)	300 – 550	325	548
Saturated Hydraulic Conductivity ($m\ s^{-1}$)	Upper Peat	$[1 – 9.9] \times 10^{-3}$	1.04×10^{-3}	5.3×10^{-3}
	Lower Peat	$[1 – 9.9] \times 10^{-4}$	9.88×10^{-4}	9.58×10^{-4}
Maximum Snow Water Storage Capacity in Detention Layer (mm)	All	0 – 100	1.1	0.08
Depression Storage (mm)	Wetland	0 – 200	17	182.7